USC
UNIVERSIDADE
DE SANTIAGO
DE COMPOSTELA

SINGLE-MOLECULE FLUORESCENCE STUDIES OF THE DYNAMICS IN SUPRAMOLECULAR SYSTEMS OF BIOLOGICAL INTEREST

Jorge Bordello Malde

PhD Thesis, 2013

Departamento de Química-Física
Universidad de Santiago de Compostela

SINGLE-MOLECULE FLUORESCENCE STUDIES OF THE DYNAMICS IN SUPRAMOLECULAR SYSTEMS OF BIOLOGICAL INTEREST

Jorge Bordello Malde

PhD Thesis, 2013

Departamento de Química-Física
Universidad de Santiago de Compostela

LOS DOCTORES MARÍA DE LA MERCED NOVO RODRÍGUEZ Y WAJIH AL-SOUFI, PROFESORES TITULARES DEL DEPARTAMENTO DE QUÍMICA-FÍSICA DE LA UNIVERSIDAD DE SANTIAGO DE COMPOSTELA

CERTIFICAN:

Que el trabajo descrito en la presente memoria, con el título **"SINGLE-MOLECULE FLUORESCENCE STUDIES OF THE DYNAMICS IN SUPRAMOLECULAR SYSTEMS OF BIOLOGICAL INTEREST"**, que presenta el Licenciado en Química **Jorge Bordello Malde** para optar al grado de doctor en Ciencias Químicas, ha sido realizado bajo su dirección en el Departamento de Química-Física de la Universidad de Santiago de Compostela.

Y para que así conste, firman la presente en Lugo, a 2 de Septiembre de 2013.

Mª de la Merced Novo Rodríguez

Wajih Al-Soufi

Acknowledgements

My work on this thesis was financially supported by a scholarship and a travel grant from the Spanish Government (FPU predoctoral fellowship programme).

I would also like to use these lines to express my gratitude to all those people who gave me the possibility to complete this thesis.

First and foremost, to my supervisors, Prof. Mercedes Novo and Prof. Wajih Al-Soufi, who provided me not only with good teaching but also with thoughtful advice and guidance. They have been for me the role model of a good researcher.

I am indebted to Dr. Carlos Penedo, leader of the Laboratory for Biophysics and Biomolecular Dynamics at the University of St. Andrews, who offered me the excellent opportunity to stay in his lab and learn modern single-molecule FRET techniques. I really appreciate his comments on Chapter V. I would also like to thank Dr. Paul Dalgarno and Steven Quinn for their great help during my time working there.

The collaboration with the Group of Prof. José Luis Mascareñas (USC) made possible the chapter about the DNA binding studies. I am especially grateful to Dr. Olalla Vázquez and Mateo Isidro Sánchez for the synthesis of the binders, and Dr. Eugenio Vázquez for his contribution to the discussion in the paper.

I also wish to thank the other co-authors of the papers included in this thesis: Dr. Belén Reija, for her collaboration in the pyronines-cyclodextrins work; Dr. María Jesús Pérez Alvite, for the synthesis of the adamantane derivative; and Daniel Granadero, not only for his contribution in the study of the cyclodextrin-adamantane interaction, but mostly for sharing this doctoral journey with me and making it worth remembering.

All my lab-mates over the last years have helped me in some way. I wish Sonia, Carlos and Lucas the best of luck with their PhDs. Special thanks to Laura from the neighbor lab, who has always provided a supportive ear when I have needed it.

Last but not least, a mention to my family and all those who kept me sane and happy outside the lab. *Thank you.*

Table of Contents

General Introduction

"Single-molecule experiments will contribute to bridge the gap between physics and biology"
A. van Oijen.

Supramolecular chemistry covers the study of those molecular systems in which the most important feature is that components are held together by noncovalent interactions. Subjects such as host-guest chemistry, molecular self-assembly, molecular recognition or conformational changes fall under the umbrella of this discipline. The scope of supramolecular chemistry is also vast comprising multitude of systems with key roles in fields as diverse as biomedicine, pharmacology, catalysis, nanochemistry or molecular sensors.

Investigations on these supramolecular systems result crucial for a better understanding of their biological function or technical application. According to this, it is important to remark the importance of collecting information not only on the thermodynamics and structure of the molecules involved but also on their mobility and dynamic properties in order to obtain a full picture of the mechanisms involved in these processes (Bohne 2006).

Several techniques are used to study supramolecular systems, depending on their specific characteristics. Among the most common are electrophoresis based on size/charge migration, mass spectroscopy, light scattering or NMR diffusion to study molecular aggregation; and crystallography, circular dichroism (CD) or electron spin resonance (ESR) to study conformational changes in macromolecules. In this context, fluorescence spectroscopy is one of the most sensitive and versatile techniques available (Böhmer and Enderlein 2003; Haran 2003; Michalet et al. 2003). Although most supramolecular systems are themselves nonfluorescent, fluorescent labels can usually be attached to some of their subunits, so that changes in the spectroscopic properties (quantum yield, spectral shift, lifetime, anisotropy, etc.) of the fluorescent label upon binding can be used to study the binding affinity and in some cases the dynamics of the process. Also the exploitation of the Förster Resonance Energy Transfer (FRET) phenomenon allows one to measure distances, detect molecular

interactions, study conformations or obtain information about metabolic or signaling pathways (Roy et al. 2008).

In the last years, single-molecule experiments have revolutionized fluorescence spectroscopy with the development of several techniques based on the detection of the individual spectral properties of single labeled molecules, instead of the mean value of molecular ensembles (Haustein and Schwille 2004; Walter et al. 2008). Working at the so-called "single-molecule level" provides as main advantage the "no-need for synchronization" to investigate molecular dynamics. Whereas conventional techniques require to displace the system from its rest state (normally, via quick changes in temperature, pressure or by inducing a chemical gradient) and to observe how it relaxes back to equilibrium conditions, single-molecule techniques analyzes the time-evolution of each individual molecule separately without the need for displacement from its equilibrium state. New relevant information about thermodynamics and kinetics obtained by the single molecule approach is often difficult to obtain in bulk experiments and can be the key to unveil the mechanisms behind many biomolecular processes (Tinoco and Gonzalez 2011).

The fluorescence detection from single fluorophores requires not only a very low concentration of the observed dye but also the suppression of the background signal from the solvent by reducing the sample volume itself (Selvin and Ha 2008; Zander et al. 2002). Single Molecule Fluorescence Detection (SMFD) techniques can be classified roughly into two groups: those observing freely diffusing molecules within a sample volume defined by a confocal microscope, such as Fluorescence Correlation Spectroscopy (FCS) or burst analysis techniques (MFD (Kuhnemuth and Seidel 2001), BIFL, PCH, etc); and those analyzing the fluorescence from molecules immobilized on a glass surface under near-field or evanescent excitation (TIRF, NSOM, etc). Their combination with FRET is common for many SMFD techniques (Selvin and Ha 2008). Single-pair FRET can report on binding events in real time and is particularly useful for studying conformational dynamics of biomolecules, which previously have been labeled with two different color dyes positioned at specific locations (Roy et al. 2008).

Given the huge amount of information they provide, single-molecule experiments impacted physical biochemistry, providing a new tool that complements standard spectroscopy and microscopy techniques and is becoming a major theme of research in modern biophysics. Any biological molecule or supramolecular system is a potential target for single-molecule studies. In fact, some single-molecule fluorescence techniques already represent standard methods for the elucidation of the structural rearrangements and association processes of biologically relevant macromolecules and, without doubt, we will not have to wait for long to find them as part of the routine techniques in any biochemical lab.

This thesis

This thesis comprises part of the results obtained during more than 4 years of Ph.D. studies at the Al-Soufi and Novo's Single Molecule Fluorescence Lab of the University of Santiago de Compostela, Spain. The purpose of this work was to study different supramolecular systems by using fluorescence spectroscopy, and very especially to prove how SMFD techniques could be applied to investigate certain systems in which the single molecule approach gave us a significant advantage over other standard techniques, either because the aimed information was not accessible by other means or because SMFD allowed to do it much easier and faster. The focus was put on Fluorescence Correlation Spectroscopy and its application to study supramolecular association in different host-guest systems such as cyclodextrins, surfactants or DNA; although a chapter on RNA folding studies using Total Internal Reflection Fluorescence (TIRF) in combination with single-molecule FRET is also included, as a result of an internship in the lab of Carlos Penedo at the University of St. Andrews, Scotland.

Chapter I is dedicated to a brief introduction into single-molecule fluorescence detection with a more detailed description of the FCS technique (setup, main equations in the data analysis, etc). Due to the necessity of very low concentrations of fluorophore, FCS is very sensitive to fluorescent impurities in samples or solvents. As the collaborations in our research group with organic chemists and biologists became closer, problems related to the unavoidable impurities arose, making it necessary to study how they affect the FCS results. A detailed discussion on the influence of impurities in FCS also appears in this first chapter. Some practical aspects concerning FCS measurements gathered through the different experiments, such as sample preparation, influence of cover-slide thickness, calibration of the confocal volume, etc. are included in a last section of the chapter.

In **Chapter II** the factors that control structure and stability of supramolecular host-guest assemblies were discussed through three different publications. Cyclodextrines complexation with Pyronines and Adamantane together with the formation of micelle-dye inclusion complexes were studied as two models of host-guest interaction using different Fluorescence Techniques. The first work addresses the study of the complexation of pyronines Y and B with γ-cyclodextrin (γCD) using UV/Vis absorption and fluorescence spectroscopy (Bordello et al. 2009), as a continuation of a previous work in the research group for the βCD. The potential of Fluorescence Correlation Spectroscopy to study a wide range of host-guest complexes without the need for a change in the spectroscopic properties of the fluorescent label upon binding is presented using as an example the study of the complexation between adamantane and cyclodextrin in the second paper collected in this Chapter (Granadero et al. 2010). Also, the use of high resolution FCS to obtain dynamic information of the host-guest inclusion, providing that the fluorescence intensity of host or guest changes upon

complexation, is discussed in this chapter through a third article (Novo et al. 2011). In this work the application of FCS to the study of inclusion complexes of dyes with hosts of different structure, such as cyclodextrins and micelles, shows how knowledge about the dynamics gives valuable information on the association mechanism, which is directly related to the structure of the host and the guest.

Chapter III is also based on a publication in which we discuss the role of a high brightness ratio of the dye during the association process in order to enhance the sensitivity of FCS for the determination of the underlying rate constant (Bordello et al. 2010). Exchange dynamics of the dye Coumarine 152 between neutral Triton X-100 micelles and the surrounding water are analyzed and compared with previous results for cationic dyes, such as Rhodamine 123, which typically show an inverse brightness variation.

As a final stage of the thesis, several experiments were conducted within the framework of collaborations with other research groups in order to use SMFD to investigate different biological systems of current interest.

The group of Prof. J. L. Mascareñas (USC) has developed non-natural synthetic agents for genome recognition capable of mimicking the DNA binding properties of naturally occurring DNA-binding transcription factors which allow the direct sensing of double-stranded DNA (dsDNA) without the need for denaturation. The goals in the design of these ligands are both high sequence-specificity and high affinity to the target DNA sequence. Both properties are difficult to study for these systems with standard analytic methods. Information about binding dynamics is not easily accessible by classic techniques.

As a result of the collaboration with Prof. Mascareñas group, successful studies were carried out to investigate the binding affinity and dynamics of the binding of synthetic agents to specific DNA sequences. This work allowed the study of minor groove association dynamics by FCS, with relevant conclusions on the association process of minor-groove binders to DNA. The most relevant results and discussions are collected in **Chapter IV**, with part of them already published as a communication (Bordello et al. 2012).

This ongoing collaboration has opened the door to new projects on this and related systems. Also, the fast binding dynamics of the DNA binders designed for these studies makes them potential labels for high resolution microscopy techniques such as PAINT (Point Accumulation for Imaging in Nanoscale Topography).

Whereas fast dynamics can be addressed using a free-diffusion correlation technique such as FCS, many biological processes occur at time scales significantly longer than that of the diffusion of a molecule through the detection volume. This situation makes it necessary to use

a different approach to SMFD. The immobilization of the molecules on a surface allows for observation-times much longer than those possible in a free-diffusion setup. We applied such an immobilization technique in the studies on RNA folding collected in **Chapter V** and carried out during a research internship in the Laboratory for Biophysics and Biomolecular Dynamics of Dr. Penedo, at the University of St. Andrews (Scotland). Here Total Internal Reflection Fluorescence (TIRF) used in combination with single molecule FRET allows us to identify conformational transitions and characterize conformational changes in the chemical denaturation pathway of the Adenine Riboswitch as well as to provide information about the kinetics of the process. This methodology has been widely used to study protein folding (Michalet et al. 2006) and is presented here as an alternative approach to the single-molecule manipulation techniques, such as atomic force microscopy (AFM) (Cao and Li 2011; Kawakami et al. 2006; Peng and Li 2008) and laser optical tweezers (LOTs) (Cecconi et al. 2007), commonly used to study the folding pathway of RNA. Using single-molecule imaging with TIR illumination, dynamics in the microseconds to hours range can be observed, limited mainly by the photostability of the immobilized dyes at the long end (photobleaching) and the time resolution of the detection at short times. By monitoring and analyzing the changes observed in the FRET efficiency during the folding studies valuable information was obtained about the folding process.

Finally, in the closing section "**Summarizing Discussion and Conclusions**" the content of this thesis is summarized highlighting the most relevant conclusions.

Objectives

The general objective of this thesis is the use of single-molecule fluorescence (SMF) techniques to study the dynamics of different supramolecular systems of biological and technological relevance. The focus is put on *Fluorescence Correlation Spectroscopy* (FCS), although a complementary SMF technique (combining FRET and *Total Internal Reflection Fluorescence Microscopy*) is also used, together with the more standard absorption and fluorescence spectroscopies.

The determination of equilibrium constants in several organized systems such as host-guest complexations or conformational changes in macromolecules provides valuable data in order to elucidate binding stoichiometries, equilibrium population distributions or affinities under different conditions. However, for a same equilibrium constant the kinetic behavior can vary widely, with the rate constants in a range of several orders of magnitude. Crucial information regarding supramolecular systems such as transition-states, binding kinetic constants and identification of intermediates or rate-limiting steps lies in the study of dynamics, which very often represents the key to unveil the mechanism of many of these processes. Despite of its importance, kinetic data is not easily available. Historically, the study of fast dynamics through ensemble-averaging techniques was based on relaxation methods, in which the system is disturbed from an existing equilibrium, observing then its decay back to equilibrium. The aim of this thesis is to apply SMF techniques to study dynamics of different supramolecular systems, which allow one to do it through steady state measurements at equilibrium conditions.

The specific objectives were set as follows:

- Tune up the FCS technique to study different host-guest systems.
  - Contribute to the technique's optimization by making adjustments to improve performance and studying the influence of different factors that affect FCS measurements.

- Set up protocols regarding most relevant aspects of the FCS measurements, such as calibration of the confocal volume, sample preparation, influence of the cover-slide thickness, etc.

- Analyze the influence of fluorescent impurities in FCS experiments.

  - Develop models and simulations to analyze the importance of impurities present in the sample on two of the most important parameters of the correlation curve: the number of molecules and the diffusion time.

  - Apply the obtained models to experimental data from different systems under study to check whether the variations in the parameters observed during the titrations can be explained on the basis of the presence of impurities or can be in fact attributed to the host-guest interaction.

  - Explain the non-expected increase in the apparent number of molecules, N, observed in titrations in which the concentration of fluorophore remains constant. Study under which conditions this behavior can be attributed to a certain level of impurities either in the stock of host or guest.

- Study the host-guest complexation of pyronines Y and B with γ-cyclodextrin using UV/Vis absorption and fluorescence spectroscopy.

  - Analyze the effect of the γ-cyclodextrin complexation on the absorption and emission spectra, quantum yield and lifetime of each pyronine.

  - Compare the results with those previously obtained in the research group for the β-cyclodextrin, with analogous structure but with a smaller cavity than γ-cyclodextrin. On the basis of these results, analyze the influence of the cavity size on the complexation.

- Review the application of FCS to the study of host-guest inclusion complexes with an emphasis on practical aspects and relevant bibliographic references.

  - Collect data of the association thermodynamics and dynamics of different types of host, such as cyclodextrins or micelles, with different fluorescent guests or fluorescently labeled molecules.

  - Analyze the influence of the host-guest geometry on the dynamics.

  - Discuss the potential and limitations of FCS to study host-guest association.

- Study the dynamics of the association of a neutral hydrophobic dye to micelles by FCS.

  - Use absorption and emission spectroscopies to study the photophysics of the Coumarine 152 as an example of neutral hydrophobic dye, both in aqueous solution and bound to Triton X-100 micelles.

  - Discuss the feasibility of overcoming the initial disadvantages of this type of dyes such as their low quantum yield, low saturation threshold and higher energetic excitation.

  - Analyze the influence of the change in the brightness of free and bound dye (brightness ratio) on the sensitivity of FCS experiments in studies of association dynamics.

- Study the association dynamics of DNA minor-groove binders to both high and low affinity DNA sequences.

  - Prove that by using of a novel fluorescently labeled derivative from the cationic bisbenzamidines family of minor groove binders, FCS allows one to obtain not only values for the binding equilibrium constant and the diffusion coefficients, but also the association and dissociation rate constants of this kind of binders.

  - Perform an estimation of the diffusion-controlled rate constants for the interaction of this binder with high and low affinity DNA sequences, in order to identify the rate-limiting step in this process and to evaluate the importance of mechanisms such as sliding or two dimensional diffusion found for the binding of proteins to DNA.

  - Study the photophysical processes responsible for the huge fluorescent enhancement of the binder under study and analyze the effect of structural changes of the binder on the association dynamics.

- Use single-molecule FRET and TIRF microscopy to study RNA folding dynamics, which are too slow to be studied by FCS.

  - Perform a comparative characterization of the folding kinetics of the Adenine riboswitch ligand-free state in presence of proline, betaine and formamide as denaturants to provide a preliminary analysis of their feasibility in single-molecule chemical denaturation studies of riboswitches folding.

  - Study the response of the add aptamer domain of the Adenine riboswitch at different concentrations of ligand, monovalent cations and divalent metal ions in presence of the denaturant formamide.

Chapter I

Single Molecule Fluorescence Detection

Contents:

1. Introduction.

In this chapter we first give a brief introduction to single molecule fluorescence detection (SMFD) in order to explain the advantages and properties of SMFD and to classify and compare the SMFD techniques used in the different studies collected in this work.

We then describe in more detail FCS as the main technique used in this thesis, the basic theory which leads to the equations used in the data analysis and some important practical aspects of FCS titrations.

In the last part we present an extensive analysis of the impact of impurities in the solutions on the two main parameters determined with FCS: the translational diffusion coefficient and the number of molecules in the sample volume. This part is in preparation to be published.

2. Single Molecule Fluorescence Detection (SMFD).

Fluorescence Spectroscopy.

Fluorescence is probably the most widely used investigative tool for studying the structure and dynamics of complex systems at molecular level (Lakowicz 2006; Valeur 2002).

Fluorescence emission can be detected with very high efficiency which makes fluorometric techniques highly sensitive, down to the single molecule level.

The microenvironment of the emitting molecule can have a strong influence on the characteristics of the emitted fluorescence. Parameters can be polarity, pH, pressure, viscosity, temperature, electric potential, quenching molecules, hydrogen bonds, etc.

The emitting molecule samples its surroundings within a very small volume, of the order of only a few cubic nanometers, and can therefore provide chemical information with very high spatial resolution.

The characteristics of the emitted fluorescence follow instantly changes in the environment and gives therefore information with high temporal resolution.

A fluorescent probe continuously samples its immediate surroundings and encodes the gathered information in the light it emits. It can be seen as a nano-scaled emitter introduced by the scientist into the microenvironment in order to gain information about its structure and dynamics.

Fluorescent probes can provide a wealth of information on their environment and are applied to a big variety of systems, such as polymers, solid surfaces, surfactant solutions, biological membranes, vesicles, proteins, nucleic acids, living cells, etc. Fluorescence allows one to study dynamics, microviscosity, pH, miscibility, degradation, polarity, rigidity, critical micelle concentration, partition coefficients, phase transitions, fluidity, order parameters, lipid–protein interactions, translational diffusion, site accessibility, structural changes, membrane potentials, complexes and binding, location of proteins, lateral organization, permeability, denaturation, conformational transition, photocleavage, ion concentrations, redox states enzyme activities, cytotoxic activity, and many more (Demchenko 2009; Lakowicz 2006; Valeur 2002).

SINGLE Molecules.

Traditionally the structure and the dynamics of molecular systems are studied with different techniques (NMR, X-Ray, SAXS, Fluorescence, etc.) applied to a huge number of molecules simultaneously in order to obtain a reliable signal. The observations are then explained by models based on the behavior of one or a few molecules, assuming that all molecules of the same kind behave in the same way, a condition not always valid in complex systems (Figure 1**Figure 1**).

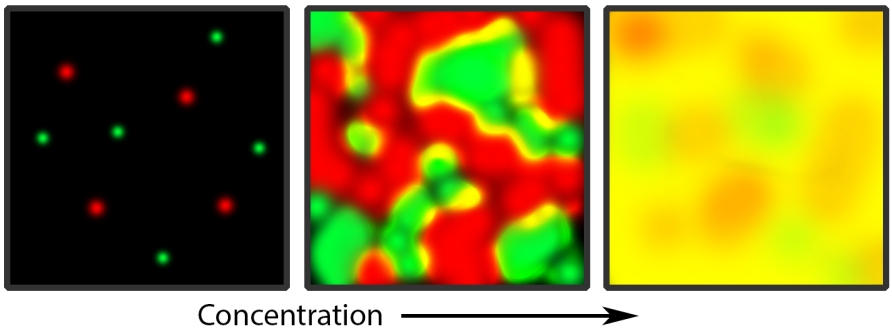

Figure 1. Conventional techniques of molecules in solution yield only average properties blurring molecular heterogeneity.

Single molecule studies offer a series of advantages over bulk measurements (Gell et al. 2006; Zander et al. 2002):

- High sensitivity: one molecule represents 1.66 10^{-24} mol (1.66 yoctomole) of the solute of interest, which is the ultimate level of sensitivity.

- High spatial resolution: one molecule samples its local environment within a few nanometers distance and overcomes thus the diffraction limit of optical microscopy by many orders of magnitude

- Resolution of heterogeneity: looking at individual molecules allows one to assess the heterogeneity of complex systems which would be hidden in the ensemble average provided by measurements of concentrated samples.

- Detection of rare intermediates in a kinetic pathway: the signal from abundantly populated states in an ensemble measurement masks that of rare intermediates. Following the kinetic pathway of single molecules allows one to detect and to classify different routes taken by the system through the energy landscape (Figure 2).

- Observation of early kinetic events: single molecule methods provide a way to study kinetics under equilibrium conditions without the need for synchronization by some external starting event (temperature or pH jump, mixing). The finite duration of a synchronization event makes it impossible to observe early kinetic events.

How many molecules do we observe in classical fluorescence measurements?

In an ensemble measurement in a spectrofluorimeter the dye has a typical concentration of 10^{-6} mol/l. Assuming that the fluorescence is collected from a detection volume of the order of 1 mm^3=10^{-6} l we actually observe about 10^{11} dye molecules!

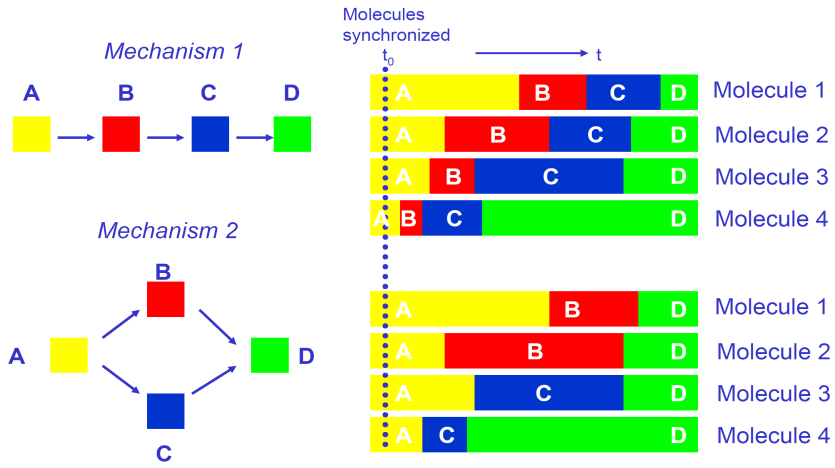

Figure 2. Studying molecular dynamics, the observation of individual molecules allows one to differentiate mechanisms and to detect dynamic heterogeneity in the population, not visible in ensemble measurements.

Can we SEE single molecules?

We cannot *see* individual molecules in an optical microscope due to the diffraction limit, but we can detect the light emitted by a single molecule with suitable detectors, sampling optics and lasers as light sources. We can localize the bright spot produced by the fluorescence of an immobilized single molecule and register the time evolution of its position, intensity, spectral characteristics, etc.

How do we isolate and detect the fluorescence of a single molecule?

The main trick in order to get single molecule resolution in solution measurements is to reduce the mean number of molecules in the observation volume to one or even less, working with a very low concentration of molecules and a microscopic observation volume. This is achieved working with concentrations below 10^{-9} mol/l and a sample volume of some cubic micrometers ($1\ \mu m^3 = 10^{-15}$ l $= 1$ femtoliter). The main challenge is then to detect the weak fluorescence emitted by a single molecule on top of background photons arising from Rayleigh and Raman scattering and from fluorescence impurities. Several conditions have to be fulfilled to obtain sufficiently high signal to noise ratios: an intense light source for excitation, such as a laser, dye molecules with high fluorescence quantum yields and high photochemical stabilities, a solvent of very high purity in order to minimize background fluorescence, and a very efficient and sensitive optical collection and detection system. A breakthrough in single molecule fluorescence detection was the use of a confocal optical microscope with high aperture objectives in order to excite and to detect fluorescent molecules only within the very small focal volume of a focused laser beam.

Single Molecule Fluorescence Techniques.

Many different experimental techniques have been developed for the detection of Single Molecule Fluorescence in the last years. We will classify them briefly.

We can distinguish two core techniques, measurements on *freely diffusing* and on *immobilized* single fluorescent molecules:

Studies on freely diffusing single molecules: In this type of studies the molecules are allowed to diffuse freely in solution. A small open sample volume is defined by the focus of a collimated laser beam in a confocal microscope with a high aperture objective. A fluorescent molecule which diffuses into this sample volume is excited by the laser light and generates a burst of fluorescence photons which are collected and monitored as a function of time. The sample volume is typically less than one femtoliter. The observation time of a molecule is

limited by the transit time through the sample volume, which is typically below 1 ms. These techniques are therefore well suited to study fast dynamic processes.

Studies on immobilized single molecules: In order to observe single molecules on a longer timescale (>1 ms) they can be immobilized in the excitation/observation volume. In Total Internal Reflection Fluorescence Microscopy (TIRF) the molecules are immobilized on a quartz slide and excited by an evanescent light wave introduced through a prism placed on top of the slide (p-TIRF) or directly through the microscope objective (o-TIRF). This evanescence wave propagates only about 100 nm into the quartz-aqueous interface where the labelled molecules are located. This thin excitation area allows TIR to discriminate against background and obtain the required signal-to-noise levels.

We can also distinguish different data analysis methods used to extract information from fluorescence intensity time traces: *fluorescence correlation spectroscopy* (FCS) (Rigler and Elson 2001), *single-molecule fluorescence resonance energy transfer* (sm-FRET) (Selvin 2000; Weiss 2000) *photon counting histograms* (PCH) (Chen et al. 1999), *fluorescence intensity distribution analysis* (FIDA) (Kask et al. 1999), *multi-parameter burst analysis* (Kühnemuth and Seidel 2001; Margittai et al. 2003), etc.

In this thesis we have used the following two SMF techniques:

- Fluorescence Correlation Spectroscopy (FCS) of freely diffusing single molecules in a confocal microscope.

- Single-Molecule Fluorescence Resonance Energy Transfer (sm-FRET) of immobilized single molecules in a TIRF microscope.

In our research group we have constructed a confocal microscope which allows to measure time resolved Fluorescence Correlation Spectroscopy (FCS), Multiparameter Fluorescence Detection (MFD) and Burst Integrated Fluorescence Lifetime (BIFL) in several variants, based on a design the laboratory of Prof. Claus Seidel of the Heinrich Heine University in Düsseldorf, Germany. Our group has pioneered the application of FCS to fast supramolecular dynamics (Al-Soufi et al. 2005, 2008). FCS is the main technique we use in this work and we therefore describe it in more detail in this chapter. The second technique (sm-FRET/TIRF) had been used during a research internship at the laboratory of Dr. Carlos Penedo of the University of St. Andrews in Scotland, UK. It will be described in more detail in Chapter V.

3. Fluorescence Correlation Spectroscopy (FCS).

FCS is a data analysis method that derives physical or chemical parameters such as translational and rotational diffusion coefficients, molecular weights, flow rates, kinetic rate constants of chemical reactions, aggregation, or triplet state lifetimes from the temporal fluctuations of the fluorescence intensity recorded from a few (1-10) molecules *freely diffusing* in an open sample volume. The fluorescence intensity fluctuations can be due to diffusion, chemical reactions, structural changes or any other process which modulates the fluorescence signal of the molecules around the equilibrium value. The timescales of the underlying modulating processes can be elegantly derived from the autocorrelation function of the intensity trace. Each of the processes appears at a correlation time which corresponds to its typical timescale.

Several excellent reviews (Elson 2011), monographs (Gell et al. 2006; Rigler and Elson 2001; Sauer et al. 2011; Selvin and Ha 2008; Thompson 1991; Zander et al. 2002), and textbooks (Lakowicz 2006; Valeur 2002) present FCS theory for different applications.

In FCS the molecules under study diffuse freely within a small sample droplet and eventually pass through the focus of a confocal epi-illuminated fluorescence microscope (Figure 3, left). The focus defines an open microscopic effective detection volume of some femtoliter (10^{-15} liter). If the concentration of the dye molecules in the droplet is low (nanomolar, 10^{-9} mol/liter), then only very few molecules are observed at a time. The molecules are excited by laser light through the microscope objective and their fluorescence is collected by the same objective and focused through a pinhole and filters onto detectors with single photon sensitivity.

The molecules move randomly through the solution due to Brownian motion (Figure 3, b) and at the same time may undergo a fast reversible reaction (Figure 3, a). Both processes introduce fluctuations at characteristic time scales in the detected total fluorescence intensity $F(t)$ (Figure 3, c). The characteristic time of the fluctuations is determined from the autocorrelation curve $G(\tau)$ of the intensity fluctuations $\delta F(t)$ (Figure 3, d with correlation time τ (Al-Soufi et al. 2005, 2008):

$$G(\tau) = \frac{\langle \delta \mathrm{F}(t)\ \ \delta \mathrm{F}(t+\tau) \rangle}{\langle \mathrm{F}(t) \rangle^2} \qquad (1)$$

The correlation function for translational diffusion G_{D} is given by (Elson and Magde 1974; Rigler and Elson 2001):

$$G_D(\tau) = \frac{1}{N}\left(1+\frac{\tau}{\tau_D}\right)^{-1}\left(1+\left(\frac{\omega_{xy}}{\omega_z}\right)^2\frac{\tau}{\tau_D}\right)^{-\frac{1}{2}} \quad (2)$$

A three-dimensional Gaussian distribution of the detected fluorescence is assumed with radial and axial $1/e^2$ radii ω_{xy} and ω_z, respectively. N is the mean number of fluorescent molecules within the sample volume and τ_D is the translational diffusion time of the molecules across the sample volume, which is related to the translational diffusion coefficient D by:

$$D = \frac{\omega_{xy}^2}{4\tau_D} \quad (3)$$

The correlation function taking into account the variation in the diffusion coefficient and in the brightness of a dye due to a *chemical equilibrium reaction* has been described previously (Al-Soufi et al. 2005). The partition equilibrium between free and bound dye is treated as a reversible chemical reaction with (partition) binding equilibrium constant $K = k_+/k_-$ defined by the entry (association) (k_+) and exit (dissociation) (k_-) rate constants.

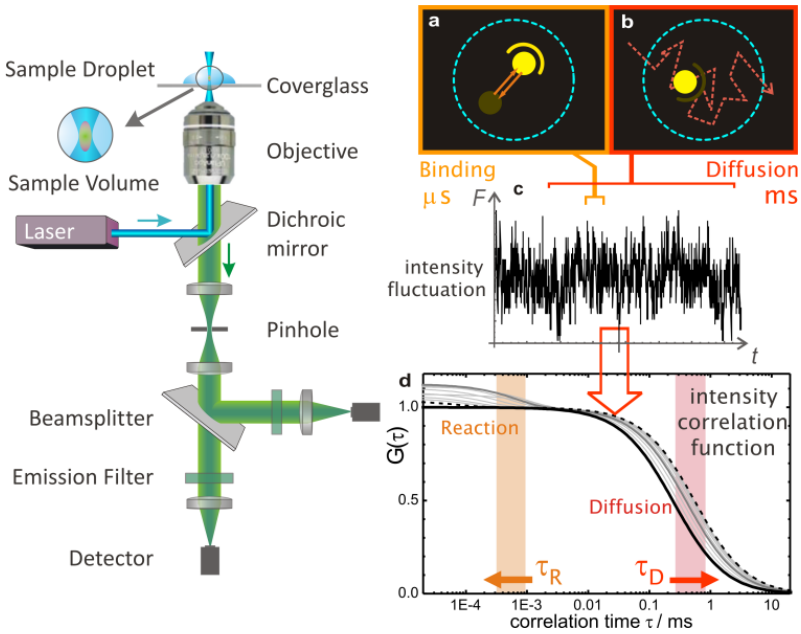

Figure 3. Principles of Fluorescence Correlation Spectroscopy. Left panel: epi-illuminated confocal microscope used to create a microscopic sample volume. Right panel: scheme of the data analysis. (a,b) The blue dashed circles indicate the border of the sample volume. The yellow dots represent dye molecules undergoing a reversible association (a), and moving randomly through the solution due to brownian motion (b). Detected fluorescence intensity (c), and autocorrelation function of the intensity fluctuations (d).

Under conditions where the host concentration [H] is always much higher than that of the dye, this concentration coincides with the initial host concentration $[H]_0$ ($[D_f] \ll [H] \approx [H]_0$), and the reaction is pseudo-first-order with the relaxation ("reaction") time τ_R given by:

$$\tau_R = (k_+[H]_0 + k_-)^{-1} \tag{4}$$

Applying the assumption that the relaxation time of the reaction is much shorter than the typical diffusion times of free, τ_f, and bound dye, τ_b, (i.e. fast exchange, $\tau_R \ll \tau_f, \tau_b$, the following correlation function for the diffusion and equilibrium reaction is obtained:

$$G_{DR}(\tau) = \frac{1}{N_f + N_b}\left(1 + \frac{\tau}{\bar{\tau}_D}\right)^{-1}\left(1 + \left(\frac{\omega_{xy}}{\omega_z}\right)^2 \frac{\tau}{\bar{\tau}_D}\right)^{-\frac{1}{2}}\left(1 + A_R\, e^{-\tau/\tau_R}\right) \tag{5}$$

where the diffusion term is defined by a mean diffusion time $\bar{\tau}_D$ and an amplitude that depends on the mean numbers N_f and N_b of free and bound dye molecules in the sample volume. The reaction term has a relative amplitude A_R and a correlation time given by the reaction time τ_R.

The parameters $\bar{\tau}_D$, τ_R, and A_R can be expressed directly as function of $[H]_0$ and K:

$$\bar{\tau}_D = \frac{\tau_f\,(1 + K\,[H]_0)}{1 + \frac{\tau_f}{\tau_b}\,K\,[H]_0} \tag{6}$$

$$\tau_R = \left(k_-(1 + K[H]_0)\right)^{-1} \tag{7}$$

$$A_R = \frac{N_f\,N_b(Q_f - Q_b)^2}{(Q_f\,N_f + Q_b\,N_b)^2} = \frac{K\,[H]_0(1-q)^2}{(1 + q\,K\,[H]_0)^2} \tag{8}$$

The reaction amplitude, A_R, depends on the brightness ratio $q = Q_b/Q_f$ of free and bound guest. The species-dependent brightness is defined by the product of the extinction coefficients, fluorescence quantum yield and detection efficiency $Q_X = \varepsilon_X\, \phi_{(F)X}\, g_X$.

4. Impact of Impurities in FCS.

The study of host-guest complexation (or protein-ligand interaction, DNA-binder aggregation or others) is among the most common applications of FCS. In a simple we need either the host or the guest to be fluorescent. On the contrary, we have to label one of them with a fluorophore.

FCS allows us to get values for the equilibrium constant and under certain conditions also the dynamic rate constants. To study these systems we typically perform titrations, getting several FCS curves at different concentrations of the unlabeled molecule (usually the host) while the concentration of the fluorescent molecule remains constant (usually the guest).

The type of complexes studied by FCS is evolving and biological systems such as DNA, proteins or membranes, are becoming more and more important. Also plenty of novel molecules are being synthesized to obtain new binders for these systems. In contrast to highly purified commercial products, many of these samples have a certain level of impurities that for different reasons can be difficult to avoid.

Even low levels of fluorescent impurities are going to have influence on the results obtained by FCS. The magnitude of this influence can be very different depending on each case. Many times it can affect certain parameters which are not relevant for our conclusions on the system. On the contrary, the influence of the impurities can also lead us to wrong conclusions from our experiment.

Here we will perform a detailed analysis of the influence of impurities on the values obtained for the fit parameters of the correlation curve. Using models and simulations, we will analyze the importance of impurities present in the sample on two of the more important parameters of the correlation curve: the *number of molecules* and the *diffusion correlation time*. If we are not aware of the presence of fluorescent impurities in our sample we can easily take apparent parameters of concentration or diffusion time of the fluorophore as the real ones, in spite being highly influenced by the signal of the impurity.

Knowing the extent of the influence of the impurities in our sample is particularly important in order not to misinterpret the changes in the different parameters of the correlation curve during a titration. We will apply the obtained models on experimental data from different systems under study in order to check whether the variations observed during the titration are due to the presence of impurities or can be in fact attributed to the host-guest interaction.

We will pay special attention to the interpretation of the non-expected increase in the apparent number of molecules, N, observed in titrations in which the concentration of fluorophore remains constant. In this case, we will study under which conditions this behavior could be attributed to a certain level of impurities either in the stock of host or guest. Note that very commonly we have only limited information about the sample: usually, we do know neither the concentration nor the brightness of the impurities and in many cases this also applies to the fluorophore itself.

4.1. Correlation Function of a Mixture.

Our model system contains two fluorescent species which contribute to the signal. The first is our fluorophore or labeled molecule under study (host or guest). The second represents the impurities, modeled as one homogeneous species.

In order to study the influence of the second species on the FCS correlation curves given by the correlation function G_{D}, we use the known model for two independent species in FCS (Krichevsky and Bonnet 2002). The correlation function for translational diffusion of two species is given by the correlation curves of the individual species weighted by the square of the contribution of each species to the total fluorescence intensity. The mean fluorescence intensity $N_{\mathrm{i}}\ Q_{\mathrm{i}}$, of each species is given by the average number of molecules in the sampling volume $N_{\mathrm{i}} = V\ C_{\mathrm{i}}$, and by the species dependent brightness Q_i, defined by the product of the extinction coefficients, fluorescence quantum yield and detection efficiency $Q_i = \varepsilon_i\ \phi_{(F)i}\ \mathrm{g}_i$.

$$G_D = \left(\frac{Q_1N_1}{Q_1N_1 + Q_2N_2}\right)^2 \frac{1}{N_1}\left(1+\frac{\tau}{\tau_1}\right)^{-1}\left(1+\frac{\tau}{\omega^2\tau_1}\right)^{-\frac{1}{2}} + \left(\frac{Q_2N_2}{Q_1N_1 + Q_2N_2}\right)^2 \frac{1}{N_2}\left(1+\frac{\tau}{\tau_2}\right)^{-1}\left(1+\frac{\tau}{\omega^2\tau_2}\right)^{-\frac{1}{2}} \qquad (9)$$

This expression can be immediately converted to the following form:

$$G_D(\tau) = \underbrace{\frac{Q_1^2N_1+Q_2^2N_2}{(Q_1N_1 + Q_2N_2)^2}}_{G_D(0)=1/N}\left[\underbrace{\frac{Q_1^2N_1}{Q_1^2N_1+Q_2^2N_2}}_{r}\left(1+\frac{\tau}{\tau_1}\right)^{-1}\left(1+\frac{\tau}{\omega^2\tau_1}\right)^{-\frac{1}{2}} + \underbrace{\frac{Q_2^2N_2}{Q_1^2N_1+Q_2^2N_2}}_{1-r}\left(1+\frac{\tau}{\tau_2}\right)^{-1}\left(1+\frac{\tau}{\omega^2\tau_2}\right)^{-\frac{1}{2}}\right] \qquad (10)$$

In the case of a single species the amplitude of the translational diffusion at time zero $G_{\mathrm{D}}(0)$ gives the inverse of the mean number of molecules in the sample volume N. In the case of a mixture the amplitude $G_{\mathrm{D}}(0)$ depends also on the brightness of each species. In this case N is only an apparent number of molecules that can be very different from the real values:

$$G_D(\tau = 0) = \frac{Q_1^2N_1+Q_2^2N_2}{(Q_1N_1 + Q_2N_2)^2} = \frac{1}{N} \qquad (11)$$

The individual factors in the former expression for G_D are the relative contributions of each (normalized) diffusion term to the full term:

$$r = \frac{Q_1^2 N_1}{Q_1^2 N_1 + Q_2^2 N_2} \qquad (1-r) = \frac{Q_2^2 N_2}{Q_1^2 N_1 + Q_2^2 N_2} \tag{12}$$

With all this we can write an abbreviated form of G_D, which is useful as fitting function:

$$G_D(\tau) = \frac{1}{N}\left(r\left(1+\frac{\tau}{\tau_1}\right)^{-1}\left(1+\left(\frac{\omega_{xy}}{\omega_z}\right)^2\frac{\tau}{\tau_1}\right)^{-\frac{1}{2}} + (1-r)\left(1+\frac{\tau}{\tau_2}\right)^{-1}\left(1+\left(\frac{\omega_{xy}}{\omega_z}\right)^2\frac{\tau}{\tau_2}\right)^{-\frac{1}{2}}\right) \tag{13}$$

Here $\tau_i = \omega_{xy}^2/(4D_i)$ is the diffusion time of the species i across the sampling volume $V = \pi^{3/2}\,\omega_{xy}^2\,\omega_z$ with aspect ratio $\omega = \omega_z/\omega_{xy}$. D_i is the diffusion coefficient of the species i. N is the apparent number of molecules:

$$\frac{1}{N} = \frac{Q_1^2 N_1 + Q_2^2 N_2}{(Q_1 N_1 + Q_2 N_2)^2} \tag{14}$$

4.2. Apparent Number of Molecules.

4.2.1. Theory.

In this work, we will analyze the apparent number of molecules, N, under different conditions of the brightness and the real number of molecules of the two species: the fluorophore (species 1), and the impurity (species 2). As it was said before, in general we do know neither the concentration (N_1, N_2) nor the brightness (Q_1, Q_2) of the fluorophore or the impurities.

We define the following ratios between impurity and fluorophore:

Brightness ratio:

$$f_Q = \frac{Q_2}{Q_1} \tag{15}$$

Number ratio:

$$f_N = \frac{N_2}{N_1} \tag{16}$$

Intensity ratio:

$$f_I = \frac{I_2}{I_1} = \frac{Q_2 N_2}{Q_1 N_1} = f_Q\ f_N \tag{17}$$

Using these ratios and equation 11 we can rewrite the expressions for the apparent number of molecules N with the following *error ratios*, expressing the *apparent* number of molecules, N, in terms of the *real* numbers N_1 and N_2.

$$N = N_1 \frac{\left(1 + f_Q\, f_N\right)^2}{1 + {f_Q}^2 f_N} \tag{18}$$

Ratio between apparent concentration and real fluorophore concentration:

$$\frac{N}{N_1} = \frac{(1 + f_I)^2}{1 + f_Q f_I} = \frac{\left(1 + f_Q\, f_N\right)^2}{1 + {f_Q}^2 f_N} \tag{19}$$

Ratio between apparent and total concentration:

$$\frac{N}{N_1 + N_2} = \frac{(f_I + 1)^2}{\left(1 + f_Q\, f_I\right)\left(f_I/f_Q + 1\right)} \tag{20}$$

Analyzing equation 19, we find that as long as the impurities are in higher number than the fluorophore, $f_N > 1$, the apparent number of molecules, N, will be always bigger than the real number of fluorophores, N_1. On the other hand, only at low concentration ($f_N < 1$) and under certain conditions a bright impurity ($f_Q > 2/(1–f_N) \approx 2$) can lead to a decrease of N.

For a fixed contribution of the impurity to the fluorescence signal, that is at constant f_I, we observe that the smaller the value of f_Q the bigger the ratio N/N_1, i. e. a higher number of less bright molecules of impurity have a bigger influence on the apparent number of molecules than fewer bright particles, at least as long as $f_Q < 1$. In the limit, when f_Q tends to *zero* ($Q_2 \ll Q_1$), we reach the situation of a very large number of molecules with very low brightness, which can be used to model the influence of the light scattered by the solvent:

$$\frac{N}{N_1}\left(f_Q \to 0\right) = (1 + f_I)^2 \tag{21}$$

This expression is equivalent to that given in the literature for the ratio between the apparent number of molecules and the number of particles calculated after correction for the influence of the uncorrelated background signal (Ruettinger et al. 2008).

$$\frac{N}{N_1} = \frac{\left(\frac{I_{\text{background}}}{I_1} + 1\right)^2}{1} \tag{22}$$

In this case, the intensity of the signal due to the solvent, $I_{\text{background}}$, would be I_2 following the notation used in this work.

According to this equation, the influence of the scattered light on the apparent number of molecules will depend on its contribution to the total intensity. It will follow the same model as the case of a fluorescent impurity when its brightness is much smaller than that of the main fluorophore, $f_Q = Q_2/Q_1 \ll 1$.

4.2.2. Simulations.

It is our aim to analyze how the apparent number of molecules, N, depends on the brightness and intensity ratios between impurity and fluorophore, f_Q and f_I respectively.

Figure 4 shows the influence of a fluorescent impurity (species 2) on the ratio N/N_1 between the apparent number of molecules and the number of molecules of the species 1. This representation is particularly instructive, since when we are not taking the impurities into account we will be taking what actually is an apparent number of molecules, N, as the number of molecules of fluorophore, N_1.

The bigger the contribution of the impurity (species 2) to the total signal, the bigger the ratio f_I, and the bigger the error ratio N/N_1. The apparent number of molecules increases nonlinearly with increasing ratio f_I.

At a given intensity ratio f_I, the error ratio N/N_1 also increases when the brightness ratio, f_Q, decreases, i. e. when the brightness of the impurity becomes smaller in relation to the brightness of the fluorophore but its number, f_N, increases. We can see this when we compare the values of N/N_1 simulated at different f_Q ratios) at the same fixed f_I in Figure 4. As an example, we can take the case in which the contribution of impurities represents a fraction, $f_I/(f_I + 1)$, of 33% of the total signal ($f_I = 0.5$). When fluorophore and impurity have the same brightness ($f_Q = 1$, blue line), the apparent number of molecules is 1.5-fold the number of molecules of fluorophore, $N/N_1 = 1.5$. When the impurity is 100-fold less bright than the fluorophore, $f_Q = 0.01$ (black line), then the ratio N/N_1 goes up to 2.2.

A lower f_Q at fixed f_I means a higher number of molecules of impurities. So we can state that, for the same contribution to the total intensity signal, the impurities have a bigger effect in N when there is a higher number of less bright molecules of impurities in comparison to the case with a lower number of brighter impurity molecules.

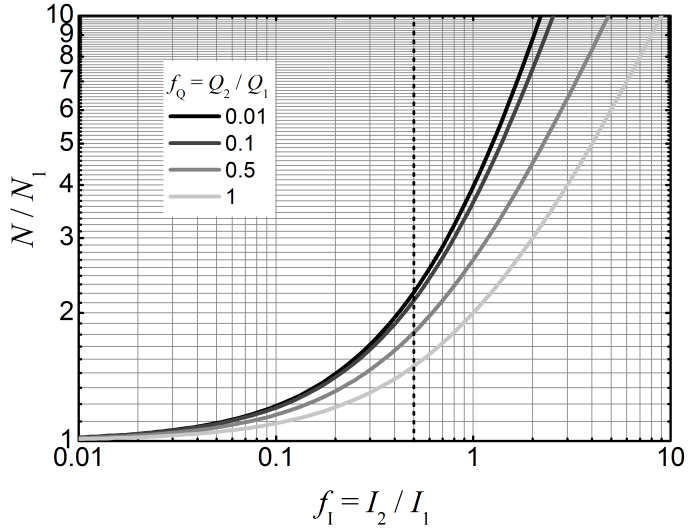

Figure 4. Simulation of the ratio N/N_1 versus the intensity ratio, f_I, at different brightness ratios, f_Q. The black curve is very close to the limit when f_Q tends to *zero*. Dashed vertical line at $f_I = 0.5$ (fraction 33%).

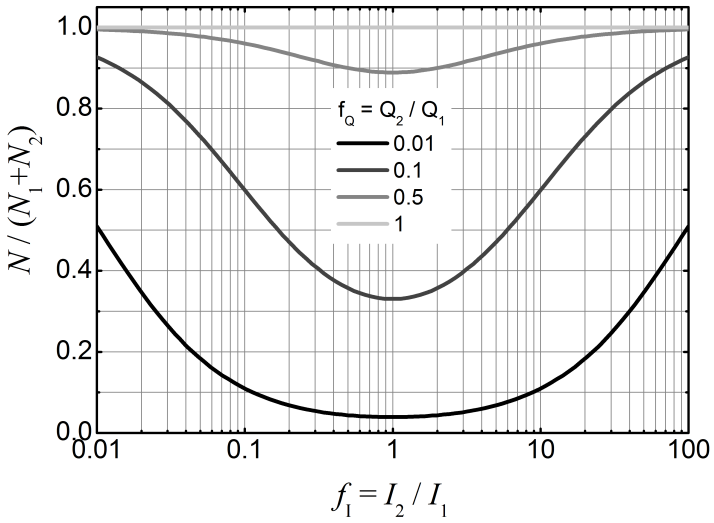

Figure 5. Simulation of the ratio $N/(N_1 + N_2)$ versus the intensity ratio, at different brightness ratios. N is the apparent number of molecules, and $N_1 + N_2$ is the real number of molecules.

When f_Q is very low, the error ratio N/N_1 becomes independent on f_Q, and the curves N/N_1 vs. f_I will then be showing the influence of the background (solvent contribution to the signal) on the apparent number of molecules, N.

Figure 5 shows the relation between the apparent number of molecules, N, and the real total number of molecules, N_1+N_2. The apparent number of molecules is equal to the total number of molecules only when the brightness of the two species are the same, in any other case N will always be *smaller* than the sum of the molecules of the species 1 and 2, N_1+N_2. The more different the brightnesses of impurity and fluorophore are, the smaller is the apparent number of molecules in relation to the real number of molecules (compare curves for $f_Q = 0.5$, green; and $f_Q = 0.01$, black, in Figure 5). Regarding to their contribution to the signal, the more similar are the values of the intensity coming from the fluorophore and from the impurity (the closer f_I is to 1), the bigger will be the decrease in the apparent number of molecules (note how the curves reach their minimum at $f_I = 1$, in Figure 5).

4.2.3. Effect of the impurities during a titration.

FCS is very often used to study host-guest association systems. Commonly there is a fluorophore or labeled molecule (guest) which forms a complex with a supramolecular system which acts as a host (micelles, cyclodextrins, DNA, etc.). A typical strategy is to perform a titration measuring fluorescence correlation curves for samples at a fixed concentration of fluorophore (guest, G) and different concentrations of host, H.

$$\mathrm{H} + \mathrm{G} \underset{}{\overset{K}{\rightleftharpoons}} \mathrm{HG}$$

In this kind of experiments, the increase in the mean diffusion coefficient is analyzed in order to determine the equilibrium constant K of the system. As long as the host is not fluorescent and there is only one guest per complex, as it occurs in the typical scenario of a 1:1 complexation, the number of fluorescent molecules should remain constant.

However, even under these conditions a variation in the apparent number of molecules can be observed during the titration, which is due to the impurities present in the system. As we will show in the following, it is necessary to take into account the influence of the impurities in order to obtain a correct estimate for the equilibrium constant K.

We propose two simple models that would explain variations in N among the different samples of a titration (Figure 6). In the first model we consider that the impurity is only present in the stock of the guest (Model A), whereas in the second model we consider that the impurity is only found in the stock of the host (Model B).

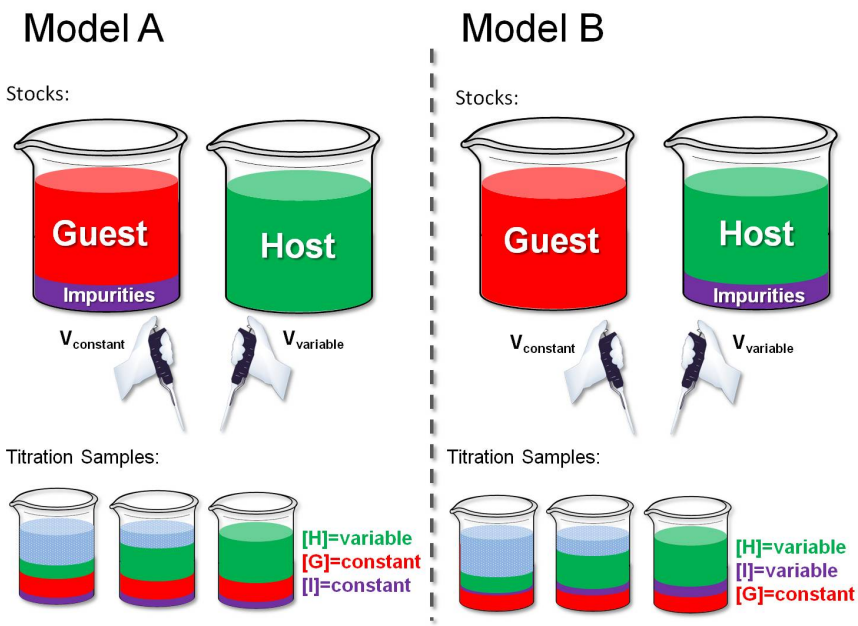

Figure 6. Scheme of the two models which consider the presence of impurities in the stock of guest (Model A) or in the stock of host (Model B) during a titration.

Model A: Impurity in the stock of the fluorophore (guest).

This model assumes that the concentrations of both, impurity and fluorophore, remain constant throughout the titration (f_N, N_1, N_2 constant). Note that always that we have an impurity responsible for part of the intensity of the detected signal, the apparent number of molecules, N, will be different to the number of molecules of the fluorophore, N_1. However, as long as f_N stays constant, then the apparent number of the molecules will not change during the titration, unless either the brightness of the fluorophore or the brightness of the impurity changes, (eq. 19).

According to this, a variation in N observed during the titration can be explained by considering a change in the brightness ratio, f_Q depending on the concentration of host, according to the chemical equilibrium. This can happen when the interaction between host and guest affects its brightness. Alternatively, an interaction between the impurity and the host could also be considered. As long as this interaction affects the brightness of the impurity this would also lead to a change in the brightness ratio, f_Q, in this case due to a change in the brightness of the impurity instead of the guest. However we consider this possibility much more unlikely to happen and will focus on changes of the brightness of the guest with the brightness of the impurities remaining constant (Q_2 constant).

Following a 1:1 equilibrium the guest would change between free and bound states. We consider two different values for the brightness of the guest: $Q_{1,f}$ which refers to the brightness of the free guest and $Q_{1,b}$ which refers to the brightness of the guest bound to the host. The brightness of the guest can be expressed as the weighted average of these two values, being X_f and X_b the molar fractions of free and bound guest, respectively (this is justified as long as the exchange between the two states is much faster than the diffusion time, which is the case in the systems we studied):

$$Q_1 = Q_{1,f}\, X_f + Q_{1,b}\, X_b \tag{23}$$

We can rewrite the equation 23 taking the molar fractions as a function of the equilibrium constant, K, and the host concentration [H] (eq. 24 to 26).

$$K = \frac{[HG]}{[G][H]} \tag{24}$$

$$K[H] = \frac{X_b}{X_f} \tag{25}$$

$$Q_1 = Q_{1,f}\left(\frac{1 + \left(Q_{1,b}/Q_{1,f}\right) K\,[H]}{1 + K[H]}\right) \tag{26}$$

The brightness ratio, f_Q, will then depend on the brightness ratio in absence of host, $f_{Q,0}$, the equilibrium constant, K, the host concentration and the ratio between the brightness of bound and free guest, q.

$$q = \frac{Q_{1,b}}{Q_{1,f}} \tag{27}$$

$$Q_1 = Q_{1,f} \cdot \left(\frac{1 + q\,K\,[H]}{1 + K\,[H]}\right) \tag{28}$$

$$f_{Q,0} = \frac{Q_2}{Q_{1,f}} \tag{29}$$

$$f_Q = \frac{Q_2}{Q_1} = f_{Q,0}\left(\frac{1 + K\,[H]}{1 + q\,K\,[H]}\right) \tag{30}$$

The ratio between the brightness of bound and free guest, q, will give the maximum change in the brightness ratio, which varies with host concentration vary from $f_Q = f_{Q,0}$, at $[H] = 0$, to $f_Q = f_{Q,\infty}$ at saturated concentrations of host ($[H] = \infty$).

$$f_{\mathrm{Q}}([\mathrm{H}]=\infty) \;=\; f_{\mathrm{Q},\infty} = \; f_{\mathrm{Q},0}\left(\frac{1}{q}\right) \tag{31}$$

$$q = \frac{f_{\mathrm{Q},0}}{f_{\mathrm{Q},\infty}} \tag{32}$$

In order to obtain a model for the change in the apparent number of molecules, we include this dependence of the brightness ratio on the concentration of host and the equilibrium constant K *(*eq. 30) in the equation 19:

$$\frac{N}{N_1} = \frac{\left(f_{\mathrm{Q},0}\, f_{\mathrm{N}}\left(\frac{1+K[\mathrm{H}]}{1+qK[\mathrm{H}]}\right)+1\right)^2}{{f_{\mathrm{Q},0}}^2 f_{\mathrm{N}}\left(\frac{1+K[\mathrm{H}]}{1+qK[\mathrm{H}]}\right)^2+1} \tag{33}$$

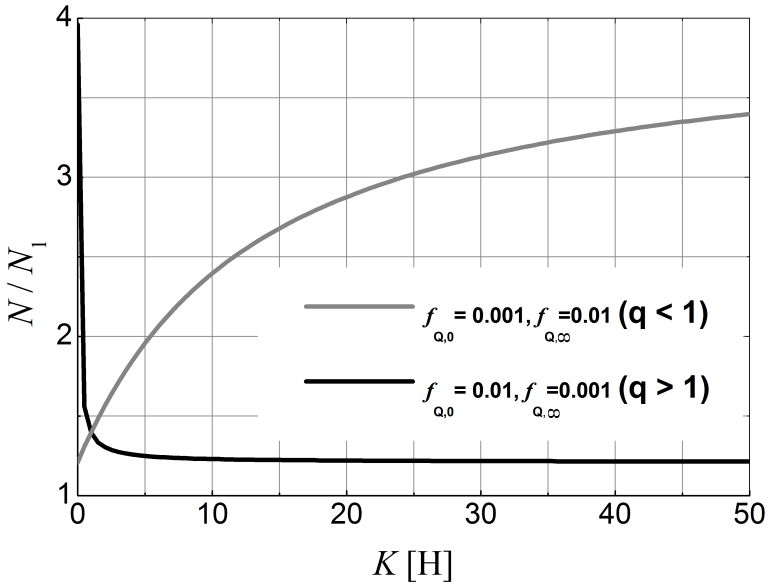

Figure 7. Simulation of the ratio between the apparent number of molecules, N, and the number of molecules of the species 1, N_1, versus the product K [H], at two different conditions of the brightness ratio, f_{Q}. In the black curve, f_{Q} changes from 0.01 to 0.001 ($q = 10$). In the grey curve, f_{Q} changes from 0.001 to 0.01 ($q = 0.1$). f_{N} was set to a value of 100 for both simulations.

Plotting the ratio N/N_1 against the product K [H] we obtain Figure 7. The curves show the behavior for two different situations an increase and a decrease in the brightness ratio, f_{Q}, with the concentration of host ($q < 1$ and $q > 1$ respectively). When the brightness of the guest increases as a result of the added host ($q > 1$, *black curve)* the ratio N/N_1 decreases from its initial value at [H] = 0. On the contrary, when the guest is less bright in the bound

state ($q < 1$, *grey curve)* the error ratio N/N_1 increases with concentration of host. In both cases, the N/N_1 tends towards a final value at saturated concentrations of host. However, for the case in which $q = 10$ the variation in f_Q happens at lower concentrations of host than for the case of $q = 0.1$. It shows how a small fraction of molecules of guest in the brighter state are enough to cause a significant decrease of the influence of impurities. At the same time we see how it needs a much higher concentration of host to increase the apparent number of molecules close to the saturation level in the case of a less bright bound state ($q < 1$).

In this model, N reaches a limit given by a saturation of the equilibrium which leads to the change in brightness of the guest. This limit will depend on the ratio of molecules, f_N, and the brightness ratio, q.

$$\frac{N_\infty}{N_0} = \frac{\left(f_{Q,0}{}^2 f_N + 1\right)\left(f_{Q,\infty} f_N + 1\right)^2}{\left(f_{Q,\infty}{}^2 f_N + 1\right)\left(f_{Q,0} f_N + 1\right)^2} \tag{34}$$

Using equation 33, the apparent number of molecules can be calculated at the value without host, N_0, and after adding enough host to saturate the equilibrium, N_∞. The ratio between these two values of N is given by the equation 34. This expression allows one to calculate which conditions of f_N and q, would be necessary according to this model to explain a change in N, from an initial value without host, N_0, to a final value, N_∞, after having the equilibrium saturated (see simulation in Figure 8).

As an example, we can see in Figure 8 the following situation: in order to explain a 3-fold increase in the apparent number of molecules due to the interaction between guest and host assuming a 10-fold decrease in the guest brightness upon complexation ($q = 0.1$) we should have a number ratio between impurity and guest, f_N, of 10. Assuming a 100-fold decrease in the guest brightness upon complexation ($q = 0.01$), the number ratio, f_N, should be 2 for the same change in the apparent number to be explained assuming impurities in the stock of guest.

If we want to explain an observed decrease in the apparent number of molecules upon addition of host at saturating concentrations of for example $N_\infty/N_0 = 0.3$, assuming a 100-fold more concentrated impurity in relation to the guest, it will require an increase for the guest brightness of 10-fold from the free to the bound state. Although we use the general term *impurity* here, this would also include those very low fluorescent molecules present in typical dirty samples of guest. Note that when working at single-molecule concentrations of fluorophore, it is not strange for some impurities to be in much higher concentration than the main fluorophore.

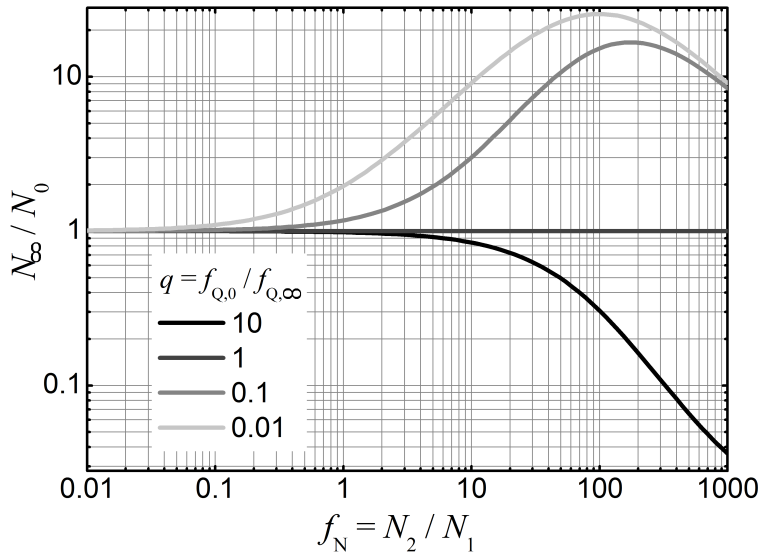

Figure 8. Simulation of the ratio between the apparent number of molecules at infinite host concentration, N_∞, and without host, N_0, for different brightness ratios between both species 1 and 2. The initial ratio of brightness, $f_{Q,0}$, is 0.01 in all cases.

As a conclusion, we can summarize a brief protocol to evaluate the possibility of explaining an observed change in the apparent number of molecules through the presence of impurities in the stock of guest. The first step would be to check the conditions under which this model applies, mainly the absence of impurities in the stock of host. Then, as a first approach we can calculate (eq. 34 or use Figure 8 to extract which pairs of parameters, q and f_N, would explain the change observed experimentally. Here we can fix the value of q if we know from previous studies the change expected in the brightness of the guest when it binds the host. Finally, we would fit the model (eq. 33) to the experimental data and observe whether it is capable of explaining the variation in N, as well as if the value of the equilibrium constant, K, for the interaction between host and guest makes sense.

Model B: Impurity in the stock of host.

This model assumes that the impurity is in the stock of host, so that its concentration will be proportional to the concentration of host in each sample.

In this case, even if we do not consider a change in the brightness ratio with the concentration of host, the apparent number of molecules, N, will change because the number ratio f_N and the intensity ratio f_I do depend on the concentration of impurities and thus on the amount of host stock added (see Figure 6) according the following equation:

$$f_{\mathrm{N}} = \frac{N_2}{N_1} = \left(\left(\frac{n_{\mathrm{imp}}}{n_{\mathrm{H}}} \right)_{\mathrm{stock}} \frac{1}{[\mathrm{G}]} \right) [\mathrm{H}] = \alpha [\mathrm{H}] \tag{35}$$

The parameter α depends on the concentration of the fluorophore and the ratio between the concentrations of impurity and host in the stock. Using this expression for the number ratio in equation 19, we get the error ratio N/N_1 as a function of the brightness ratio, f_{Q}, the parameter α, and the concentration of host, [H]:

$$\frac{N}{N_1} = \frac{\left(f_{\mathrm{Q}} [\mathrm{H}] \alpha + 1 \right)^2}{{f_{\mathrm{Q}}}^2 [\mathrm{H}] \alpha + 1} \tag{36}$$

$$\frac{N}{N_1} = \frac{\left(f_{\mathrm{Q},0} [\mathrm{H}] \alpha \left(\frac{1 + K[\mathrm{H}]}{1 + qK[\mathrm{H}]} \right) + 1 \right)^2}{f_{\mathrm{Q},0}^2 [\mathrm{H}] \alpha \left(\frac{1 + K[\mathrm{H}]}{1 + qK[\mathrm{H}]} \right)^2 + 1} \tag{37}$$

As we can see for the black and red curves in Figure 9 the influence of the impurities on N is almost linear with the concentration of impurities or host. As could be expected, the increase in the apparent number is much bigger for the case of bright impurities (black line).

Similarly to the model A, we can also consider a dependence of the brightness ratio on the host concentration and an equilibrium constant, K. The variation in the apparent number of molecules N will now follow a curve during the titration (see Figure 9) given by equation 37.

With data of the signal intensity for host and guest separately we can establish a relation between f_{Q} and α, using the intensity signal of the impurities in the host stock (I_{imp}), the intensity signal of the guest in absence of host ($I_{1,0}$), and the concentration of the host stock, $[\mathrm{H}]_{\mathrm{stock}}$:

$$\frac{I_{\mathrm{imp}}}{I_{1,0}} = \frac{n_{\mathrm{imp}} Q_2}{n_1 Q_{1,0}} = \frac{n_{\mathrm{imp}}}{n_1} f_{\mathrm{Q},0} = \alpha [\mathrm{H}]_{\mathrm{stock}} f_{\mathrm{Q},0} \tag{38}$$

Using eq. 38, we can replace parameter α in eq. 37 to obtain equation 39.

$$\frac{N}{N_1} = \frac{\left(f_{Q,0} \frac{[\mathrm{H}]}{[\mathrm{H}]_{stock}} \frac{I_{\mathrm{imp}}}{I_{1,0}} \left(\frac{1 + K[\mathrm{H}]}{1 + qK[\mathrm{H}]} \right) + 1 \right)^2}{f_{Q,0}^2 \frac{[\mathrm{H}]}{[\mathrm{H}]_{stock}} \frac{I_{\mathrm{imp}}}{I_{1,0}} \left(\frac{1 + K[\mathrm{H}]}{1 + qK[\mathrm{H}]} \right)^2 + 1} \tag{39}$$

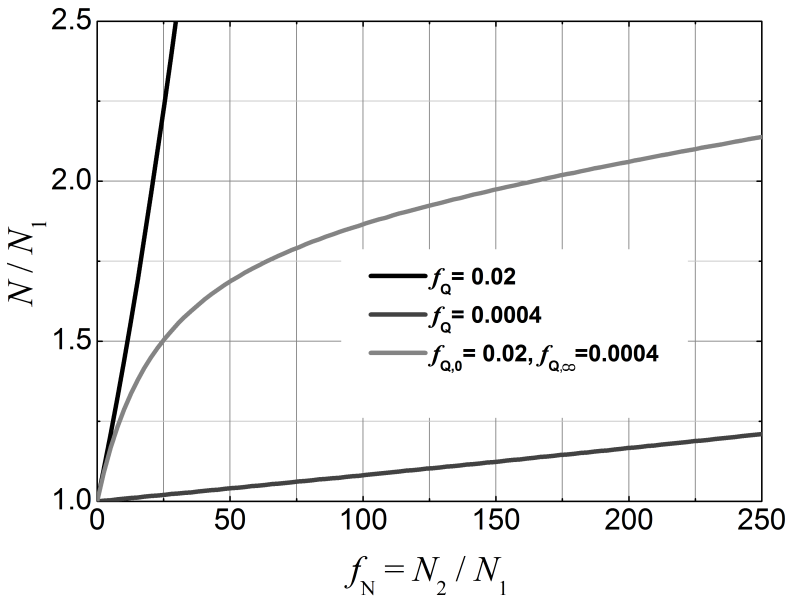

Figure 9. Simulation of the ratio between the apparent number of molecules, N, and the number of molecules of species 1, N_1, versus the number ratio, f_N, at three different conditions of the brightness ratio, f_Q. In the top and bottom curves, f_Q is constant at 0.02 and 0.0004 respectively. In the middle curve f_Q changes from 0.02 to 0.0004 according to an equilibrium, which depends on the concentration of host.

We can conclude that the presence of impurities in the stock of *host* can also increase the apparent number of molecules. This case is much easier to quantify since there is the possibility of performing independent measurements of the host in absence of guest that will allow one to quantify the amount and the brightness of the impurities. In contrast to the impurities in the stock of guest, when the impurity is in the stock of host the apparent number of molecules will always increase with the host concentration. The presence of impurities in the stock of host will increase the error factor N/N_1 almost linearly with the host concentration or the number ratio, f_N. Additionally to the presence of impurities in the stock of host it can also happen that the brightness of the guest depends on the complexation equilibrium. In this case the plot of the error ratio N/N_1 versus [H] or f_N, will be curved (green curve, Figure 9). This curve will be similar to those obtained with model A (impurities in the stock of guest) with $q < 1$, but with a remarkable difference: in this case the curvature also disappears when the equilibrium saturates, however, the error ratio will keep increasing linearly after that due to the addition of more and more impurities.

4.2.4. Experiments.

We will analyze experimental data in order to verify the two-species model for the correlation curve. Also, using the equations deduced before, we will check whether the variations in N for some experiments can be explained by the presence of impurities in the samples.

Checking the two independent species model using fluorescent beads.

Here we will use two types of fluorescent beads with different size (G25: 25 nm and G100: 100 nm) and different brightness in order to verify equations 19 and 40. As a simulation of a real system, the larger and brighter G100 particles would represent the fluorophore (species 1), whereas G25 beads, less bright and in higher number, would represent the impurity (species 2), see Table 1.

Table 1. Fluorescence intensity (I), number of molecules (N) and brightness ($Q = I/N$) for the samples of G100 beads, G25 beads and the mixture (G25+G100) determined from fits to the correlation curves shown in Figure 10. Estimated and experimental values of the parameter r and the ratio $N_{1/}N$ for the sample with both species.

Sample	I /kHz	N	$Q = I/N$
G100 (species 1)	11.5	0.092 ± 0.001	126
G25 (species 2)	14.0	3.54 ± 0.01	3.96
G25 + G100 (1+2)	24.5	0.377 ± 0.001	65.1
r (simulation)	**r (fit)**	**N_1/N (simulation)**	**N_1/N (fit)**
0.96	0.97 ± 0.01	0.21	0.24 ± 0.01

We measured the correlation curves for both types of beads separately, and then for a third sample which is a mixture of both species, with each concentration equal to that of the separate solution (Figure 10). The parameters obtained from the fit to the correlation curve for the sample with both species are compared with those estimated according to the model using the parameters from the fits to the correlation curves of both species measured separately (Table 1).

From the fits to the correlation curves of the pure G25 and G100 samples we get the number of molecules for each species (N_1 and N_2), the signal intensity (I_1 and I_2) and the brightness (Q_1 and Q_2).

Using the equations 19 and 40, we can predict the apparent number of molecules, N, and the parameter r for the third sample where both types of beads are mixed.

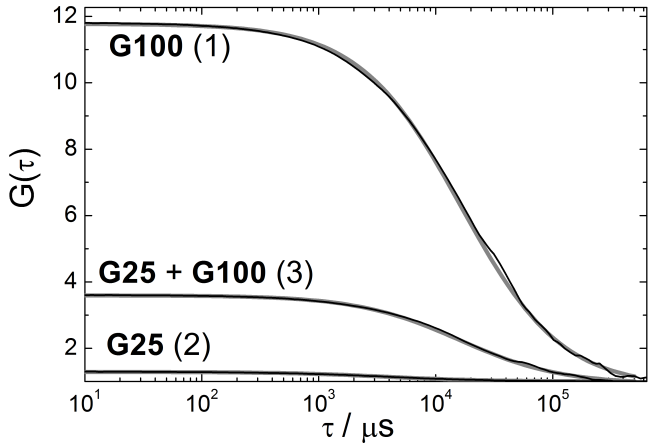

Figure 10. Experimental (black) and fitted (grey) correlation curves for the samples of G100 beads (1), G25 beads (2) and a mixture of G25 and G100 (3). One species model was used for samples 1 and 2, while the two species model (eq. 13) was used for the mixture.

According to the values in Table 1 for the samples 1 and 2, we predict an increase in the number of molecules of almost 5-fold with respect to the number in sample 1, $N/N_1 = 4.8$, after we mix the G100 and G25 beads keeping the concentration of samples 1 and 2. However, the predicted r shows that the influence of the G100 beads on the diffusion term is 0.96, very close to 1, which indicates that G25 beads will barely have influence on the diffusion correlation time.

These results of the simulations show very good match with the parameters obtained experimentally of 4.2 for N/N_1 and 0.97 for r, proving that the model works satisfactorily.

This experiment also illustrates the influence of typical impurities in FCS. A very important impurity contribution to the intensity signal (57% in this example) can affect drastically the apparent number of molecules (in this case N is more than 4-fold the number or molecules of the G100 beads, which would represent the species of interest). However, the diffusion term is barely affected by the G25 beads - that is because the G100 beads are much brighter than the G25 beads, $Q_1/Q_2 = 32$ (in the same way as the fluorophore is normally much brighter than the impurity). Therefore, we can conclude that as long as the brightness of our fluorophore is much higher than the brightness of the impurity over the whole range of concentrations in the titration, we can get very accurate values for the diffusion time of the fluorophore even at high levels of impurity (in this example, the G25 beads contribute more than half the intensity). We should, however, take into account that the apparent number of molecules can be strongly affected.

Checking the model for scattered light.

In a FCS signal, there is always a certain level of background intensity due to scattered light by the solvent. The scattered light can reach important contributions, depending on the type of buffer, the use of some biological samples, or due to a low brightness of the fluorophore. We can easily estimate this contribution of the scattered light by measuring the solvent or buffer before adding the fluorophore.

As we saw in section 3.1.1, the influence of scattered light on the apparent number of molecules, N, can be modeled as an impurity, with very high concentration but very low brightness.

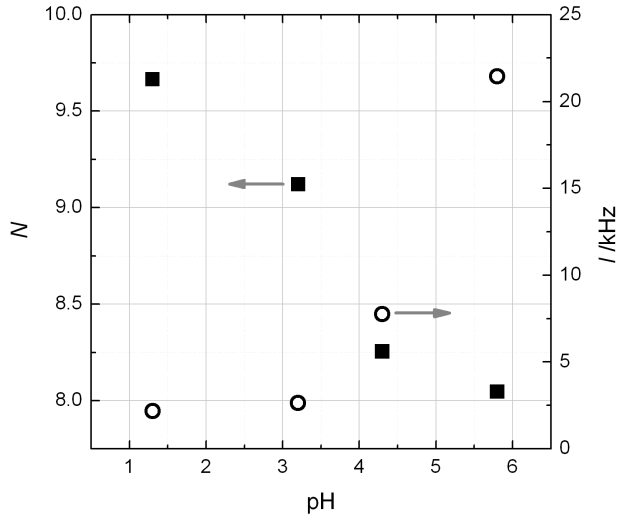

Figure 11. Solid squares (left Y-axis scale): Values of the apparent number of molecules, N, obtained from the fit of the FCS correlation curves when measuring OG488 at a fixed concentration and different pHs. Open circles (right Y-axis scale): Mean count rate, I, for the FCS measurements of the OG488 at different pHs.

We perform an experiment to check the model with scattered light by measuring the fluorophore Oregon Green 488 (OG488) at different pHs. The brightness of this fluorophore is very sensitive to pH, showing a strong increase around its pKa of ~ 4.7. This allows us to change the brightness of the fluorophore without affecting the number of molecules, N_1. Changing the pH, the intensity coming from scattered light is always the same, but its contribution with respect to the total signal changes because of the change in the OG488 brightness with pH.

When we measure correlation curves for the OG488 at different pHs (see Figure 11), the intensity signal (right scale, circles) is observed to increase with the pH in the range from 1 to 6, whereas the apparent number of molecules (left scale, squares) decreases.

We fitted the two functions for the variation in the apparent number of molecules, N, to the experimental data, assuming a second fluorescent species (equation 19) and the scattered light (equation 22, Figure 12).

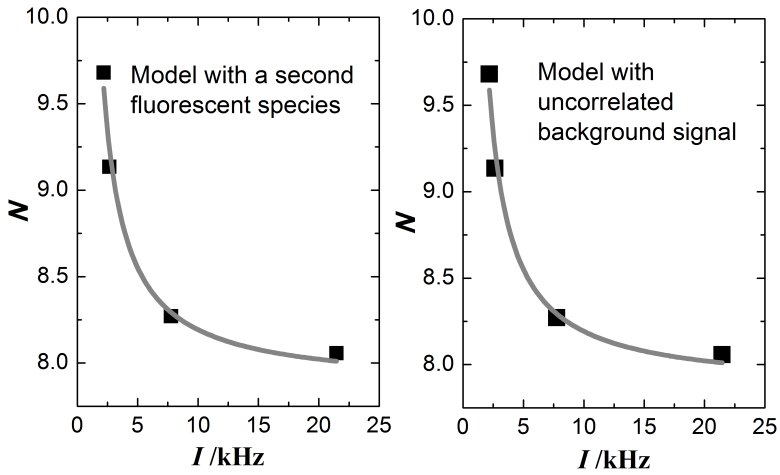

Figure 12. Scatter: Values of the apparent number of molecules, N, obtained from the fit of the FCS correlation curves when measuring OG488 at a fixed concentration and different pHs versus the mean count rate, I. (Note: brightness of the OG488 increases when increasing the pH, see Figure 11). Lines: Curves obtained by fitting the equations for the model which describes the influence on N by a second species (eq. 19), (left), and that one simplified when the second contribution comes from uncorrelated background signal (eq. 22) (right) which models the scattered light.

Both functions can describe satisfactorily the variation observed in the experimental data. Using the model for a second fluorescent species, we get a very high value for the ratio N_2/N_1 (see Table 2) — condition under which both functions become equivalent, confirming that the observed effect in the number of molecules is caused by the increase in the contribution of the scattered light when the brightness of the fluorophore is reduced by the decrease in pH.

Table 2. Values of the number of OG488 molecules, N_1, the intensity of the second species or background signal (I_2), and ratio N_2/N_1 for the fits represented in Figure 12.

Model	N_1	I_2 ($I_{background}$) /kHz	$f_N = N_2/N_1$
second species	7.9	0.21	10^{19}
uncorrelated background signal	7.9	0.21	-

As a result of this analysis we get interesting information, such as the real number of OG488 molecules, N_1, which is 7.9. Logically, this value is very close to the apparent number of molecules in those samples in which the brightness of the OG488 is higher (pH = 5.8). In contrast, at pH = 1.3 the increase in the apparent number of molecules in comparison with the real one is more than 20%.

We also obtain a value for the intensity of the scattered light, which is 0.21 kHz, representing a 1% of the signal at pH = 5.8, but almost a 10% at pH = 1.3.

4.2.5. Variations in the number of molecules during titrations.

In order to study many complexation systems by FCS we perform titrations, in which the concentration of the labeled molecule remains constant at a low value (single-molecule regime) to measure several samples at different concentrations of the second species (typically the host, when we are studying host-guest systems).

When we study this kind of systems in FCS, a common manifestation of the presence of impurities is the change in the apparent number of molecules during the titration, when it should remain constant. In such a case, it becomes necessary to analyze the variation in the apparent number of molecules to determine whether it can be attributed to impurities present in the stocks of host or guest.

Impurities in the interaction between a Surfactant and a fluorophore. (Triton X-100/Coumarine 152).

Here we study the influence of impurities in an additive, such as a surfactant, on the apparent number of molecules of fluorescent guest. Surfactants are difficult to purify and, given their high concentrations in the milli-molar range in a typical solution, even a very small fraction of impurities can be comparable in concentration to that of the guest. The guest in this complexation is the dye Coumarine 152 (C152) and micelles of the surfactant Triton X-100 (TX100) act as a host.

The concentration of C152 is kept constant, so that the number of molecules should not change when we add surfactant. In Figure 13 we show the data for a preliminary titration for this system, where we observe an unexpected increase in the number of molecules. In separate measurements of the surfactant we detected a small fluorescent signal. This makes it necessary to check whether the impurities in the TX100 solutions can explain the behavior in the apparent number of molecules.

We try to fit the two models proposed before (see section 4.2.3.): model A which assumes fluorescent impurities in the stock of fluorophore, and model B which considers the impurities are in the stock of host, in this case, the surfactant TX100. By trying to fit model B using equation 37 we will check whether the intensity of the signal measured in samples of TX100 without C152 can be responsible for the observed increase in the number of molecules. The fit of model A to the experimental data will show us which characteristics should have an impurity present in the stock of C152 to explain the variation in N.

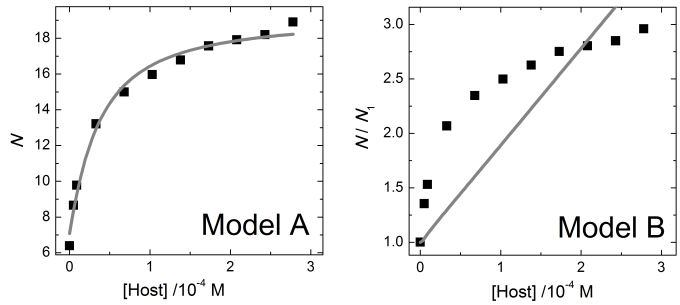

Figure 13. Scatter: Different values of the apparent number of molecules, N, obtained from the fit of the FCS correlation curve when measuring different concentrations of surfactant TX100 at a fixed concentration of Coumarine 152 (Note: data are the same in both graphs, however for the fit of Model B we use ratio N/N_1 instead of the absolute N value because in that case we know the value of N_1 from the sample without TX100). Lines: Curves obtained by fitting the equations for the models A (left) and B (right) described before, to the scatter points. Fit-parameters are in both cases highly correlated and their values are discussed in the text.

Although both models can explain the variation in the experimental data when we leave all the fitting parameters free, we must fix those about which we have some information. In this case, we know that C152 increases its brightness upon binding the TX100 micelles, so q was fixed in a value of 4 (see Chapter III). Model B is unable to successfully fit the data with the other fit-parameters fully correlated, whereas Model A can describe pretty well the variation in the experimental data. Fit-parameters in model A are also highly correlated, so this makes necessary to fix some of them to get reasonable values. In order to explain the observed change in N, Model A considers an impurity in the stock of C152 which has to be brighter than C152 (f_Q was fixed in 10, which means 10-fold brighter), then according to the fit, this impurity will be around 10-fold less concentrated. This makes clear that the impurity has to be another fluorophore, being much brighter and much less concentrated than C152 itself. This impurity decreases the apparent number of molecules when there is no TX100, in relation with the real number of molecules of C152. When TX100 is added, the brightness of the C152 goes up and therefore also its contribution to the apparent number of molecules, so that the apparent N increases. The value obtained for the equilibrium constant, K, is consistently lower (about 10-fold) than that expected for the interaction C152-TX100. This

fact can be easily explained under the assumption that the interaction with the TX100 affects the impurity brightness; in this case the K in the model will be actually an apparent equilibrium constant since the interaction of both dyes with the TX100 affects their brightness ratio.

We know from separate measurements that TX100 presents a significant intensity in the total fluorescent signal. However, by trying to fit the model B we determine that this contribution by itself cannot explain the variation in the apparent number of molecules, N. Additionally, by fitting the model A we could easily determine what kind of impurity present in the guest stock could explain the variation in the experimental data.

From this fit, we can obtain the parameters, f_{I}, f_{Q} and f_{N}. Using the equations in section 4.2.1, we could also predict the influence of this impurity on the diffusion term.

Impurities in the interaction between labeled DNA and a non-fluorescent binder.

In this system, the hybrid binder binds simultaneously to both, the minor and major dsDNA grooves. The study was performed with Oregon Green 488 labeled DNA. Therefore, in order to apply the models note that the binder would have the role of host, in the sense that the titration is performed by progressively increase its concentration in the samples at a fixed and low concentration of labeled DNA, which would be acting as the guest.

Model A (eq. 33) fits perfectly well to the experimental data (see Figure 14), keeping the fit-parameters at reasonable values although with high correlation among them. This result makes clear that a variation in N can be explained by the presence of impurities in the stock of labeled DNA.

Considering the nature of the sample, a labeled macromolecule, there is a certain probability for the impurity to be free Oregon Green, residue from the labeling or result of degradation of the labeled DNA. According to this hypothesis, the impurity is as bright as the fluorophore, since the attachment to the DNA does not affect OG brightness as long as DNA and binder are not forming a complex. By including this condition and fixing $f_{\mathrm{Q},0} = 1$ (note this parameters refers to the situation with $[\mathrm{binder}] = 0$), we can get from the fit very good estimations for f_{N}, q, N_1 and K in this system (see Table 3).

The value obtained for q is very close to *zero*, which means an enormous decrease in the brightness of the conjugated OG488, Q_1. This result together with the observed decrease in intensity observed upon addition of binder can be explained by a quenching of this Oregon Green when the DNA forms a complex with the binder. Therefore, when the binder is added, the brightness of the conjugated Oregon Green, Q_1, decreases and the brightness ratio, f_{Q},

increases, which leads to a $q < 1$. The free Oregon Green does not interact with the binder, so it maintains its brightness.

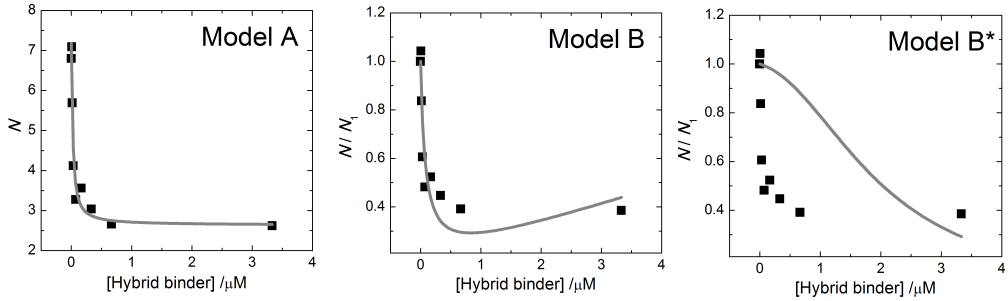

Figure 14. Scatter: Different N values obtained from the fit of the FCS correlation curve when measuring different concentrations of hybrid binder at a fixed concentration of Oregon Green 488-labeled DNA. Lines: Curves obtained by fitting the equations 33 and 37 for models A (left) and B (right) respectively. (Note: experimental data are the same in both graphs, however for the fit of Model B we use ratio N/N_1 instead of the absolute N value because in that case we know the value of N_1 from the sample without binder).

The value of 0.6 for the parameter $f_N = N_2/N_1$ shows us that approximately a 40% of the Oregon Green is free, compared to a 60% that would be conjugated to the DNA. We confirmed this fact separating the free Oregon Green from the labeled DNA by chromatography and getting very similar proportions.

Table 3. Values of the parameters: f_N, q, N_1 and K, obtained by fitting the equation 33 for model A to the data of the variation in N for the titration of Oregon Green labeled DNA with hybrid binder.

Fit-parameters (model A)				
f_Q	$f_N = N_2/N_1$	q	N_1	K /μM^{-1}
1 (fixed)	0.6 ± 0.1	≈ 0	4.6 ± 0.4	111 ± 31

The value for the equilibrium constant is in the order of magnitude of that one we would expect for the interaction between the binder and the DNA, 111 μM^{-1}. In this case, monitoring the change in the number of molecules during the titration could represent an alternative to the use of other variables, such as the diffusion time, for the determination of the equilibrium constant.

In order to check whether the presence of impurities in the stock of binder can explain the variation in N eq. 37 and eq. 39 were fitted to the experimental data (Figure 14, center and right plot respectively). The former leads to nonsense values for the fit-parameters (see

Table 3), such as an impurity 13 times brighter than the Oregon Green or a value of *zero* for the equilibrium constant. The latter introduces more constraints to the fit by using data of the intensity signal for the samples of DNA and binder (model B*). For this fit, concentration of the binder stock, its intensity signal, together with the intensity signal of the labeled DNA sample without binder were fixed using the values of each individual measurement. The third plot in Figure 14 shows how model B is unable to fit the data, which means that this behavior in the apparent number of molecules during the titration cannot be attributed to an impurity in the stock of the hybrid binder.

Table 4. Values of the parameters for the fitting of equations 37 (model B) and 39 (model B*) to the data of the variation in N during the titration of Oregon Green labeled DNA with hybrid binder.

Fit-parameters (model B)					
f_Q	K /µM^{-1}	q	α /µM^{-1}		
13	≈ 0	≈ 0	0.08		
Fit-parameters (model B*)					
f_Q	K /µM^{-1}	q	$I_{1,0}$ /kHz	I_{imp} /kHz	$[\mathbf{H}]_{stock}$ /µM^{-1}
1610	0.42	≈ 0	20 (fixed)	0.35 (fixed)	1.7 (fixed)

Impurities in the interaction between a labeled binder and DNA.

In this preliminary titration for the system Oregon Green 488 labeled Bisbenzamidine/DNA we observed a very important increase in the number of molecules when DNA is added at a constant concentration of labeled binder.

N values obtained from individual fits to the correlation curves of each sample of the titration. In order to explain a non-linear variation of N during a titration, Models A and B require that the brightness of the dye changes upon adding DNA, which is known to occur with this labeled binder. Since the stock of DNA presents a relatively important signal, it is reasonable to consider an impurity in any of the stocks, the OG488-labelled Bis-benzamidine (bbaOG) or the DNA.

Both models were fit to the values of N vs. DNA concentration obtained during the titration (see Figure 15).

Model A considers an impurity in the binder stock. The fit-parameters although highly correlated indicate that the impurity should be brighter than the binder and less concentrated ($f_Q > 1$, $f_N < 1$). Thus, when we add DNA, the binder brightness increases and

so does its contribution to the apparent number of molecules. Knowing the process to synthesize the binder, it is very likely that the impurity is free Oregon Green, from an uncompleted purification or degradation of the labeled binder. We also know that Oregon Green conjugated to the binder is around 10 times less bright than the free OG, and that it recovers its brightness when binder and DNA form a complex. Taking this into account the values of f_Q and q can be fixed in the fit (see Table 5). Although the curve (Figure 15-A) does not change due to the correlation among the fit-parameters, this allows us to obtain a much better estimation for the number ratio between impurity and binder, f_N, the equilibrium constant for the complexation binder-DNA, K, and the number of binder molecules in the sampling volume, N_1.

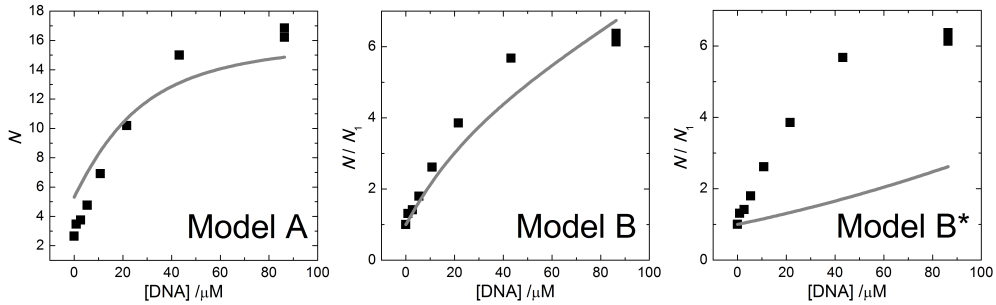

Figure 15. Scatter: Different N values obtained from the fit of the FCS correlation curve when measuring different concentrations of DNA at a fixed concentration of Benzamidine-OregonGreen488 (Note: data are the same in both graphs, however for the fit of Model B the ratio N/N_1 is preferred instead of the absolute N value). Lines: Curves obtained by fitting the eqs. for the models A (left), B (center) and B* (right) described before, to the scatter points.

Table 5. Values of the parameters for the fitting of equations 33 (model A), 37 (model B) and 39 (model B*) to the data of the variation in N during the titration to study the interaction between a OG488-labeled binder and DNA.

Fit-parameters (model A)					
f_Q	K /µM^{-1}	q	$f_N = N_2/N_1$	N_1	
10 (fixed)	0.008	10 (fixed)	0.1	15	
Fit-parameters (model B)					
f_Q	K /µM^{-1}	q	α /µM^{-1}		
0.01	0.006	10 (fixed)	8.35		
Fit-parameters (model B*)					
f_Q	K /µM^{-1}	q	$I_{1,0}$ /kHz	I_{imp} /kHz	$[H]_{stock}$ /µM^{-1}
≈0	≈0	10 (fixed)	4.11 (fixed)	2.83 (fixed)	96 (fixed)

Model B is able to fit the experimental data when equation 37 is used (see Figure 15, model B). The change in brightness of this binder from free to bound state can be again fixed in 10 (see Chapter IV), the equilibrium constant, K, shows a reasonable value contrarily to what happens with the correlated values of α and f_Q, which do not match the experimental data of signal intensities as it is proved when fitting equation 39 (model B* in Figure 15). Intensity signal of the DNA stock was measured in absence of binder allowing to fix additional values in the fit of equation 39 (see Table 5). This final fit clearly shows that the variation in N cannot be explained just in terms of the impurities present in the DNA stock when the model takes into account data of the intensity signals. However, given the fact that DNA without added binder presents a relatively high signal, the influence of these impurities could explain why model A is not able to completely reproduce by itself the variation in N. Therefore we can conclude that, in this case, there is a major effect on the apparent number of molecules due to the free OG present in the binder stock; with and additional but lesser influence of the impurities in the stock of binder.

4.3. Apparent Diffusion Time.

4.3.1. Theory.

The impurities in FCS samples not only affect to the apparent number of molecules, but also the diffusion term and, therefore, the diffusion times obtained from the fit to the correlation curves.

In order to analyze the influence of impurities on the diffusion term we will use the same model as for the case of the apparent number of molecules (Figure 3). In this model we consider a homogeneous impurity, behaving like a second fluorescent species.

Using the ratios f_Q and f_I defined before, we can rewrite the expression for the parameter r from equation 12 as follows:

$$r = \frac{1}{f_Q f_I + 1} \tag{40}$$

Performing simulations for the value of r, we can estimate how the diffusion time will be affected by the presence of the second species or impurity. The contribution of the main species in the diffusion term is given by r, whereas $1–r$ represents the contribution of the impurity. In situations in which either the brightness or the signal intensity from the impurity is very low with respect to the main species ($f_Q\, f_I \ll 1$), r will remain very close to 1. On the contrary, the bigger the product $f_Q\, f_I$, the more r will move away from 1.

We can compare the contribution of species 1 in the diffusion with its molar fraction combining equations 19, 20 and 40, getting an idea of the contribution of the species 1 to the diffusion term in relation with its number ratio.

$$\frac{r}{N_1/(N_1+N_2)} = \frac{f_I/f_Q + 1}{f_Q f_I + 1} \tag{41}$$

4.3.2. Simulations.

Contribution of the impurity to the diffusion term.

Figure 16 shows the contribution of the impurity (species 2) to the diffusion term, $1–r$, as a function of the brightness ratio, f_Q, and the intensity ratio, f_I, according to the equation 40. As expected, the contribution of the impurity to the diffusion term increases with f_I. However, in contrast to the behavior of the apparent number of molecules (see Figure 4), the higher f_Q the bigger the influence of the impurity on the diffusion time (Remember that at given f_I a higher f_Q implies a smaller f_N). As an illustrative example we take a dim but numerous impurity: if we have a contribution of the impurity (species 2) to the fluorescence intensity of 50% ($f_I = 1$) and a brightness ratio $f_Q = 0.01$, then the influence of the impurity on the apparent number of molecules will be very high, $N/N_1 = 4$ (Figure 4), but very low on the diffusion term, $1–r < 0.05$ (Figure 16, black curve at $f_I = 1$).

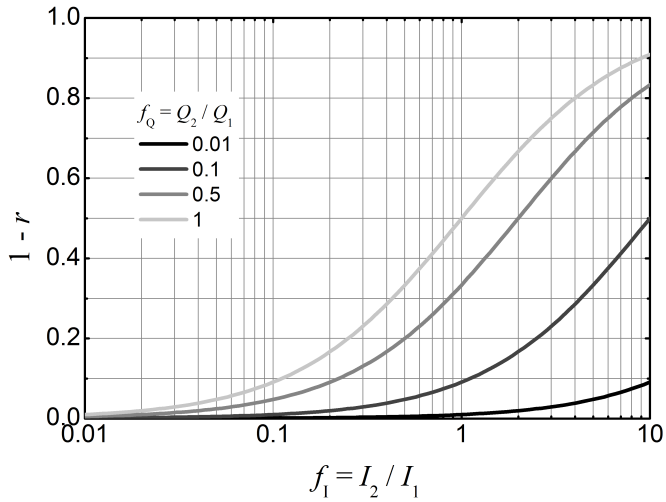

Figure 16. Simulation of the factor $1–r$ versus the intensity ratio, at different brightness ratios. $1–r$ is the contribution of the species 2 (impurity) to the diffusion term of the correlation curve.

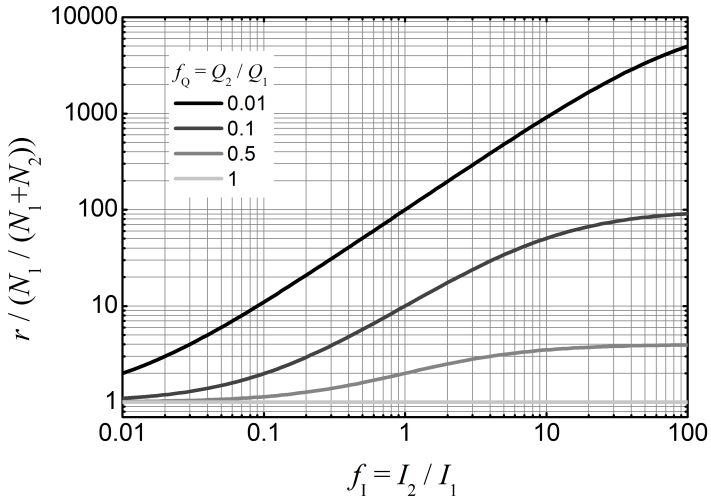

Figure 17. Simulation of the ratio between the factor r and the number ratio of the species 1, versus the intensity ratio, f_I, at different brightness ratios. The ratio between the factor r and the number ratio of the species 1, gives an idea of the contribution of the species 1 to the diffusion term in relation with its number ratio.

Using equation 41, we observe that when both species have the same brightness their contributions to the diffusion term coincide with their molar fractions. However, when the species 1 is brighter than species 2, its contribution in the diffusion term will be higher than that corresponding to its molar fraction (see Figure 17). We observe also in this case that the higher the intensity from species 2 (less bright) the higher the contribution in the diffusion of the species 1 (brighter species) with respect to its molar fraction.

Apparent diffusion time.

Once we know how impurities affect to the value of r, it is very interesting to determine how r affects the apparent diffusion time that we obtain in the analysis of correlation curves of samples with impurities.

Commonly, although there are two species in the sample (fluorophore and impurity) the correlation curve can be fitted satisfactorily using the model for a single species. This situation can occur especially when we are not aware of the presence of an impurity in our system and when it has a diffusion time similar to that of main fluorophore. In these cases, as a result of the fit, we get a value of the diffusion time (apparent diffusion time) that will depend on the parameter r, but also on the diffusion times of both species.

In order to study this dependence, several correlation curves were simulated using the two-species model (equation 13). Five different values for the diffusion times τ_1 and τ_2 were

chosen, covering the range 0.1 to 10 for the ratio τ_2 / τ_1. For each pair of diffusion time values, five different correlation curves were simulated with the parameter r set in values from 0.5 to 0.99. As a result we got a matrix of 5×5=25 correlation curves, with the rest of the parameters in common for all of them. The single-species model (equivalent to the two-species model when $r = 1$) was then used to fit each of these curves, obtaining the corresponding value for the apparent diffusion time, τ_{app} (see Figure 18, for an example of five of these curves with their correspondent fits).

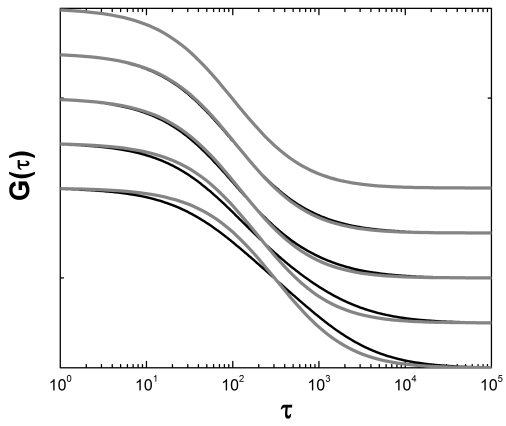

Figure 18. Example of five simulated correlation curves in a stacked plot. In *black*, simulated curves using the two-species model with the following parameters: $N = 5$, $\theta = 5$, $\tau_1 = 100$ µs, $\tau_2 = 1000$ µs, $r = 0.5$, 0.7, 0.9, 0.95 and 0.99 (from bottom to top curve, respectively). In *grey*, fitted curves using the single-species model, which gives the following values for the apparent diffusion time (from bottom to top curve): $\tau_{app} = 319$ µs, 191 µs, 122 µs, 110 µs and 102 µs.

If we plot the ratio τ_{app}/τ_1 versus the ratio τ_2/τ_1, for different values of r (Fig. 19), we can see that they follow a power function as indicated in the Fig. 15, whose exponent depends on r.

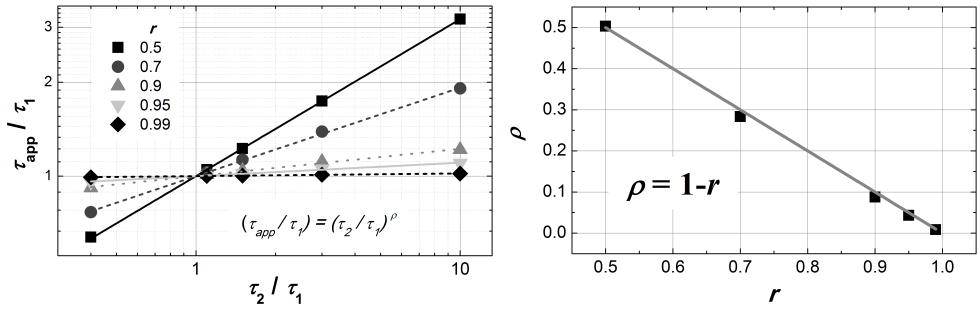

Figure 19. Left panel: Fit to the generated data τ_{app}/τ_1 vs. τ_2/τ_1 at different values of the parameter r, using a power fit function. r is the contribution of species 1 to the diffusion term of the correlation curve. τ_1 and τ_2 are the diffusion correlation times for the species 1 and 2, respectively. τ_{app} is the diffusion correlation time obtained from the fit of the 1-species model to the two species correlation curve, simulated with the values of τ_1, τ_2 and r. Right panel: Linear fit to ρ (exponents obtained in the fit τ_{app}/τ_1 vs. τ_2/τ_1) vs. r values.

If we represent the exponent of the power function, $\rho(r)$, versus the values of r, we get the linear dependence $\rho(r) = 1–r$ as shown in (Figure 19, right). This leads to the empirical function for τ_{app} given in equation 42. Note that this equation was obtained simulating a maximum 10-fold difference between the diffusion times, range in which it would make sense trying to use a single diffusion time fit.

$$\tau_{app} = {\tau_1}^{r} \; {\tau_2}^{1-r} \tag{42}$$

In this expression the apparent diffusion time, τ_{app}, is given as the geometric mean of the values τ_1 and τ_2 weighted by the parameter r. In order to perform simulations we rewrite the equation 42 more conveniently in relative terms as follows:

$$\frac{\tau_{app}}{\tau_1} = \left(\frac{\tau_2}{\tau_1}\right)^{1-r} \tag{43}$$

Figure 20 shows that, as expected, the bigger $1–r$ is and the more different the diffusion times of species 1 and 2 are, the more the apparent diffusion time moves away from the main species diffusion time. However, the influence of an impurity on the apparent diffusion time is much smaller than on the apparent number of molecules, especially in the case of a not too big contribution r and similar diffusion times of the two species. In the case of significantly different diffusion times these can be usually well separated in a fit of a two-species model to the correlation curve.

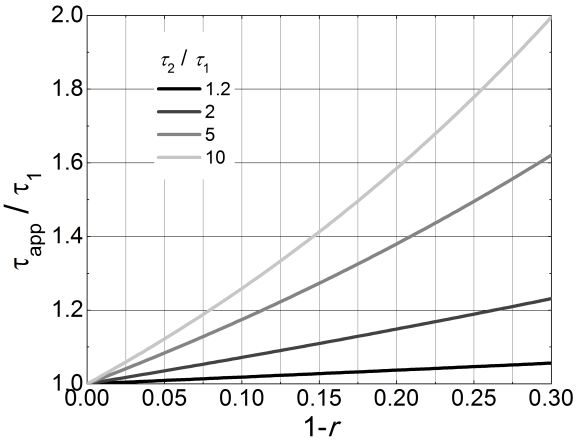

Figure 20. Simulation of the ratio τ_{app}/τ_1 vs. $(1–r)$ at different values of the ratio τ_2/τ_1, according to equation 43. τ_1 and τ_2 are the diffusion correlation times for the species 1 and 2, respectively. τ_{app} is the diffusion correlation time obtained from the fit of the 1-species model to the two species correlation curve. r is the contribution of the species 1 to the diffusion term of the correlation curve, the contribution of the species 2 is $1–r$.

4.3.3. Experiments: influence of impurities on the diffusion term.

In some of the systems we have studied, the impurities in the stock of host presented a diffusion time higher than the diffusion time of the fluorophore (guest). Then, we had the problem of deciding whether the increase in the diffusion time observed when we add host to the fluorophore was due to the interaction between host and guest or it was due to the influence of the impurities in the host stock.

In order to solve this problem, first, we need to measure the correlation curves for guest and host separately. Then, using equation 40 and 42 we can predict the apparent diffusion time assuming no interaction between host and guest. If this predicted time matches the diffusion time obtained from the fit to the experimental correlation curve for the mixture of host and guest, it will mean that the increase in the diffusion time is mainly due to the impurities in the stock of host. On the contrary, if the experimental diffusion time is bigger than the one estimated for the non-interaction case, we can conclude that the increase in the diffusion time is the result of an interaction between host and guest.

In Table 6 and Table 7, we present the data for two different host-guest systems where the host stock was contaminated with fluorescent impurities, whose diffusion times could be measured and happen to be higher than the diffusion time of the fluorophore. In these cases, an increase in the diffusion time of the fluorophore upon addition of the host can be misinterpreted as a host-guest interaction being maybe only an effect of the impurities.

Impurities in the interaction between a labeled binder and DNA.

When we study the interaction of small binders, such as this Coumarine labeled Bisbenzamidine (bbaCou), with DNA, the DNA commonly presents high levels of fluorescent impurities, with diffusion times bigger than the diffusion time of the binder. This, together with the fact that the proportion of binder molecules, which attach to the DNA is low at these DNA concentrations, make it difficult to decide whether the increase observed in τ_D was due to the impurity or due to the interaction of the binder with the DNA.

For this binder, it is clear that there is interaction with the sequence of high affinity (AAATTT), because the experimental diffusion time is bigger than the diffusion time of the impurity (see Table 6). However, for the low affinity sequence (GGCCC) the increase in the diffusion time after adding DNA is very small, and the experimental diffusion time, $\tau_{D,exp}$, is still lower than the diffusion time of the impurity.

With the experimentally determined ratios f_I and f_Q for this system, we can calculate the value for r using equation 40 and then with eq. 42 the apparent diffusion time after the

addition of the impurity to the binder considering no interaction between binder and DNA, $\tau_{D,sim}$.

Table 6. Parameters (τ_D, I, N and Q) obtained from the measured FCS curves of the guest (bbaCou) and host (DNA_{AATTT} or DNA_{GGCCC}) separately. Parameters (f_I, f_Q, r) calculated from the individual curves of host and guest to obtain an estimation of the diffusion time for the sample with both ($\tau_{D,sim}$). The experimental diff. time, $\tau_{D,exp}$, was obtained from the fit to the measured FCS curve for the sample with binder and DNA.

	τ_D /µs	I /kHz	N	Q	
bbaCou	34.2	4.93	2.82	1.75	
AATTT 7.08 µM	63.2	1.16	1.03	1.13	
GGCCC 8.5 µM	55.7	0.87	0.62	1.41	
	f_I	f_Q	r	$\tau_{D,sim}$ /µs	$\tau_{D,exp}$ /µs
bbaCou + AATTT 7.08 µM	0.23	0.64	0.87	37	87.4
bbaCou + GGCCC 8.5 µM	0.18	0.81	0.88	36	52.6

If we compare the value for the $\tau_{D,sim}$ with $\tau_{D,exp}$, we can see that the influence of the impurity on the apparent diffusion time is still far away from explaining the experimental values. This clearly indicates an interaction between binder and DNA, even for the low affinity sequence (GGCCC) in spite of the very low increase in the diffusion time.

Impurities in the system Alexa/Cyclopeptide.

Here we study the interaction of a cyclopeptide (CP) as host, with two different guests, the dye Alexa 488 (Alexa) and this same dye bound to trichloromethane (CCl_3-Alexa), see Figure 21.

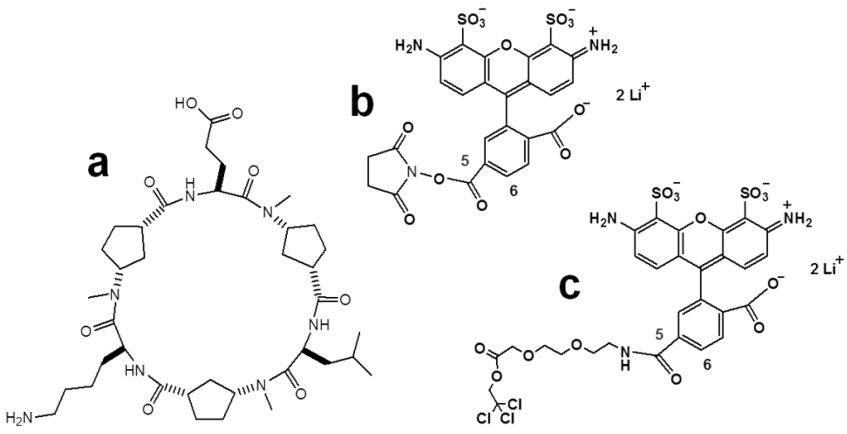

Figure 21. Structures of the cyclopeptide (*a*) and dyes: Alexa (*b*) and CCl_3-Alexa (*c*) used in this experiment.

We observed that the stock of cyclopepide has some kind of fluorescent impurity and, after measuring a correlation curve in FCS, we get a value for its diffusion time which is bigger than any of both Alexa dyes (see Table 7).

Adding cyclopeptide to the fluorophores we observe a small increase in the diffusion time as compared to that of the dye alone, but in both cases the apparent diffusion time is below that of the impurity in the cyclopeptide stock.

Again, from the values of f_I and f_Q for this system and using equations 40 and 42 we can calculate the estimated diffusion time for the sample with dye and cyclopeptide, assuming that the observed variation is only due to the addition of a second fluorescent species (impurity) without any interaction between them.

For both dyes, Alexa and CCl_3-Alexa, the apparent diffusion time obtained experimentally, $\tau_{D,exp}$, is significantly higher than the simulated diffusion time, $\tau_{D,sim}$ (Table 7). We conclude therefore, that complexation of the cyclopeptide occurs with both Alexa dyes.

Table 7. Parameters (τ_D, I, N and Q) obtained from the measured FCS curves of the guest (Alexa or CCl_3-Alexa) and host (Cyclopeptide) separately. Parameters (f_I, f_Q, r) calculated from the individual curves of host and guest to obtain an estimation of the diffusion time for the sample with both ($\tau_{D,sim}$). The experimental diffusion time, $\tau_{D,exp}$, was obtained from the fit to the measured FCS curve for the sample with dye and cyclopeptide.

	τ_D /µs	I /kHz	N	Q	
CCl_3-Alexa	62.6	35.4	4	8.9	
Alexa	55	20	2.1	9.5	
Cyclopeptide (CP)	69	1.51	0.24	6.3	
	f_I	f_Q	r	$\tau_{D,sim}$ /µs	$\tau_{D,exp}$ /µs
CCl_3-Alexa + CP	0.04	0.71	0.97	63	70.4
Alexa + CP	0.08	0.66	0.95	56	64.5

Although in the examples given here, the increase in the diffusion time was low upon addition of the host, for both systems the experimental diffusion time was significantly bigger than that estimated as an influence of the addition of impurities. Consequently, we could proof that the increase in the diffusion time was always caused by an interaction between host and guest, and not by the influence of the impurities in the stock of host.

We can conclude that performing the calculations explained in this section is very useful to correctly interpret small variations in the diffusion time, even when we have a contamination in the stock of host, which would move the diffusion time in the same direction than the effect of the interaction we are studying.

Bright impurity in the stock of the guest.

A stock of a DNA minor-groove binder labeled with the dye Oregon Green (BBA-OG) has a purity of better than 95% in concentration as determined from HPLC. The impurity is known to be free Oregon Green (OG), which has a brightness about 8 times higher than the fluorescent label in BBA-OG ($f_Q \approx 8$). This is the case of a small fraction of a very bright impurity. The aim is to predict the influence of the OG-impurity in the BBA-OG-stock in the FCS experiment.

FCS curves of solutions of BBA-OG yield correlation curves which can be well fitted with a single diffusion time of $\tau_{app} = 305$ µs which is intermediate between that estimated for BBA-OG ($\tau_1 = 360$ µs) and the value of free OG ($\tau_2 = 250$ µs).

Which amount of impurity (free OG) is necessary in order to explain the observed apparent diffusion time?

From equation 42 we obtain easily estimation for r:

$$r \approx ln\frac{\tau_{app}}{\tau_2}\Big/ln\frac{\tau_1}{\tau_2} = ln\frac{305\,\mu s}{250\,\mu s}\Big/ln\frac{360\,\mu s}{250\,\mu s} = 0.55 \tag{44}$$

From equation 40 and the known values of f_Q we can then estimate the number ratio f_N=0.13*:*

$$f_N = \frac{1-r}{r}\frac{1}{f_Q^2} \approx \frac{1-0.55}{0.55}\frac{1}{8^2} = 0.13 \tag{45}$$

This corresponds to a *number fraction* of the impurity ($N_1/(N_1+N_2) = 1/(1+f_N)$) of only 1.3 %. This example demonstrates the strong sensitivity of FCS measurements to impurities of high brightness.

4.4. Conclusions.

In FCS, special care must be taken with impurities and the effect they have on parameters obtained in the fit to the correlation curves. Certain levels of impurities can be common when we are using non-ultrapure reactants, products from synthesis not perfectly purified, or some commercial chemicals which are not available at high grade of purity (DNA, surfactants, cyclodextrins).

In many bulk spectroscopy techniques or those single molecule techniques in which the molecules are fixed to a surface, these impurities can be neglected or removed. However, when we use a single molecule technique in solution, such as FCS, without applying any kind of

filtering to the data (cross-correlation, FLCS, etc.) the impurity can have a significant influence on the measurement results.

Knowing the extent of the influence of the impurities in FCS experiments, we can evaluate whether they are affecting our results and decide whether it is worth trying to remove them from the system. Sometimes it will be enough to be able to quantify their effect, and to take it into account to interpret the results.

Impurities in FCS have a strong influence on the apparent number of molecules, N. In this case, the easiest way to quantify the effect is through their contribution to the intensity signal. With this value we can calculate the maximum influence on N, which will be given by a situation with a highly concentrated impurity with very low brightness.

In cases in which the impurity are molecules that are much less bright than the fluorophore we are interested in (less than 1%) but with huge contributions to the intensity (up to a 50%), the influence on the number of molecules will be very high, but neglectable on the diffusion time. The scattered light coming from the solvent is a clear example of this situation.

On the contrary to what happens with the number of molecules, the diffusion time will be much more affected by impurities with high brightness. Also, the more different in size are the fluorophore and the impurity the bigger will be the influence on the diffusion time.

In this work we presented different examples of host-guest complexations with unexpected increases in the apparent number of molecules during titrations at constant concentration of fluorophore. This behavior could be explained as an effect of impurities present either in the stock of fluorophore or in the stock of host. Probably in some case, we observe the influence of both types of impurities.

During a titration, if the brightness ratio between fluorescent guest and impurity is dependent on the concentration of added host, it will cause a variation in the number of molecules following a saturation curve.

We can detect an impurity in the stock of guest by an unexpected change in the apparent number of molecules during a titration, as long as the brightness ratio between guest and impurity depends on the concentration of added host. The knowledge of two of the three ratios f_I, f_N and f_Q allows us to estimate the effect of the impurity on N and τ_D. For this reason, even once we know an impurity is present in the stock of guest, we would need the comparison with a clean sample of fluorophore to be able to quantify its effect.

In the case of an impurity in the stock of an unlabeled host, we can easily measure impurity and fluorophore separately, and calculate the ratios f_I, f_N and f_Q. With these values and the equations we have proposed we can predict the influence on the number molecules and on the diffusion time. It allows us to interpret correctly the data in FCS, and distinguish between those effects caused by the impurity and those due to the interaction between host and guest. Calculations and analysis discussed in this work make possible to study systems with certain levels of impurities even when the effects of the interaction between host and guest are weak.

5. Practical Aspects of FCS.

5.1. Laser Beam Diameter Determination.

The small detection volume is crucial in SMD. In FCS experiments, however the optimum size of the focus will depend on each system under study, as we will discuss later in this chapter it. One can change the focus size by tuning the size of the laser beam, which can be easily done using different collimators.

The radius of the laser beam before entering the objective depends on the numerical aperture of the optical fiber, NA, and the focal length of the collimator, f_{col}:

$$R_{\mathrm{beam}} = \mathrm{NA}\, f_{\mathrm{col}} \tag{46}$$

Then the radius of the focus will depend not only on the radius of the laser beam, but also on the focal length of the objective, f_{obj}, and the wavelength of the laser, λ.

$$R_{\mathrm{focus}} = \frac{\lambda\, f_{\mathrm{obj}}}{\pi\, R_{\mathrm{beam}}} \tag{47}$$

According to these expressions, in Table 8 the radius of the laser beam and focus are calculated for the different setups used in this thesis.

It results very interesting to be able to experimentally determine the laser beam diameter, not only to check the previous calculations but also to assure that the beam is perfectly collimated. The knife-edge method is among the most common ways to measure the diameter of a Gaussian laser beam, in which the full beam power is recorded with a laser power meter as a razor blade is translated through the beam mounted on a calibrated translation stage. Moving the razor blade into the beam and noting the micrometer reading of the stage, the curve on the left side of Figure 22 is obtained.

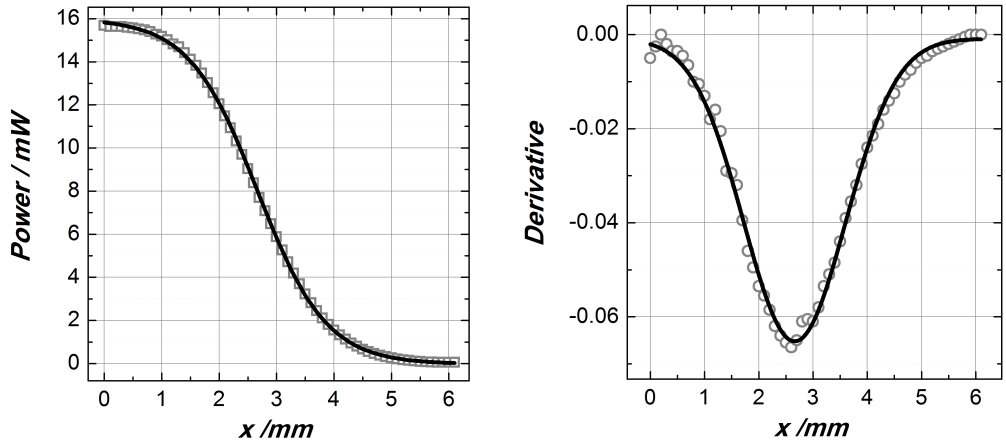

Figure 22. The left side shows the power meter read as function of the translation of the blade into the laser beam. The right side is the derivative of the plot on the left.

This first plot represents the integral of the Gaussian beam between -∞ and the position of the blade, starting at the total beam power and decreasing to zero power. The width of the beam can be calculated using the points of the measured curve at which the power output is 10% and 90% of the maximum value, X_{10} and X_{90}, respectively, being $X_{10\text{-}90}$ the distance between them. Then the $1/e^2$ diameter, d, of the Gaussian beam can be calculated using the following shorthand expression $d = 1.56\ X_{10\text{-}90}$.

Table 8. Parameter calculation for the different collimators and lasers. The radius of the laser beam, R_{beam}, and the radius of the focus, R_{focus}, depend on the numerical aperture of the optical fiber, NA, the focal length of the collimator, f_{col}, the focal length of the objective (3 mm), and the laser wavelength, λ.

λ /nm	NA	f_{col} /mm	R_{beam} /mm	R_{focus} /µm
405	0.065	30 (60FC-4-M30-13-DI)	1.95	0.20
405	0.065	6.24 (60FC-4-6,2-01-DI)	0.41	0.95
488	0.09	30 (60FC-4-M30-13-DI)	2.70	0.17
488	0.09	6.24 (60FC-4-6,2-01-DI)	0.56	0.83

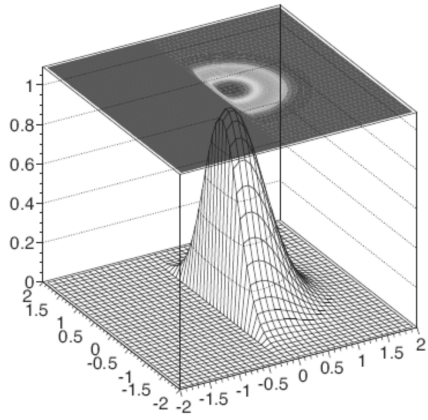

Figure 23. Gaussian beam cut by a razor blade that has advanced almost to its center.

Note that a correct calculation of the total transmitted light energy would involve a two-dimensional integral. Although the integration in one dimension is straightforward, the other is intractable and no analytic form is known. However we can calculate the derivative of this curve (plotted on right side of Figure 22), which gives a good approximation to the Gaussian beam profile, similar to Figure 23. Then we can determine the width from the $1/e^2$ points of this curve where the intensity has dropped to 13.5% of the maximum value.

Table 9. Diameter determination collimator 60FC-4-M30-13-DI (#500695) at 405 nm.

x_{10} /mm	x_{90} /mm	$x_{10\text{-}90}$ /mm	d /mm	d^* /mm
3.99	1.36	2.66	4.1	3.8

* from a Gaussian fit to the derivative plot.

As diameter of the beam generated at 405 nm with the collimator 60FC-4-M30-13-DI we obtain $d = 3.8$ mm. This is in good agreement with the calculated value of 2 $R_{\text{beam}} = 3.9$ mm (see Table 8).

5.2. Influence of the Photon Package Size for the Correlation.

LABVIEW software used to build the correlation curves requires splitting the photons from a measurement in several packages. Then a filtering is applied to remove those packages with a mean intensity signal statistically far from the average. Then each package is analyzed separately and the final correlation curve is calculated as the average of the curves corresponding to each package of photons. The smaller the packages the better the filtering, this way also power drifts from the laser can be suppressed. However the time window

corresponding to each package has to be long enough in order not to trunk the correlation affecting the longer diffusion times.

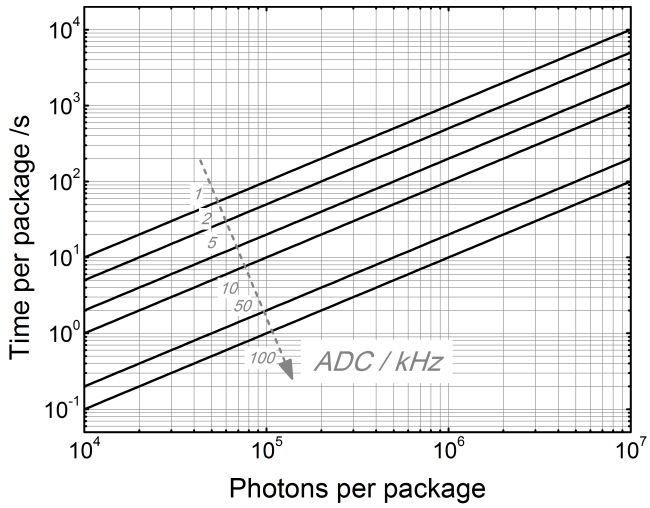

Figure 24. Plot of the *Time per package* vs. *Photons per package* depending on the intensity signal of the sample (ADC, photon counts per second). *The Time per package* value selected must be at least 5000 times higher than the diffusion time to avoid influence on the diffusion time.

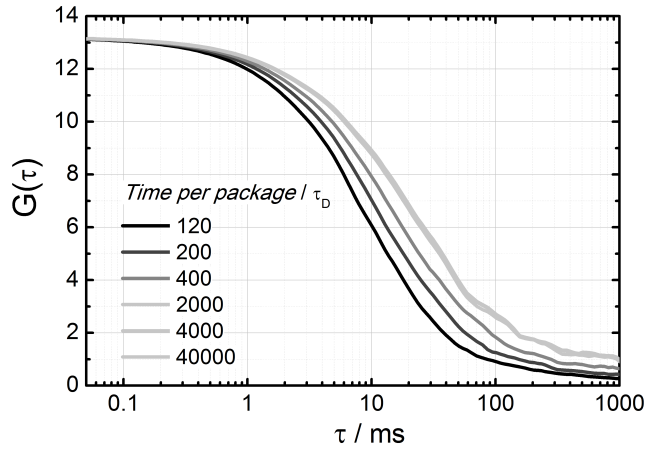

Figure 25. Series of FCS correlation curves obtained from the same measurement of 100 nm fluorescent beads using different sizes of the photons packages to build the correlation curves using LABVIEW software. For small package sizes the apparent diffusion time appears severely shifted to smaller correlation times.

The input parameter which determines the size of these packages is the so-called *photons per package*, which, using the average intensity signal, can be converted to the temporal length of the package (*Time per package*).

Using the photons collected for a measurement of 100 nm fluorescent beads and performing analysis for different package sizes it can be observed that for small package sizes the apparent diffusion time appears severely shifted to smaller correlation times (see Figure 25).

The Plot in Figure 24 can be used to select the appropriate value for the *Photons per package* parameter depending on the recorded fluorescence intensity of the sample (ADC, photon counts per second), as shown in Figure 25. In our experience the *Time per package* value must be at least 5000 times higher than the diffusion time in order to avoid a detectable distortion of the correlated correlation curve.

5.3. Influence of Cover-Slide Thickness.

The optical properties of the high aperture microscope objective used in the FCS setup depend sensitively on the thickness of the air and glass media positioned between its front lens and the object. The geometry of the focus is significantly affected by the thickness of the cover glass. The effect of the cover glass thickness on the diffusion time has already been reported in detail (Enderlein et al. 2005). In order to assure a constant geometry of the focus, the microscope objective has to be adjusted to the specific thickness value of the cover-slide through the adjustment ring or correction collar of the objective.

In Figure 26, we can see how the measured diffusion time of Rhodamine 123 increases when the correction collar position deviates from the actual thickness of the cover-slide.

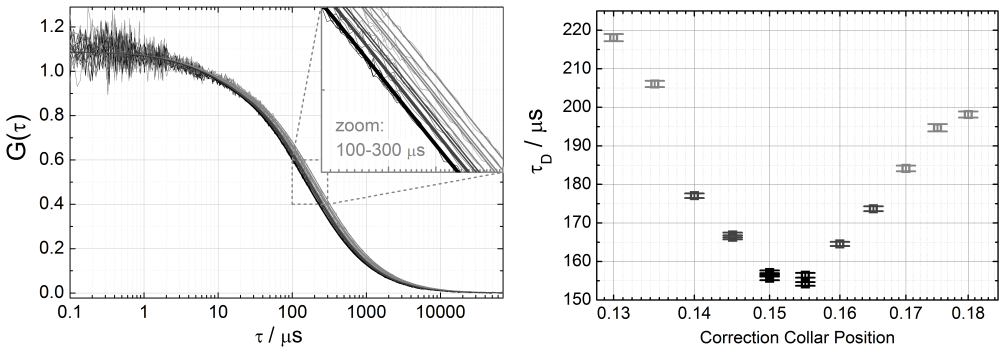

Figure 26. Left plot: FCS correlation curves for the same sample of R123 measured using different positions of the correction collar. Right plot: Apparent diffusion time, τ_D, against the position of the correction collar. The diffusion time increases when the correction collar position deviates from the actual thickness of the surface.

We have found an important deviation in thickness among the different batches of cover slides we used, so it became necessary to measure the thickness at every measurement. Even a single cover-slide presents a significant variation in thickness along the surface, making it necessary to measure the thickness right on the spot where the drop is placed. The direct measurement with a micrometer caliper would contaminate the glass surface. Using the scale on the fine focus wheel of the microscope, we therefore determine the thickness optically from the distance between the two reflections of the focus at both *glass-water interfaces.* This is sufficiently precise to adjust the collar or at least to reject cover slips with strong deviations from a mean value.

Given the strong influence of the cover-slide thickness on the diffusion times, its variability and the inconvenience of adjusting the correction collar for each measurement, in the final stage of this thesis we decided to change from cover-slips to well plates which allow one to prepare the different samples of a titration in the same well avoiding the deviations due to the cover slide thickness. In addition, the use of larger sample volumes and the possibility of covering the well with a cap allow one to measure the same sample for long periods of time without the evaporation problems that occur with the drop on a cover slide.

5.4. Calibration of the Confocal Volume.

The determination of absolute diffusion coefficients from the diffusion times obtained in FCS requires knowing the exact value of the focus size. In conventional FCS, a calibration is needed to determine the focus size using the diffusion time of a substance with well known diffusion coefficient.

$$D = \frac{\omega_{xy}^2}{4\,\tau_D} \tag{48}$$

A new calibration is necessary each time the conditions that affect the confocal volume change (temperature, excitation power, wavelength, coverslide thickness, solvent, etc.).

The reference value used in this thesis was that of D(Rh6G) = $\mathbf{(4.14 \pm 0.05)\ 10^{-10}\ m^2\,s^{-1}}$ for the Rhodamine 6G (Rh6G) determined at 25°C using dual focus FCS (2fFCS) (Muller et al. 2008) which allows one to obtain absolute values. With this value for the Rh6G we can determine the diffusion coefficients for other rhodamines using the ratios among the different values given by Gendron et al. (2008) which includes Rhodamine 6G, Rhodamine B (RhB), Rhodamine 110 and Rhodamine 123 (Rh123). Rh123 and RhB are the substances that we use for calibration at 480 nm and 405 nm, respectively.

Table 10. Values of the diffusion coefficients determined by Gendron et al. (2008) at 22.5°C.

Dye	D /10^{-10} m^2s^{-1}	D/D_{Rh6G}
Rh6G	4 ± 0.3	1
RhB	4.2 ± 0.3	1.05
R123	4.4 ± 0.3	1.1
R110	4.3 ± 0.3	1.075

The conversion of these diffusion coefficients at 25°C to other temperatures can be easily done by taking into account the dependence of the diffusion coefficients with the temperature and viscosity of the solvent (Kapusta 2010):

$$\frac{D_1}{D_2} = \frac{T_1}{T_2}\frac{\eta_1}{\eta_2} \tag{49}$$

5.5. Key Points in FCS Measurements.

5.5.1. Important characteristics of the dye.

The selection of a proper dye is crucial for satisfactory FCS experiments. The most relevant characteristics of the fluorophore are the following:

Absorption and emission spectra: It is necessary to know them beforehand to select the laser and filters to be used in the experiment.

Diffusion coefficient: It is directly related to the size of the dye molecule. It is determined measuring its diffusion time, once the size of the focus is known. Some host-guest complexations are studied just through the change in diffusion time of the dye. In these cases, the smaller the dye the bigger the contrast and therefore the resolution of the technique.

CPM vs. Irradiance curve: The recorded fluorescence intensity per dye molecule, *cpm* (counts per molecule), shows an initial linear dependency with the irradiance. The linearity disappears at high values of the irradiance due to optical saturation and photobleaching artifacts. The measurements must be performed always at an irradiance below the saturation threshold, within the linear region.

The two important parameters of the *cpm vs. irradiance curve* are the slope of the linear section and the irradiance value at which the saturation starts. The slope depends on the photophysical properties of the fluorophore, and it will change when its emission does (for example upon complexations involving change in brightness). The level of irradiance for saturation depends not only on the photophysical properties of the fluorophore but also on its

exposure time to the irradiation, given by the diffusion time. The diffusion time depends on the focus size. However, it will also change when the dye undergoes complexation, that is why this threshold must be determined for both free and bound dye and at the same focus size that will be used in the titration.

The *cpm* can be easily calculated for the cases with only one fluorescent species in the sample through the ratio I^*/N, where I^* is the intensity signal after subtracting the solvent contribution and N is the number of fluorescent molecules, obtained from correlation curve fits.

As with the other single-molecule spectroscopy techniques, in general FCS requires bright dyes (high slope in the linear section) which can be highly irradiated without undergoing optical saturation.

Triplet state contribution: An excited state fluorophore that relaxes to the triplet excited state becomes virtually dark, since it cannot generate fluorescence photons during the time it spends in this state. At high enough irradiance levels, intersystem crossing to the triplet state reduces the fluorescence yield causing the loss of linearity in the cpm vs. irradiance curve (optical saturation). Even in the linear section of the curve, the fraction of molecules undergoing relaxation through the triplet state pathway will affect the correlation curve. This so-called triplet contribution is taken into account as an additional term in the correlation function. However, in cases in which the triplet state relaxation time (usually a few microseconds) overlaps with the dynamics of interest in the system, it is desirable to perform the measurement at irradiances low enough to avoid considering the triplet contribution.

5.5.2. Parameters to optimize.

Focus size.

The diameter, ω_{xy}, of the detection volume depends on the diameter of the laser beam before entering the objective, which in turn is determined by the collimator (see section 0).

In general, a small focus has more advantages, e.g.:

- It increases the signal to background ratio (dye molecules vs. solvent). Also, by reducing the focus size the amplitude of the correlation curve can be increased without affecting the signal/background ratio.

- It reduces the diffusion times, so that the saturation level is displaced to higher irradiances.

However, in some cases it can be interesting to use a bigger focus size to keep the correlation function valid. For example, in order to increase the diffusion times so the diffusion term can be separated from other processes such as reaction dynamics. The focus size is also critical when the molecules under study are too big in relation to the focus size, since the fit model considers point-like particles.

The detection volume diameter, ω_{xy}, is usually determined by a calibration measurement with a solution of a fluorophore with known diffusion coefficient using the following expression $\tau_D = \omega_{xy}^2/(4D)$ (only valid when working at an irradiance below the saturation level).

Dye concentration.

The signal/background ratio increases with the dye concentration (the background refers to the signal from the solvent, without fluorophore). However, a high number of molecules in the focus reduces the amplitude of the signal fluctuations and consequently the amplitude of the correlation curve is also reduced.

Optimum: a focus size small enough to get a high S/B ratio ($S/B > 100$), with a number of molecules in the focus as low as possible ($N < 15$).

Irradiance.

Irradiance is the power per unit of area in the focus. At high irradiance the measurement time is reduced, which has several positive effects on the quality of the measurement: lower probability of artifacts, less sample evaporation problems, reduces the problem with the power drift in the laser, etc. However, the irradiance has an upper limit to avoid certain phenomena such as optical saturation or the increase in the triplet contribution.

Irradiance is determined using the power and the focus size. The power in the sample is calculated using a previously determined ratio between the power measured at the exit of the optical fiber and at the focal distance of the objective. For the same focus size, power and irradiance are proportional.

Number of photons.

The bigger the number of collected photons the better, since it will reduce the noise in the correlation curve. The only limitation is the duration of the measurement, because too long measurements (> 40 min) will increase the probability of artifacts, sample evaporation problems, power drift in the laser, etc.

5.5.3. Summary: steps to follow to first measure a host-guest system in FCS.

- Select laser and adequate filters, adjust collimator and dichroic to the laser wavelength.

- Determine the main characteristics of the new system (diffusion coefficients, *cpm* vs. irradiance curve, triplet contribution, etc.) for both free and bound dye (this is crucial in cases in which the brightness of the dye changes upon complexation).

- Change the focus size if necessary and possible, and determine the optimum concentration. Recalculate the *cpm* vs. irradiance curve if the focus size was changed.

- Select the irradiance level (the highest before the appearance of saturation or photobleaching), and according to the intensity of the signal design the experiment (number of samples, number of photons collected, etc).

5.6. Precise Titrations with Very Small Sample Volumes.

Titrations with limited sample amounts (for example when working with some biomolecules, such as DNA, or molecules from complex and costly synthesis) make it necessary to plan efficiently the preparation of the different samples to save as much substance as possible.

In such situations a dilution-extraction method was used to prepare the different samples for the FCS titrations at variable host concentration.

This procedure allows not only carrying out titrations using a minimal amount of host but also performing the measurements in the same well, which avoids problems due to variations in the cover glass thickness.

Three different stock solutions must be available: two solutions of dye (or labeled guest) in buffer and the solution of host.

- *dye stock:* solution of the dye or labeled guest in buffer at the desired concentration for the titration. It can be prepared by a ten-fold dilution of the *dye stock 10×*.

- *dye stock 10×:* solution of the dye or labeled guest in buffer, 10-fold more concentrated than the *dye stock*.

- *host stock:* solution of the host in buffer, with a volume that allows at least the load of a well.

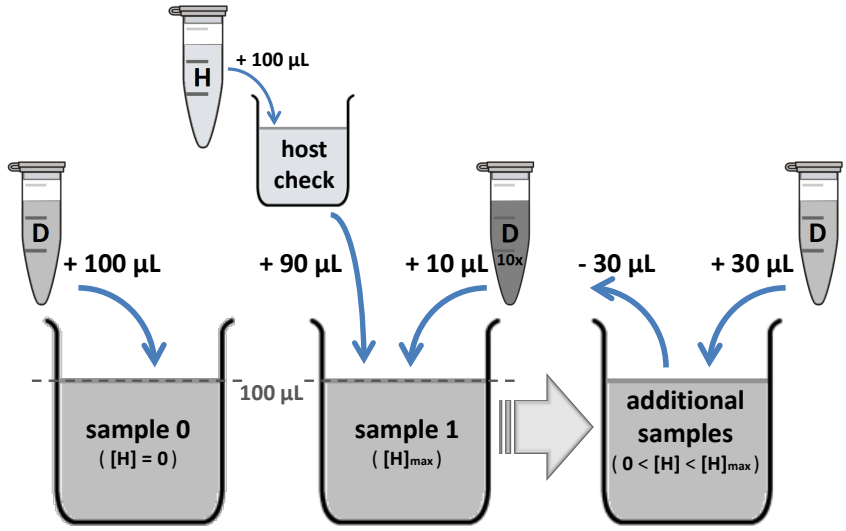

Figure 27. Scheme of the procedure used for sample preparation in titrations using minimal sample amounts. Eppendorf tubes represent the three stock solutions used to prepare all the different samples. Arrows represent the addition or removal of volumes in the well. In this example: $V_{load} = 100$ µL and $V_i = 30$ µL.

The samples will then be prepared from these stock solutions as follows (see Figure 27):

Sample 1 (maximum host concentration) is prepared by mixing in the same well nine parts of host stock with one part of *dye stock 10×*. As a function of the necessary volume to load a well, V_{load}, the required volumes are *0.9* V_{load} and *0.1* V_{load}, respectively.

Additional samples are prepared in the same well by first removing a certain volume, V_i, of the previous sample in the well and then adding the same volume of *dye stock*. This way, the dye concentration remains constant and the concentration of host, [H], in each sample is calculated from the previous one as follows:

$$[H]_i = [H]_{i-1}(1 - V_i/V_{load}) \quad (50)$$

Sample 0, at zero concentration of host, can be measured previously in the same well of the titration by measuring an aliquot of *dye stock*.

The stock of host must be measured beforehand in a different well to check the contribution of the possible fluorescent impurities. This solution can be used afterwards to prepare sample 1.

In order to keep the sample volume constant, especially if long measurement times are needed, it is important to avoid evaporation by covering the well with a cap.

Chapter II

Host-Guest Interactions studied by Bulk and Single Molecule Fluorescence Titrations

Contents:

PAPER 2: *Host-Guest Complexation studied by Fluorescence Correlation Spectroscopy: Adamantane-Cyclodextrin Inclusion.*

PAPER 3: *Host-Guest Association studied by Fluorescence Correlation Spectroscopy.*

Host-Guest Interactions studied by Fluorescence Techniques.

This chapter presents three publications to which the doctoral candidate has contributed. Through these three works the factors that control the structure and the stability of supramolecular host-guest assemblies are discussed together with the potential of Fluorescence Correlation Spectroscopy to obtain dynamic information of these interactions, which is essential for a full understanding of the mechanisms involved in this type of systems.

The first contribution *Host-Assisted Guest Self-Assembly: Enhancement of the Dimerization of Pyronines Y and B by γ-Cyclodextrin* (Bordello et al. 2009) represents the initial stage in the candidates thesis, in which UV/Vis absorption and fluorescence spectroscopy combined with advanced data analysis were used to study the role of small variations in the structural properties of host and guest molecules on the stoichiometry and strength of supramolecular associations. Previous studies in the research group using β-cyclodextrin as host and pyronines B or Y as guest showed that the stability and dynamics of the association between host and guest are both highly dependent on the substituents of the guest (Al-Soufi et al. 2005; Reija et al. 2005).

In this work the association between these two pyronines and a cyclodextrin with a bigger cavity (γ-cyclodextrin) was studied. The absorption spectra of the pyronines show complex variations with cyclodextrin concentration indicating that pyronine dimerization is strongly enhanced inside the cavity of the cyclodextrin. A full model was proposed and the equilibrium constants of the involved processes and the absorption and emission spectra of the different species (free dye, dye dimers, 1:1 and 2:1 complexes) were determined, showing that the equilibrium constant of the formation of complexed dimers are much higher than those for free dimerization or for the inclusion of a single guest. The role of the γ-cyclodextrin can be illustrated as a belt which assists the self-assembly of the pyronines. The differences in the stability of pyronine B and pyronine Y dimers were explained on the basis of their structure and geometry. Applying exciton theory, important structural differences between the two pyronines can be established regarding self-assembly, attributed to steric hindrance between the ethyl substituents in PB which would not allow parallel dimerization.

The dynamics of this system was studied by FCS in our research group, showing that the increase of the cavity size leads to an increase of the association rate constant and a decrease of the dissociation rate constant (Al-Soufi et al. 2008).

Standard fluorescence spectroscopic methods, although widely used due to their sensitivity, have an important limitation for the study of host-guest complexation: the requirement of a variation in a spectroscopic property of a fluorescent species due to the complexation. In

cases in which host and guest are nonfluorescent, FCS represents an excellent alternative for the determination of the stoichiometry and the association equilibrium constant in this type of systems. With a careful selection of the experimental conditions, FCS is a fast and relatively straightforward technique that needs only minimal amounts of host and guest. The equilibrium constant is determined by analyzing the variation in the diffusion coefficient of one of the species upon complexation, being the only requirement that the guest or host can be fluorescently labelled and that the complexation increases sufficiently the molar mass of the fluorescent species. Following this strategy, the complexation of a labelled adamantane and β-cyclodextrin was studied, determining a very high value of the association equilibrium constant which agrees well with that given in the literature for the inclusion of similar adamantane derivatives into βCD, studied with different techniques. This work is described in the second paper: *Host-guest Complexation studied by Fluorescence Correlation Spectroscopy: Adamantane-Cyclodextrin Inclusion* (Granadero et al. 2010).

As it was pointed out before, FCS gives also access to the association/dissociation rate constants of the host-guest inclusion providing that the fluorescence intensity of the fluorescent probe changes upon complexation. The potential and the limitations of FCS to study host-guest association and exchange dynamics are discussed in a third contribution, *Host-Guest Association studied by Fluorescence Correlation Spectroscopy* (Novo et al. 2011), in which the application of FCS to the study of host-guest inclusion complexes is reviewed. Also the influence of the host-guest geometry on the dynamics is analyzed through the comparison between two different types of host: cyclodextrins and micelles. The results show that cyclodextrin cavities act as “hard” cages which put geometric and orientational restrictions on the inclusion of a hydrophobic guest, whereas micelles behave as “soft” cages without geometrical requirements.

Host-Assisted Guest Self-Assembly: Enhancement of the Dimerization of Pyronines Y and B by γ-Cyclodextrin

Jorge Bordello, Belén Reija, Wajih Al-Soufi and Mercedes Novo

ChemPhysChem (2009), 10(6), 931-939.

Abstract: *The role of small variations in the structural properties of host and guest molecules on stoichiometry and strength of supramolecular association is analyzed. In previous works we found that a change in substituents from pyronine B to pyronine Y has a dramatic effect on both the stability and the dynamics of the association of these guests with β-cyclodextrin as host. Now we study the association between these two pyronines and a cyclodextrin with a bigger cavity (γ-cyclodextrin) using UV-Visible absorption and fluorescence spectroscopies. The absorption spectra of the pyronines show complex variations with cyclodextrin concentration indicating that pyronine dimerization is strongly enhanced inside the cavity of the cyclodextrin. A full model is proposed and the equilibrium constants of the involved processes and the absorption and emission spectra of the different species are estimated. The equilibrium constants of the formation of complexed dimers are much higher than those for free dimerization or for the inclusion of a single guest. The γ–cyclodextrin host assists like a belt the guest self-assembly. The differences in the stability of pyronine B and pyronine Y dimers are explained on the basis of their structure and geometry.*

1. Introduction.

The knowledge about the structural factors controlling non-covalent host-guest interactions is fundamental for the understanding of molecular recognition phenomena in biological systems, and it is also of great importance for the design of functional supramolecular systems with a wide range of applications. Structure and stability of supramolecular host-guest assemblies depend sensitively on the properties of host and guest molecules. Analysis of the dynamics of supramolecular association by fluorescence correlation spectroscopy (FCS) has shown the important interplay between geometrical requirements and specific interactions between host and guest.[1;2] The overall stability of the assembly depends on the balance between the geometric and orientational requirements limiting the association rate constant and the

strength of specific interactions controlling the dissociation process. Subtle changes in the geometry or electronic structure of host or guest can have a big influence on this balance and may lead to strong changes in the stability or even on the type of the supramolecular species formed.

Cyclodextrin inclusion complexes are simple and useful models for the study of this kind of intermolecular host-guest interactions. Cyclodextrins (CDs) are toroidally shaped polysaccharides with a highly hydrophobic central cavity which allows them to form inclusion complexes with many organic substrates.

In previous works we studied the host-guest interactions between the pyronines Y (PY) and B (PB) and β-cyclodextrin (βCD).[1;3] It was found that these two xanthene dyes (Figure 1) form inclusion complexes of stoichiometry 1:1 with βCD. The values of the corresponding stability constants show that the complex PB:βCD is about five times more stable than the complex PY:βCD. Specific interactions between the xanthene moiety and the electron-rich oxygens of the cyclodextrin cavity were suggested to be responsible for the stability of the complexes, as well as for their different photophysical properties with respect to free pyronines in aqueous solution. Dynamic studies performed by FCS yielded the individual rate constants of the association and dissociation processes.[1] The association rate constants of the two pyronines with βCD were found to be very similar but much lower than that of a diffusion-controlled collision process, which was attributed to geometrical and orientational requirements during the inclusion. The dissociation rate constant of the complex PB:βCD was, however, significantly smaller than that of PY:βCD. These results confirmed that the different stability of the two complexes is due to the specific host-guest interactions controlling the dissociation rate and not to the guest geometry itself.

In order to understand more deeply the factors controlling the stability of cyclodextrin complexes, further studies were performed with the same pyronines and a cyclodextrin of wider cavity, the γ-cyclodextrin (γCD). γCD is built up from 8 glucopyranose units instead of the 7 units of βCD so that the diameter of its inner cavity is increased in about 20% with respect to βCD (see Figure 1).[4] FCS studies yielded values of the association rate constants of the pyronines with γCD significantly larger than with βCD, as expected due to the lower geometrical restrictions imposed by the bigger cavity during inclusion of the guest.[2] Nevertheless, the dissociation rate constants increase even more due to weaker specific interactions between guest and host in the bigger cavity of γCD, so that the overall stability of the pyronine:γCD complexes is much lower than that of the pyronine:βCD complexes.

Apart from those differences in the association dynamics, the increase of the cavity size from βCD to γCD leads to further interesting changes in the complexation behavior of the

pyronines which are analyzed in this contribution. The association equilibriums between the pyronines and γCD are studied by means of absorption and fluorescence spectroscopies in order to determine the stoichiometries of the complexes formed, to obtain their corresponding stability constants and to characterize their structures on the basis of their photophysical properties.

The formation of inclusion complexes between pyronines PB and PY and the three natural cyclodextrins was studied earlier by Schiller et al. using equilibrium and temperature-jump visible spectrophotometries.[5-7] Nevertheless, the experimental conditions used (low CD concentrations and presence of 1.0 mol dm^{-3} NaCl in the aqueous solutions) and the strong approximations applied in the data analysis make their results unreliable. It is known that high ionic strengths have a great influence on the dye aggregation processes, which are important in the systems under study.[8]

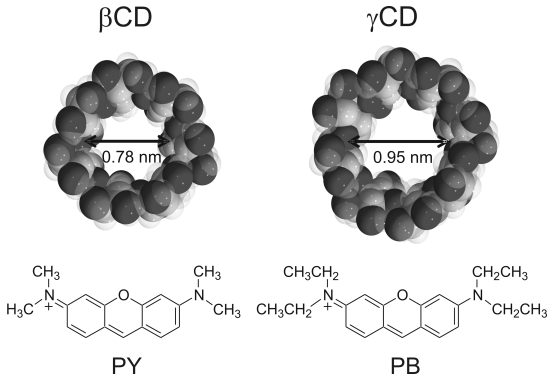

Figure 1. Structures and cavity sizes of βCD and γCD and structures of pyronines Y and B.

2. Results.

Series of absorption spectra (about 15 spectra in each series) of each pyronine in the presence of different concentrations of γCD were measured. Figure 2 shows some of the spectra for each series. As the concentration of γCD is increased, a decrease of the apparent molar absorptivity at the pyronine absorption maximum is first observed together with an increase of the absorptivity at the shoulder (see insets in Figure 2). At higher γCD concentrations the molar absorptivity at the shoulder decreases again and, in the case of PB, also an increase of molar absorptivity is observed at the pyronine absorption maximum. There are no clear isosbestic points for the whole range of γCD concentrations.

The possible aggregation of PY and PB in aqueous solution was studied by measuring series of absorption spectra of solutions with increasing pyronine concentrations (20 to 30 spectra in each series). Those absorption spectra are represented in Figure 3 in terms of the apparent

molar absorptivity, which allows to appreciate better the spectral changes as the concentration of pyronine is increased.

A systematic decrease of the apparent molar absorptivity at the pyronine absorption maxima with increasing pyronine concentrations is observed, together with an increase of the absorption at the shoulder in the case of PY. Clear isosbestic points are observed for both pyronines. In accordance, the plots of absorbance versus pyronine concentration show clear deviations from linearity at concentrations higher than 2 10^{-5} mol dm^{-3}. Stray light effects were ruled out since the experimental conditions were chosen to be within the linear range of the spectrophotometer, but a small contribution of the pyronine fluorescence emission was detected at the highest concentrations in the wavelength range where absorption and emission spectra overlap.

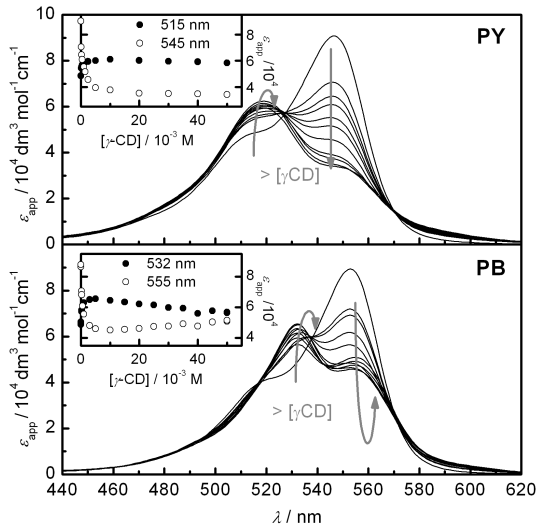

Figure 2. Absorption spectra of PY and PB in aqueous solution in the presence of different concentrations of γCD (0 to 0.050 mol dm^{-3}) at fixed pyronine concentrations (3.6 10^{-5} mol dm^{-3} for PY and 6.6 10^{-5} mol dm^{-3} for PB). Insets: Plots of the apparent molar absorptivity (in dm^3 mol^{-1} cm^{-1}) at two selected wavelengths versus γCD concentration.

Series of emission spectra of the two pyronines in the presence of different concentrations of γCD were measured (Figure 4). In both cases a decrease of the fluorescence intensity is observed as the concentration of γCD is increased, together with a slight shift of the emission spectrum to higher wavelengths. The plots of the fluorescence intensity versus γCD concentration (insets in Figure 4) show that the decrease is steeper for PB than for PY.

Also time-resolved fluorescence measurements were performed for solutions of the pyronines with different concentrations of γCD. Table 1 gives the fluorescence lifetimes and amplitudes obtained in the fits of a multiexponential model to the fluorescence decays. In the absence of

γCD and at low concentrations the decays are monoexponential for PY and biexponential for PB, although in the latter the second lifetime has a minor contribution that is independent of γCD concentration. At a γCD concentration of 0.050 mol dm^{-3} and larger, a shorter lifetime is detected whose amplitude seems to increase slightly with the concentration of γCD. Since all the lifetimes are short for the time resolution of the instrument used, it was necessary to fix one of the lifetime values in some of the fits to avoid parameter correlation. This might have some effect on the amplitude values, which are highly dependent on slight changes of the lifetime values.

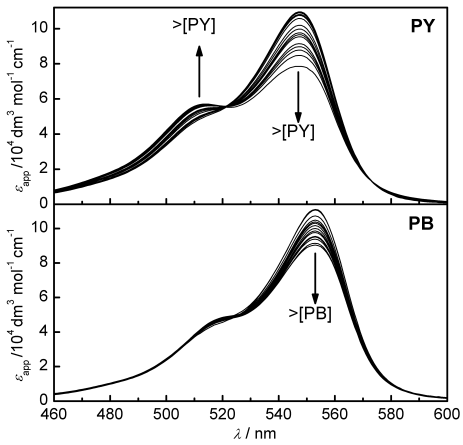

Figure 3. Absorption spectra of PY and PB in aqueous solution as a function of pyronine concentration, varying from 8 10^{-6} to 1.1 10^{-4} mol dm^{-3} for PY and from 3 10^{-6} to 1.0 10^{-4} mol dm^{-3} for PB.

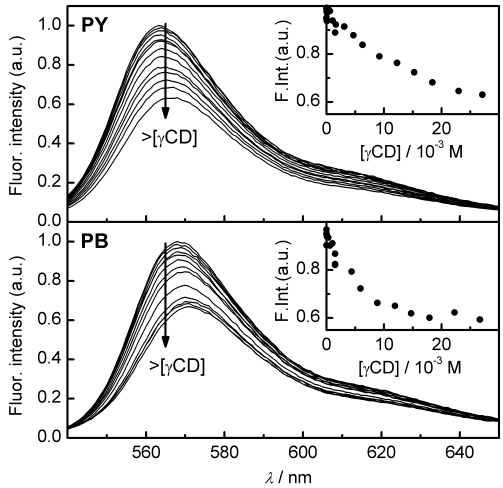

Figure 4. Corrected emission spectra of PY and PB in aqueous solution in the presence of different concentrations of γCD (0 to 0.027 mol dm^{-3}) at fixed pyronine concentration (2.0 10^{-7} mol dm^{-3} for PY and PB). Insets: Plots of fluorescence intensity at 565 nm vs. [γCD].

Table 1. Fluorescence lifetimes, amplitudes and chi square values obtained in the individual fits of a multiexponentional model to the fluorescence decays of PY and PB in the presence of different concentrations of γCD (pyronine concentration = 1.0 10^{-6} mol dm^{-3}). The sum of the amplitudes (A_i) has been normalized to 100 to facilitate comparison.

[γCD] /mol dm^{-3}	τ_1 /ns (A_1)	τ_2 /ns (A_2)	τ_3 /ns (A_3)	χ^2
		PY + γCD		
0		1.687 ± 0.004 (100)		1.10
0.00025		1.689 ± 0.004 (100)		1.01
0.0015		1.689 ± 0.004 (100)		1.16
0.0050	1.2 ± 0.2 (30)	1.81 ± 0.06 (70)		1.09
0.0100	1.09 ± 0.05 (30)	1.8 (fixed) (70)		1.07
0.0300	1.07 ± 0.05 (30)	1.8 (fixed) (70)		1.13
0.0500	1.1 ± 0.1 (36)	1.85 ± 0.04 (64)		1.13
		PB + γCD		
0		1.07 ± 0.02 (97)	2.3 ± 0.4 (3)	1.08
0.00025		1.08 ± 0.02 (97)	2.6 ± 0.6 (3)	1.11
0.00075		1.049 ± 0.006 (97)	2.5 (fixed) (3)	1.13
0.0015		1.03 ± 0.02 (97)	2.1 ± 0.4 (3)	1.18
0.0050	0.75 ± 0.09 (30)	1.2 (fixed) (67)	4 ± 1 (1)	1.21
0.0100	0.79 ± 0.08 (44)	1.2 (fixed) (53)	3.2 ± 0.7 (3)	0.98
0.0300	0.76 ± 0.08 (44)	1.2 (fixed) (53)	3.0 ± 0.5 (3)	1.04
0.0500	0.55 ± 0.08 (30)	1.2 (fixed) (68)	2.9 ± 0.3 (3)	1.16

3. Discussion.

3.1. Stoichiometry and Model Determination.

The variations of the absorption spectra of PY and PB in the presence of different concentrations of γCD (Figure 2) cannot be explained by a simple 1:1 association as in the case of βCD.[3] The lack of clear isosbestic points and the nonmonotonic dependence of the apparent molar absorptivity with the γCD concentration (see insets in Figure 2) show that there must be more than two absorbing species in equilibrium. Moreover, analysis of the series of absorption spectra with PCA yield for both pyronines 3 to 4 structural components contributing to the experimental spectra (see Figures 1S and 2S in the Supporting Information). Therefore, formation of complexes of higher stoichiometries must be considered. Taking into account the tendency of xanthene dyes to aggregate in aqueous solutions[8] and the bigger cavity of γCD compared to βCD, pyronine dimers and/or inclusion complexes of the dimers (2:1 pyronine:CD complexes) are possible species contributing to the observed absorption spectra. As mentioned above, formation of 2:1 and even 2:2 complexes of these pyronines with γCD has been reported in the literature, but formation of pyronine dimers was not taken into account.[5-7] However, the experimental conditions used in those works were very different to ours and the models proposed were not satisfactorily justified.

In order to investigate the dimerization of the pyronines in aqueous solution, absorption measurements were performed with varying pyronine concentrations in absence of γCD (Figure 3). Experimental absorption spectra show systematic variations of the apparent molar absorptivity with clear isosbestic points as the concentration of pyronine is increased, suggesting formation of dimers. This is confirmed by the results of the PCA analysis of these series of absorption spectra up to pyronine concentrations of (6 - 8) 10^{-5} mol dm^{-3}, that yield two structural components which are attributed to pyronine monomers and dimers (see Figures 3S and 4S in the Supporting Information). It must be noted that, if the spectra of the solutions with even higher pyronine concentrations are included in the PCA analysis, a third component is observed due to the contribution of fluorescence emission at long wavelengths as mentioned before.

Taking into account all these experimental findings, a general mechanism is proposed for the association of the pyronines with γCD, where 1:1 and 2:1 pyronine: γCD inclusion complexes are included (P: γCD and P2: γCD in Scheme 1, respectively). Formation of the 2:1 complexes can take place by association of a second pyronine molecule with a 1:1 complex as well as by inclusion of a pyronine dimer (P2) into the γCD cavity. Thus, the proposed mechanism is cyclic with four species present in equilibrium. If the concentration of pyronine is too low to yield dimers, the 2:1 complexes can anyhow be formed from the 1:1 complexes.

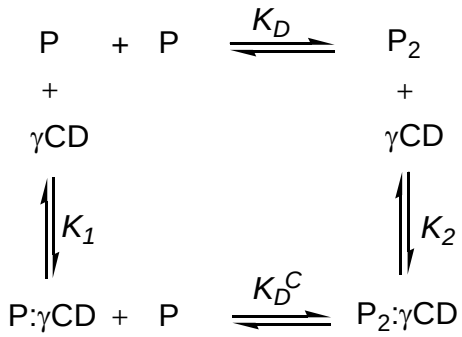

Scheme 1. Mechanism proposed to explain the association of PY and PB with γCD in aqueous solution including four absorbing species: pyronine monomer (P), pyronine dimer (P_2), 1:1 complex (P:γCD) and 2:1 complex (P_2:γCD). These species are interconnected through four equilibria characterized by their corresponding equilibrium constants K_D, K_1, K_2 and K_D^C.

The equilibrium constants in Scheme 1 are functions of the equilibrium concentrations of the different species as given by equations (1-4):

$$K_1 = \frac{[\mathrm{P{:}\,\gamma CD}]}{[\mathrm{P}][\gamma\mathrm{CD}]} \tag{1}$$

$$K_2 = \frac{[\mathrm{P_2{:}\,\gamma CD}]}{[\mathrm{P_2}][\gamma\mathrm{CD}]} \tag{2}$$

$$K_\mathrm{D} = \frac{[\mathrm{P_2}]}{[\mathrm{P}][\mathrm{P}]} \tag{3}$$

$$K_\mathrm{D}^\mathrm{C} = \frac{[\mathrm{P_2{:}\,\gamma CD}]}{[\mathrm{P}][\mathrm{P{:}\,\gamma CD}]} \tag{4}$$

From the definitions of the equilibrium constants it is easily deduced that only three of them are independent, being the fourth a combination of the others:

$$K_\mathrm{D}^\mathrm{C} = \frac{K_\mathrm{D} K_2}{K_1} \tag{5}$$

The mechanism proposed in Scheme 1 must also be in agreement with the results of fluorescence measurements. The series of emission spectra with varying γCD concentration (Figure 4) are very similar to those obtained with βCD, where only free pyronine and 1:1 complex were observed.[3] As in that case, analysis with PCA yields only two structural components contributing to the experimental emission spectra (see Figures 5S and 6S in the Supporting Information). This seems to be in disagreement with the proposed mechanism but, taking into account that the pyronine concentration used in fluorescence measurements

is much lower than in absorption measurements, the equilibrium concentrations of pyronine dimers should be negligible and also insignificant concentrations of 2:1 complex are expected to be present. Moreover, the dimers of xanthene dyes are typically non fluorescent[8] so that even if some small amounts of those species were present, they would not be detected in fluorescence measurements. Therefore, the emission spectra of the pyronines with varying γCD concentration are considered to be contributed by only two fluorescence species in equilibrium, free pyronine P and 1:1 complex P:γCD.

The results of time-resolved fluorescence measurements are in perfect agreement with the above interpretation. Single fluorescence lifetimes corresponding to those of the free pyronines are obtained in the absence of γCD and at low concentrations of γCD, whereas second shorter lifetimes are observed at higher γCD concentrations. As in the case of βCD, the shorter lifetimes are attributed to the 1:1 complexes of the pyronines with γCD.[3] The equilibrium concentrations of these complexes increase with γCD concentration and therefore the amplitudes corresponding to those lifetimes increase whereas the amplitudes of the pyronine lifetimes decrease. In the case of PB, the third residual lifetime is attributed to a hydrolysis product of this pyronine, which was also observed in the measurements with βCD.

3.2. Quantitative Analysis.

Now a quantitative analysis of the experimental data must be performed in order to check the validity of the proposed mechanism and to determine the spectra of the different species present and the equilibrium constants involved. However, resolving such a complex mechanism makes it necessary to follow a systematic analysis procedure. In a first step, the dimerization of the pyronines in the absence of γCD is analyzed in order to determine the corresponding equilibrium constants K_D and the absorption spectra of the dimers. The second step is the analysis of the series of emission spectra to obtain information about the 1:1 complexation process, specially the association equilibrium constants K_1. Using all this information, the series of absorption spectra of the pyronines with different concentrations of γCD are analyzed on the basis of the complete mechanism to obtain the equilibrium constants K_2 and the absorption spectra of the 1:1 and 2:1 complexes.

In the absence of γCD only the dimerization process in Scheme 1 must be considered, as shown in Scheme 2.

$$P + P \overset{K_D}{\rightleftharpoons} P_2$$

Scheme 2. Dimerization of PY and PB in absence of γCD.

Taking into account the definition of K_D (equation 3), the equilibrium concentrations of the pyronine monomers and dimers are related to the total pyronine concentration $[P]_0$ as follows:

$$[P] = \frac{-1 + \sqrt{1 + 8K_D[P]_0}}{4K_D} \quad (6)$$

$$[P_2] = \frac{[P]_0}{2} + \frac{1 - \sqrt{1 + 8K_D[P]_0}}{8K_D} \quad (7)$$

and the apparent molar absorptivity at a wavelength λ is the sum of contributions of these two species:

$$\varepsilon_{app}(\lambda) = \varepsilon_P(\lambda)\frac{[P]}{[P]_0} + \varepsilon_{P_2}(\lambda)\frac{[P_2]}{[P]_0} \quad (8)$$

where $\varepsilon_x(\lambda)$ denotes the molar absorptivity of species X at λ.

Table 2. Values of the equilibrium constants defined in Scheme 1 for PY and PB with γCD. The values of K_D and K_2 were obtained in the fits of absorption data and those of K_1 in the fits of emission data, except for the value given in parenthesis which results from the analysis of absorption data (see text). The values of K_D^C were calculated using equation 5.

	PY + γCD	PB + γCD
K_D / 10^3 mol^{-1} dm^3	3.0 ± 0.5	5.0 ± 0.8
K_1 / 10^3 mol^{-1} dm^3	0.04 ± 0.01 (≈0.07)	0.19 ± 0.04
K_2 / 10^3 mol^{-1} dm^3	26 ± 4	8.3 ± 0.5
K_D^C /10^3 mol^{-1} dm^3	(2.0 ± 0.7) 10^3	(2.2 ± 0.6) 10^2

Equation 8 can now be used as fit function in the global analysis of the series of absorption spectra with varying pyronine concentrations (Figure 3). Nevertheless, for these fits to be correct, the distorting effect of fluorescence emission on the absorption spectra detected at high pyronine concentrations and long wavelengths should be eliminated. This implies that either the concentration range or the wavelength range must be limited for the analysis. For the determination of the dimerization equilibrium constants, the whole concentration range should be used in order to increase the contribution of the dimer to absorption. Therefore, fits of equation 8 were performed using the whole concentration dataset but only the short wavelengths range (440-525 nm for PY and 440-540 nm for PB). In these fits, the values of K_D listed in Table 2 were obtained. The order of magnitude of these values is typical for

xanthene dyes,[8] but they are somewhat higher than those reported for these pyronines in aqueous solution.[9] Afterwards the complete absorption spectra of the pyronines monomer and dimer were determined in further fits using the whole wavelength range but a limited concentration range (up to 5-6 10^{-5} mol dm^{-3}) and fixing K_D to the value obtained before (Figure 5). The spectra of the monomers coincide perfectly with the experimental absorption spectra of PY and PB at the lowest concentrations, validating the analysis procedure. The spectra of the dimers are slightly dependent on the concentration range and/or the value of K_D used. However, absorption maximum and band splitting are not significantly affected (see Figure 7S in the Supporting Information). These spectra coincide very well with those published before,[9;10] except for the absolute values of the molar absorptivities reported for the dimers which are a half of the true values due to an error in the dimer concentrations that these authors used.

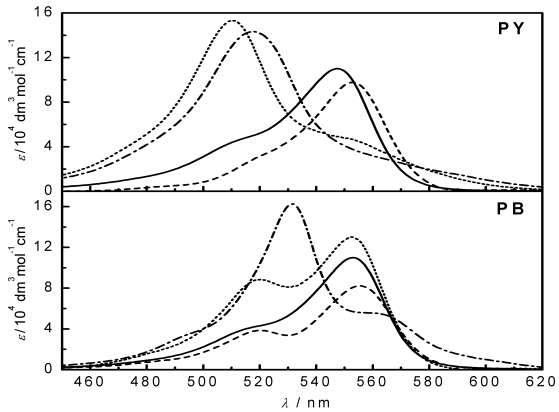

Figure 5. Absorption spectra of the different species present in equilibrium in aqueous solutions of the pyronines PY and PB in the presence of γCD: free pyronine monomer P (solid line), pyronine dimer P_2 (dotted line), P:γCD complex (dashed line) and P_2:γCD complex (dashed-dotted line).

The next step is the analysis of the series of emission spectra. Also in this case the mechanism in Scheme 1 can be simplified, since the only fluorescent species present are the free pyronines and their 1:1 complexes linked by the equilibrium given in Scheme 3:

$$P + \gamma CD \underset{}{\overset{K_1}{\rightleftharpoons}} P{:}\gamma CD$$

Scheme 3. Equilibrium of 1:1 association between pyronines PY and PB and γCD.

Under the assumptions that no interconversion processes take place in the excited state (since the association and dissociation rates cannot compete with the deactivation rates of the excited species[1;2]) and that the cyclodextrin equilibrium concentration coincides with its initial concentration (excess of γCD compared to pyronine), the following equation is obtained

for the dependence of the fluorescence intensity at a certain wavelength, $F(\lambda)$, with γCD concentration:

$$F(\lambda) = \frac{F_{\mathrm{P}}(\lambda) + F_{\mathrm{P:\gamma CD}}(\lambda)\, K_1\, [\gamma\mathrm{CD}]_0}{1 + K_1[\gamma\mathrm{CD}]_0} \qquad (9)$$

where $F_{\mathrm{P}}(\lambda)$ and $F_{\mathrm{P:\gamma CD}}(\lambda)$ are the fluorescence intensities at wavelength λ when all the pyronine were free and complexed, respectively.

Using equation 9 as fit function, global analysis was performed for the series of emission spectra of the two pyronines with γCD. The fits were very satisfactory and gave the values of the 1:1 association equilibrium constants K_1 listed in Table 2 and the emission spectra of species P and P:γCD (Figure 6). The uncertainties in the K_1 values reflect the differences found among several series of data. The spectra of the free pyronines obtained from our fits coincide with those measured experimentally in the absence of cyclodextrin, validating again the proposed model. The emission spectra calculated for the complexes P: γCD are similar to those of the complexes P:βCD,[3] as shown in Figure 6. The good fits and the satisfactory spectra of the species involved confirm that there is no contribution of the pyronine aggregates to the emission, as it was also observed for the aggregates of these pyronines in colloidal solutions.[11]

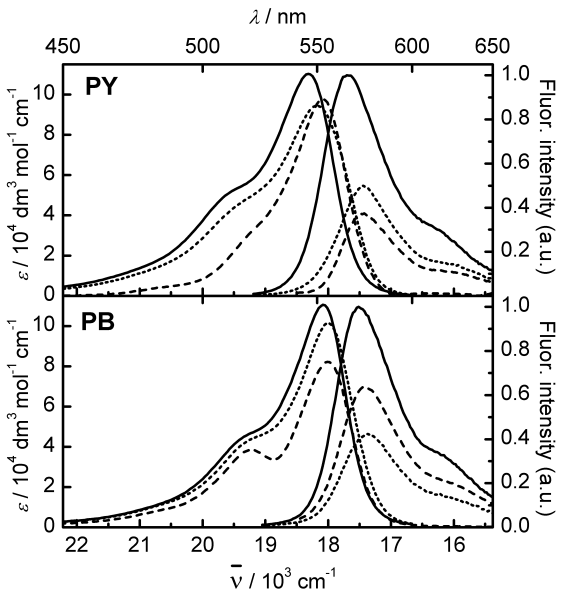

Figure 6. Absorption and emission spectra of PY and PB as free monomers in aqueous solution (solid lines) and forming 1:1 complexes with βCD[3] (dotted lines) and with γCD (dashed lines).

The results of time-resolved fluorescence measurements (Table 1) are in agreement with the analysis above. For each pyronine two lifetimes are observed whose values do not vary with the concentration of γCD, indicating that the association process in the excited-state does not compete with the deactivation process. The shorter lifetime, which was attributed to the complex P:γCD, is not observed at the lowest γCD concentrations, since the equilibrium constants K_1 are relatively low (Table 2) and therefore the concentration of complex is small at those concentrations. Moreover, it must be noted that both the lifetimes of the free pyronines and those of their complexes are short for the time resolution of our system so that it is difficult to obtain accurate values of these lifetimes. This problem also affects the preexponential factors, which approximately show the expected tendencies (the amplitude of the free-pyronine lifetime decreases with the concentration of γCD and that corresponding to the complex increases) but are too inaccurate to be quantitatively analyzed as it was done in the case of βCD.[3]

Finally, we will deal with the analysis of the series of absorption spectra of the pyronines in the presence of different concentrations of γCD (Figure 2). As proposed above, these spectra are contributed by the four species in equilibrium shown in Scheme 1. Taking into account the definitions of the equilibrium constants (equations 1 to 4) and the matter balances for γCD and for the pyronines, the following equations are obtained for the equilibrium concentrations of the four species under conditions of excess of γCD ($[\gamma\mathrm{CD}]_0 \gg [\mathrm{P}]_0$):

$$[\mathrm{P}] = \frac{-(1 + K_1[\gamma\mathrm{CD}]_0) + \sqrt{(1 + K_1[\gamma\mathrm{CD}]_0)^2 + 8K_\mathrm{D}(1 + K_2[\gamma\mathrm{CD}]_0)[\mathrm{P}]_0}}{4K_\mathrm{D}(1 + K_2[\gamma\mathrm{CD}]_0)} \tag{10}$$

$$[\mathrm{P_2}] = K_\mathrm{D}[\mathrm{P}]^2 \tag{11}$$

$$[\mathrm{P{:}\gamma CD}] = K_1[\gamma\mathrm{CD}]_0[\mathrm{P}] \tag{12}$$

$$[\mathrm{P_2{:}\gamma CD}] = K_\mathrm{D}K_2[\gamma\mathrm{CD}]_0[\mathrm{P}]^2 \tag{13}$$

The apparent molar absorptivity measured at a certain wavelength λ is the sum of the contributions of the four species:

$$\varepsilon_{\mathrm{app}}(\lambda) = \frac{1}{[\mathrm{P}]_0}\left(\varepsilon_\mathrm{P}(\lambda)[\mathrm{P}] + \varepsilon_{\mathrm{P_2}}(\lambda)[\mathrm{P_2}] + \varepsilon_{\mathrm{P{:}\gamma CD}}(\lambda)[\mathrm{P{:}\gamma CD}] + \varepsilon_{\mathrm{P_2{:}\gamma CD}}(\lambda)[\mathrm{P_2{:}\gamma CD}]\right) \tag{14}$$

This equation was used as fit function in the global analysis of the series of absorption spectra of the pyronines with fixed pyronine concentrations and varying concentrations of γCD (Figure 2) applying PCGA. The global nonlinear fit parameters are the three equilibrium constants (K_1, K_2 and K_D). The molar absorptivities of the four contributing

species, which make up their characteristic absorption spectra, were fitted as linear global parameters. Nevertheless, in order to minimize statistical correlation among these parameters, K_1 and K_D were fixed at the values obtained in the analysis above (Table 2) as well as the molar absorptivities of monomer and dimer of each pyronine (absorption spectra shown in Figure 5). In the case of PB the fits were straightforward and very satisfactory and yielded the value of K_2 listed in Table 2 and the spectra of the complexes PB:γCD and PB2:γCD shown in Figure 5. Varying the value of K_1 within its uncertainty interval leads to small changes in the fitted spectrum of PB:γCD but has a negligible effect on the absorption spectrum of PB_2:γCD (see Figure 8S in the Supporting Information). Nevertheless, in the case of PY, there is a strong correlation among the fit parameters K_2 and the molar absorptivities of the complexes PY:γCD and PY_2:γCD that must be controlled to get a satisfactory fit. For this purpose, a preliminary spectrum for PY_2:γCD was determined using only the experimental data at concentrations of γCD higher than $1.5\ 10^{-3}$ mol dm^{-3}, at which the contribution of the dimer PY_2 can be neglected. Then the whole data set was analyzed in an iterative process looking for the chi-square minimum where either the spectrum of PY_2:γCD or the value of K_1 was fixed as well as K_D and the spectra of PY and PY_2. The best fit was achieved for the values of K_1 and K_2 given in Table 2 and for the spectra shown in Figure 5 of the complexes PY:γCD and PY_2:γCD. The value of K_1 is higher than that obtained from emission measurements but of the same order of magnitude. Lower values of K_1 provoked significant distortions of the PY:γCD spectrum at the low wavelength range, but the value of K_2 (Table 2) and the spectral properties of PY_2:γCD were not significantly affected (see Figure 8S in the Supporting Information).

The values obtained for K_2 are in good agreement with the values reported in the literature for PY and PB, although in those works the experiments were performed in aqueous solutions of 1.0 mol dm^{-3} NaCl and at 25°C.[5;6] Also absorption spectra for the P_2:γCD complexes were estimated in those works, which have similar properties as our spectra. Nevertheless, in those estimations it was assumed that the spectra of the P:γCD complexes were the same as the spectra of the monomers, which is a very strong assumption. Our analysis shows that the absorption spectra of the P:γCD complexes are quite different to those of the free monomers (Figure 5) and that they have a strong influence on the spectra determined for the P_2:γCD complexes.

3.3. Discussion of Results.

On the basis of the results presented so far we will first discuss the properties of P:CD (1:1) complexes, then the formation of complexed dimers P_2:γCD and finally the relative orientation of the guests in the dimers.

As already determined in dynamic studies of these systems, the increase of cavity size in γCD with respect to βCD has a great effect on the stability of the P:CD complexes.[1;2] The values obtained for the 1:1 association equilibrium constant of the pyronines with γCD (K_1 in Table 2) are one order of magnitude smaller than those determined with βCD,[3] a result that has been explained on the basis of the association dynamics of these systems studied by FCS. Moreover, the complexes PB:CD are about 5 times more stable than those formed by PY both with βCD and γCD. This is due to the stronger interaction of PB with the interior of the CD cavity that is reflected in the smaller dissociation rate constants.[2] Nevertheless, P:γCD and P:βCD complexes show very similar photophysical properties, as shown in Figure 6. Both the absorption and the emission spectra of these complexes are slightly red shifted with respect to the spectra of the corresponding free pyronines. Fluorescence quantum yield decreases in the complexes with respect to free pyronines as well as fluorescence lifetime, due to the increase of the nonradiative deactivation rate constant (see Table 3). This increase is smaller in the complexes P:γCD reflecting again the weaker specific interactions of the pyronines with the CD of bigger cavity.

Table 3. Fluorescence lifetimes, fluorescence quantum yields, radiative deactivation rate constants and nonradiative deactivation rate constants of PY and PB in aqueous solution and their 1:1 complexes with βCD and with γCD.

	τ /ns	φ	k_r / 10^9 s^{-1}	k_{nr} / 10^9 s^{-1}
PY[3]	1.76	0.47	0.27	0.30
PY:βCD[3]	1.08	0.27	0.25	0.68
PY:γCD	1.1	0.33	0.30	0.61
PB[3]	1.20	0.36	0.31	0.56
PB:βCD[3]	0.50	0.19	0.38	1.6
PB:γCD	0.75	0.27	0.36	0.97

But the larger cavity size of γCD with respect to βCD has another important effect on the complexation behavior of these systems: the efficient formation of P_2:γCD complexes which are highly stabilized through cooperative interactions. These complexed pyronine dimers are observed already at low pyronine concentrations where formation of free dimers is negligible. The addition of γCD causes thus a strong enhancement of pyronine dimerization. This effect

illustrates the great potential of CDs as molecular reactors and catalyzers[12;13] and as a tool to assist guest self-assembly. The different complexation stoichiometries lead to a complicated mechanism for the interaction of the pyronines with γCD (Scheme 1), where pyronine dimerization is included as a second pathway for the formation of P_2:γCD complexes. For the interaction of these pyronines with βCD the mechanism is much simpler, since the cavity size is too small for the formation of 2:1 complexes and, at the concentrations used in those measurements, pyronine dimerization needs not to be taken into account.[3]

The values of the equilibrium constants given in Table 2 allow us to calculate the equilibrium concentrations of each species present as functions of γCD concentration using equations 10 to 13. As expected, the relative concentrations of species P_2 and P_2:γCD are highly dependent on the total pyronine concentration, being negligible at the concentrations used for emission measurements. This supports the assumption made for the analysis of the series of emission spectra. The concentration of P_2 decreases rapidly when adding γCD, whereas that of P_2:γCD increases at low γCD concentrations and decreases afterwards. In spite of the low values of K_1 and the high values of K_D^C, P:γCD concentration increases as the concentration of γCD is increased and it is the predominant species at high γCD concentrations, except in the case of high dye concentrations. This can be understood since in our studies the total pyronine concentration is much lower than that of γCD, so that a P:γCD complex has a very low probability to find a second free pyronine molecule to form a P_2:γCD complex. This would not be the case if dye and γCD concentrations were comparable.

The capacity of γCD to enhance pyronine dimerization can be quantified by comparing the equilibrium constant K_D with the product $K_1 K_D^C$ (see Scheme 1 and Table 2). Their values indicate that dimer formation inside the γCD cavity is 8 and 26 times enhanced, for PB and PY respectively, with respect to aqueous solution. Although no dynamic information is available for the dimer formation, the high value of K_D^C suggests the importance of cooperative effects during the formation of the P_2:γCD complexes and that hydrophobic interactions play an important role in the stability of the pyronine dimers, as already proposed for other dyes.[8] Comparing the two pyronines, the dimerization enhancement is significantly larger for PY than for PB, as reflected in the higher stability constant K_2 of the complex PY_2:γCD compared to PB_2:γCD (see Table 2). This difference may be attributed to the better fit of two PY molecules inside the γCD cavity in comparison to the bulkier PB, but the necessary reorientation of the PB dimers could also play an important role, as it will be discussed below.

The absorption spectra of species P_2 and P_2:γCD obtained by global analysis of the experimental data (Figure 5) provide interesting information about the geometries of the dimers of the two pyronines by applying exciton theory.[14;15] For both pyronines the

absorption spectra of the P_2:γCD complexes show single bands which are blue shifted with respect to the spectra of the monomers, indicating a parallel geometry (H-type or "sandwich") in both cases. On the contrary, the free dimers of PY and PB have different spectral properties. The spectrum of PY_2 shows a single blue-shifted absorption band typical of a "sandwich" H-type aggregate, whereas the spectrum of PB_2 has two bands indicating a geometry in between a parallel dimer and a head-to-tail dimer (J-type). In order to obtain more quantitative information about the geometries of the dimers, their absorption spectra were decomposed in several Gaussian curves and the oscillator strength ratios between blue and red bands were calculated. For PY_2 and the two complexed dimers, PY_2:γCD and PB_2:γCD, these ratios are higher than 1.3, confirming that they are H-type (see Figure 7).[16] In the case of PB_2, the ratio of oscillator strengths corresponds to an oblique head-to-tail dimer with an angle between the monomer units of about 100°, as represented in Figure 7. These results suggest that PB_2 has to undergo a great geometrical change when it is included inside the γCD cavity, which should reduce the association rate constant and may explain the lower stability of the complex PB_2:γCD in comparison to PY_2:γCD.

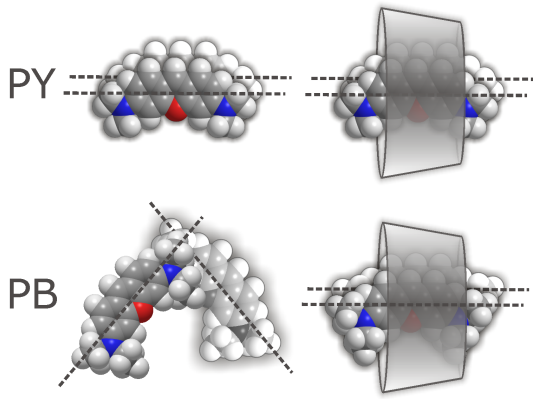

Figure 7. Approximate geometries of the free dimers PY_2 and PB_2 and of the complexed dimers PY_2:γCD and PB_2:γCD as derived from their absorption spectra.

The results obtained in this work give again evidence of the important differences in the aggregation and complexation behavior of the two pyronines derived from the simple substitution of the methyl groups by ethyl groups. In the case of the P:CD complexes, the stability is determined by the strength of the specific interactions between the xanthene moiety and the interior of the CD cavity, being potential steric effects of the side groups negligible. On the contrary, the bulkier ethyl groups of PB hinder parallel dimerization in the free dimers and decrease the stability of the complexed dimer. The γCD cavity assists like a belt the self-assembly of the pyronines stabilizing dimers which do not significantly form on their own.

4. Experimental Section.

Materials.

PY was purchased from Sigma (51% dye content) and PB from Aldrich (57% dye content). The main impurities of these materials are not water soluble, so that they can be separated by filtration of the aqueous solutions.[6] γCD (Sigma-Aldrich) was used as delivered. The pH of the solutions was controlled by addition of $HClO_4$ (Merck, p.a.). Water was purified with a Milli-Q system.

Sample Preparation.

Stock solutions of PY and PB were prepared as reported before and were stable within 2-3 days when kept protected from light.[3] The absence of fluorescence impurities in these stocks was checked by comparing the excitation and the emission fluorescence spectra of diluted aqueous solutions monitored at different emission and excitation wavelengths, respectively. The concentrations of the stocks were estimated using the literature value of $\varepsilon = 1.1\ 10^5\ mol^{-1}\ dm^3\ cm^{-1}$ for the molar absorptivity of both PY[17] and PB[5] at their respective absorption maxima. Very diluted samples were used for this estimation to avoid the effect of pyronine aggregation. The inaccuracy of these concentrations, inferred from the disagreement of the reported molar absorptivity values, has a direct effect on the absolute values obtained for the equilibrium constants but has not been taken into account for the estimation of their errors.

Aqueous solutions for measurements were freshly prepared by dilution of the stocks, with pyronine concentrations in the range $(0.03\text{-}1)\ 10^{-4}\ mol\ dm^{-3}$ for absorption and $(0.2\text{-}1)\ 10^{-6}\ mol\ dm^{-3}$ for fluorescence. Dilution was made using $HClO_4$ solutions of pH 4.0 ± 0.5 instead of water in order to minimize the hydrolysis of the pyronines. Samples of varying CD concentration were prepared by addition of different volumes of a γCD stock solution (concentration about 0.050 mol dm^{-3}). Adsorption of the pyronines on glass surfaces caused poor reproducibility of fluorescence intensity, especially in the case of PB. In order to minimize this problem the glass flasks were rinsed several times with pyronine solutions of the desired concentration and small amounts of γCD were added to the PB stocks for the titration experiments. Also quartz cells were used, since the adsorption on this material was negligible. No deoxygenation of the samples for time-resolved measurements was necessary since these pyronines have short fluorescence lifetimes.

Absorption Measurements.

Absorption spectra were recorded in a Varian-Cary 300 spectrometer using quartz cells. Baselines of 0% and 100% transmittance were recorded with water in both sample and reference cells. Cells of 10.0 mm and 4.0 mm path length (ℓ) were used to cover a wide range of concentrations in each series assuring that the absorbance values were within the linear range of the spectrometer. The linear range of the spectrometer was checked to be up to an absorbance of 4.25, as determined with solutions of different concentrations of methyl orange. These solutions were also measured with the two cells of different path lengths in order to obtain the exact conversion factor. The absorption spectra are shown in units of apparent molar absorptivity ε_{app} (i.e., $A/\ell C_0$) to eliminate the effect of the different path lengths and dye concentrations on the measured absorbances. The optical effect of the cyclodextrin on the absorption spectra was corrected using a γCD solution with the same concentration as the sample solution as reference. Temperature was kept constant at 20 ± 1 °C during the measurements.

Fluorescence measurements.

Both steady-state and time-resolved fluorescence measurements were performed with an Edinburgh-Instruments F900 spectrofluorimeter, equipped with a Xenon lamp of 450 W as excitation source for steady-state measurements and a hydrogen-filled nanosecond flashlamp for lifetime measurements using the time-correlated single photon counting technique. Excitation wavelengths were 515 nm for steady-state emission spectra and 310 nm in time-resolved measurements. Fluorescence decays were measured at 565 nm with a TAC resolution of 0.053 ns but were limited by the pulse width (typical half width 1.5 ns). All decays were measured up to 10000 counts at maximum. Emission spectra were corrected for the wavelength dependence of the detection system. All experiments were carried out at 20 ± 1 °C.

Absolute quantum yields were determined using rhodamine B in basic ethanol as the standard, with a reported value of 0.70 for its fluorescence quantum yield.[18]

Data analysis.

The series of absorption and emission spectra obtained in the titrations with γCD were analyzed using Principal Components Global Analysis (PCGA).[19] This method can be applied to series of spectra which vary with an external parameter, as the γCD concentration or the pyronine concentration in our case. The first step of PCGA is a Principal Components Analysis (PCA), where the minimal number of spectral components responsible for the observed variations is obtained. This information helps to draw up a theoretical model that is

used in the second step as a fit function for a nonlinear least-squares global analysis using the whole spectra as a dataset. The results of this global fit are the values of the physicochemical parameters involved in the model and the individual spectra of the components.

Individual fits of fluorescence decays were performed with the software package from Edinburgh Instruments using deconvolution of the lamp pulse. The series of decays at different γCD concentrations were also analyzed with the above-described PCGA using a modified procedure that allows deconvolution of the lamp pulses.

References.

[1] W. Al-Soufi, B. Reija, M. Novo, S. Felekyan, R. Kühnemuth, C. A. M. Seidel, *J. Am. Chem. Soc.* 2005, *127* 8775.

[2] W. Al-Soufi, B. Reija, S. Felekyan, C. A. M. Seidel, M. Novo, *ChemPhysChem,* 2008, *9* 1819

[3] B. Reija, W. Al-Soufi, M. Novo, J. Vázquez Tato, *J. Phys. Chem. B* 2005, *109* 1364.

[4] J. Szejtli, *Chem. Rev.* 1998, *98* 1743.

[5] R. L. Schiller, S. F. Lincoln, J. H. Coates, *J. Chem. Soc., Faraday Trans. 1* 1986, *82* 2123.

[6] R. L. Schiller, S. F. Lincoln, J. H. Coates, *J. Chem. Soc., Faraday Trans. 1* 1987, *83* 3237.

[7] R. L. Schiller, S. F. Lincoln, J. H. Coates, *J. Incl. Phenom. Macrocyclic Chem.* 1987, *5* 59.

[8] Ó. Valdés-Aguilera, D. C. Neckers, *Acc. Chem. Res.* 1989, *22* 171.

[9] L. P. Gianneschi , T. Kurucsev, *J. Chem. Soc., Faraday Trans. 2* 1974, *70* 1334.

[10] L. P. Gianneschi, A. Cant, T. Kurucsev, *J. Chem. Soc., Faraday Trans. 2* 1977, *73* 664.

[11] M. Arik, Y. Onganer, *Chem. Phys. Lett.* 2003, *375* 126.

[12] K. Takahashi, *Chem. Rev.* 1998, *98* 2013.

[13] L. Barr, P. Dumanski, C. Easton, J. Harper, K. Lee, S. Lincoln, A. Meyer, J. Simpson, *J. Incl. Phenom. Macrocyclic Chem.* 2004, *50* 19(6).

[14] E. G. McRae, M. Kasha, in *Physical process in radiation biology*, Academic Press, New York 1964, p. 23.

[15] M. Kasha, R. Rawls, M. Ashraf, *Pure Appl. Chem.* 1965, *11* 371.

[16] V. Martínez Martínez, F. López Arbeloa, J. Prieto Bañuelos, T. López Arbeloa , I. López Arbeloa, *J. Phys. Chem. B* 2004, *108* 20030.

[17] M. El Baraka, M. Deumie, P.Viallet, T.J. Lampidis, *J.Photochem.Photobiol.,A* 1991, *56* 295.

[18] F. López Arbeloa, T. López Arbeloa, M. J. Tapia Estévez, I. López Arbeloa, *J. Phys. Chem.* 1991, *95* 2203.

[19] W. Al-Soufi, M. Novo, M. Mosquera, *Appl. Spectrosc.* 2001, *55* 630.

Acknowledgements.

B.R. and J.B. thank the *Ministerio de Ciencia e Innovación* for research scholarships. M.N. and W.A.S. thank the *Ministerio de Ciencia e Innovación* and *Xunta de Galicia* for financial support (projects CTQ2007-68057-CO2-O2, INCITE07PXI209034ES, INCITE08E1R209060 ES, Network 2006/124).

Supporting Information.

1. Principal component analysis (PCA) of emission and absorption spectra.

Legend for the Figures 1S - 6S (PCA of emission and absorption spectra).

Panels a and b: first four or five spectral eigenvectors and eigenvector profiles:

Eigenvector	Line	Color
First	solid	light gray
Second	dash dot	light gray
Third	solid	black
Fourth	dash	black
Fifth (where necessary)	dot	black

Panel c: logarithmic plot of eigenvalues versus number of components.

Panel d: logarithmic plot of mean error values versus number of included components.

Panel e: plot of mean Durbin-Watson test values of residual spectra (circles) and residual profiles (triangles) versus number of included components.

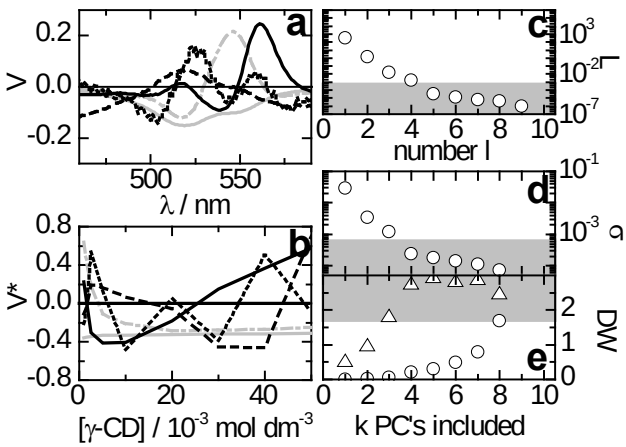

Figure 1S. Results of PCA of the series of absorption spectra of PY in aqueous solution in the presence of different concentrations of γCD (0 to 0.050 mol dm^{-3}) at a fixed concentration of PY (3.6 10^{-5} mol dm^{-3}) as shown in Figure 2. PCA yields 3-4 structural components contributing to the experimental spectra. As known for absorption spectra, the *spectral eigenvectors* (a) are distorted by baseline fluctuations and drifts and are not a reliable criterion for the determination of structural components in PCA. In these cases the *eigenvector profiles* (b) are found to be more stable: The first three eigenvector profiles (gray lines and black solid line) show systematic variations with the γCD concentration, whereas the fourth and all following profiles fluctuate randomly. This indicates three structural components. The other statistical criteria support this: The first four *eigenvalues* (c) have significantly higher values than the following ones and represent the structural variance of the data. The inclusion of four components reduces the value of the *mean error* (d) down to the level of the residual mean error. And the *mean Durbin-Watson test values (e)* calculated as a function of γCD concentration (triangles) show that it is necessary to include 3-4 components in order to obtain uncorrelated residuals.

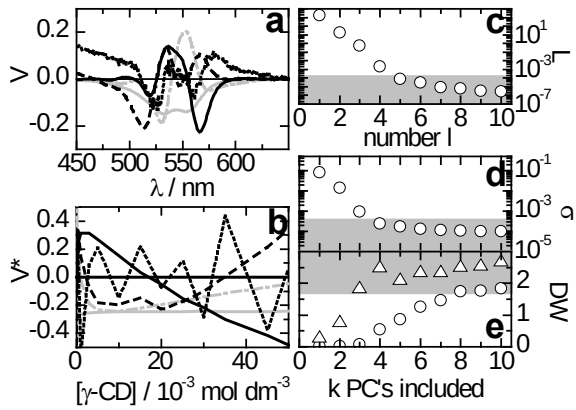

Figure 2S. Results of PCA of the series of absorption spectra of PB in aqueous solution in the presence of different concentrations of γCD (0 to 0.050 mol dm^{-3}) at a fixed concentration of PB (6.6 10^{-5} mol dm^{-3}) as shown in Figure 2. PCA yields 3-4 structural components contributing to the experimental spectra. *Spectral eigenvectors* (a): see comments in Figure 1S. *Eigenvector profiles* (b): The first four eigenvector profiles (gray lines and black solid and dashed lines) show systematic variations with the γCD concentration, whereas the fifth and all following profiles fluctuate randomly. This indicates four structural components. The other statistical criteria support this: The first 4-5 *eigenvalues* (c) have significantly higher values than the following ones and represent the structural variance of the data. The inclusion of four components reduces the value of the *mean error* (d) down to the level of the residual mean error. And the *mean Durbin-Watson test values (e)* calculated as a function of γCD concentration (triangles) show that it is necessary to include three to four components in order to obtain uncorrelated residuals.

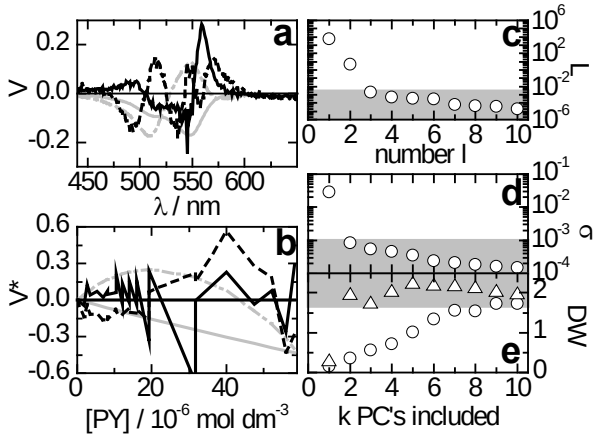

Figure 3S. Results of PCA of the series of absorption spectra of PY in aqueous solution as a function of pyronine concentration (0 to 60 10^{-6}, see also Figure 3). PCA yields 2 structural components contributing to the experimental spectra. *Spectral eigenvectors* (a): see comments in Figure 1S. *Eigenvector profiles* (b): Only the first two eigenvector profiles (gray lines) show systematic variations with the PY concentration, whereas the third and all following profiles fluctuate randomly. This indicates two systematic components. The other statistical criteria corroborate this: The first two *eigenvalues* (c) have significantly higher values than the following ones and represent the structural variance of the data. The inclusion of two components reduces the value of the *mean error* (d) down to the level of the residual mean error. The *mean Durbin-Watson test values (e)* calculated as a function of wavelength (circles) are again distorted by the baseline instabilities, but the DW-values calculated as a function of PY concentration (triangles) lie well above the critical value of 1.7 with the inclusion of the second component, indicating that two components are necessary to obtain uncorrelated residuals.

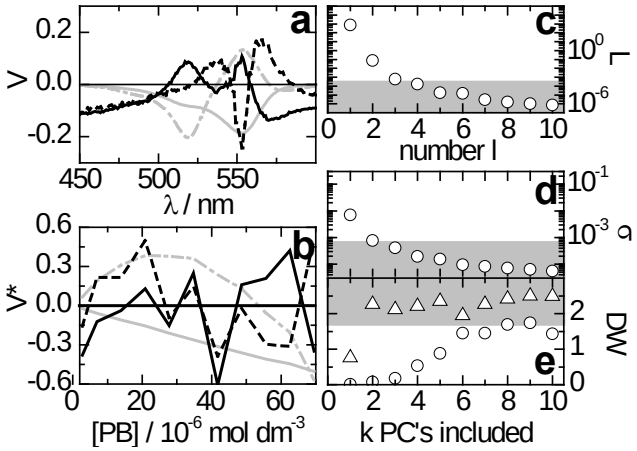

Figure 4S. Results of PCA of the series of absorption spectra of PB in aqueous solution as a function of pyronine concentration (0 to 70 10^{-6} mol dm^{-3}, see also Figure 3). PCA yields two structural components contributing to the experimental spectra. *Spectral eigenvectors* (a): see comments in Figure 1S. *Eigenvector profiles* (b): the first two eigenvector profiles (gray lines) show strong systematic variations with the PB concentration, whereas the third and fourth profiles (black lines) fluctuate randomly. This indicates two systematic components. The other statistical criteria are not conclusive except for the *mean Durbin-Watson test values (e)* calculated as a function of PB concentration (triangles): inclusion of two components is sufficient to obtain uncorrelated residuals.

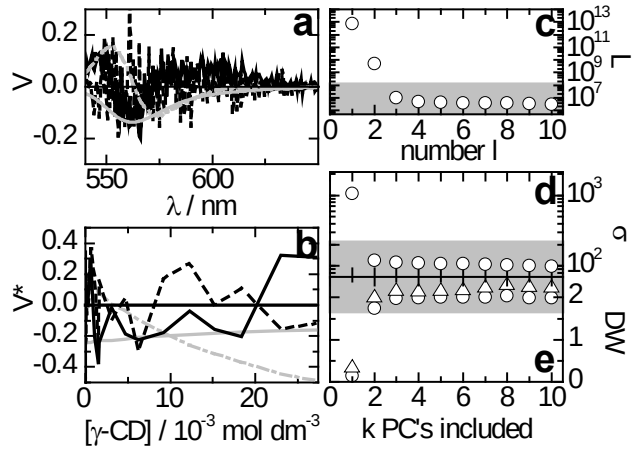

Figure 5S. Results of PCA of the series of emission spectra of PY in aqueous solution in the presence of different concentrations of γCD (0 to 0.027 mol dm^{-3}) at fixed concentration of PY ($2.0\ 10^{-7}$ mol dm^{-3}) as shown in Figure 4. PCA yields two structural components contributing to the experimental spectra. *Spectral eigenvectors* (a) and *Eigenvector profiles* (b): Only the first two eigenvectors (gray lines) show systematic variations with the wavelength (a) or with the γCD concentration (b), whereas the third and all following profiles fluctuate randomly. This indicates clearly two systematic components. The other statistical criteria corroborate this: The first two *eigenvalues* (c) have significantly higher values than the following ones and represent the structural variance of the data. The inclusion of two components reduces the value of the *mean error* (d) down to the level of the residual mean error. The *mean Durbin-Watson test values (e)* calculated as a function of wavelength (circles) and those calculated as a function of γCD concentration (triangles) lie well above the critical value of 1.7 with the inclusion of the second component, indicating that two components are necessary to obtain uncorrelated residuals.

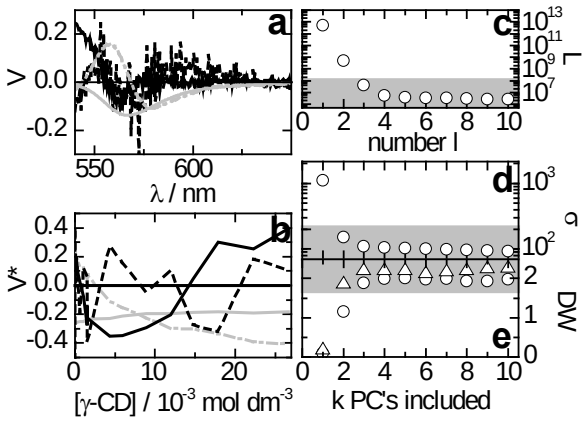

Figure 6S. Results of PCA of the series of emission spectra of PB in aqueous solution in the presence of different concentrations of γCD (0 to 0.027 mol dm^{-3}) at fixed concentration of PB (2.0 10^{-7} mol dm^{-3}) as shown in Figure 4. PCA yields two structural components contributing to the experimental spectra. *Spectral eigenvectors* (a) and *Eigenvector profiles* (b): Only the first two eigenvectors (gray lines) show systematic variations with the wavelength (a) or with the γCD concentration (b), whereas the third and all following profiles fluctuate randomly. This indicates clearly two systematic components. The other statistical criteria corroborate this: The first two *eigenvalues* (c) have significantly higher values than the following ones and represent the structural variance of the data. The inclusion of two components reduces the value of the *mean error* (d) down to the level of the residual mean error. The *mean Durbin-Watson test values (e)* calculated as a function of γCD concentration (triangles) lie well above the critical value of 1.7 with the inclusion of the second component, indicating that two components are necessary to obtain uncorrelated residuals, whereas those calculated as a function of wavelength (circles) suggest three components. Two systematic components is taken as result of PCA for this series since most of the criteria indicate that.

2. Pure absorption spectra.

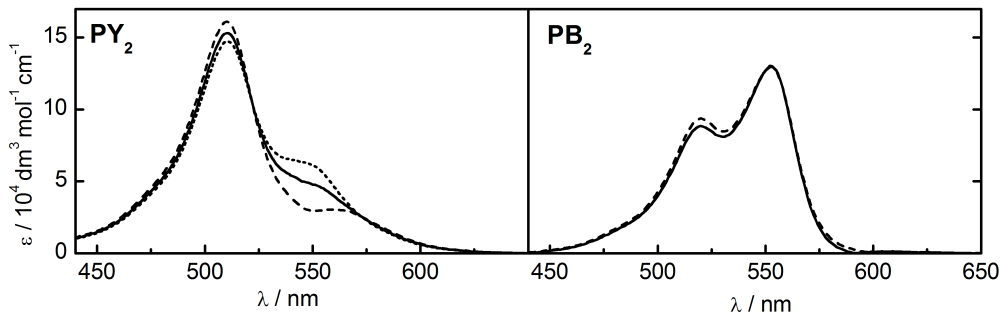

Figure 7S. Dependence of the absorption spectra of the pyronine dimers on the value of the dimerization constant K_D used in the fits for PY_2 (dashed line: $K_D = 2.5$ mM^{-1}, solid line: $K_D = 3.0$ mM^{-1}, dotted line: $K_D = 3.5$ mM^{-1}) and on the PB concentration range used in the fits for PB_2 (dashed line: up to 6 10^{-5} mol dm^{-3}, solid line: up to 4 10^{-5} mol dm^{-3}).

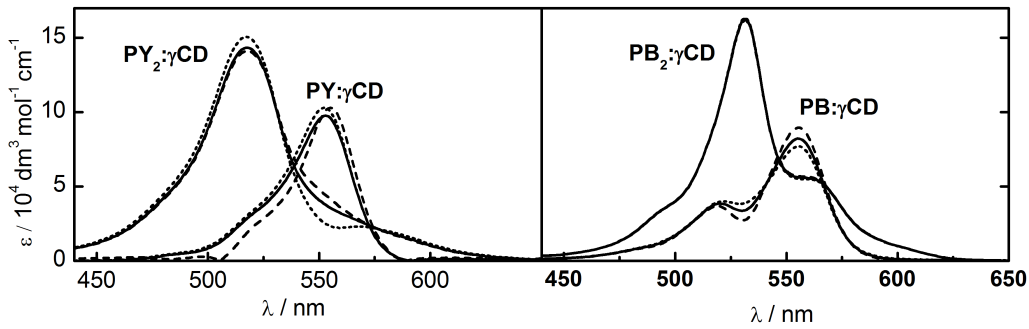

Figure 8S. Dependence of the absorption spectra of the 1:1 and 2:1 complexes formed between the pyronines and γCD on the value of the association constants K_1, K_2 used in the fits (see text).
PY: dashed line, $K_1 = 0.042$ mM^{-1}, $K_2 = 26$ mM^{-1}; solid line, $K_1 = 0.066$ mM^{-1}, $K_2 = 26$ mM^{-1}; dotted line, $K_1 = 0.097$mM^{-1}, $K_2 = 26$ mM^{-1}.
PB: dashed line, $K_1 = 0.16$ mM^{-1}, $K_2 = 8.4$ mM^{-1}; solid line, $K_1 = 0.19$ mM^{-1}, $K_2 = 8.3$ mM^{-1}; dotted line, $K_1 = 0.22$ mM^{-1}, $K_2 = 8.1$ mM^{-1}.

Host-Guest Complexation studied by Fluorescence Correlation Spectroscopy: Adamantane-Cyclodextrin Inclusion

Daniel Granadero; **Jorge Bordello**; Mª J. Pérez-Alvite; Mercedes Novo and Wajih Al-Soufi

International Journal of Molecular Sciences (2010), 11, 173–188.

Abstract: *The host-guest complexation between an Alexa 488 labelled Adamantane derivative and β-cyclodextrin is studied by Fluorescence Correlation Spectroscopy (FCS). A 1:1 complex stoichiometry and a high association equilibrium constant of $K = 5.2\ 10^4\ M^{-1}$ are obtained in aqueous solution at 25°C and pH = 6. The necessary experimental conditions are discussed. FCS proves to be an excellent method for the determination of stoichiometry and association equilibrium constant of this type of complexes, where both host and guest are nonfluorescent and which are therefore not easily accessible to standard fluorescence spectroscopic methods.*

1. Introduction.

Supramolecular host-guest chemistry describes the formation of molecular complexes composed of small molecules (guest) noncovalently bound to larger molecules (host) in a unique structural relationship.[1] Host-guest complexes are of great technological importance an have been extensively studied.[2] Several techniques are used to determine their stoichiometry and stability, such as calorimetry, conductivity, pH potentiometry, capillary electrophoresis, and absorption or fluorescence spectroscopy. Among them, fluorescence spectroscopy is widely used, because it is a sensitive and relatively straightforward technique. Standard fluorescence spectroscopy analyses the variation of a spectroscopic property (quantum yield, spectral shift, lifetime, or anisotropy) of a fluorescent guest or host due to the complexation. A significant variation of any of these parameters requires an intimate participation of the fluorophore in the complexation process, which limits the use of this technique to cases where the fluorophore itself is included as guest (Figure 1 a) or is expulsed from the interior of the host by a nonfluorescent guest in a competitive process or where some specific interactions take place. Most technologically interesting host-guest complexes are themselves nonfluorescent and the attachment of a fluorescent label in order to use them in

standard fluorescence spectroscopy leads to a dilemma: on one hand, the fluorophore should not interfere in the host-guest complexation under study, but on the other hand a sufficiently strong interaction between fluorophore and host or guest is necessary in order to detect a change in the spectral properties upon complexation. Although many specific solutions have been found, the study of fluorescently labelled host-guest systems by standard fluorescence spectroscopy is still challenging.

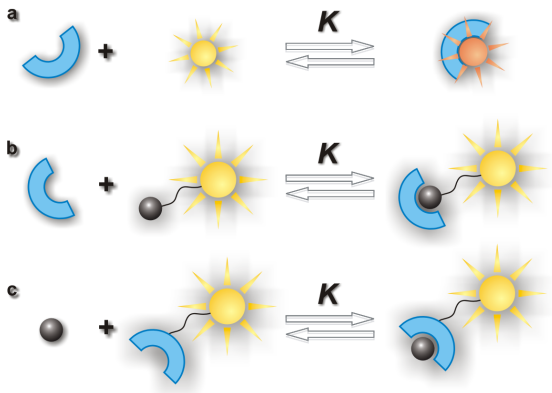

Figure 1. Fluorescent labeling of a host-guest complex (a) inclusion of a fluorescent guest (b) guest with attached fluorophore (c) host with attached fluorophore.

Fluorescence Correlation Spectroscopy (FCS) can solve the described problem in a more general way. Instead of the change in the spectral properties FCS analyses the variation in the diffusion coefficient of a fluorophore attached to guest or host due to the increase in the molecular weight upon complexation (see Figure 1, b and c). The fluorophore itself needs not to interact directly with the host-guest complex except for a common diffusive movement. This relaxes the conditions imposed on the fluorophore which can be selected independently of the specific host-guest system, so that bright and photostable dyes can be attached at convenient positions in guest or host.

FCS is a well established fluctuation correlation method that extracts information about the dynamics of molecular processes from the small changes in molecular concentration or chemical states that arise from spontaneous fluctuations around equilibrium.[3] FCS allows one to study dynamic and photophysical processes that take place in a wide time scale in one and the same experiment. It is a single molecule technique which uses very small sample volumes determined by a confocal setup and nanomolar fluorophore concentrations. FCS is used in a wide range of fields, but surprisingly few applications to the study of host-guest complexation can be found. We studied recently by FCS host-guest dynamics and determined the fast entry/exit rate constants of fluorescent dyes within cyclodextrins.[4, 5]

In this contribution we will study by FCS the stoichiometry and the stability of the inclusion complex formed between the host β-cyclodextrin (βCD) and the nonfluorescent guest adamantane labelled with Alexa 488 as fluorescent probe (see Figure 2).

Cyclodextrins (CD) are naturally occurring water-soluble toroidally shaped polysaccharides with a highly hydrophobic central cavity that have the ability to form inclusion complexes with a variety of organic and inorganic substrates.[6-12] The three major natural cyclodextrins are α, β and γCD built up from 6, 7 and 8 glucopyranose units, respectively. CDs are often found as building blocks of supramolecular systems, self-assemblies or chemical sensors.[13-18] The ability of CDs to form inclusion complexes, in which the physicochemical properties of the guest molecules change with respect to the free molecules, has led to a variety of applications.[19-25]

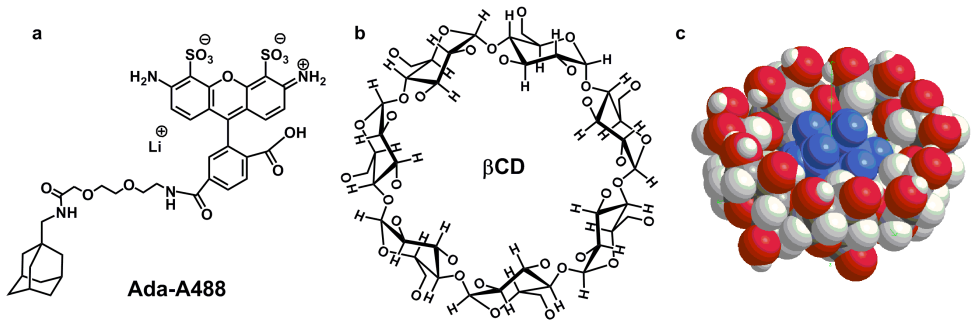

Figure 2. (a) Structure of Ada-A488 (b) Structure of βCD. (c) Sketch of an adamantane-βCD inclusion complex.

Adamantane (tricyclo[3.3.1.1(3,7)]decane, $C_{10}H_{16}$) is formed by four cyclohexanes fused to each other in chair conformations achieving a strain free and highly symmetrical stable structure. The adamantyl group is a spherical group with a diameter of 7 Å which perfectly matches the cavity diameter of βCD. Adamantane derivatives form therefore 1:1 inclusion complexes with βCD with high values of the association equilibrium constant, typically between 10^4 -10^5 M^{-1}.[26-31] Due to their high stability βCD-adamantane complexes have found several important applications both in supramolecular chemistry and in biomedical applications, such as hydrogels,[32] affinity biosensors,[33] surface-mediated gene delivery,[34] cyclodextrin polymer-based particles,[35] or supramolecular polymers.[36, 37]

In this work we demonstrate how FCS can be used to study the inclusion complex formation between βCD and adamantane labelled with the fluorescent probe Alexa 488 (Ada-A488 as shown in Figure 2). We discuss the necessary experimental conditions, determine the stoichiometry and the equilibrium constant and compare the results with those published for similar guests obtained with other methods.

2. Theory.

2.1. Mechanism.

The association of the fluorescent guest A and the nonfluorescent host H yielding a fluorescent complex B is treated as a reversible chemical reaction with (association) equilibrium constant K:

$$\mathrm{A} + \mathrm{H} \underset{}{\overset{K}{\rightleftharpoons}} \mathrm{B} \tag{1}$$

The equilibrium constant K is related to the entry (association) (k_+) and exit (dissociation) (k_-) rate constants as follows:

$$K = \frac{k_+}{k_-} \tag{2}$$

Under conditions where the host concentration [H] is always much higher than that of the fluorescent guest, this concentration coincides with the initial host concentration $[\mathrm{H}]_0$, and the complexation "reaction" is pseudo-first-order with relaxation ("reaction") time τ_R given by:

$$\tau_R = (k_+[\mathrm{H}]_0 + k_-)^{-1} \tag{3}$$

2.2. FCS.

FCS analyzes the fluorescence intensity fluctuations that are caused by the spontaneous variations in the number of fluorescent molecules in the confocal sample volume due to translational diffusion.[5,38-40] The observed fluorescence intensity fluctuates at a time scale given by the mean residence time of a fluorophore in the sample volume. The intensity fluctuations $\delta F(\mathrm{t}) = F(\mathrm{t}) - \langle F \rangle$ are analyzed by the normalized temporal autocorrelation function $G(\tau)$ as function of the correlation time τ as given in eq. 4.

$$G(\tau) = \frac{\langle \delta \mathrm{F}(t)\ \delta \mathrm{F}(t+\tau) \rangle}{\langle \mathrm{F}(t) \rangle^2} \tag{4}$$

The time dependent part of the correlation function describing pure translational diffusion of a single fluorescent species in and out of a sample volume G_D is given in eq. 5. Here a three-dimensional Gaussian sample volume is assumed with radial and axial $1/e^2$ radii ω_{xy} and ω_z, respectively. N is the mean number of fluorescent molecules within the sample volume and τ_D is the translational diffusion (transit) time of the molecules across the sample volume, which is related to the translational diffusion coefficient D by eq. 6.[3, 41]

$$G_D(\tau) = \frac{1}{N}\left(1 + \frac{\tau}{\tau_D}\right)^{-1}\left(1 + \left(\frac{\omega_{xy}}{\omega_z}\right)^2 \frac{\tau}{\tau_D}\right)^{-\frac{1}{2}} \tag{5}$$

$$D = \frac{\omega_{xy}^2}{4\tau_D} \tag{6}$$

At higher excitation power the dark triplet state of the dye may be significantly populated and a superimposed fast flickering of the fluorescence intensity may be observed with a time constant τ_T given by the triplet lifetime of the fluorophore. This leads to an additional exponential term in the correlation function as described in eq. 7.

$$G_{DT}(\tau) = G_D(\tau)\left(1 + A_T\, e^{-\tau/\tau_T}\right) \tag{7}$$

In the case that the exchange of the fluorophore between free and bound states is much faster than the typical transit time of the fluorophore across the sample volume ($\tau_R \ll \tau_D$) these states of the fluorophore will not be seen by FCS as two distinct species, but as a single one with a mean diffusion time $\bar{\tau}_D$. The value of $\bar{\tau}_D$ depends then on the individual diffusion coefficients D_f and D_b of free and bound fluorophore and on the molar fractions $X_x = N_x/(N_f+N_b)$ of these species:

$$\bar{\tau}_D = \frac{\omega_{xy}^2}{4(X_f D_f + X_b D_b)} = (X_f(\tau_f)^{-1} + X_b(\tau_b)^{-1})^{-1} \tag{8}$$

The full correlation curve describing translational diffusion of two fluorescent species in fast exchange and a common triplet term is given in eq. 9 where the diffusion term is defined by the mean diffusion time $\bar{\tau}_D$.

$$G_{DT}(\tau) = \frac{1}{N}\left(1 + \frac{\tau}{\bar{\tau}_D}\right)^{-1}\left(1 + \left(\frac{\omega_{xy}}{\omega_z}\right)^2 \frac{\tau}{\bar{\tau}_D}\right)^{-\frac{1}{2}}\left(1 + A_T\, e^{-\tau/\tau_T}\right) \tag{9}$$

In the case of a fluorescent guest, a 1:1 stoichiometry, and under the conditions that the free host concentration is always much higher than that of the guest, [A] ≪ [H], the mean diffusion time $\bar{\tau}_D$ can be expressed as function of the total host concentration $[H]_0$, the equilibrium association constant K and the limiting values of the diffusion times of free and bound dye, τ_f and τ_b, respectively.

$$\bar{\tau}_D = \frac{\tau_f(1 + K[H]_0)}{1 + \frac{\tau_f}{\tau_b}K[H]_0} \tag{10}$$

The equilibrium association constant K can then be determined from a fit to a series of mean diffusion times measured at different host concentrations or directly from a global fit to the series of correlation curves.

3. Results and Discussion.

The determination of absolute diffusion coefficients with standard FCS can be affected by several experimental errors.[42] For the determination of the equilibrium constant and the stoichiometry of the complexation only relative values of the diffusion times are needed, but even these may be distorted at high excitation irradiance due to saturation or photodestruction of the fluorophore. The residence time of the complex in the focal volume is longer than that of the free fluorophore, which may increase the photobleaching probability and thus shorten the apparent diffusion times. This in turn flattens the titration curve and leads to an underestimation of the equilibrium constant. Therefore, as a first step the irradiance dependence of the fluorescence count rate and of the diffusion coefficient of free and complexed Ada-A488 has been studied. Figure 3 shows that the registered fluorescence count rate per Ada-A488 molecule (the molecular brightness) (filled black squares) increases linearly at low irradiance but levels off slightly at higher values. The presence of βCD ([CD] = 6.4 10^{-3} mol dm^{-3}) has only small influence on the brightness of the fluorophore, with a reduction of about 5% at low and about 25% at highest irradiance. This change may be due to different photobleaching probabilities of free and complexed dye, to polarization effects in the detection optics, to a change of the refractive index of the solution, or to increased scattering, but it may also be due to some direct interaction between the Alexa 488 chromophore and the adamantane-cyclodextrin complex. However, the Alexa 488 fluorophore is too big to be included into the βCD cavity and no efficient competition with the adamantane inclusion is to be expected.

The diffusion time of Ada-A488 (open squares in Figure 3), increases significantly on the addition of βCD (open circles). At highest irradiance a very similar slight decrease of the diffusion times (of about 5%) is observed in both cases, probably due to some saturation effect. For the titration measurements an irradiance of $I_0/2 = 27$ kWcm^{-2} was chosen, which is at the upper end of the linear increase of the brightness.

The normalized fluorescence intensity correlation curves $G(\tau)$ of Ada-A488 in water at different βCD concentrations are shown as grey lines in Figure 4. The detected fluorescence intensity is strongly correlated at very short correlation times, but then two decorrelation terms are observed at around 5 μs and 200 μs. The amplitude of the first term increases strongly at higher irradiance (not shown) but is independent of the βCD concentration. It can therefore be safely assigned to the population of the triplet state of Alexa 488. The

second term shifts to longer correlation times at increasing βCD concentration and is assigned to the diffusion of the fluorophore in and out of the sample volume. All correlation curves can be well fitted with correlation function G_{DT} (eq. 9) yielding the diffusion times τ_D shown in the inset of Figure 4a.

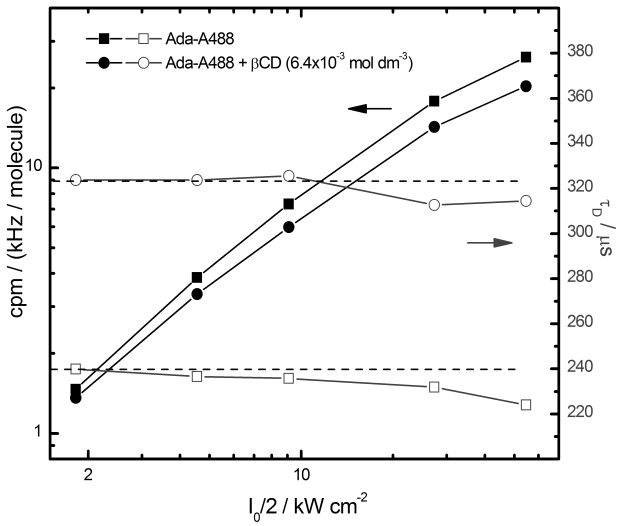

Figure 3. Power series of the FCS signal of Ada-A488 in aqueous solution (squares, $[\beta CD]_0 = 0$ mol dm^{-3}) and at high concentration of βCD (circles, $[\beta CD]_0 = 6.4\ 10^{-3}$ mol dm^{-3}). [Ada-A488] ≈ 10^{-9} mol dm^{-3}). Left scale, filled symbols: count rate per single Ada-A488 molecule. Right scale, open symbols: diffusion time of Ada-A488. All data obtained from FCS correlation curves similar to those shown in Figure 4 at different excitation irradiances. Counts per molecule (cpm) is the total detected fluorescence count rate divided by the mean number of molecules in the focus *N*.

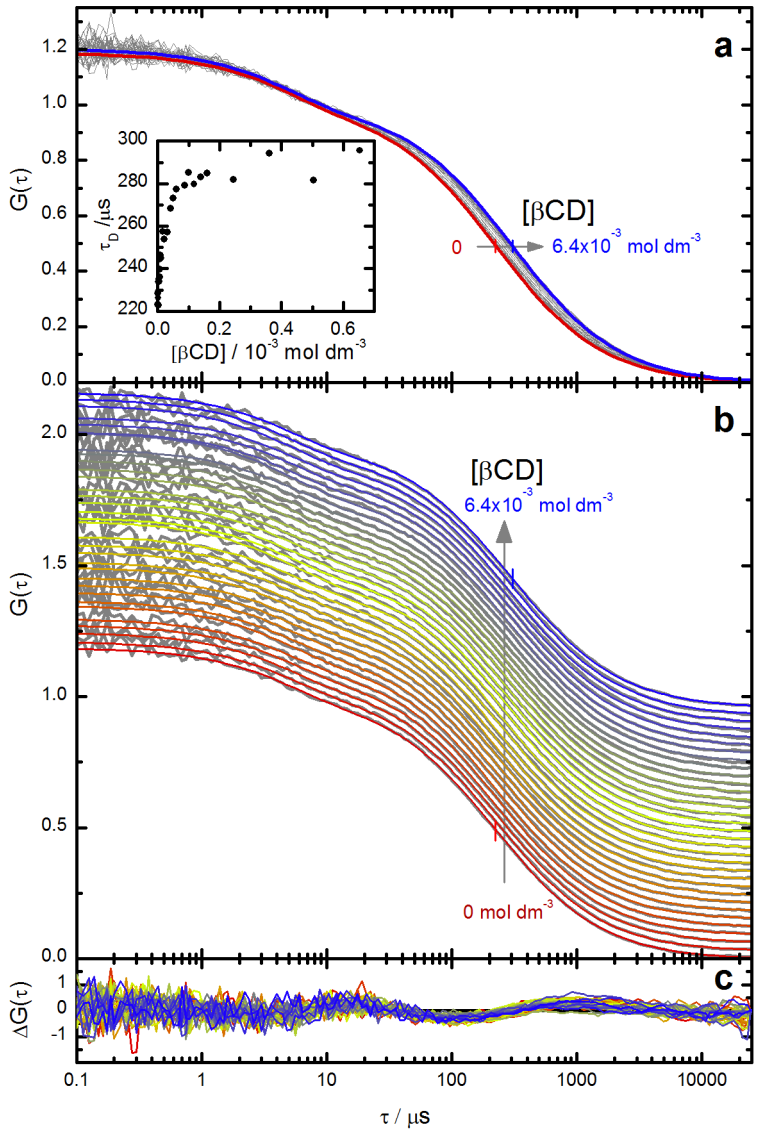

Figure 4. Fluorescence intensity correlation curves $G(\tau)$ of Ada-A488 in the presence of increasing concentrations of βCD ([CD] = 0 to 6.4 10^{-3} mol dm^{-3}) in aqueous solution. ([Ada-A488] ≈ 10^{-9} mol dm^{-3}). Panel a: normalized experimental correlation curves at increasing βCD concentration (grey curves) and two representative curves from the global fit of Equations. 9 and 10 at [βCD] = 0 mol dm^{-3} (red curve) and [CD] = 6.4 10^{-3} mol dm^{-3} (blue curve) to the correlation curves. The intermediate fit curves are not shown for clarity. Small vertical bars indicate the diffusion time obtained from the fit. Inset: mean diffusion times $\bar{\tau}_D$ as function of βCD concentration determined from individual fits of the equation 9 to the correlation curves. The highest concentrations are not shown. See also Figure 5. Panel b: stacked representation of the same correlation curves as in panel a. Panel c: weighted residuals from the global fit (vertical scale is arbitrary).

The strong increase of τ_D already at very low βCD concentration cannot be explained by an increase of the solvent viscosity, which is not significant at these low cyclodextrin concentrations.[43] We interpret these values of τ_D as mean diffusion times $\bar{\tau}_D$ of the fluorophore in fast exchange between free and bound states as described by equations 8-10. The fit of these mean diffusion times $\bar{\tau}_D$ by the model of a complexation with stoichiometry 1:1 (eq. 10) is very satisfactory as shown in Figure 5. More precise values of the parameters are obtained by a direct global target fit of the correlation curves by equations 9 and 10 as shown in Figure 4. The results of this global fit are listed in Table 1, together with calculated values of the diffusion coefficients and the hydrodynamic radii of free dye and the complex.

Table 1. Results of the global target fit of equations 9 and 10 to the correlation curves shown in Figure 4 and calculated values. All values at 25.0 ± 0.5 °C.

	Ada-A488 + βCD
K /10^3 M^{-1}	52 ± 2
τ_f /ms	0.222 ± 0.002
τ_b /ms	0.300 ± 0.002
A_T	0.20
τ_T /µs	4.8
D_f /10^{-10} $m^2 s^{-1}$	3.15 ± 0.30
D_b /10^{-10} $m^2 s^{-1}$	2.33 ± 0.20
$R_{h,f}$ /Å	7.8 ± 0.7
$R_{h,b}$ /Å	10.5 ± 0.9

The limiting diffusion times obtained from the fits to the series of correlation curves were converted to translational diffusion coefficients D using eq. 6 with the radial $1/e^2$ radius of the sample volume obtained from a calibration with Rhodamine 123 as reference (see experimental section). The uncertainty in this calibration and other systematic errors are not included in the indicated standard deviations. The hydrodynamic radii R_h of free Ada-A488 and of the complex Ada-A488:βCD were estimated applying the Stokes-Einstein relation (eq. 11) with the viscosity of water $\eta(25°C) = 0.8905$ cP:

$$R_h = \frac{k\,T}{6\,\pi\,\eta\,D} \tag{11}$$

As expected the free guest Ada-A488 has a higher diffusion coefficient than the complex Ada-A488:βCD. The diffusion coefficient of homogeneous spherical particles is expected to change with the inverse of the cubic root of their molar mass $D \sim R_h^{-1} \sim M^{-1/3}$. As shown previously this is well fulfilled for small globular molecules and for inclusion complexes of different cyclodextrins.[4] In this case the ratio between the diffusion coefficients $D_b/D_f = 0.74$

coincides perfectly with that expected from the ratio of their molar masses $(M_b/M_f)^{-1/3} = (2.37)^{-1/3}$. The absolute values of the diffusion coefficients compare very well with those obtained before for complexes between pyronines and βCD and γCD.[4, 5]

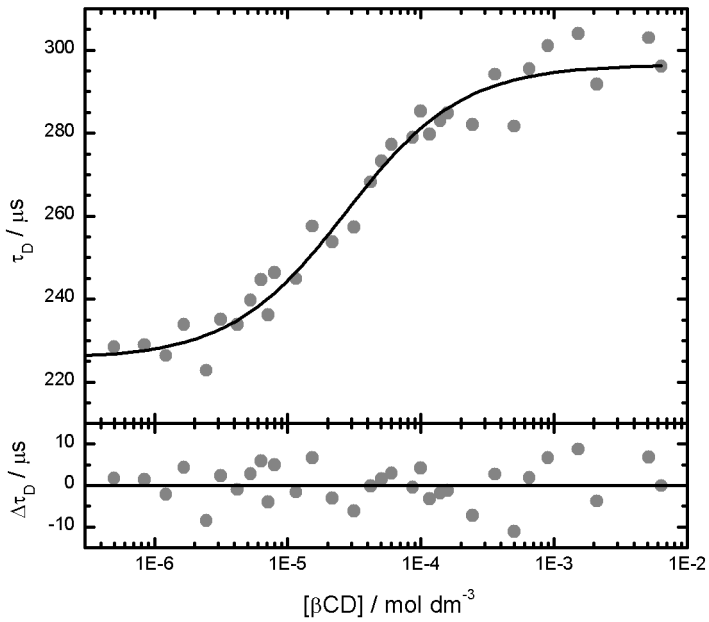

Figure 5. Upper panel: Mean diffusion times $\bar{\tau}_D$ as function of βCD concentration determined from individual fits of correlation function G_{DT} (eq. 9) to the normalized correlation curves of Figure 4. Parameter of the fit as given in the text. The black curve represents the best fit of equation 10 to $\bar{\tau}_D$ with the parameter $\tau_f = 225 \pm 2$ µs, $\tau_b = 297 \pm 2$ µs, and $K = (48 \pm 7)\ 10^3$ mol^{-1}dm^3. Note that due to the logarithmic concentration scale the values at [CD] = 0 M are not visible in the figure, although they are included in the fit. Lower panel: residuals of the fit.

As can be deduced from the residuals in Figure 5, the precision in the measurement of the diffusion times in these experiments is about $\sigma(\tau_D)/\tau_D \approx 2\%$. This translates to a minimal detectable relative change of the molar mass of the fluorophore from this data of about 20%.

The very high value of the association equilibrium constant $K = 5.2\ 10^4$ M^{-1} agrees well with that given in the literature for the inclusion of different adamantane derivatives into βCD with values of K = 1-10 10^4 M^{-1}.[26-31, 44]

Finally, the fact that in spite of the high association equilibrium constant a fast exchange of Ada-A488 between free and complexed state is observed indicates that the association rate constant must be similar or even slightly higher than that observed for the dynamics of the association of pyronines to βCD.[4, 5] An additional correlation term due to the exchange itself is not observed as the fluorophore does not change its brightness upon complexation.

4. Experimental Section.

4.1. Materials.

βCD (Sigma-Aldrich) (M = 1134.98 g mol^{-1}) was used as delivered. βCD was checked for fluorescence impurities and was found to be clean enough for classical fluorescence measurements and for FCS experiments. Water was purified with a Milli-Q system. The synthesis of the Ada-A488 compound (M = 825.88 g mol^{-1}) is described in section 4.4.

4.2. Sample Preparation.

Stock aqueous solutions of βCD were freshly prepared with a concentration of about 8 10^{-3} mol dm^{-3}. Stock solutions of Ada-A488 were prepared as follows: the solid compound Ada-A488 was first dissolved in ethanol in order to facilitate its solubilisation. Then, an aliquot of this solution was diluted 1000 times in 0.1 mol dm^{-3} phosphate buffer to adjust the pH at 6. The concentrations of Ada-A488 in these stock solutions were still 25-fold higher than that necessary for the FCS measurements (approximately 10^{-9} mol dm^{-3}). The FCS samples were finally prepared by dilution of a constant volume of the corresponding Ada-A488 stock together with different volumes of the βCD stock solution and addition of water to adjust to a certain total volume. All these volumes were weighed so that concentration corrections could be performed. Special care was taken in order to avoid any possible contamination of the samples with fluorescent impurities. At the highest βCD concentrations a slight turbidity was observed in the samples, which explains an additional small very slow term in the correlation curves.

4.3. FCS Measurements.

The confocal epi-illuminated setup used for the FCS measurements is similar to that described elsewhere.[4,45] A 40 µL drop of each sample was deposited on a borosilicate coverslip (Menzel Gläser, NO 1 DE). The samples were excited by the continuous linearly polarized light of a 489 nm laser diode (Becker&Hickl, BDL-485-SMC, DE) coupled to a monomode optical fiber (Point-Source, kineFLEX-P-1-S-405-0.7, UK). The light output of the fiber was collimated (Schäfter&Kirchhoff, 60FC-4-6,2-01-DI, DE), spectrally cleaned (Semrock, Brightline HC 482/18, US), redirected by a dichroic mirror (Semrock, Brightline BS R488, US) and focused into the sample by a high aperture microscope objective (Olympus, UPLSAPO 60xW/1.20, water immersion) mounted in an inverted microscope (Olympus, IX-71). The fluorescence was collected by the same objective and then refocused through the dichroic mirror onto a pinhole (Thorlabs, ∅=50 µm, US) in the image plane. The light passing the pinhole was collimated, then split into two beams by a nonpolarizing beamsplitter

cube (Newport, 05BC17MB.1, US) and each focused onto avalanche photodiodes (MPD50CTC APD, ∅=50 µm, MPD, Italy). Band-pass filters (Semrock, Brightline HC 525/45, US) in front of the detectors discriminated fluorescence from scattered laser light. Both output signals were processed and stored by TCSPC-modules (SPC 132, Becker & Hickl GmbH, Berlin, Germany). Correlation curves were calculated with a fast home-built routine that runs under LabVIEW (National Instruments).[45] Typically 20 million photons were collected for each correlation curve with count rates around 50 kHz. All measurements were made at stabilized temperature, 25.0 ± 0.5°C. The excitation power as measured in the focus of the microscope objective by a power meter (Thorlabs, PM30-120, US) was typically 240 µW, corresponding to a mean irradiance of $I_0/2 = P/(\pi\ \omega_{xy}^2) = 27$ kW cm^{-2}, assuming a Gaussian intensity distribution along the optical axis. P is the excitation power in the sample).[46]

The focal area and the detection volume were calibrated with Rhodamine 123 in aqueous solution at low irradiance yielding a radial $1/e^2$ radius of $\omega_{xy} = 0.53$ µm. The value of $D_{R123} = (4.6 \pm 0.4)\ 10^{-10}$ m^2 s^{-1} is estimated from recent PFG-NMR[47] and dual-focus FCS[48] data. The diffusion coefficients are given for 25°C. All given uncertainties correspond to one standard deviation from the fits and do not include calibration errors.

Series of FCS curves measured at different host concentrations were analyzed by global "target" analysis programmed in OriginPro 8.0 (OriginLab Corporation, US). An empirical weighting function was used in order to take into account the strong variation of the noise in the FCS curves.

4.4. Synthesis of the Ada-A488 Compound.

Preparation of compound 1 (see Scheme 1):

1-adamantanemethylamine (85.8 mg, 0.52 mmol) was dissolved in dry DCM (10.4 mL) and Fmoc 8-amino-3,6-dioxaoctanoic acid (200mg, 0.52 mmol), HATU (217 mg, 0.57 mmol) and DIEA (546 mL, 3.12 mmol) were successively added.

After 1 hour stirring at room temperature, the solution was poured into a separation funnel and washed with HCl (5%) and $NaHCO_3$ (sat). The organic layers were dried over Na_2SO_4, filtered and concentrated under reduce pressure, providing a yellow oil that when purified by flash chromatography (2–4% MeOH in DCM) gave (**1**, 222 mg) of the compound as a white foam [80%, Rf = 0.5 (5% MeOH in DCM)].

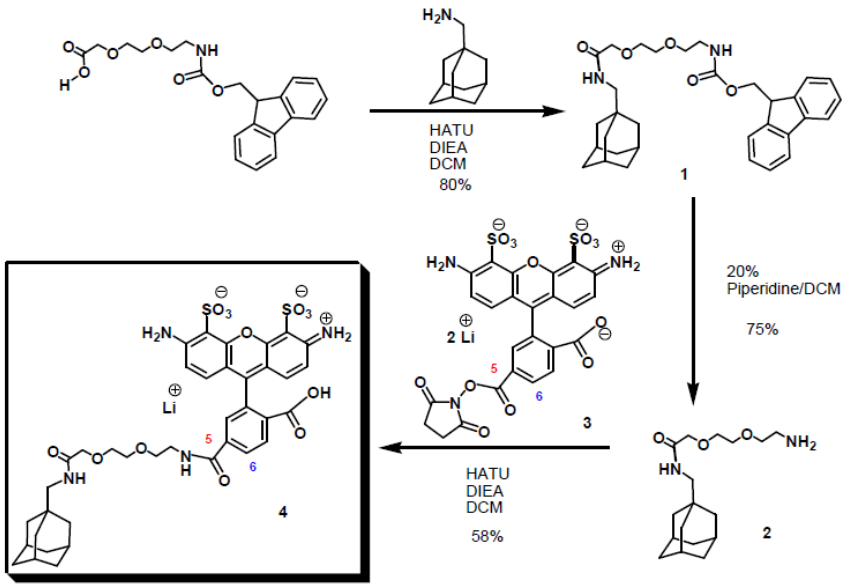

Scheme 1. Synthesis of the Ada-A488 compound (4).

Preparation of compound 2:

A solution of Fmoc 8-amino-3,6-dioxaocta-methyladamantane amide (**1**, 25 mg, 0.047 mmol) in piperidine-DCM mixture (1:4, 0.5 mL) was stirred at rt for 20 min, the solvent was removed *in vacuo*, and the residue was dissolved in DCM . This solution was washed with NaOH (1M). The organic phase was concentrated and dissolved in H2O. The resulted solution was centrifugated and the supernatant was liofilized giving 8-amino-3,6-dioxaocta-methyladamantane amide (**2**, 11 mg) as a yellow oil which was used without further purification [75%, Rt = 15.3 min (Eclipse Inertsil analitic column, 50–80 % MeOH 0.1%TFA in H2O 0.1%TFA in 19 min)].

^{1}H NMR (CD_3CN, 250.13 MHz, d): 7.04–6.85 (m, 2H, NH_2), 3.9 (s, 2H, CH_2 ester), 3.65–3.52 (m, 6H, CH_2 ether), 3.01–2.89 (bs, 2H, CH_2 amine), 2.83 (d, J = 6.57 Hz, 2H, CH_2 amide), 1.72–1.47 (m, 7H, CH and CH_2 Ad), 1.4 (s, 6H, CH_2 Ad).

Preparation of compound 4:

8-amino-3,6-dioxaocta-methyladamantane amide (**2**, 0.35 mg, 1.12 mmols) and Alexa Fluor 488 carboxylic acid succinimidyl ester (mixed isomers) (**3**, 0.2 mg, 0.31 mmols) were dissolved in dry DCM (500 mL) and dry DMF (20 mL), DIEA (1 mL, 5.5 mmols) was added and the mixture was stirred under argon for 1 h. The crude was purified by HPLC, affording (**4**,

0.15 mg) of compound as a pink solid [58%, Rt = 15 min and 16min for 2 isomers (Eclipse Inertsil analitic column, 50–80% MeOH 0.1%TFA in H_2O 0.1%TFA in 19 min)].

MS (MALDI-TOF) [m/z (%)]: 825 ([M^-], 100), 779.4 (8), 604.2 (16).

Abbreviations Used:

CD_3CN: Deuterated acetonitrile; DCM: Dichloromethane; DIEA: Diisopropylethylamine; DMF: dimethylformamide; Fmoc: Fluorenylmethoxycarbonyl; HATU:O-(7-azabenzotriazol-1-yl)-1,1,3,3-tetramethyluronium hexafluorophosphate; ^1H NMR: Proton nuclear magnetic resonance; HPLC: High Performance Liquid Chromatography; MALDI-TOF: Mass Spectrometry of Laser Desorption/Ionization-Time of Flight; bs: broad singlet; d: doublet; m: multiplet; s: singlet; rt: room temperature.

Suppliers:

Fmoc 8-amino-3,6-dioxaoctanoic acid: Commercially available from Bachem; Alexa Fluor 488 carboxylic acid succinimidyl ester (mixed isomers): Commercially available from Molecular Probes.

5. Conclusions.

Fluorescence correlation spectroscopy has been proved to be an excellent method for the determination of the stoichiometry and the association equilibrium constant of host-guest complexes with fluorescently labelled guests. FCS requires only that guest or host can be fluorescently labelled and that the complexation increases sufficiently the molar mass of the fluorescent species. FCS needs only minimal amounts of host and guest, is fast and relatively straightforward, as long as the experimental conditions are carefully selected. All commercially available systems allow this type of measurements.

A very high value of the association equilibrium constant between Ada-A488 and βCD was determined, which agrees well with that given in the literature for the inclusion of similar adamantane derivatives into βCD.

References.

[1] Turro, N. J. Supramolecular Structure and Dynamics Special Feature: Molecular structure as a blueprint for supramolecular structure chemistry in confined spaces. *PNAS* 2005, *102*, 10766-10770.

[2] Dodziuk, H. *Introduction to Supramolecular Chemistry* Springer: Dordrecht, 2002.

[3] Rigler, R.; Elson, E. S. *Fluorescence correlation spectroscopy: theory and applications* Springer Verlag: Berlin, 2001.

[4] Al-Soufi, W.; Reija, B.; Novo, M.; Felekyan, S.; Kühnemuth, R.; Seidel, C. A. M. Fluorescence Correlation Spectroscopy, a Tool to investigate Supramolecular Dynamics: Inclusion Complexes of Pyronines with Cyclodextrin. *J. Am. Chem. Soc.* 2005, *127*, 8775-8784.

[5] Al-Soufi, W.; Reija, B.; Felekyan, S.; Seidel, C. A.; Novo, M. Dynamics of supramolecular association monitored by fluorescence correlation spectroscopy. *Chemphyschem* 2008, *9*, 1819-1827.

[6] Cramer, F.; Hettler, H. Inclusion compounds of cyclodextrins. *Naturwissenschaften* 1967, *54*, 625-32.

[7] Szejtli, J. Introduction and General Overview of Cyclodextrin Chemistry. *Chem. Rev.* 1998, *98*, 1743-1754.

[8] Dodziuk, H. *Cyclodextrins and Their Complexes: Chemistry, Analytical Methods, Applications* Wiley-VCH: 2006.

[9] Carrazana, J.; Reija, B.; Ramos Cabrer, P.; Al-Soufi, W.; Novo, M.; Vázquez Tato, J. Complexation of Methyl Orange with beta-cyclodextrin: Detailed Analysis and Application to Quantification of Polymer-bound Cyclodextrin. *Supramolecular Chemistry* 2004, *16*, 549-559.

[10] Bordello, J.; Reija, B.; Al-Soufi, W.; Novo, M. Host-assisted guest self-assembly: enhancement of the dimerization of pyronines Y and B by gamma-cyclodextrin. *Chemphyschem* 2009, *10*, 931-939.

[11] Reija, B.; Al-Soufi, W.; Novo, M.; Vázquez Tato, J. Specific interactions in the inclusion complexes of Pyronines Y and B with beta-cyclodextrin. *J Phys Chem B* 2005, *109*, 1364-1370.

[12] Bohne, C. Supramolecular dynamics of guest complexation to cyclodextrins. *The Spectrum* 2000, *13*, 14-19.

[13] Harada, A.; Li, J.; Kamachi, M. Synthesis of a tubular polymer from threaded cyclodextrins. *Nature* 1993, *364*, 516.

[14] Lehn, J. M. *Supramolecular Chemistry* VCH: Weinheim, 1995.

[15] Nepogodiev, S. A.; Stoddart, J. F. Cyclodextrin-Based Catenanes and Rotaxanes. *Chem. Rev.* 1998, *98*, 1959-1976.

[16] Alvarez Parrilla, E.; Ramos Cabrer, P.; Al-Soufi, W.; Meijide del Río, F.; Rodríguez Núñez, E. A.; Vázquez Tato, J. Dendritic growth of a supramolecular complex. 2000.

[17] Ogoshi, T.; Harada, A. Chemical Sensors Based on Cyclodextrin Derivatives. *Sensors* 2008, *8*, 4961-4982.

[18] Hennig, A.; Bakirci, H.; Nau, W. M. Label-free continuous enzyme assays with macrocycle-fluorescent dye complexes. *Nature methods* 2007, *4*, 629-632.

[19] Breslow, R.; Belvedere, S.; Gershell, L.; Leung, D. The chelate effect in binding, catalysis, and chemotherapy. *Pure and Applied Chemistry* 2000, *72*, 333-342.

[20] Loftsson, T.; Brewster, M. E. Pharmaceutical Applications of Cyclodextrins. 1. Drug Solubilization and Stabilization. *J. Pharm. Sci.* 1996, *85*, 1017-1025.

[21] Uekama, K.; Hirayama, F.; Irie, T. Cyclodextrin Drug Carrier Systems. *Chem. Rev.* 1998, *98*, 2045-2076.

[22] Hirayama, F.; Uekama, K. Cyclodextrin-based controlled drug release system. *Adv. Drug Deliv. Rev.* 1999, *36*, 125-141.

[23] Lezcano, M.; Al-Soufi, W.; Novo, M.; Rodríguez-Núñez, E.; Vázquez Tato, J. Complexation of several benzimidazole-type fungicides with alpha- and beta-cyclodextrins. *J. Agric. Food Chem.* 2002, *50*, 108-112.

[24] Ritter, H.; Tabatabai, M. Cyclodextrin in Polymer Synthesis: A Green Way to Polymers. *Progress in Polymer Science* 2002, *27*, 1713-1720.

[25] Davis, M. E.; Brewster, M. E. Cyclodextrin-based pharmaceutics: past, present and future. *Nat. Rev. Drug Discov.* 2004, *3*, 1023-1035.

[26] Eftink, M. R.; Andy, M. L.; Bystrom, K.; Perlmutter, H. D.; Kristol, D. S. *J. Am. Chem. Soc.* 1989, *111*, 6765-6772.

[27] Cromwell, W. C.; Bystrom, K.; Eftink, M. R. Cyclodextrin-adamantanecarboxylate inclusion complexes: studies of the variation in cavity size. *J. Phys. Chem.* 1985, *89*, 326-332.

[28] Gelb, R. I.; Schwartz, L. M. Complexation of Admantane-Ammonium Substrates by Beta-Cyclodextrin and its O-Methylated Derivatives. *Journal of Inclusion Phenomena and Molecular Recognition in Chemistry* 1989, *7*, 537-543.

[29] Palepu, R.; Reinsborough, V. C. β-cyclodextrin inclusion of adamantane derivatives in solution. *Aust. J. Chem.* 1990, *43*, 2119-2123.

[30] Kwak, E. S.; Gomez, F. A. Determination of the binding of β-cyclodextrin derivatives to adamantane carboxylic acids using capillary electrophoresis. *Chromatographia* 1996, *43*, 659-662.

[31] Harries, D.; Rau, D. C.; Parsegian, V. A. Solutes probe hydration in specific association of cyclodextrin and adamantane. *J. Am. Chem. Soc.* 2005, *127*, 2184-2190.

[32] Koopmans, C.; Ritter, H. Formation of Physical Hydrogels via Host-Guest Interactions of β-Cyclodextrin Polymers and Copolymers Bearing Adamantyl Groups. *Macromolecules* 2008, *41*, 7418-7422.

[33] Holzinger, M.; Bouffier, L.; Villalonga, R.; Cosnier, S. Adamantane/β-cyclodextrin affinity biosensors based on single-walled carbon nanotubes. *Biosensors and Bioelectronics* 2009, *24*, 1128-1134.

[34] Park, I.; von Recum, H. A.; Jiang, S.; Pun, S. H. Spatially-Controlled Delivery of Cyclodextrin-Based Polyplexes from Solid Surfaces. *Mol.Ther.* 2006, *13*, S67-S67.

[35] Bellocq, N. C.; Pun, S. H.; Jensen, G. S.; Davis, M. E. Transferrin-Containing, Cyclodextrin Polymer-Based Particles for Tumor-Targeted Gene Delivery. *Bioconjug. Chem.* 2003, *14*, 1122-1132.

[36] Munteanu, M.; Choi, S.; Ritter, H. Cyclodextrin-click-cucurbit[6]uril: Combi-Receptor for Supramolecular Polymer Systems in Water. *Macromolecules* 2009, *42*, 3887-3891.

[37] Soto Tellini, V. H.; Jover, A.; Carrazana Garcia, J.; Galantini, L.; Meijide, F.; Vázquez Tato, J. Thermodynamics of Formation of Host-Guest Supramolecular Polymers. *J. Am. Chem. Soc.* 2006, *128*, 5728-5734.

[38] Widengren, J.; Rigler, R. Fluorescence correlation spectroscopy as a tool to investigate chemical reactions in solutions and on cell surfaces. *Cell Mol. Biol.* 1998, *44*, 857-879.

[39] Widengren, J. In *Photophysical aspects of FCS measurements;* Rigler, R., Elson, E. S., Eds.; Springer Verlag: Berlin, 2001; p 276.

[40] Haustein, E.; Schwille, P. In *Fluorescence correlation spectroscopy in vitro and in vivo;* Selvin, P. R., Ha, T., Eds.; Cold Spring Harbor Laboratory Press: Cold Spring Harbor, N.Y., 2008; p 259.

[41] Elson, E. L.; Magde, D. Fluorescence correlation spectroscopy. I. Conceptual basis and theory. *Biopolymers* 1974, *13*, 1-27.

[42] Enderlein, J.; Gregor, I.; Patra, D.; Dertinger, T.; Kaupp, U. B. Performance of Fluorescence Correlation Spectroscopy for Measuring Diffusion and Concentration. *Chemphyschem* 2005, *6*, 2324-2336.

[43] Alcor, D.; Allemand, J. F.; Cogne-Laage, E.; Croquette, V.; Ferrage, F.; Jullien, L.; Kononov, A.; Lemarchand, A. Stochastic Resonance to Control Diffusive Motion in Chemistry. *J Phys Chem B* 2005, *109*, 1318-1328.

[44] Carrazana, J.; Jover, A.; Meijide, F.; Soto, V. H.; Vázquez Tato, J. Complexation of Adamantyl Compounds by beta-Cyclodextrin and Monoaminoderivatives. *J Phys Chem B* 2005, *109*, 9719-9726.

[45] Felekyan, S.; Kuhnemuth, R.; Kudryavtsev, V.; Sandhagen, C.; Becker, W.; Seidel, C. A. M. Full correlation from picoseconds to seconds by time-resolved and time-correlated single photon detection. *Rev. Sci. Instrum.* 2005, *76*.

[46] Eggeling, C.; Widengren, J.; Rigler, R.; Seidel, C. A. M. Photobleaching of fluorescent dyes under conditions used for single-molecule detection: evidence of two-step photolysis. *Anal. Chem.* 1998, *70*, 2651-2659.

[47] Gendron, P. O.; Avaltroni, F.; Wilkinson, K. J. Diffusion coefficients of several rhodamine derivatives as determined by pulsed field gradient-nuclear magnetic resonance and fluorescence correlation spectroscopy. *J. Fluoresc.* 2008, *18*, 1093-1101.

[48] Muller, C.; Loman, A.; Pacheco, V.; Koberling, F.; Willbold, D.; Richtering, W. Precise measurement of diffusion by multi-color dual-focus fluorescence correlation spectroscopy. *Europhys. Lett.* 2008, *83*.

Acknowledgements.

J.B. thanks the *Ministerio de Ciencia e Innovación* for a research scholarship. M.J.P.A thanks the Spanish MICINN for her FPI Fellowship. M.N. and W.A. thank the *Ministerio de Ciencia e Innovación* and the *Xunta de Galicia* for financial support (CTQ2004-07683-C02-02, INCITE07PXI209034ES, INCITE08E1R209060ES).

Host-Guest Association studied by Fluorescence Correlation Spectroscopy

Mercedes Novo, Daniel Granadero, **Jorge Bordello** and Wajih Al-Soufi

Journal of Inclusion Phenomena and Macrocyclic Chemistry (2011), 70(3-4), 259-268.

Abstract: *Fluorescence Correlation Spectroscopy (FCS) is a powerful single molecule technique for the study of the stability and the association dynamics of supramolecular systems and, in particular, of host-guest inclusion complexes. With FCS the host-guest binding equilibrium constant is determined analysing the variation in the diffusion coefficient of the fluorescent guest or host with no need for a change in the photophysical properties of the fluorescent probe. FCS gives also access to the association/dissociation rate constants of the host-guest inclusion providing that the fluorescence intensity of host or guest changes upon complexation. These rate constants can be compared with that of a diffusion-controlled process estimated from the same FCS experiment allowing for a better understanding of the association dynamics. The results show that cyclodextrin cavities act as "hard" cages which put geometric and orientational restrictions on the inclusion of a hydrophobic guest, whereas micelles behave as "soft" cages without geometrical requirements. In our contribution to this special issue we review briefly the application of FCS to the study of host-guest inclusion complexes with an emphasis on practical aspects and relevant bibliographic references.*

1. Introduction.

Host-Guest complexes are supramolecular aggregates stabilized by non-covalent bonds and are ubiquitous in biochemical, pharmaceutical, environmental, cosmetic, food, and other chemical systems and applications.[1] Different approaches are necessary to fully understand a supramolecular system: structural studies yield stoichiometry, geometry, association sites and heterogeneity, thermodynamic studies provide information about stability, equilibrium constants and reversibility, and finally dynamic studies are necessary to describe the association/dissociation dynamics, diffusional properties or conformational dynamics. Most published studies focus on structure and thermodynamics of supramolecular association, which, however, give very few information about the dynamics of the system. As pointed out

by C. Bohne "Dynamic studies are necessary to provide the 'movie' in addition to the 'snapshots' taken from structural and thermodynamic measurements".[2]

In this contribution we briefly summarize how to use Fluorescence Correlation Spectroscopy (FCS) for the study of supramolecular association and, more specifically, of the stability and the binding dynamics in host-guest systems (as usual we use "binding" as a general term for an attractive noncovalent interaction. In the context of "host-guest" systems it refers to a "complexation" or more specifically to "inclusion"). We show how knowledge about the dynamics gives valuable information about the association mechanism, which is directly related to the structure of the host and the guest. For details we refer to relevant bibliography.

2. Association Dynamics.

Host-Guest complexes are typically formed by the association of host H with guest G to give a 1:1 complex HG (see Figure 1). The association rate (on-rate) $v_+ = k_+$ [H] [G] is described by the bimolecular association rate constant k_+, whereas the dissociation rate (off-rate) $v_- = k_-$ [HG] is defined by the unimolecular dissociation rate constant k_-. Both processes, association and dissociation, are rate-limited by molecular diffusion and thus upper limits are given by diffusion-controlled rate constants: i.e. $k_+ < 10^{10}\,M^{-1}\,s^{-1}$, $k_- < 10^{9}\,s^{-1}$ in aqueous solution.

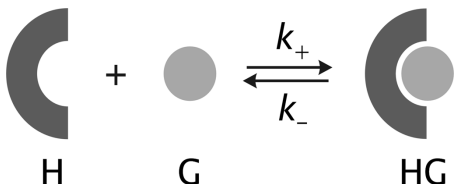

Figure 1. Host H and guest G form complex HG with association rate constant k_+ and separate with dissociation rate constant k_-.

At equilibrium both rates are equal, $v_+ = v_-$, and the binding equilibrium constant K is derived as ratio of the association and dissociation rate constants as given in eq. 1.

$$K = \frac{[HG]_{eq}}{[H]_{eq}[G]_{eq}} = \frac{k_+}{k_-} \qquad (1)$$

Dynamic studies give information on how fast the complex associates or dissociates. For a 1:1 complexation the corresponding rate law (eq. 2) and the typical condition of excess host concentration ($[H]_0 \gg [G]_0$) lead to a pseudo-first order association rate and to kinetics which are mono-exponential with an observed relaxation rate constant k_R as given in eq. 3. Here we

assume that the guest acts as fluorescent probe. Being FCS a single molecule technique, the total concentration of the fluorescent probe is very low, of the order of $[G]_0 \approx 10^{-8}$ M. Thus the condition ($[H]_0 \gg [G]_0$) is fulfilled even for hosts of low solubility or high affinity systems. Don't confuse the time dependence of the guest concentration $[G](t)$ with the autocorrelation of the intensity fluctuations $G(\tau)$ defined in eq. 4.

$$\frac{d[HG]}{dt} = k_+[H][G] - k_-[HG] \tag{2}$$

$$[G](t) \sim e^{-k_R t}, [HG](t) \sim 1 - e^{-k_R t}, k_R = k_+[H]_0 + k_- \tag{3}$$

The relaxation rate constant k_R depends on the two rate constants, k_+ and k_-. The contribution of the association process can be modulated by varying the host concentration $[H]_0$, but not that of the dissociation.[3, 4]

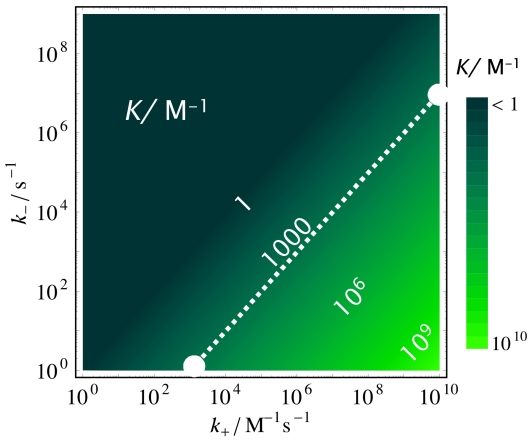

Figure 2. Very different values of the association rate constant k_+ and the dissociation rate constant k_- can lead to the same value of the binding equilibrium constant K.

Can we infer information about the relaxation rate constant k_R of the binding equilibrium from the corresponding equilibrium constant K? In other words: does knowledge about the stability (thermodynamics) of a complex give information about the dynamics of the host guest association? The answer is "not so much"; systems with similar values of their stability constant K may present very different values of their association and dissociation rate constants. For example, for a typical intermediate stability constant, $K = 1000\ M^{-1}$, the association rate constant can fall in a very wide interval, between very low values, e.g. $k_+ = 10^3\ M^{-1} s^{-1}$ or very high ones, only limited by diffusion ($k_+ = 10^{10}\ M^{-1} s^{-1}$), with the corresponding values of the dissociation rate constants as indicated in Figure 2.

That host-guest complexes with similar stability can present very different dynamics, had already been demonstrated by the classical work of Cramer et al. for the inclusion of different azoderivatives by α-cyclodextrin (αCD) studied by the temperature-jump technique.[5] Substitution of the azoderivatives with ethyl or methyl side groups changes only very slightly the stability of the αCD inclusion complex but decreases the association and dissociation rate constants by several orders of magnitude.

How fast is the association/dissociation process? The time scale of this process is given by the relaxation time $\tau_R = k_R^{-1}$ which is the inverse of the relaxation rate constant k_R (eq. 3). Again, as an example, for $K = 1000\ M^{-1}$, we can analyse the two above-mentioned cases as depicted in Figure 3, right panel: slow dynamics with $k_+ = 10^3\ M^{-1}s^{-1}$, $k_- = 1\ s^{-1}$ (upper red curve) correspond to long relaxation times of $\tau_R = 1$ s. Fast, diffusion-controlled dynamics with $k_+ = 10^{10}\ M^{-1}\ s^{-1}$, $k_- = 10^7\ s^{-1}$ (lower, blue curve) lead to short relaxation times of $\tau_R = 100$ ns or faster. These relaxation rates correspond to conditions of very low host concentration where the dissociation process controls the relaxation rate. In both cases the observed relaxation time is shortened with increasing host concentration. As can be seen, binding dynamics cover a very wide time range and the upper limit corresponds to very fast reactions experimentally not easily accessible.

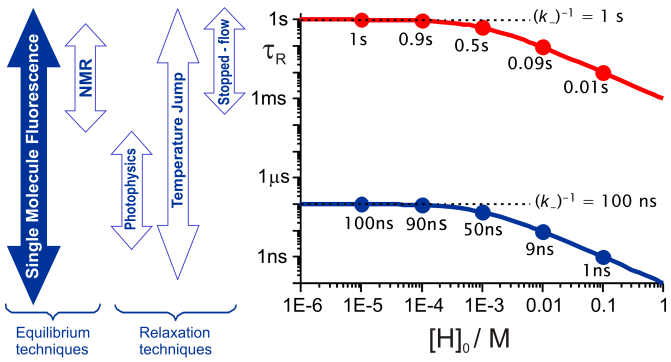

Figure 3. Right panel: For the same typical intermediate binding equilibrium constant, $K = 1000\ M^{-1}$, the relaxation time $\tau_R = k_R^{-1}$ of the equilibrium can vary in a very wide time interval from seconds to nanoseconds. Upper curve: slow dynamics with $k_+ = 10^3\ M^{-1}s^{-1}$, $k_- = 1\ s^{-1}$, and $\tau_R < 1$ s. Lower curve: fast dynamics with $k_+ = 10^{10}\ M^{-1}s^{-1}$, $k_- = 10^7\ s^{-1}$, and $\tau_R < 100$ ns. Left panel: Dynamic range covered by some frequently used fast techniques for the determination of the rate constants of supramolecular association/dissociation.

Frequently used fast techniques for the determination of the rate constants of supramolecular association/dissociation are temperature-jump (T-Jump), time-resolved fluorescence (TRF), laser flash photolysis (LFP), ultrasonic relaxation and stopped-flow (see Figure 3, left panel).[2, 6-8] These methods analyze the relaxation of the system back to equilibrium after a perturbation. TRF and LFP rely on the photophysics of chromophores with fluorescent excited states or long lived triplet states and/or on the presence of a quenching molecule.

Ultrasonic relaxation needs no chromophore but requires detailed knowledge about the molecular process being disturbed. Laser T-Jump covers a wide time range from nanoseconds to seconds, whereas TRF, LFP and ultrasonic relaxation are limited to dynamics of nano- to microseconds. Stopped-flow techniques can only be used to study slow dynamics. There are other techniques that allow dynamic study of systems at thermodynamic equilibrium. The most known is NMR, which is, however, limited to slow dynamics

3. Single Molecule Fluorescence.

The study of supramolecular dynamics require methodologies which cover a very wide range of time scales, ideally within the same experiment. It is also preferred not to rely on unique photophysical properties of the host guest system and to avoid perturbation of the system. Techniques which analyze the fluorescence of single molecules have the potential to cover these needs. They analyze variations in the fluorescence intensity of a molecular system due to spontaneous fluctuations around the equilibrium, without the need for an external perturbation and they can cover a very wide dynamic range.[9, 10]

Although standard "bulk" fluorescence experiments already use low dye concentrations of about 10^{-6} mol dm^{-3} and small detection volumes around 1 mm^3, the observed fluorescence is still an average of the light emitted by about 10^{11} dye molecules! This huge number average hides any static and temporal heterogeneities in the molecular ensemble and, more important for our case, makes it practically impossible to follow directly the dynamics of the unsynchronized molecular processes. Kinetic measurements at these "bulk" concentrations require therefore some external perturbation which synchronizes the molecular processes, so that their relaxation back to equilibrium can be followed as a macroscopic variation of the ensemble properties (Figure 4, a).

Single molecule fluorescence techniques observe a very small number or even a single molecule at a time (Figure 4, b) and avoid thus the loss of information due to averaging. Observing a few molecules allows one to follow directly the dynamics of the reversible association process as significant fluctuations in the fluorescence intensity, provided that the association affects the brightness of the fluorescent guest (or host). The species dependent *brightness* is given by the product of the extinction coefficient, fluorescence quantum yield and detection efficiency and is a measure for the detected fluorescence count rate from each species.

In order to detect fluorescence from single fluorophores it is not sufficient to reduce the concentration of the observed dye but it is also necessary to suppress the background signal (Raman scattering, impurities) by reducing the sample volume itself. Different techniques are used for this aim. For slow dynamics one of the reaction partners is typically immobilized on

a glass surface and the fluorescence is excited only within a very thin layer above this surface by means of special illumination techniques (e.g. total internal reflection, TIR). The fluorescence from this layer can then be detected with highly sensitive CCD cameras.[9] Dynamics in the microsecond to hour range can be observed, limited mainly by the photostability of the dyes at the long end and the time resolution of the detection at short times.

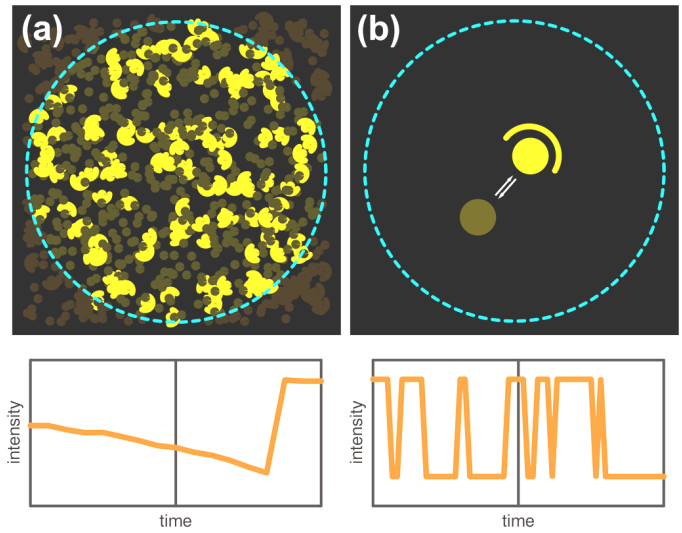

Figure 4. Simulated kinetic experiments for the study the dynamics of a reversible (association) reaction assuming that the guest increases its fluorescence intensity upon complexation. Upper panels: scheme of the sample volume (blue dashed circle) with bright yellow complex and dark brown free guest. Lower panels: observed total fluorescence intensity as function of time (time increases to the left). (a) Standard "bulk" measurement: the ensemble relaxes back to equilibrium after an external perturbation. The relaxation time is determined from the exponential change in the "bulk" fluorescence intensity. (b) Single molecule measurement: the system is at equilibrium and the reversible process is followed directly from the change in fluorescence intensity provoked by the reaction. Depending on the single molecule technique the rate constants k_+ and k_- are determined directly from the time the system stays in each of the two states (free, bound) or the relaxation time τ_R is determined from the characteristic time of the fluorescence fluctuations.

Faster dynamics are typically observed with molecules which diffuse freely through a very small open detection volume defined by the focus of an epi-illuminated confocal microscope (see Figure 5). During the transit through the sample volume the fluorophore is repeatedly excited and the change in fluorescence intensity due to the reversible reaction is detected. Here the dynamic range is limited by the fluorescence lifetime of some nanoseconds of the dye itself and the mean transit time of the fluorophore through the sample volume, typically in the millisecond range. The fluorescence intensity fluctuations can be analyzed by different techniques, and we will present in the following Fluorescence Correlation Spectroscopy (FCS) as one of the most widely used.

For all Single Molecule Fluorescence techniques several conditions have to be fulfilled. One needs very bright and photostable dyes, very efficient excitation and detection setups, very low dye concentrations and highly purified solvents and solutes. In order to observe the dynamics one also relies on a highly fluorescent probe molecule which undergoes some change in its photophysical properties during the association/dissociation process.

4. Fluorescence Correlation Spectroscopy.

4.1. Principles.

FCS analyzes the spontaneous temporal fluctuations of the fluorescence intensity emitted by a few (1-10) molecules in a small open sample volume. These intensity fluctuations may be due to various processes at the molecular level: changes in the singlet or triplet excited-state population, changes in the local concentration due to translational motion of the fluorophores in and out of the sample volume or changes in their physicochemical properties, for example due to a chemical reaction or, as in our case, supramolecular association. Each of these processes modulates the fluorescence intensity at a characteristic timescale which can in principle be derived from the autocorrelation function of the intensity trace. Several excellent reviews,[11-15] monographs,[9,16-19] and textbooks[20,21] present FCS theory for different applications. We will point out briefly the most important aspects.

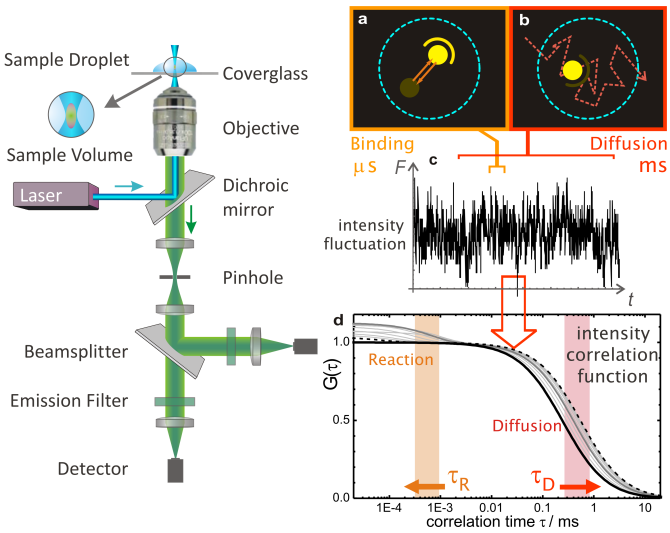

Figure 5. Principles of Fluorescence Correlation Spectroscopy. Left panel: epi-illuminated confocal microscope used to create a microscopic sample volume. Right panel: scheme of the data analysis. (a,b) The blue dashed circles indicate the border of the sample volume. The yellow dots represent dye molecules undergoing a reversible association (a), and moving randomly through the solution due to brownian motion (b). Detected fluorescence intensity (c), and autocorrelation function of the intensity fluctuations (d).

In FCS the molecules under study diffuse freely freely within a small sample droplet and eventually pass through the focus of a confocal epi-illuminated fluorescence microscope (Figure 5, left). The focus defines an open microscopic effective detection volume of some femtoliter (10^{-15} liter). If the concentration of the dye molecules in the droplet is low (nanomolar, 10^{-9} mol/liter) then only very few molecules are observed at a time. The molecules are excited by laser light through the microscope objective and their fluorescence is collected by the same objective and focused through a pinhole and filters onto detectors with single photon sensitivity. The molecules move randomly through the solution due to brownian motion (Figure 5, b) and at the same time undergo a fast reversible reaction (Fig. 5, a). Both processes introduce fluctuations at characteristic time scales in the detected total fluorescence intensity $F(t)$ (Figure 5, c). The characteristic time of the fluctuations is determined from the autocorrelation curve $G(t)$ of the intensity fluctuations $\delta F(t)$ (Fig. 5, d).[3,4]

$$G(\tau) = \frac{\langle \delta F(t)\, \delta F(t+\tau)\rangle}{\langle F(t)\rangle^2} \tag{4}$$

Under the conditions discussed in the following sections the full correlation function for translational diffusion and a fast reversible (association) reaction is given by eq. 5 with the mean diffusion (transit) time $\bar{\tau}_D$, the mean number of fluorescent molecules in the sample volume N, the ratio between radial and axial radii of the sample volume ω_{xy}/ω_z, and the amplitude A_R of the reaction term.

$$G_{DR}(\tau) = \frac{1}{N}\left(1+\frac{\tau}{\bar{\tau}_D}\right)^{-1}\left(1+\left(\frac{\omega_{xy}}{\omega_z}\right)^2\frac{\tau}{\bar{\tau}_D}\right)^{-\frac{1}{2}}(1+A_R\, e^{-k_R\tau}) \tag{5}$$

4.2. Translational Diffusion.

On the millisecond time scale the observed fluorescence intensity depends on the number of dye molecules present in the open sample volume, a number which fluctuates due to the entry and exit of dyes under Brownian motion. The characteristic time of these fluctuations reflects the mean transit (or diffusion) time τ_D of the fluorescent species through the sample volume, which depends on the translational diffusion coefficient of the fluorophore and on the size of the sample volume. A calibration of this size with a reference dye allows one then to determine the diffusion coefficient of the fluorophore from measurements of τ_D. The translational diffusion coefficient D is inversely proportional to the diffusion time τ_D according to eq. 6, with ω_{xy} being the radial radius of the sample volume. The diffusion coefficient D is also related to the hydrodynamic radius R_h as given for homogeneous spheres by the

Stokes-Einstein relation on the right hand in eq. 6, where k is the Boltzmann constant and η the viscosity of the solvent.

$$D = \frac{\omega_{xy}^2}{4\tau_D} = \frac{k\,T}{6\,\pi\,\eta\,R_\mathrm{h}} \tag{6}$$

The amplitude of the correlation function (eq. 5) is inversely proportional to the number of fluorophores in the detection volume (N), which is a peculiarity of the technique: the lower the concentration of dye the higher the amplitude of the fluctuations and, consequently, of the correlation function.

4.3. Binding Equilibrium Constant.

The diffusion coefficient of a fluorescent guest decreases when it binds to a host. The association of the guest to the host introduces a variation in the observed diffusion coefficient (or diffusion time) of the guest which depends on the third root of the molar mass ratio, as given by eq. 7 for homogeneous compact spheres.

$$\frac{D_\mathrm{HG}}{D_\mathrm{G}} = \frac{\tau_\mathrm{G}}{\tau_\mathrm{HG}} \approx \frac{R_\mathrm{h,G}}{R_\mathrm{h,HG}} \approx \sqrt[3]{\frac{M_\mathrm{G}}{M_\mathrm{HG}}} \tag{7}$$

FCS is used here for binding dynamics that are much faster than the mean diffusion time of the fluorophore through the detection volume (fast exchange). In this case the fluorescent guests will associate and dissociate many times during their transit, changing rapidly between free (G) and bound (HG) state. The observed mean diffusion time $\bar{\tau}_\mathrm{D}$ depends then on the fraction of the time that the fluorescent guests spent in the free or in the bound state. This can be expressed by the number-weighted mean diffusion coefficient $\overline{D}$ obtained from the individual coefficients D_G and D_HG of free and bound dye and the number fractions $X_\mathrm{x} = N_\mathrm{x}/(N_\mathrm{G}+N_\mathrm{HG})$ as given in eq. 8.

$$\bar{\tau}_D = \frac{\omega_{xy}^2}{4\overline{D}} \qquad \overline{D} = X_G D_G + X_{HG} D_{HG} \tag{8}$$

In the case of the equilibrium of Fig. 1 and eq. 1 the fractions can be expressed by the equilibrium constant K and the host concentration $[\mathrm{H}]_0$ which leads to eq. 9.

$$\bar{\tau}_D([\mathrm{H}]) = \frac{\tau_\mathrm{G}\,(1 + K\,[\mathrm{H}]_0)}{1 + \frac{\tau_\mathrm{G}}{\tau_\mathrm{HG}} K\,[\mathrm{H}]_0} \tag{9}$$

Titrations of this mean diffusion time at different host concentrations $[H]_0$ allows one to determine the binding equilibrium constant K and the limiting diffusion coefficients of free and bound guest.[4]

The binding equilibrium constant K can be determined solely from the change in the hydrodynamic properties of the guest upon complexation. For the determination of K it is therefore not necessary (but allowed) that the fluorophore changes its brightness during the binding. This makes it possible to study nonfluorescent hosts labelled with a fluorophore which does not need to interact itself with the host. This is an advantage of FCS over other fluorescence techniques which rely on a significant change of some fluorescence properties of the guest in order to detect its binding.

An example is the inclusion of the nonfluorescent guest adamantane by βCD.[22] The fluorescent label (Alexa 488) attached to the adamantane presents no change in its fluorescent properties due to the inclusion of the adamantane moiety by βCD. The inclusion equilibrium is therefore not easily accessible by standard fluorescence techniques. A FCS titration, however, shows immediately a systematic increase of the diffusion time of the fluorescently labelled adamantane ($M_G = 826$ g mol^{-1}) on the addition of βCD ($M_H = 1135$ g mol^{-1}), as shown in Figure 6.

The experimentally determined ratio of the limiting values $D_{HG}/D_G = \tau_G/\tau_{HG} = 0.74$ coincides perfectly with the expected value $(M_G/M_{HG})^{1/3} = (0.422)^{1/3} = 0.75$ (see eq. 7).[22] The equilibrium constant obtained from these FCS titrations is in good agreement with that obtained by other techniques.

In order to follow with FCS the relatively small variations in the diffusion coefficient D_{HG}/D_G observed with small hosts such as cyclodextrins great care has to be taken during the experiments and artifacts introduced by triplet state population, saturation and photobleaching, background signal, variation in solvent viscosity, sample temperature and deformations of the effective detection volume (due, for example, to very small variations in the cover slide thickness) have to be taken into account.[22-24]

For an accurate determination of the binding equilibrium constant it is very important to make sure that the observed diffusion time is not affected by saturation and photobleaching of the fluorophore due to too high excitation irradiance. The diffusion time has to be independent of the excitation power, both at zero and at high host concentrations, which has to be checked experimentally for each host-guest combination. Too high irradiance shortens the observed diffusion time as a function of the host concentration and leads to strongly erroneous results for the equilibrium constant.

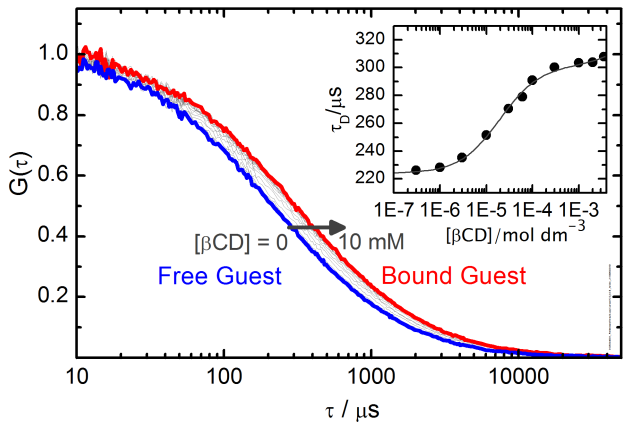

Figure 6. Inclusion equilibrium between βCD and adamantane labeled with Alexa 488 dye studied by FCS. Main panel: the diffusion term of the correlation curves shifts to longer times on the addition of increasing amounts of βCD due to the increase in the mean diffusion time $\bar{\tau}_D$ of the guest. Inset: Plot of $\bar{\tau}_D$ versus $[\beta CD]_0$ (note the logarithmic concentration scale). Fitting of $\bar{\tau}_D$ with eq. 9 yields the high equilibrium constant $K = (52 \pm 2)\ 10^3\ M^{-1}$.[22]

4.4. Binding Dynamics.

Binding dynamics can be observed when the fluorescence brightness of the guest changes between its free and bound states. Binding leads then to fluorescence blinking which can be analysed by FCS. To be detectable in FCS the blinking must be much faster than the transit through the sample volume, that is the relaxation time τ_R of the binding process (eq. 2) must be shorter than the diffusion time τ_D (fast exchange). The fluorescence intensity fluctuations due to the binding dynamics introduce then an additional term in the correlation function (eq. 5) at the relaxation time τ_R with an amplitude A_R which depends strongly on the brightness ratio $q = Q_{HG}/Q_G$ of bound and free fluorophore (Figure 7, insets τ_R and A_R). Again both τ_R and A_R can be expressed as function of the host concentration and the binding constant as given in eq. 10 and 11.[3]

$$\tau_R([H]) = \left(k_-(1 + K[H]_0)\right)^{-1} \tag{10}$$

$$A_R = \frac{K[H]_0(1-q)^2}{(1+qK[H]_0)^2} \tag{11}$$

The amplitude of the reaction term A_R is zero both at very low and at very high host concentrations when the guest is either totally free or fully bound (see Figure 7). The highest amplitude A_R is reached at a host concentration $[H]_{0,max} = (K\ q)^{-1}$ which depends on the brightness ratio q. Fluorophores which increase strongly their brightness upon binding make it possible to detect the dynamics already at a very small degree of binding (low host concentrations) and at relatively long relaxation times.[25]

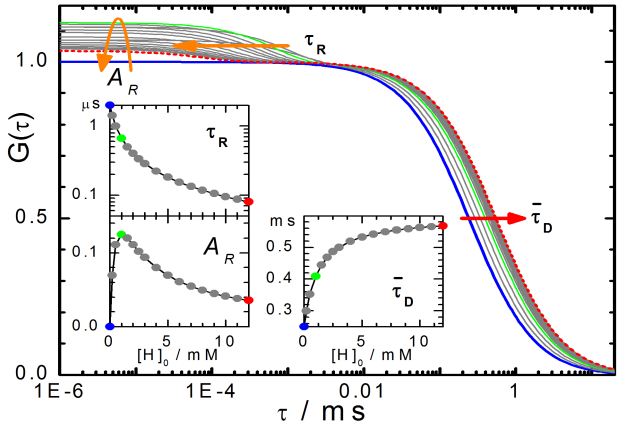

Figure 7. Main panel: Correlation curves from simulated FCS experiments (eq. 5) of an inclusion equilibrium as depicted in Figure 5. Thick blue line: free guest, $[H]_0 = 0$. Thin grey lines: intermediate host concentrations. Dashed red line: highest host concentration $[H]_0 = 12$ mM. Insets: Dependence of the amplitude of the relaxation term A_R, of the relaxation time τ_R, and of the mean diffusion time $\bar{\tau}_D$ on $[H]_0$. (Parameters used for simulation: $N = 1$, $\tau_G = 0.25$ms, $\tau_{HG} = 0.6$ ms, $q = 0.5$, $K = 2000$ M^{-1}, $k_+ = 10^9$ M^{-1} s^{-1}, $k_- = 5\ 10^5$ s^{-1}).

From fits of the corresponding correlation function (eq. 5, 9, 10 and 11) to the experimental correlation curves one determines both the equilibrium constant K and the dissociation rate constant k_-. From eq. 1 also the association rate constant k_+ is obtained.[3]

Complications may arise when additional terms appear in the correlation curves, mainly due to excited-state dynamics of the fluorophore. Transitions in and out of the dark triplet state of the fluorophore introduce fluorescence fluctuations with the triplet lifetime of some microseconds.[26] The population of the triplet state is strongly dependent on the excitation power and can in principle be reduced working at low irradiance.

5. Influence of Host-Guest Geometry on the Dynamics.

In order to study the influence of the geometry of host and guest on the binding dynamics we studied two parent cyclodextrins, βCD and γCD, and two analogous guest molecules, pyronine Y (PY) and pyronine B (PB), which have the same xanthene skeleton but methyl and ethyl substituents, respectively, at the amino side groups (Figure 8).

Electronic absorption and fluorescence spectroscopic studies showed that in all cases 1:1 pyronine:CD complexes are formed, although also 2:1 complexes with γCD are observed for both pyronines at dye concentrations much higher than those used in FCS.[27,28] The values of the (1:1) association equilibrium constants, K, differ significantly between the four host-guest combinations (Table 1). In contrast to what may be expected, for each type of CD the

binding constant is larger with PB than with PY in spite of the bulkier side groups of PB. Moreover, larger association equilibrium constants are obtained for the CD of smaller cavity.

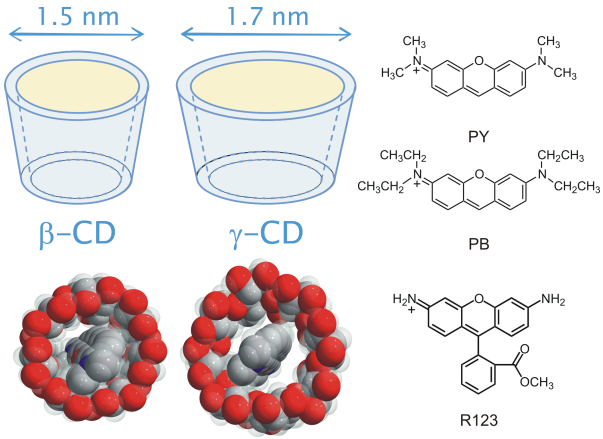

Figure 8. Geometry of βCD and γCD. Structures of the dyes PY, PB, and R123.

The pure emission spectra of free and bound dyes allow one to estimate the brightness ratio q as given in Table 1. In the systems studied here, the brightness of the dyes decrease significantly when they are bound to the hosts.

As an example Figure 9 shows a series of correlation curves obtained in titration experiments of PY with βCD. Due to the fast exchange of the pyronine guest in and out of the CD complex only a single diffusion term with a mean diffusion time, $\bar{\tau}_D$, is observed which increases as the host concentration is increased (compare insets $\bar{\tau}_D$ in Figure 7 and Figure 9). The second term in the correlation curves due to the association/dissociation dynamics is described by the relaxation time, τ_R, and an amplitude A_R that varies with the concentration of the host as expected (compare insets τ_R in Figure 7 and Figure 9). In all cases it has to be checked that the relaxation time is in fact much shorter than the diffusion time, in order to allow for the separation of the two terms in the correlation function. The small contribution of the triplet-state formation to the correlation curves which appears at about the same correlation time as the reaction term must also be taken into account in the analysis.

Global target analysis of the FCS curves as a function of host concentration with the correlation function as given in eq. 5 yields the association/dissociation rate constants.[3] The results of the fits for the systems under study are shown in Table 1. In most cases the value of K obtained from bulk fluorescence and absorption titrations was fixed in the fits of the correlation curves, in order to improve the accuracy of other fit parameters such as k_-. For the system PY:γCD it was not possible to determine the association and dissociation rate

constants since the reaction term appears at too short correlation times overlapping with the fluorescence lifetime of PY.

Table 1. Results from Global target fits of series of FCS curves and derived values as explained in the text.[3, 4]

	PB:βCD	PY:βCD	PB:γCD	PY:γCD	R123:TX100
K / 10^3 M^{-1}	2.1 ± 0.2	0.40 ± 0.04	0.19 ± 0.03	0.04 ± 0.01	65 ± 3
q	0.49 ± 0.04	0.6 ± 0.2	0.67 ± 0.02	0.34 ± 0.02	0.42 ± 0.03
τ_A / ms	0.30 ± 0.02	0.25 ± 0.02	0.27 ± 0.02	0.23 ± 0.02	0.263 ± 0.002
τ_B / ms	0.40 ± 0.04	0.45 ± 0.06	0.46 ± 0.05	0.41 ± 0.05	1.66 ± 0.05
k_+ /10^9 $M^{-1}s^{-1}$	0.15 ± 0.05	0.2 ± 0.1	0.56 ± 0.11	> 1	14 ± 1
k_- / 10^4 s^{-1}	7.6 ± 2.7	50 ± 30	300 ± 30	-	22 ± 1
k_d /10^9 $M^{-1}s^{-1}$	7.7 ± 0.5	8.0 ± 0.5	8.0 ± 0.5	8.4 ± 0.3	16 ± 1
k_{-d} / 10^9 s^{-1}	2.0 ± 0.1	2.6 ± 0.2	2.1 ± 0.2	2.7 ± 0.1	0.11 ± 0.01
k_r / 10^9 s^{-1}	0.04 ± 0.01	0.07 ± 0.03	0.16 ± 0.03	-	-
k_{-r} / 10^4 s^{-1}	7.7 ± 2.7	50 ± 30	320 ± 100	-	-
D_G / 10^{-10} m^2 s^{-1}	4.8 ± 0.4	5.8 ± 0.4	4.8 ± 0.4	5.8 ± 0.4	4.3 ± 0.4
D_{HG} / 10^{-10} m^2 s^{-1}	3.6 ± 0.4	3.2 ± 0.3	3.1 ± 0.4	3.5 ± 0.4	0.7 ± 0.1
R_G / R_{HG} (Å)	5.1 / 6.8	4.2 / 7.6	5.1 / 7.8	4.2 / 7.0	5.7 / 36
$M_{w,G}$ / $M_{w,HG}$ (Da)	324 / 1459	267 / 1402	324 / 1621	267 / 1564	381 / 95000

The diffusion coefficients D and all derived values were recalculated for a new reference value for Rhodamine 6G, $D_{R6G}(25°C) = (4.0 \pm 0.3)$ 10^{-10} m^2 s^{-1}.[29, 30] The uncertainties represent one standard deviation as given by the fits and do not include the uncertainty in the reference value. All values given for 25°C. The molar mass does not include that of the counterions of the charged dyes.

From the hydrodynamic properties of host and guest the collision rate constants k_d for a purely diffusion-controlled association process between two species can be estimated applying the Smoluchowski equation (eq. 12) as given in Table 1.

$$k_d = 4\,\pi\,(D_G + D_H)\,(R_G + R_H)\,N_0 \qquad (12)$$

(D_G, R_G and D_H, R_H are diffusion coefficients and hydrodynamic radii of guest G and host H, respectively, and N_0 is the Avogadro constant.) This diffusion limited rate constant k_d will be compared later with the rate constant k_+ of association between guest and host determined from the same FCS data. It is clearly an advantage of FCS to yield in the same measurement information about both diffusional and association dynamics.

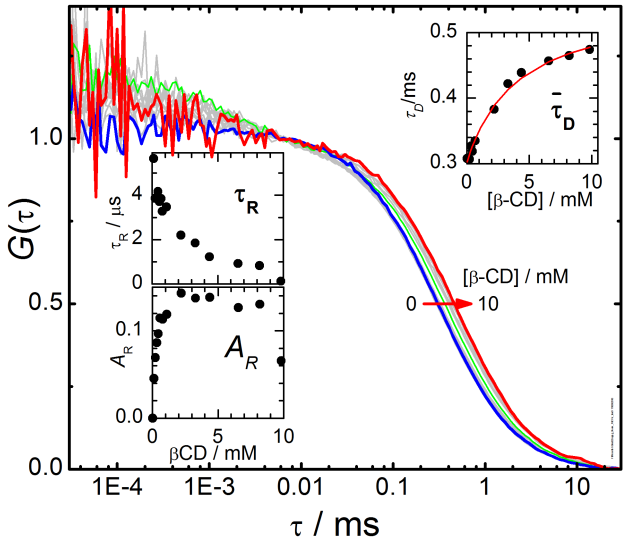

Figure 9. Main panel: Experimental normalized correlation curves of PY in aqueous solution with increasing βCD concentrations. Insets: Variation of the mean diffusion time τ_D, the relaxation time τ_R and the amplitude of the reaction term A_R with the concentration of βCD as determined from individual fits of eq. 5.[3]

Binding Dynamics of "Hard" and "Soft" Cages.

The rate constants k_+ of association of the guests PY and PB to βCD are both similar with a very high value of about $k_+ = 0.2\ 10^9\ M^{-1}\ s^{-1}$ (Table 1). This is, however, still about 40 times lower than the estimated collision rate constant $k_d = 8\ 10^9\ M^{-1}s^{-1}$, with which host and guest collide due to Brownian motion in the solvent (eq.12, Table 1). The overall association (inclusion) is thus much slower than expected for a diffusion-controlled process. This can be understood on the basis of a two step process (see Figure 10, a).[3] First host and guest collide with rate constant k_d and form an encounter complex within a common solvent cage. If no specific interactions are assumed a lifetime of the encounter complex of about 1 ns can be estimated. During this lifetime host and guest collide of the order of 100 times changing randomly their relative orientation. In most cases they separate again with rate constant k_{-d} without inclusion. Depending on the geometrical requirements for the inclusion of the guest into the host a small fraction of the relative orientations may be favourable so that inclusion can occur with a rate constant of inclusion, k_i. The overall association rate is thus mostly controlled by this inclusion step.

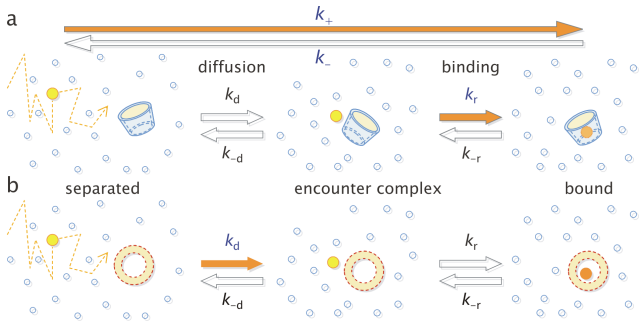

Figure 10. Two step mechanism for supramolecular association involving the formation of an encounter complex, for a "hard" cage (cyclodextrin) (a) and a "soft" cage (micelles) (b).

Both guests, PY and PB, have similar association rate constants in spite of their different side groups. On one hand, simulations indicate that the side groups may not change significantly the critical dimension which determines the probability to enter the βCD cavity[3] and, on the other hand, the high flexibility of the CD molecule probably allows for an induced fit compensating part of the difference in the guest geometry.[31]

Another interesting result is the fact that the difference in the stability of these inclusion complexes is determined by their dissociation and not by the association process. The dissociation rate constants of PY and PB with βCD (Table 1) differ in about one order of magnitude, reflecting the stronger interaction of PB than PY with the interior of the βCD cavity, as already proposed on the basis of "bulk" fluorescence studies.[32]

What happens if we increase the size of the host cavity? The data for the inclusion of PY and PB by γCD, a host with a 20 % bigger diameter of its cavity, show that the association rate constant, k_+, of the PB:γCD complex is about four times higher than in the case of PB:βCD (Table1). The wider γCD cavity increases the fraction of favourable relative orientations which lead to an inclusion, although the association process is still not diffusion controlled.

However, the wider cavity weakens also the specific interactions between host and included guest resulting in a strongly increased dissociation rate constant. The overall stability of the pyronine/γCD complexes is therefore much lower than that of the pyronine/βCD complexes.

What do we expect for hosts without geometric restrictions? Micelles are themselves highly dynamic supramolecular self-assemblies of surfactants. Dyes such as the xanthene dye, rhodamine 123 (R123) exchange dynamically between the aqueous and the micellar pseudophase in a process similar to the inclusion described before. But, as opposed to the cyclodextrins, the micelle presents no geometric restrictions for the association of the dye, they act as "soft" hosts.

R123 is a typical probe for FCS, and is very suitable for dynamic studies in micellar systems since it presents a partition equilibrium between the aqueous phase and the micellar pseudophase formed by neutral micelles such as those formed by the aggregation of a well-known non-ionic surfactant, Triton X-100 (TX100) (Figure 8).[4, 33, 34] The 1:1 binding equilibrium constant for the partition equilibrium of the R123 with TX100 micelles is given in Table 1. Due to the low dye concentrations an occupancy number of more than one dye molecule per micelle is negligible.

A strong change in the brightness of R123 during the association process to TX100 micelles makes it possible to follow the association dynamics with FCS as described before (Table 1).[4, 25, 33] As expected, the rate constant of the association of R123 to a TX100 micelle is as fast as the diffusion controlled collision rate constant itself: $k_+ \approx k_d \approx 15\,10^9\,M^{-1}s^{-1}$. This shows that the association is diffusion controlled, in accordance with the picture of an unspecific association without orientational or geometrical requirements (see Figure 10, b). In this sense, the micelles may be seen as "soft" cages, as opposed to the cyclodextrin "hard" cages, which, although highly flexible, impose orientational restrictions to the inclusion.

References.

[1] Dodziuk, H.: Introduction to Supramolecular Chemistry. Springer, Dordrecht (2002)

[2] Bohne, C.: Supramolecular Dynamics Studied Using Photophysics. *Langmuir*. 22, 9100-9111 (2006)

[3] Al-Soufi, W., Reija, B., Novo, M., Felekyan, S., Kühnemuth, R., Seidel, C.A.M.: Fluorescence Correlation Spectroscopy, a Tool to investigate Supramolecular Dynamics: Inclusion Complexes of Pyronines with Cyclodextrin. *J. Am. Chem. Soc.* 127, 8775-8784 (2005)

[4] Al-Soufi, W., Reija, B., Felekyan, S., Seidel, C.A., Novo, M.: Dynamics of supramolecular association monitored by fluorescence correlation spectroscopy. *Chemphyschem*. 9, 1819-1827 (2008)

[5] Cramer, F., Saenger, W., Spatz, H.C.: Inclusion Compounds. XIX. The Formation of Inclusion Compounds of alpha-Cyclodextrin in Aqueous Solutions. Thermodynamics and Kinetics. *J. Am. Chem. Soc.* 89:1, 14-20 (1967)

[6] Kleinman, M.H., Bohne, C. In: Ramamurthy, V., Schanze, K.S. (eds.) Organic Photochemistry, , p. 391, Marcel Dekker Inc, New York (1997)

[7] Pace, T.C.S., Bohne, C.: Dynamics of Guest Binding to Supramolecular Systems: Techniques and Selected Examples. *Advances in Physical Organic Chemistry*. 42, 167-223 (2008)

[8] Zana, R.: Dynamics of Surfactant Self-Assemblies: Micelles, Microemulsions, Vesicles, and Lyotropic Phases. Taylor & Francis/CRC Press, Boca Raton (2005)

[9] Selvin, P.R., Ha, T.: Single-Molecule Techniques: A Laboratory Manual. Cold Spring Harbor, N.Y. : Cold Spring Harbor Laboratory Press (2008)
[10] Walter, N.G., Huang, C.Y., Manzo, A.J., Sobhy, M.A.: Do-it-yourself guide: how to use the modern single-molecule toolkit. *Nature Methods*. 5, 475-489 (2008)
[11] Widengren, J., Rigler, R.: Fluorescence correlation spectroscopy as a tool to investigate chemical reactions in solutions and on cell surfaces. *Cell Mol. Biol*. 44, 857-879 (1998)
[12] Van Craenenbroeck , E., Engelborghs, Y.: Fluorescence Correlation Spectroscopy: Molecular Recognition at the Single Molecule Level. *Journal of Molecular Recognition*. 13, 93-100 (2000)
[13] Krichevsky, O., Bonnet, G.: Fluorescence correlation spectroscopy: the technique and its applications. *Reports on Progress in Physics*. 65, 251-297 (2002)
[14] Hess, S.T., Huang, S., Heikal, A.A., Webb, W.W.: Biological and Chemical Applications of Fluorescence Correlation Spectroscopy: A Review. *Biochemistry* (N.Y.). 41, 697-705 (2002)
[15] Gösch, M., Rigler, R.: Fluorescence correlation spectroscopy of molecular motions and kinetics: Advances in Fluorescence Imaging: Opportunities for Pharmaceutical Science. *Adv. Drug Deliv. Rev*. 57, 169-190 (2005)
[16] Thompson, N.L. In: Lakowicz, J.R. (ed.) Topics in Fluorescence Spectroscopy. Techniques, , p. 337, Plenum Press, New York(1991)
[17] Rigler, R., Elson, E.S.: Fluorescence Correlation Spectroscopy: Theory and Applications. Springer Verlag, Berlin (2001)
[18] Zander, C., Enderlein, J., Keller, R.A.: Single-Molecule Detection in Solution - Methods and Applications. VCH-Wiley, Berlin/New York (2002)
[19] Gell, C., Brockwell, D., Smith, A.: Handbook of Single Molecule Fluorescence Spectroscopy. Oxford University Press, USA (2006)
[20] Valeur, B.: Molecular Fluorescence: Principles and Applications. Wiley-VCH, Germany (2002)
[21] Lakowicz, J.R.: Principles of Fluorescence Spectroscopy. Springer, USA (2006)
[22] Granadero, D., Bordello, J., Pérez-Alvite, M.J., Novo, M., Al-Soufi, W.: Host-Guest Complexation Studied by Fluorescence Correlation Spectroscopy: Adamantane–Cyclodextrin Inclusion. *Int. J. Mol. Sci*. 11, 173-188 (2010)
[23] Enderlein, J., Gregor, I., Patra, D., Fitter, J.: Art and artefacts of fluorescence correlation spectroscopy. *Curr. Pharm. Biotechnol.* 5, 155-161 (2004)
[24] Enderlein, J., Gregor, I., Patra, D., Dertinger, T., Kaupp, U.B.: Performance of Fluorescence Correlation Spectroscopy for Measuring Diffusion and Concentration. *Chemphyschem.* 6, 2324-2336 (2005)

[25] Bordello, J., Novo, M., Al-Soufi, W.: Exchange-Dynamics of a Neutral Hydrophobic Dye in Micellar Solutions Studied by Fluorescence Correlation Spectroscopy. *J. Colloid Interface Sci.* 345, 369-376 (2010)

[26] Widengren, J., Mets, U., Rigler, R.: FCS of triplet states in solution: a theoretical and experimental study. *J. Phys. Chem.* 99, 13368-13379 (1995)

[27] Reija, B., Al-Soufi, W., Novo, M., Vázquez Tato, J.: Specific interactions in the inclusion complexes of Pyronines Y and B with beta-cyclodextrin. *J Phys Chem B.* 109, 1364-1370 (2005)

[28] Bordello, J., Reija, B., Al-Soufi, W., Novo, M.: Host-assisted guest self-assembly: enhancement of the dimerization of pyronines Y and B by gamma-cyclodextrin. *Chemphyschem.* 10, 931-939 (2009)

[29] Gendron, P.O., Avaltroni, F., Wilkinson, K.J.: Diffusion coefficients of several rhodamine derivatives as determined by pulsed field gradient-nuclear magnetic resonance and FCS. *J. Fluoresc.* 18, 1093-1101 (2008)

[30] Müller, C.B., Eckert, T., Loman, A., Enderlein, J., Richtering, W.: Dual-focus fluorescence correlation spectroscopy: a robust tool for studying molecular crowding. *Soft Matter.* 5, 1358-1366 (2009)

[31] Dodziuk, H.: Rigidity Versus Flexibility. A Review of Experimental and Theoretical Studies Pertaining to the Cyclodextrin Nonrigidity. *J. Mol. Struct.* 614, 33-45 (2002)

[32] Almgren, M., Wang, K., Asakawa, T.: Fluorescence Quenching Studies of Micellization and Solubilization in Fluorocarbon-Hydrocarbon Surfactant Mixtures. *Langmuir.* 13, 4535-4544 (1997)

[33] Novo, M., Felekyan, S., Seidel, C.A.M., Al-Soufi, W.: Dye-Exchange Dynamics in Micellar Solutions Studied by FCS. *J Phys Chem B.* 111, 3614-3624 (2007)

[34] Freire, S., Bordello, J., Granadero, D., Al Soufi, W., Novo, M.: Role of Electrostatic and Hydrophobic Forces in the Interaction of Ionic Dyes with Charged Micelles. *Photochem. Photobiol. Sci.* 9, 687-696 (2010)

Acknowledgements.

MN and WAS thank the *Xunta de Galicia* and the *Ministerio de Educación y Ciencia* for financial support (CTQ2007-68057-C02-02/BQU, INCITE09E2R209064ES, INCITE09262304 PR, 2009/029). J.B. thanks the *Ministerio de Educación y Ciencia* for a research scholarship.

Chapter III

Exchange-Dynamics of a Neutral Hydrophobic Dye in Micellar Solutions studied by FCS

Contents:

Exchange-Dynamics of a Neutral Hydrophobic Dye in Micellar Solutions studied by Fluorescence Correlation Spectroscopy

Jorge Bordello, Mercedes Novo and Wajih Al-Soufi

Journal of Colloid and Interface Science (2010), 345(2), 369-376.

Abstract: *The dynamics of the exchange of the moderately hydrophobic neutral dye Coumarine 152 between the aqueous phase and the phase formed by neutral Triton X-100 micelles is studied by Fluorescence Correlation Spectroscopy. The changes in the photophysical properties of the dye in presence of the micelles are discussed. The low quantum yield, the low saturation threshold and the necessary high energetic excitation of this dye requires a careful selection of the experimental conditions in order to obtain dynamic and diffusional properties with reasonable precision. It is shown that the contrast between the brightness of free and bound dye has a strong influence on the sensitivity of the FCS experiment. The entry rate constant of the dye to the micelles,* $k_{+}=(0.8\pm0.3)\ 10^{10}\ M^{-1}s^{-1}$*, is very near to the diffusion controlled limit. The high association equilibrium constant of* $K=(129\pm3)\ 10^{3}\ M^{-1}$ *is mainly determined by the low exit rate constant,* $k_{-}=(0.6\pm0.2)\ 10^{5}\ s^{-1}$.

1. Introduction.

Micelles are highly cooperative, dynamically organized molecular assemblies, stabilized mainly by hydrophobic interactions. Both surfactants and solubilized molecules are constantly exchanged between the micelles and the surrounding aqueous solution. The study of the dynamics of the exchange processes of solubilizates and surfactant molecules is of critical importance for the characterization of a micellar system and also essential for a more detailed theoretical understanding of their formation.[1] Micellar exchange dynamics have significant influence on the performance of a given surfactant solution in technological processes, such as detergency, foaming, solubilisation, emulsification or wetting.[2]

Recently we have shown how the typically very fast dye exchange dynamics can be conveniently studied with fluorescence correlation spectroscopy (FCS), using micelles as

membrane mimetic systems and a typical mitochondrial fluorescence marker, Rhodamine 123 (R123), as probe.[3,4] We also demonstrated the advantages of FCS to determine the association/dissociation rate constants of fluorescent dyes with cyclodextrins.[5]

FCS is a fluctuation correlation method that extracts information about the dynamics of molecular processes from the small changes in molecular concentration or chemical states that arise from spontaneous fluctuations around equilibrium. Therefore FCS yields direct information about the dynamics of a fluorescent probe without the need for external disturbances. FCS allows one to study dynamic and photophysical processes that take place in a wide time scale in one and the same experiment. FCS is a single molecule technique, using very small sample volumes determined by a confocal setup and nanomolar fluorophore concentrations.[6]

Fluorophores used in FCS are typically very bright and highly photostable dyes, such as Rhodamines or other Xanthene derivatives. Unfortunately, most of these dyes are charged molecules. This complicates the systematic study of the interaction of a hydrophobic dye with different micellar systems, many of the surfactants being themselves ionic species. The resulting strong electrostatic interactions between a charged dye, ionic surfactant and the counterions present in solution mask the weaker hydrophobic forces which control the exchange of neutral guests. A charged dye is not a good probe for the study of matter exchange in ionic micelles, except in the case that the electrostatic interactions themselves are the main interest.

Looking for neutral fluorophores one finds that most of them have less adequate properties for FCS. They typically present a lower brightness, worse photostability and mostly need an excitation at lower wavelength with the resulting increase in background signal. The use of these dyes requires a very careful selection of the experimental conditions. On the other hand some of these dyes compensate these disadvantages at least partially by the fact that they show a strong increase in their brightness upon association to a micelle (see Figure 3), just opposite to the behaviour of typical FCS dyes. This is a big advantage as we will show in this contribution. It makes it much easier to detect even small amounts of associated dye and allows one to study the dynamics of the association at low surfactant concentration and in a time interval better accessible to standard FCS equipment.

As a representative example for this type of neutral hydrophobic probes we use coumarine 152 (C152). C152 partitions between the micellar pseudo-phase and the aqueous solution. 7-aminocoumarines have relatively low fluorescence quantum yields in aqueous solution and a poor photostability.[7,8] In addition, coumarines need a more energetic excitation at shorter wavelengths, which also excites more fluorescent impurities. However, in spite of these

drawbacks, the neutral coumarines have certain advantages which make them interesting for the study presented here. They are characterized by two excited singlet states, an intramolecular charge transfer state (ICT) and a twisted intramolecular charge transfer state (TICT).[9] It is known that the ICT states in 7-aminocoumarins are highly fluorescent whereas their TICT states are non fluorescent.[10-12] In the nonpolar and restrictive environment of micelles the formation of TICT states is suppressed, resulting in an appreciable enhancement and blue shift of the fluorescence of the dye within the micellar pseudo-phase (bound dye) as compared to that of the dye in the aqueous phase (free dye). The result is a strong increase in the detected molecular brightness of the 7-aminocoumarins as they associate to a micelle.[13] Additionally, coumarines generally show a much higher Stokes Shift than for example rhodamines, which make it easier to separate the dye fluorescence from the Raman signal of the excitation laser light.

We use the neutral surfactant Triton X-100 (TX100, t-Oct-C_6H_4-$(OCH_2CH_2)_n$OH, n=9-10, M_w=646.85 g mol^{-1}), formed by a polar polyethylene glycol chain and a hydrophobic aromatic chain. Although this surfactant has been extensively studied, there is still some discrepancy about its properties regarding micelle formation. Recent studies reported significant variations of the aggregation number and the *cmc* depending on surfactant concentration, temperature and the technique used.[14-16] We use the following most cited values: critical micelle concentration *cmc*=2.6 10^{-4} mol dm^{-3} and aggregation number N_{agg}=143.[17] The choice of these values has direct effect on the absolute values of our reported rate constants but does not affect the overall conclusions.

We first determine quantum yields, the brightness ratio, and the partition equilibrium constant from ensemble steady state absorption and fluorescence spectra. Then we discuss the experimental conditions in the FCS measurements with respect to the brightness contrast, saturation and photobleaching. Finally we present the diffusional properties and the exchange dynamics as determined from FCS.

2. Materials and Methods.

2.1. Materials.

Coumarine 152 (see Figure 1Sa, in the *Supporting Information*) was purchased from Sigma-Aldrich and used as received. The surfactant TX100 (Fluka BioChemika, see Figure 1Sb, in the *Supporting Information*) was checked for fluorescence impurities and was found to be clean enough for classical fluorescence measurements and for FCS experiments. Water was purified with a Milli-Q system.

2.2. Sample Preparation.

Stock aqueous solutions with concentrations of 15-35 10^{-3} mol dm^{-3} of the surfactant TX100 were prepared. Stock solutions of C152 were prepared with 10-fold higher concentrations than those necessary for the titrations (approximately 10^{-8}-10^{-9} mol dm^{-3} in FCS). The measuring samples were prepared by dilution of a constant volume of the corresponding C152 stock together with different volumes of the surfactant stock solution and addition of water to adjust a certain total volume. The accuracy of these volumes was checked by weighing, and concentration corrections were made. Utmost care had been taken not to contaminate the samples with fluorescent impurities.

Due to the low solubility of C152 in water aqueous solutions of C152 for the stock were stirred over night at room temperature and then filtered. The final concentration of C152 in the filtered solution was then determined from its absorption at 405 nm. The molar absorption coefficient of C152 in water at this wavelength ($\varepsilon^{405}_{water}$= 2532 ± 10 $mol^{-1}\,m^2$) was once determined from the following procedure: first the molar absorption coefficient of C152 was determined in ethanol, in which C152 is well soluble (ε^{405}_{EtOH}= 2034.3 ± 9.0 $mol^{-1}\,m^2$). Then the concentration of a filtered aqueous solution of C152 of known absorbance was obtained by evaporating the water of a given volume, redissolving it in ethanol and measuring its absorbance in this solvent. With ε^{405}_{EtOH} the concentration and thus $\varepsilon^{405}_{water}$ can be calculated.

2.3. Equipment.

Absorption spectra were measured with a Varian-Cary 300 spectrophotometer. Fluorescence emission spectra were recorded with a Edinburgh Intruments F900 spectrofluorimeter.

The setup used for the FCS measurements has been described elsewhere.[18] A 40 µL drop of each sample was deposited on borosilicate coverslips (Menzel Gläser, NO 1 DE). The autofluorescence of these coverslips was sufficiently suppressed in the confocal setup. The samples were excited by the linearly polarized light of a 405 nm continuous wave laser diode (Becker&Hickl, BDM-405-SMC, DE) which was spectrally cleaned (Semrock, Maxdiode LD01-405/10, US), redirected by a dichroic mirror (AHF Analysentechnik, z405 RDC, DE) and focused into the sample by a microscope objective (Olympus, UPLSAPO 60xW/1.20, water immersion) mounted in an inverted microscope (Olympus, IX-71). The fluorescence was focused onto a pinhole (Thorlabs, ∅=50 µm, US) and then split into two beams by a nonpolarizing beamsplitter cube (Newport, 05BC17MB.1, US). Each beam was then focused onto an avalanche photodiode (MPD50CTC APD, ∅=50 µm, MPD, Italy). A band-pass filter (HQ550/100M, AHF Analysentechnik, Tübingen, Germany) in front of the beamsplitter

discriminated fluorescence from scattered light. The detector signals were processed and stored by two TCSPC-modules (SPC 132, Becker & Hickl GmbH, Berlin, Germany). Typically 20 million photons were collected for each correlation curve with count rates between 5 and 20 kHz. All measurements were made at stabilized temperature, 25.0 ± 0.5°C. The excitation power as measured in the focus of the microscope objective by a power meter (Thorlabs, PM30-120, US) was typically 300 µW, corresponding to a mean irradiance of $I_0/2 = P/(\pi\ \omega_{xy}^2) = 26$ kW cm^{-2}, assuming a Gaussian intensity distribution along the optical axis. P is the excitation power in the sample).[7]

The focal area and the detection volume have been calibrated with Rhodamine B (RB) in aqueous solutions at low irradiance. Recent PFG-NMR[19] and dual-focus FCS[20] measurements of the diffusion coefficients of typical rhodamine dyes determine much higher values than those used before in FCS. The diffusion coefficient of RB was estimated from these references to $D_{RB} = (4.4 \pm 0.4)\ 10^{-10}$ m^{2}s^{-1}, yielding a radial $1/e^2$ radius of $\omega_{xy} = 0.50$ µm. However, the very low absorption of RB at the excitation wavelength of 405nm may introduce systematic errors in the calibration. All diffusion coefficients are corrected for temperature and viscosity effects and are given for 25°C.

2.4. Data Analysis.

The series of absorption and emission spectra obtained in the titrations of C152 with the surfactant were analyzed using principal components global analysis (PCGA).[21] For FCS curves two levels of nonlinear data analysis have been applied: (1) Individual correlation curves were fitted by a fast home-built routine that runs under LABVIEW (National Instruments). (2) Series of correlation curves measured at different surfactant concentrations were analyzed by global "target" analysis programmed in OriginPro 8.0 (OriginLab Corporation, US) or in Matlab (The MathWorks, US).

3. Theory.

The necessary theory has been described in more detail elsewhere and only a brief overview will be given here.[3, 4, 18]

3.1. Mechanism.

When a dye is added to a surfactant solution above the *cmc*, depending on the nature of the dye, it can either associate totally with the micelles or it can partition between the aqueous solution and the micellar pseudo-phase. In the latter case a partition equilibrium model is considered between free dye (D_f) and dye bound to the micelles (D_b):

$$\mathrm{D_f} + \mathrm{M} \rightleftarrows \mathrm{D_b} \tag{1}$$

where K is the equilibrium binding constant.[17] As for any other equilibrium process, absorption and fluorescence titrations with constant concentration of dye and varying concentrations of micelles (i.e., surfactant) allow for the determination of the binding constant.

The concentration of micelles [M] can be obtained from the total surfactant concentration [S] as follows:

$$[\mathrm{M}] = \frac{[\mathrm{S}] - cmc}{N_{\mathrm{agg}}} \tag{2}$$

3.2. FCS.

FCS analyzes spontaneous fluorescence intensity fluctuations that may be caused by various processes at the molecular level.[4, 22-24] The normalized autocorrelation function $G(\tau)$ of the intensity fluctuations $\delta F(t) = F(t) - \langle F \rangle$ is given by equation 3:

$$G(\tau) = \frac{\langle \delta F(t)\ \delta F(t+\tau) \rangle}{\langle F(t) \rangle^2} \tag{3}$$

The correlation function for translational diffusion G_{D} is given by:[6, 25]

$$G_D(\tau) = \frac{1}{N}\left(1 + \frac{\tau}{\tau_D}\right)^{-1}\left(1 + \left(\frac{\omega_{xy}}{\omega_z}\right)^2 \frac{\tau}{\tau_D}\right)^{-\frac{1}{2}} \tag{4}$$

A three-dimensional Gaussian distribution of the detected fluorescence is assumed with radial and axial $1/e^2$ radii ω_{xy} and ω_{z}, respectively. N is the mean number of fluorescent molecules within the sample volume and τ_{D} is the translational diffusion time of the molecules across the sample volume, which is related to the translational diffusion coefficient D by:

$$D = \frac{\omega_{xy}^2}{4\,\tau_D} \tag{5}$$

3.3. Correlation Function for the Partition Equilibrium.

The correlation function taking into account the variation in the diffusion coefficient and in the brightness of a dye due to a chemical equilibrium reaction has been described previously.[5] The partition equilibrium (eq. 1) between free and bound dye is treated as a reversible chemical reaction with (partition) binding equilibrium constant $K = k_+/k_-$ defined by the entry (association) (k_+) and exit (dissociation) (k_-) rate constants.

Under conditions where the micelle concentration [M] is always much higher than that of the dye, this concentration coincides with the initial micelle concentration $[M]_0$ ($[D_f] \ll [M] \approx [M]_0$), and the reaction is pseudo-first-order with the relaxation ("reaction") time τ_R given by:

$$\tau_R = (k_+[H]_0 + k_-)^{-1} \tag{6}$$

Applying the assumption that the relaxation time of the reaction is much shorter than the typical diffusion times of free, τ_f, and bound dye, τ_b, (i.e. fast exchange, $\tau_R \ll \tau_f$, τ_b, the following correlation function for the diffusion and equilibrium reaction is obtained:

$$G_{DR}(\tau) = \frac{1}{N_f + N_b}\left(1 + \frac{\tau}{\bar{\tau}_D}\right)^{-1}\left(1 + \left(\frac{\omega_{xy}}{\omega_z}\right)^2 \frac{\tau}{\bar{\tau}_D}\right)^{-\frac{1}{2}}\left(1 + A_R\, e^{-\tau/\tau_R}\right) \tag{7}$$

where the diffusion term is defined by a mean diffusion time $\bar{\tau}_D$ and an amplitude that depends on the mean numbers N_f and N_b of free and bound dye molecules in the sample volume. The reaction term has a relative amplitude A_R and a correlation time given by the reaction time τ_R.

The parameters $\bar{\tau}_D$, τ_R, and A_R can be expressed directly as function of $[M]_0$ and K:

$$\bar{\tau}_D = \frac{\tau_f(1 + K[M]_0)}{1 + \frac{\tau_f}{\tau_b}K[M]_0} \tag{8}$$

$$\tau_R = \left(k_-(1 + K[M]_0)\right)^{-1} \tag{9}$$

$$A_R = \frac{N_f\, N_b (Q_f - Q_b)^2}{(Q_f\, N_f + Q_b\, N_b)^2} = \frac{K[M]_0(1-q)^2}{(1 + q\, K[M]_0)^2} \tag{10}$$

The reaction amplitude, A_R, depends on the brightness ratio $q = Q_b / Q_f$ of free and bound guest. The species-dependent brightness is defined by the product of the extinction coefficients, fluorescence quantum yield and detection efficiency $Q_X = \varepsilon_X\, \phi_{(F)X}\, g_X$.

It is interesting to analyse the amplitude of the correlation function G_{DR} (eq. 7) at different correlation times. At very short times $\tau \ll \tau_R$ the amplitude is exactly that of two non-interacting species weighted by their fractional intensities, as shown in eq. 11. At these short times the dye exchange is frozen and the two species, free and bound dye, contribute independently to the total intensity.

$$G_{DR}(0) = \frac{1}{N_f + N_b}(1 + A_R) = \frac{Q_f{}^2 N_f + Q_b{}^2 N_b}{(Q_f N_f + Q_b N_b)^2} = \left(\frac{Q_f N_f}{Q_f N_f + Q_b N_b}\right)^2 \frac{1}{N_f} + \left(\frac{Q_b N_b}{Q_f N_f + Q_b N_b}\right)^2 \frac{1}{N_b} \qquad (11)$$

However, at an intermediate time range typical for the diffusion through the sample volume the fast exchange of the dye between free and bound states smears out their properties and the dye appears as one single diffusive species with a mean brightness and a mean diffusion time $\bar{\tau}_D$ (eq. 8). Therefore, as long as the exchange is much faster than the diffusion, $\tau_R \ll \tau_D$, only a single diffusional term is observed with an amplitude given by the inverse of the total number of dye molecules $G_{DR}(\tau_R \ll \tau \ll \tau_D) = (N_f + N_b)^{-1}$, independent of the individual brightness, just as expected for the single (mean) species.

3.4. Brightness Ratio.

We will analyze more generally the influence of the ratio between the brightness of free and bound dye, $q = Q_b/Q_f$, on the sensitivity of the FCS measurement to the dynamics of the dye exchange. The observations are also valid for other similar reversible reactions and other hosts. As explained before, the rate constants of the reaction are determined from series of reaction times, τ_R (eq. 6), which in turn are estimated from fits of eq. 7 to series of FCS curves in a titration experiment with varying micelle concentrations. The reaction times are best determined from reaction terms which both have high amplitudes A_R and appear at long correlation times. The advantage of a high amplitude is directly the increase in the signal to noise ratio. Longer reaction times shift the reaction term away from the limited time resolution of the FCS equipment and towards regions of the correlation curve with lower noise. An upper limit for the value of the reaction time τ_R that can be conveniently determined is imposed by the assumptions of a fast exchange ($\tau_R \ll \tau_D$) in eq. 7.

The dependence of the amplitude of the reaction term A_R on the micelle concentration, eq. 10, is illustrated in Figure 1 and Figure 2S for different values of the brightness ratio q. For convenience both the concentration ratio $K\,[M]_0 = N_b/N_f$ (upper nonlinear scale) and the molar fraction of bound dye ($X_b = K\,[M]_0/(1+K\,[M]_0)$ (lower linear scale) are given as scales. The linear dependence of the reaction time τ_R $k_- = 1-X_b = (1+K\,[M]_0)^{-1}$ (eq. 9) on the fraction of bound dye is also indicated in the figure (grey dashed line).

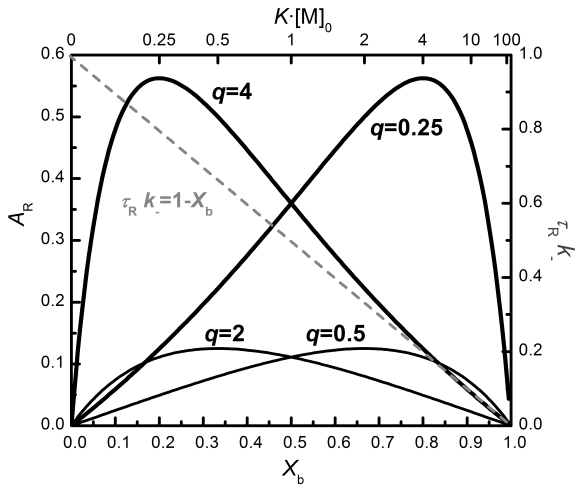

Figure 1: Reaction amplitude, A_R, at different brightness ratios, q, (left-hand scale, black curves) and the dimensionless product between reaction time and exit rate constant, ($\tau_R\ k_-$) (right-hand scale, grey dashed line), versus the molar fraction of bound dye, X_b (bottom scale), or the concentration ratio $K\,[M]_0 = N_b/N_f$ (upper nonlinear scale).

The micelle concentration $[M]_{0,max}$ and the molar fraction $X_{b,max}$ at which the reaction term amplitude A_R reaches its maximum, as well as the value of the maximum itself, $A_{R,max}$, depend only on the brightness ratio q (see Figure 3S in the *Supporting Information*):

$$K[M]_{0,max} = \frac{1}{q}; \qquad X_{b,max} = \frac{1}{1+q}; \qquad A_{R,max} = \frac{(1-q)^2}{4\,q} = \frac{(Q_f - Q_b)^2}{4\,Q_f\,Q_b} \tag{12}$$

The reaction time which corresponds to this maximum amplitude is given by equation 13.

$$\tau_{R,max} = \frac{1}{k_-}\,\frac{q}{1+q} \tag{13}$$

High amplitudes A_R are obtained for high brightness contrasts, that is both for $q \gg 1$ and $q \ll 1$. However, in the case of dyes with lower brightness in the bound state, $q < 1$ ($q = 0.5$ and $q = 0.25$ in Figure 1 and Figure 2S), high micelle concentrations ($K\,[M]_0 > 1$, $X_b > 0.5$) are necessary to achieve a significant increase in the reaction amplitude. In the case of dye-surfactant systems with low binding constants K the necessary micelle concentrations can be very high, exceeding many times the *cmc* of the surfactant. This has several drawbacks: (1) surfactant solutions are difficult to purify and usually introduce some residual fluorescent impurities. Adding millimolar concentrations of surfactant to nanomolar concentrations of dye can be a serious problem in FCS measurements. (2) at high surfactant concentrations the properties of the micelles, such as size, form or aggregation number may change. (3) the

reaction terms with high amplitudes correspond to short reaction times, τ_R, (see equation 9 and dotted line in Figure 1), with the mentioned disadvantages.

These problems are reduced by dyes which show an increase in their brightness upon binding, that is that have high values of $q > 1$ ($q = 2$ and $q = 4$ in Figure 1 and Figure 2S). In this case the reaction amplitude increases strongly already at low micelle concentrations and reaches its maximum at low fractions of bound dye ($K\,[\mathrm{M}]_0 < 1,\ X_b < 0.5$). Comparing two cases of the same 1:4 contrast, for $q = 0.25$ the maximum of the amplitude is reached at $K\,[\mathrm{M}]_0 = 4$, whereas with $q = 4$ already at $K\,[\mathrm{M}]_0 = 1/4$, that is a sixteen times lower micelle concentration (note the nonlinear upper scale of $K\,[\mathrm{M}]_0$ in Figure 1). Thus for this type of dyes only very small micelle concentrations are necessary for the determination of the reaction term, which in turn appears at longer reaction times, easier to resolve with typical FCS equipment.

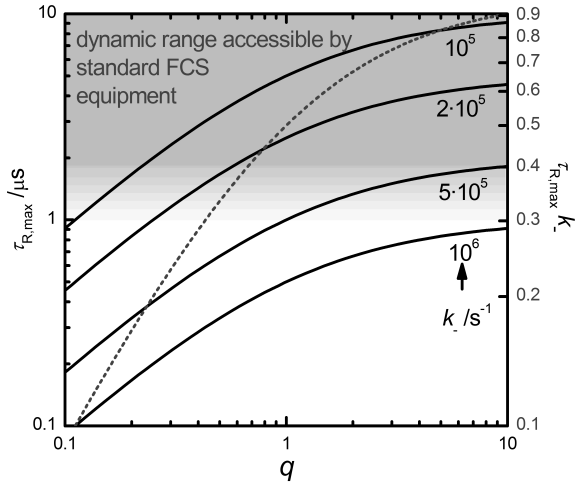

Figure 2: Left scale and black lines: reaction time at the reaction amplitude maximum, $\tau_{R,max}$ versus the brightness ratio, q, for different exit rate constants k_-. Right scale and grey dotted curve: the dimensionless product of reaction time at the reaction amplitude maximum and exit rate constant ($\tau_{R,max}\,k_-$) versus brightness ratio, q. The grey area indicates approximately the range of reaction times which can be determined with standard FCS equipment.

Summarizing, Figure 2 represents the dependence of the reaction time at the reaction amplitude maximum, $\tau_{R,max}$, (eq. 13) on the brightness ratio for different typical values of the exit rate constant k_-. For an acceptable determination of the reaction dynamics from series of FCS curves at different micelle concentrations, the FCS curves with high amplitude of the reaction term should be well resolved. The reaction time given by $\tau_{R,max,}$ thus indicates the minimum reaction time which has to be well resolved by the measurement. Due to dead-time limitations of the counting electronics, standard commercial FCS equipment allows one to determine reaction times down to about one microsecond (although the time resolution itself

may be somewhat higher). This accessible reaction time interval is shown as shaded area in Figure 2. High brightness ratios increase therefore the sensitivity and allow one to study systems with higher exit rate constants. Depending on the exit rate constant of the system, the brightness ratio may be decisive for the accessibility of the reaction dynamics by a given FCS equipment.

4. Results and Discussion.

4.1. Partition Equilibrium.

Absorption and fluorescence titration measurements were registered in aqueous solution at a constant concentration of C152 but different concentrations of TX100. Fluorescence emission spectra (Figure 3) of C152 showed no changes after addition of surfactant at concentrations smaller than the *cmc* of TX100. On the contrary, at higher surfactant concentrations, systematic spectral variations were observed: a significant blue shift and a huge increase in intensity.

The dependence observed indicates a partition equilibrium of C152 between the aqueous solution and the micellar pseudo-phase with an equilibrium binding constant K (eq. 1). Under the experimental conditions used (fixed dye concentration and excess of micelles compared to total dye concentration) and in the absence of excited-state association/dissociation processes, the following relation can be deduced between the fluorescence intensity (or the absorbance) at a certain wavelength, $F(\lambda)$, and the concentration of micelles:

$$F(\lambda) = \frac{F_{\mathrm{f}}(\lambda) + F_{\mathrm{b}}(\lambda)\, K[\mathrm{M}]_0}{1 + K[M]_0} \tag{14}$$

where $F_{\mathrm{f}}(\lambda)$ and $F_{\mathrm{b}}(\lambda)$ are the limiting fluorescence intensities (or absorbances) at wavelength λ of the dye free in the aqueous solution and bound to the micelles, respectively.

Global non-linear analysis using PCGA to the full emission spectra of Figure 3 yield an excellent fit and a precise value of the equilibrium binding constant (Table 1) as well as the "pure" spectra of the two species involved, i.e., free dye and dye bound to the micelles (Figure 4).

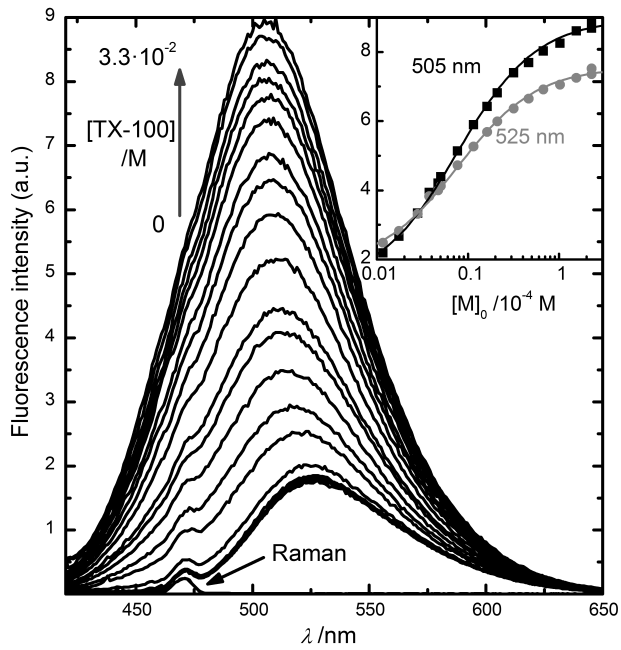

Figure 3. Fluorescence emission spectra of C152 in the presence of different concentrations of TX100 in aqueous solution ([C152] = 1.98 10^{-7} mol dm^{-3}, λ_{exc} = 405nm). Inset: Fluorescence intensities of C152 at two wavelengths (505 nm and 525 nm) versus micelle concentration of TX100 (logarithmic scale). Symbols represent experimental data and lines fitted curves of eq.14 with the parameters given in the text obtained from a global fit at all measured wavelengths.

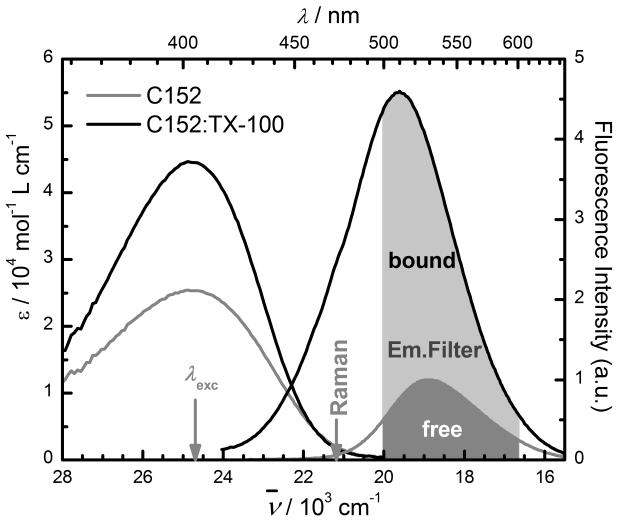

Figure 4. "Pure" absorption and fluorescence emission spectra of C152 in aqueous solution (gray lines), and bound to TX100 micelles (black lines) obtained as described in the text. Also indicated are the excitation wavelength (λ_{exc} = 405 nm), the Raman band and the range of emission wavelength detected (λ_{em}) in the FCS measurements as determined by the band-pass filter used (CWL=550nm, FWHM=100nm).

As compared to the values obtained with R123, the binding constant K of the C152/TX100 system is approximately twice as high (see Table 1). This may be because C152 is a neutral dye whereas R123 has a positive charge, so C152 would have a higher affinity to the apolar micellar pseudo-phase.

Absorption titration data are not shown here, since the spectral change with TX100 concentration is much smaller than that observed in emission. The quantitative analysis of these small changes in absorption is complicated due to several reasons: (1) TX100 shows a residual absorbance that overlaps with that of C152. (2) in order to distinguish the C152 absorbance from that of TX100 relatively high C152 concentration have to be used, much higher than in the emission measurements. Under these conditions the probability that micelles are occupied by more than one C152 molecule (occupancy numbers above 1) is no longer negligible. Assuming that the mean occupancy number is based on Poisson statistics, we use the value of the constant for the 1:1 binding equilibrium determined from our emission data to calculate the probability of double occupancy (see eq. S1 to S5 and Figure S5 in the *Supporting Information*). This probability remains negligible in the concentrations range used for emission and FCS series, but rises above 10% in the absorption measurements. Therefore, Global fits with the 1:1 complexation model to the absorption data are not satisfactory and we take the measurement at the highest TX100 concentration as an acceptable approximation for the "pure" absorption spectrum of C152 bound to the micelles and use it to estimate the quantum yield of this complex. This approximation does not affect the determination of the brightness ratio.

Figure 4 shows the "pure" absorption and fluorescence emission spectra of free C152 in aqueous solution and of C152 bound to the micelles of TX100. The corresponding absorption spectra present no significant spectral shift but a higher molar absorption coefficient for bound C152. Emission spectra show a significant intensity increase (which includes that of the absorption at the excitation wavelength) and a small blue shift for bound C152. The ratio between the fluorescence intensities of free and bound C152 that will be observed in FCS measurements with a given excitation wavelength and emission filter, the brightness ratio q, can be determined integrating the corresponding pure fluorescence emission spectra within the limits of the emission filters (gray areas in Figure 4). The relative quantum yields ϕ_b/ϕ_f are calculated from the same spectra but integrating the full spectral range and correcting for the different molar absorption coefficients of the species at the excitation wavelength. The results are given in Table 1. The boost in the brightness of C152 in the presence of TX100 micelles is determined by the increase of the molar absorption coefficient at the excitation wavelength (405 nm) and especially of the fluorescence quantum yield. This way, the entry/exit processes of C152 into/out of a micelle results in an effective variation ("blinking") of the brightness, which can be observed in FCS measurements.

4.2. FCS Measurements.

In order to achieve optimal conditions for the determination of the dynamics of the reaction process of a given surfactant-dye system several experimental parameters have to be balanced: (1) a low excitation irradiance avoids saturation, photobleaching and triplet population but may increase the measuring time unacceptably, especially in the case of dyes with low brightness (2) a bigger confocal volume increases the diffusion time and improves the separation between reaction and diffusion terms ($\tau_R \ll \tau_D$) but also raises the background signal and the probability of photobleaching, especially at high host concentrations (3) the range of micelle concentrations in the titration has to be optimized both for the resolution of the reaction term at high amplitudes A_R and for the determination of the diffusional properties of free and bound dye. In the case of a dye with $q > 1$ it may be convenient to separate the determination of the reaction term at low micelle concentrations ($K\,[M]_0 < 1$) from the titration at high concentrations ($K\,[M]_0 \gg 1$) necessary for the estimation of the diffusion time τ_b of bound dye.

Table 1. Binding equilibrium constants, photophysical parameters, and properties determined from FCS of the dye C152 bound to TX100 micelles.

	C152/TX100
K /10^3 M^{-1}	129 ± 3
$q = Q_b / Q_f$ [a]	3.8 ± 0.2
ϕ_f [b]	0.064 ± 0.003
ϕ_b [b]	0.21 ± 0.01
ϕ_b / ϕ_f [b]	3.2 ± 0.2
τ_f /ms	0.122 ± 0.002
τ_b /ms	1.22 ± 0.03
D_f /10^{-10} m^2s^{-1}	5.2 ± 0.6
D_b /10^{-10} m^2s^{-1}	0.52 ± 0.05
$R_{h,f}$ /Å	4.7 ± 0.2
$R_{h,b}$ /Å	47 ± 5
k_- /10^5 s^{-1}	0.6 ± 0.2
k_+ /10^{10} $M^{-1}s^{-1}$	0.8 ± 0.3
k_d /10^{10} $M^{-1}s^{-1}$	2

[a] Brightness ratio estimated from em. spectra for λ_{exc} =405nm and interference filter: 550/100nm.
[b] Fluorescence quantum yields of free C152 and C152 bound to micelles.
All values are given for 25°C

In order to determine the optimal excitation irradiance power series were measured for free and bound C152 under the same experimental conditions as used later for the FCS curves. Saturation and photobleaching at too high irradiance will reduce the apparent diffusion time

and introduce therefore significant error in the determination of the diffusional properties.[26,27] Figure 5 shows a double logarithmic plot of the fluorescence count rate of the dye calculated as the difference between the fluorescence intensity detected from samples with and without dye, versus the mean irradiance (I_0 / 2).

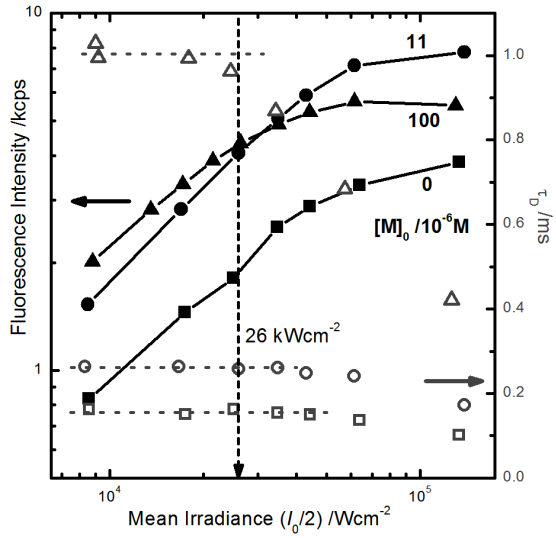

Figure 5. Detected fluorescence intensity (filled symbols, left scale) and apparent diffusion time (open symbols, right scale) of C125 versus mean irradiance (I_0/2) at different micelle concentrations as indicated (squares: $[M]_0 = 0$ M, circles: $[M]_0 = 0.011$ mM, triangles: $[M]_0 = 0.10$ mM). The solvent signal (water or water + TX100) was measured separately and was subtracted from the total photon count for each sample. The vertical dashed arrow indicates the irradiance used for the FCS measurements of the reaction dynamics.

The fluorescence count rate registered from C152 in the absence of TX100 (filled black squares in Figure 5) increases linearly at low irradiance but levels off at about 50 kW cm^{-2} due to saturation. The addition of an intermediate concentration of TX100 micelles ($[M]_0 = 0.011\ 10^{-3}$ mol dm^{-3}, $K\,[M]_0 \approx 1.4$) increases the registered intensity (filled black circles) according to the expected increase in brightness of the dye. Saturation is observed at approximately the same irradiance. At a much higher micelle concentration ($[M]_0 = 0.10\ 10^{-3}$ mol dm^{-3}, $K\,[M]_0 \approx 13$) the registered intensity (filled black triangles) increases still, but levels off strongly at high irradiance due to saturation and photobleaching, falling even below the intensity found at lower micelle concentrations. Due to the binding equilibrium the presence of micelles increases the mean residence time of the dye in the focal volume which leads to a higher photobleaching probability. The effect of saturation and photobleaching is well appreciated comparing the values of the diffusion time τ_D of C152 determined from FCS curves at different micelle concentrations and at increasing irradiance

as indicated as open symbols in the same Figure 5. At zero or intermediate micelle concentrations τ_D is constant within the experimental error up to about 40 kW cm^{-2}, whereas at high micelle concentrations already at about 30 kW cm^{-2} a strong decrease is observed. At high irradiance the real transit time is not observed but the time until the dye is bleached. In order to minimize the effects of saturation and photobleaching an irradiance of about 26 kW cm^{-2} (207 μW in the sample) was chosen. This irradiance is high enough to assure acceptable measurement times for the determination of the reaction term at intermediate micelle concentrations and is just acceptable for the estimation of τ_D at highest concentrations.

The next step is the evaluation of the influence of the triplet reaction. For this aim FCS correlation curves were measured at different excitation irradiances for C152 in aqueous solution and in the presence of high TX100 concentration ([TX100] = 14.8 10^{-3} mol dm^{-3}, $[M]_0 = 0.10\ 10^{-3}$ mol dm^{-3}, concentration ratio $K\,[M]_{0,max} \approx 13$). The triplet-state population depends directly on the excitation power,[6,28] whereas the dynamics of the dye-micelle association reflected in the reaction term does not depend on excitation power but changes with the concentration of micelles (see eqs. 9 and 10). At all irradiances the curves without TX100 need only one diffusion term for the model to fit satisfactorily. In the presence of TX100 micelles no excitation power dependent term was found and therefore no triplet term has been taken into account in the fits.

As pointed out before, the exchange dynamics are best determined at micelle concentrations which lead to high amplitudes in the reaction term. In this system the maximum reaction term amplitude, A_R, corresponds to a very low micelle concentration of $[M]_{0,max} \approx 0.002\ 10^{-3}$ mol dm^{-3} ($K\,[M]_{0,max} \approx 0.3$) as estimated from eq. 12 and the values of q and K determined from bulk measurements (Table 1) (see also Figure 6). For the titration finally five FCS curves were measured at concentration ratios of $K\,[M]_{0,max} = 0$, 0.3, 1.4, 2.3 and 13 as shown in Figure 6. Beside the curve at $[M]_{0,max}$ other higher concentrations were added in order to improve the statistics and to separate better between diffusion and reaction term in the global fit. The curves at cero and at the highest micelle concentrations contain no information about the reaction, but help to estimate the diffusion coefficients of free and bound dye. For the reasons discussed before, this experiment is not optimized for the determination of the diffusion coefficients or the equilibrium constant. These would require a lower irradiance and a higher number of curves which cover a wide range of at micelle concentrations. This is not the aim of this study and the values of the diffusion coefficients given here are therefore only rough estimations.

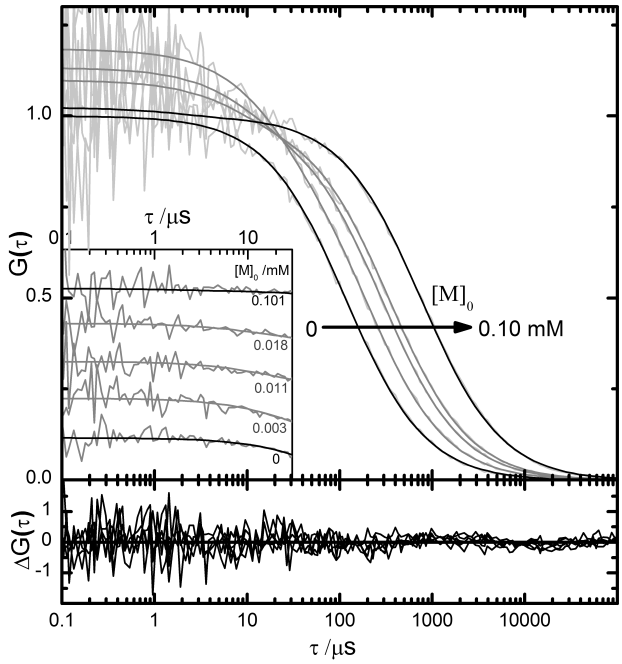

Figure 6. Upper panel: Normalized correlation curves of C152 in aqueous solution in the presence of different concentrations $[M]_0$ of TX100 micelles ($[M]_0$ = 0 to 0.10 mM corresponding to $K\,[M]_0$ = 0, 0.3, 1.4, 2.3 and 13) (gray noisy lines), measured at an irradiance of 26 kW cm^{-2}. The smooth curves are obtained from a global fit of equation 7 to the experimental data with fitting parameters given in Table 1). All curves were normalized by multiplication by N, the total number of molecules obtained from the fit. Inset: stacked view of the fast part of the same FCS curves. Lower panel: corresponding weighted residuals in arbitrary units. The weighting amplifies the residuals at long correlation times.

Global "Target" Analysis of this series of FCS curves using equation 7 lead to satisfactory fits, as shown by the accordance of the fitted curves with the experimental data and the randomly distributed residuals (see Figure 6). Leaving all parameters of equation 7 free in the fits leads to a binding equilibrium constant of $K = (140 \pm 10)\ 10^3\ M^{-1}$, in good concordance with the value $K = (129 \pm 3)\ 10^3\ M^{-1}$ determined from bulk measurements. This later value was then kept fixed in the fits. The brightness ratio of $q = 2.5$ obtained from these fits coincides with that estimated directly from the total fluorescence intensities registered in the FCS measurements, but is significantly smaller than that observed in the bulk (see Table 1). This is probably due to the spectral responses of the FCS-detectors and to polarization effects. The results of the fits are shown in Table 1. The entry rate constant k_+ is not a direct fit parameter, but it is calculated from the binding equilibrium constant K and the exit rate constant k_-.

4.3. Diffusional Dynamics.

The diffusion times obtained from the analysis of the fluorescence correlation curves (Table 1) are converted to diffusion coefficients using eq. 5 and then to the corresponding hydrodynamic radii R_h applying the Stokes-Einstein relation:

$$R_h = \frac{k\,T}{6\,\pi\,\eta\,D} \tag{15}$$

where k is the Boltzmann constant and η the viscosity of water (0.8905 cP at 25°C). The values obtained are also given in Table 1.

As expected, the diffusion coefficient of bound C152 is much lower than that of free dye and coincides well with the diffusion coefficient of empty TX100 micelles determined by Dynamic Light Scattering ($D = 0.54\ 10^{-10}\ m^2\ s^{-1}$)[14] (values from some other references are significantly lower but they are not based on such a detailed study as in the reference cited). The presence of a small, noncovalently bound neutral dye has no significant effect on the translational motion of the micelles, as opposed to large fluorescent probes which perturb the micellar structure and lead to a significant decrease of the diffusion constant.[29]

A comparison to the values of D_b and R_h obtained for the association of R123 to TX100 micelles shows significant differences.[3] This may be due to the uncertainty in the calibration of the focal area of different FCS equipment, the use of different dyes as references, and the general limitations of standard FCS to accurately determine absolute diffusion coefficients.[27] However, these differences may also be explained by the influence of the micellar concentration itself on the micellar self-diffusion coefficient, D_b, due to changes in shape and aggregation (N_{agg}) of the micelles with increasing surfactant concentration.[30]

4.4. Partition Dynamics.

Table 1 gives the values of the rate constants of dye entry (k_+) and exit (k_-) obtained from the fits of the fluorescence correlation curves. Neither the entry nor the exit processes take place during the lifetime of the excited state, since both the rate at which the coumarine molecules enter into the micelles (k_+ [M]) and the exit rate (k_-) are, for all studied concentrations, much lower than the fluorescence deactivation rate of C152. Lifetimes for 7-aminocoumarines range between 0.4 and 5 ns depending on the solvent, that of C152 in water being about 2 ns.[12]

The high value obtained for the entry rate constant (k_+) of about $10^{10}\ M^{-1}s^{-1}$ suggests a diffusion-controlled process for the entry of the neutral dye C152 to the TX100 micelles. The

rate constant corresponding to a purely diffusion-controlled association process between dye and the micelle (k_d), can be roughly estimated applying the Smoluchowski equation:

$$k_d = 4\pi\, D_{DM}\, R_{DM}\, N_0 \qquad (16)$$

where D_{DM} and R_{DM} are the sums of diffusion coefficients and hydrodynamic radii of the dye (free C152) and the micelles (bound C152), respectively, and N_0 is the Avogadro constant. Comparing the values of k_+ with that of $k_d \approx 2\ 10^{10}\ M^{-1}s^{-1}$ a good agreement is found, which corroborates a diffusion-controlled entry rate constant (see Table 1). This behaviour of the micelle as a "soft" supramolecular cage is similar to that found before for the entry of the cationic dye R123 in the same micelles.[3] The entry rate constant found in this study are of the same order of magnitude as those reported for other solubilizates and different types of micelles determined with other techniques.[1, 17, 31]

The exit rate constant $k_- = 6\ 10^4\ s^{-1}$ is much lower than that found for the R123-TX100 system. It is known that the exit rate constant varies strongly with the hydrophobicity of the solubilizate, which is higher in the case of C152. This is reflected in the much higher binding equilibrium constant of the C152 system. Given that in both cases the entry is diffusion limited, the overall affinity of the dyes to the micelles is mainly determined by the exit process.

5. Conclusions.

Matter exchange is a fundamental process in colloid and interface science. Fluorescence Correlation Spectroscopy has the potential to reveal these typically very fast exchange-dynamics. The study of hydrophobic interactions in ionic colloidal systems requires neutral fluorescent probes, which typically present a lower brightness, worse photostability and mostly need an excitation at lower wavelength as compared to the charged dyes mostly used in FCS. We have shown in this contribution that the dynamics of the (host-guest) association of a neutral hydrophobic dye to micelles can be studied by FCS in spite of the low quantum yield, low saturation threshold and higher energetic excitation of the dye. The careful selection of the experimental conditions allows one to obtain the dynamic and diffusional properties with reasonable precision. We discuss that the contrast in the brightness of free and bound dye (brightness ratio q) has a strong influence on the sensitivity of the FCS experiment to the association dynamics. A strong contrast $q > 1$ leads to high amplitudes of the reaction term already at low micelle concentrations.

We found again that the micelles act as a soft cage which allows a diffusion-limited entry of the dye into the micelle.. Being the association rate constant diffusion-limited, both the

binding equilibrium constant and the overall exchange (relaxation) rate of different micellar systems will be determined mainly by the exit rate constant, which shows a strong dependence on the specific interactions between dye and micelle. This leads to a broad dynamic range of the exchange in micellar systems, which can be well covered by FCS.

The use of both neutral and charged dyes opens the way to systematic studies of the dynamics of matter exchange in series of neutral and ionic colloidal systems and to evaluate the role of electrostatic as compared to other weak interactions.

References.

[1] R. Zana, in Dynamics of Surfactant Self-assemblies: Micelles, Microemulsions, Vesicles, and Lyotropic Phases, R. Zana (Ed.), Taylor & Francis/CRC Press, Boca Raton, 2005.

[2] A. Patist, J.R. Kanicky, P.K. Shukla, D.O. Shah, J. *Colloid Interface Sci.* 245 (2002) 1.

[3] M. Novo, S. Felekyan, C.A.M. Seidel, W. Al-Soufi, *J Phys Chem B.* 111 (2007) 3614.

[4] W. Al-Soufi, B. Reija, S. Felekyan, C.A. Seidel, M. Novo, *Chemphyschem.* 9 (2008) 1819.

[5] W. Al-Soufi, B. Reija, M. Novo, S. Felekyan, R. Kühnemuth, C.A.M. Seidel, J. Am. Chem. Soc. 127 (2005) 8775.

[6] R. Rigler, E.S. Elson, Fluorescence Correlation Spectroscopy: Theory and Applications, Springer Verlag, Berlin, 2001.

[7] C. Eggeling, J. Widengren, R. Rigler, C.A.M. Seidel, *Anal. Chem.* 70 (1998) 2651.

[8] C. Eggeling, J. Widengren, R. Rigler, C.A.M. Seidel, in Applied Fluorescence in Chemistry, Biology and Medicine, W. Rettig, B. Strehmel, S. Schrader, H. Seifert (Eds.), Springer-Verlag, Germany, 1999, p. 193.

[9] J. Shobini, A.K. Mishra, K. Sandhya, N. Chandra, *Spectrochim. Acta*, Pt. A: Mol. Biomol. Spectrosc. 57A (2001) 1133.

[10] P. Dahiya, M. Kumbhakar, T. Mukherjee, H. Pal, *Chemical Physics Letters*. 414 (2005) 148.

[11] R.W. Yip, Y.X. Wen, A.G. Szabo, *J. Phys. Chem.* 97 (1993) 10458.

[12] G.I. Jones, W.R. Jackson, C.Y. Choi, W.R. Bergmark, *J. Phys. Chem.* 89 (1985) 294.

[13] A. Chakraborty, D. Seth, P. Setua, N. Sarkar, *J Phys Chem B.* 110 (2006) 16607.

[14] G.D.J. Phillies, J. Stott, S.Z. Ren, *J. Phys. Chem.* 97 (1993) 11563.

[15] G.D.J. Phillies, J.E. Yambert, Langmuir. 12 (1996) 3431.
[16] K.R. Acharya, S.C. Bhattacharya, S.P. Moulik, *J. Photochem. Photobiol.* A. 109 (1997) 29.
[17] K. Kalyanasundaram, Photochemistry in Microheterogeneous Systems, Academic Press, New York, 1987.
[18] D. Granadero, J. Bordello, M.J. Pérez-Alvite, M. Novo, W. Al-Soufi, *ijms.* 11 (2010) 173.
[19] P.O. Gendron, F. Avaltroni, K.J. Wilkinson, J. Fluoresc. 18 (2008) 1093.
[20] C. Muller, A. Loman, V. Pacheco, F. Koberling, D. Willbold, W. Richtering, *Europhys. Lett.* 83 (2008) .
[21] W. Al-Soufi, M. Novo, M. Mosquera, *Appl. Spectrosc.* 55 (2001) 630.
[22] J. Widengren, R. Rigler, Cell Mol. Biol. 44 (1998) 857.
[23] J. Widengren, in Fluorescence correlation spectroscopy: theory and applications, R. Rigler, E.S. Elson (Eds.), Springer Verlag, Berlin, 2001, p. 276.
[24] E. Haustein, P. Schwille, in Single-molecule techniques: a laboratory manual, P.R. Selvin, T. Ha (Eds.), Cold Spring Harbor Laboratory Press, Cold Spring Harbor, N.Y., 2008, p. 259.
[25] E.L. Elson, D. Magde, *Biopolymers.* 13 (1974) 1.
[26] C. Eggeling, A. Volkmer, C.A.M. Seidel, *Chemphyschem.* 6 (2005) 791.
[27] J. Enderlein, I. Gregor, D. Patra, J. Fitter, *Curr. Pharm. Biotechnol.* 5 (2004) 155.
[28] J. Widengren, R. Rigler, *Bioimaging.* 4 (1996) 149.
[29] M.A. Hink, A. Van Hoek, A.J.W.G. Visser, *Langmuir.* 15 (1999) 992.
[30] I.D. Charlton, A.P. Doherty, *Journal of Physical Chemistry B.* 104 (2000) 8327.
[31] M.H. Gehlen, F.C. De Schryver, *Chem. Rev.* 93 (1993) 199.

Acknowledgments.

J.B. thanks the *Ministerio de Ciencia e Innovación* for a research scholarship. M.N. and W.A. thank the *Ministerio de Ciencia e Innovación* and the *Xunta de Galicia* for financial support (CTQ2004-07683-C02-02, INCITE07PXI209034ES, INCITE08E1R209 060ES) and C.A.M. Seidel and S. Felekyan for help with the FCS setup.

Supplementary Information.

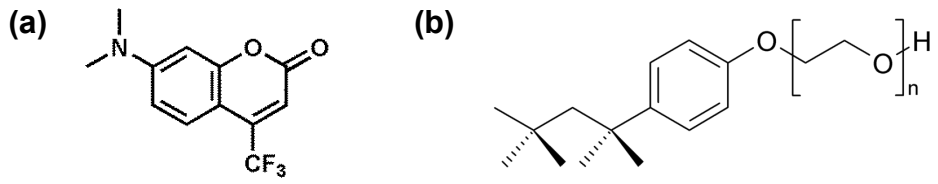

Figure 1S. Molecular structures for dye Coumarine 152 (a) and surfactant Triton X-100, n=9-10, (b).

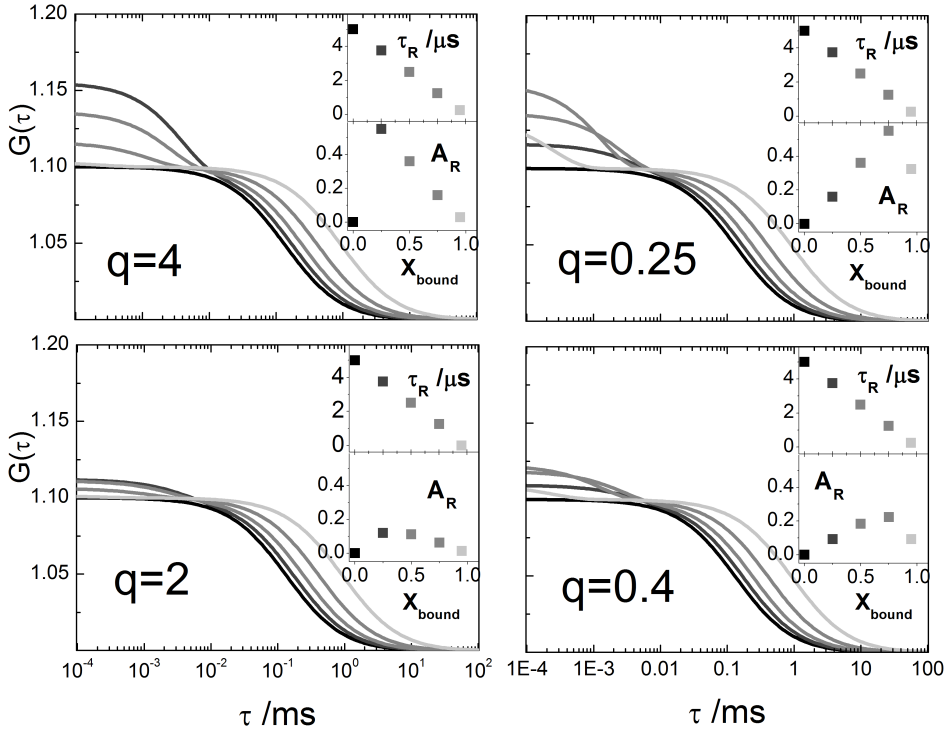

Figure 2S. Simulated FCS Curves for the system TX 100 and C152 to observe the influence of the brightness ratio. Insets: Variation in A_R and τ_R versus the fraction of dye bound to TX100 micelles. Different colours correspond to different values of the fraction of dye bound to TX100 micelles: 0 (black), 0.25 (dark grey), 0.5 (grey), 0.75 (grey), 0.95 (light grey). Four different values for q were selected: 0.25, 0.4, 2 and 4.

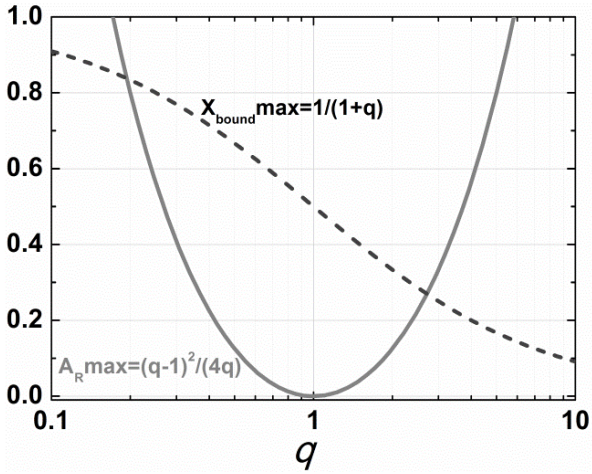

Figure 3S. Maximum in reaction amplitude, A_R (solid line), and corresponding fraction of bound dye, $X_{b,max}$ (dashed line), versus the brightness ratio, q.

Study based on Poisson statistics to calculate the probability of double occupancy (two dyes per micelle) in the different series: Absorption, Emission and FCS.

Poisson statistics considers a random association between C152 molecules and TX 100 micelles. Using the equations S1 to S3, the probability of having empty micelles, P(0), micelles with one C152 molecule, P(1), or micelles with two C152 molecules, P(2), can be calculated.

$$P(0) = e^{-N} \tag{S1}$$

$$P(1) = N\, e^{-N} \tag{S2}$$

$$P(2) = \frac{1}{2}\, N^2\, e^{-N} \tag{S3}$$

N is the mean occupancy number. It is calculated from the constant for the 1:1 association equilibrium, K_1, determined before from emission data and the initial C152 concentration $[C152]_0$, by using equations S4 and S5.

$$N = K_1[C152] \tag{S4}$$

$$[C152] = \frac{[C152]_0}{1 + K_1[M]} \tag{S5}$$

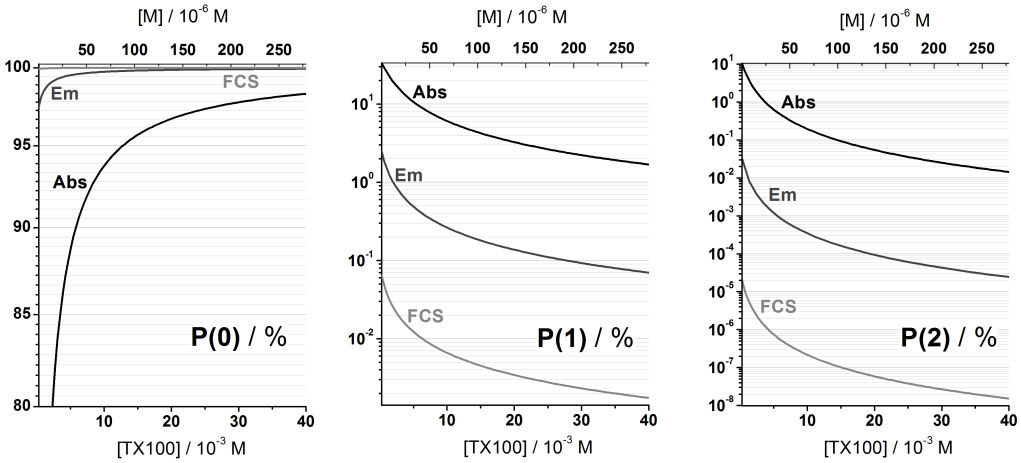

Figure 4S. Poisson statistics. Each plot represents probabilities of having micelles with 0, 1 and 2 C152 molecules: P(0), P(1), and P(2), respectively. In each graph there are three curves corresponding to different initial concentrations of dye: for absorption series (in black, $[C152]_0 = 4.9\ 10^{-6}$ mol dm^{-3}), for emission series (in dark grey, $[C152]_0 = 2.0\ 10^{-7}$ mol dm^{-3}) and for FCS titration series (in light grey, $[C152]_0 = 5.0\ 10^{-9}$ mol dm^{-3}).

Chapter IV

Dynamics of a DNA Minor-Groove Binder studied by Fluorescence Correlation Spectroscopy

Contents:

1. Introduction.

The recognition of specific DNA sequences has an enormous diagnostic and clinical potential that has promoted the development of high-affinity, sequence-specific DNA binders for the direct sensing of double-stranded DNA (Neidle 2001; Neidle 2008).

Focusing on small molecules that bind non-covalently and reversibly to DNA, we can identify three main types of DNA binding modes (Waring 2006): external electrostatic binding, groove binding, and intercalation.

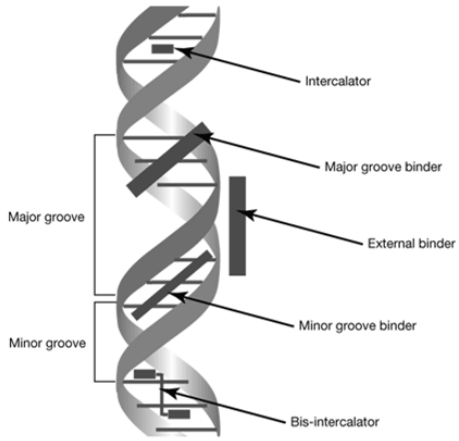

Figure 1.1. Schematic of DNA binding modes.

Sequence-specific DNA-binding proteins generally bind into the major groove, while the considerably narrower minor groove is used by the smaller ligands. Minor-groove binding molecules with modest sequence discrimination ability are of current interest having potential for anticancer and anti-PCP chemotherapy, in addition to a variety of human diseases (Neidle 2001). These binders block replication and transcription of their DNA, by competition at regulatory sites during these processes or by perturbing local DNA structure upon binding, in a way that protein binding cannot occur.

The compounds related in structure to pentamidine have proven antimicrobial and antifungal activity (Bell et al. 1990; Del Poeta et al. 1998), correlated with their ability to interact strongly with the DNA minor groove in AT sequences with subsequent inhibition of one or more DNA directed enzymes. Understanding the binding kinetics of the naturally occurring Distamycin A with DNA have been reported as an important step toward evaluating the potential of polyamide drugs as efficient inhibitors of intracellular processes (Baliga and Crothers 2000a, 2000b).

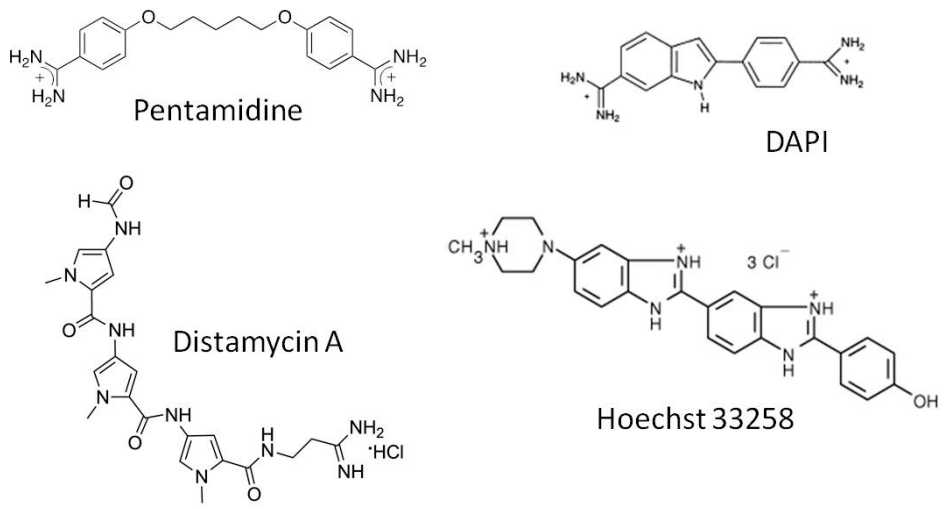

Figure 1.2. Examples of broadly studied minor groove binders.

Since DNA is not fluorescent by itself, staining of the DNA with dye molecules which exhibit an enhanced quantum yield of fluorescence when bound to DNA represents also a field of interest of the minor-groove DNA binders. Asymmetric cyanine dyes (Eriksson et al. 2003, 2006) or the dye Hoechst 33258 (Breusegem et al. 2002), a bis-benzimidazole derivative with an *N*-methylpiperazine and a phenyl group at the ends, are useful spectroscopic probes for DNA used in microscope imaging, electrophoresis and PCR. The dye DAPI, 4,6-diamidino-2-phenylindole, is routinely used to quantify DNA fluorimetrically in solution (Breusegem et al. 2001, 2002).

DNA minor-groove binders are typically arch-like positively-charged molecules with high affinity and specificity for AT-rich sequences (Neidle 2001). Several electrostatic, van der Waals and hydrophobic factors are involved in the binding specificity for AT regions, although their relative importance is still controversial (Neidle 2001). The minor groove is narrower in the AT regions with close van der Waals contacts stabilizing the complex (Laughton and Luisi 1999). Also, in these regions the minor groove is more electronegative, when almost all minor-groove binding ligands carry cationic charge (Breusegem et al. 2001; Wilson et al. 1990); and the surfaces of the groove walls are more hydrophobic than in sequences of GC base pairs, due to the backbone hydrogen atoms. In addition, minor groove at GC rich sequences is more sterically blocked by the 2-amino group in guanine (Breusegem et al. 2001). However, according to some authors (Haq et al. 1997) the key factor to explain this selectivity is a favorable increase in entropy upon complexation, caused by the release of ordered water molecules from the "spine of hydration" and from a decrease in solvent-accessible surface areas of the reactants.

The optimization of DNA binders requires detailed kinetic and structural information that helps to a better understanding of the binding mechanism. However, the very low dissociation rates of high-affinity binders result in very slow binding dynamics, which is experimentally not easily accessible. In consequence information about structural features which determine the DNA minor-groove association dynamics is still limited (Pace and Bohne 2008; Waring 2006). Stopped-flow measurements seem to indicate that the association process is very fast and nearly diffusion limited, which is surprising, given the high geometric constraints imposed on the inclusion of a binder into the minor groove (Baliga and Crothers 2000; Breusegem et al. 2002).

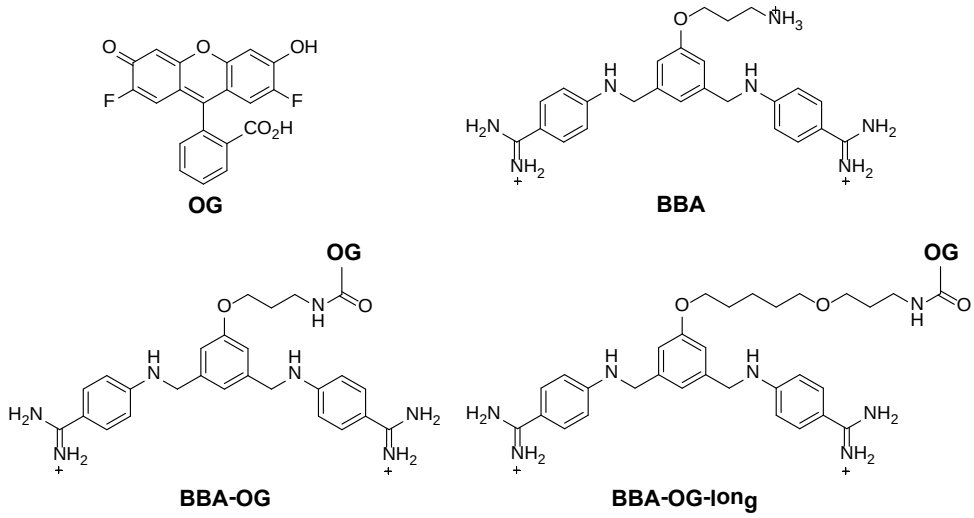

Figure 1.3. Molecular structures of the molecules used in this work.

In order to shed light on the association dynamics of this important class of DNA binders, we use the BBA-OG (Figure 1.3), a novel fluorescently labeled derivative from the cationic bis-benzamidines family of minor groove binders (Vazquez et al. 2010), where the labeling with the negatively charged dye Oregon Green leads to a huge increase of the dissociation rates. This makes it possible to study the binding dynamics to both high and low affinity DNA sequences with Fluorescence Correlation Spectroscopy (FCS), which yields values for the binding equilibrium constant, the association and dissociation rate constants, and also the diffusion coefficients, which are necessary to estimate the diffusion-controlled rate constants (Al-Soufi et al. 2005, 2008). To the best of our knowledge this highly sensitive single-molecule technique has not been previously used to analyze the dynamics of DNA minor groove binders.

The comparison of the dynamics of the association of BBA-OG to different DNA sequences and to DNA of a different length allows us to identify the rate-limiting step in this process and evaluate the importance of mechanisms such as sliding or two dimensional diffusion found for the binding of proteins to DNA (Berg and von Hippel 1985; Vuzman et al. 2010).

Also the use of a modified binder with a lengthened linker between the BBA and OG units (BBA-OG-long) provides us information on how this factor affects the binder photophysics and more generally how modifications in the attachment of the dye influence the DNA binding dynamics.

2. Materials and Methods.

2.1. Sample Preparation.

All samples were prepared in buffer (Tris HCl 20 mM, NaCl 100 mM, pH=7.5). Note that the NaCl concentration does not take into account the ions from the Tris HCl.

Stock solutions of BBA-OG and of the different DNAs were freshly prepared for each series. BBA-OG stock solutions had 10-fold higher concentrations than those necessary for the titrations (approximately 10^{-9} mol dm^{-3} in the FCS experiments).

The measuring samples were prepared by dilution of a constant volume of the BBA-OG stock together with different volumes of the corresponding DNA stock solution and addition of buffer to adjust to a certain total volume. The accuracy of these volumes was checked by weighing, and concentration corrections were made.

Series of FCS measurements at different DNA concentrations were carried out by measuring first the sample at the highest DNA concentration, being then successively diluted by replacing a fixed volume of sample by the same volume from a stock with the same binder concentration but without DNA (a more detailed explanation of the procedure can be found in the section of *Practical Aspects of FCS* in Chapter I).

2.2. Oligonucleotides.

Oligonucleotides were purchased lyophilized from Thermo Fisher Scientific Inc. They were reconstituted in buffer (Tris HCl 20 mM, NaCl 100 mM, pH=7.5) and annealed by heating to 95°C (1:1 mixture of complementary strands for the AAATTT-ds) followed by slow cooling to room temperature.

The concentration of DNA samples was determined by measuring the amount of UV irradiation absorbed by the bases (Barbas et al. 2007). The number of micrograms of the oligonucleotides was calculated from the reading at 260 nm, Abs260, using the following conversions: 1 OD = 50 µg/mL (dsDNA) or 33 µg/mL (ssDNA). The OD refers to the Abs260 using an optical path of 1 cm. Abs260/Abs280 ratio was checked to be always between 1.7 and 1.8, as an indicator of purity.

Table 2.1. Sequences of the oligonulceotides used in this work.

DNA	Sequence (5' to 3')	bp
AAATTT-hp	GGC **AAATTT** CGC TTTTT GCG **AAATTT** GCC	12 + loop
AATTT-hp	GGCG **AATTT** CGC TTTTT GCG **AAATT** CGCC	12 + loop
GGCC-hp	GGCA **GGCC C**AGC TTTTT GCT**G GGCC** TGCC	12 + loop
AAATTT-ds	GCGCACTGCGTCAGCGACTGCGTCAGCGACTGCGTCAGCG**AAATTT**GCGC (and its complementary)	50

2.3. FCS Setup.

The confocal epi-illuminated setup used for the FCS measurements is similar to that described in previous chapters and elsewhere (Granadero et al. 2010). 100 µL samples were deposited on a glass bottom microplate (Whatman Ltd.). The samples were excited by the continuous linearly polarized light of a 489 nm laser diode (Becker&Hickl, BDL-485-SMC, DE) coupled to a monomode optical fiber (Point-Source, kineFLEX-P-1-S-405-0.7, UK). The light output of the fiber was collimated (Schäfter&Kirchhoff, 60FC-4-6,2-01-DI, DE), spectrally cleaned (Semrock, Brightline HC 482/18, US), redirected by a dichroic mirror (Semrock, Brightline BS R488, US) and focused into the sample by a high aperture microscope objective (Olympus, UPLSAPO 60xW/1.20, water immersion) mounted in an inverted microscope (Olympus, IX-71). The fluorescence was collected by the same objective and then refocused through the dichroic mirror onto a pinhole (Thorlabs, ∅=50 µm, US) in the image plane. The light passing the pinhole was collimated, then split into two beams by a nonpolarizing beamsplitter cube (Newport, 05BC17MB.1, US) and each focused onto avalanche photodiodes (MPD50CTC APD, ∅=50 µm, MPD, Italy). Band-pass filters (Semrock, Brightline HC 525/45, US) in front of the detectors discriminated fluorescence from scattered laser light. Both output signals were processed and stored by TCSPC-modules (SPC 132, Becker & Hickl GmbH, Berlin, Germany). Correlation curves were calculated with the Single Photon Counting software by Becker & Hickl GmbH.

Typically 20 million photons were collected for each correlation curve with count rates in the range of 2.5 to 29 kHz, depending on the sample. All measurements were made at stabilized temperature, 25.0 ± 0.5°C. The excitation power as measured in the focus of the microscope objective by a power meter (Thorlabs, PM30-120, US) was typically 80 µW, corresponding to a mean irradiance of $I_0/2 = P/(\pi\ \omega_{xy}^2) = 9$ kW cm^{-2}, assuming a Gaussian intensity distribution along the optical axis. P is the excitation power in the sample (Eggeling et al. 1998).

The focal area and the detection volume were calibrated with Rhodamine 123 in aqueous solution at low irradiance yielding a radial $1/e^2$ radius of $\omega_{xy} = 0.53$ µm. The value of $D_{R123} = (4.6 \pm 0.4)\ 10^{-10}$ m^{2}s^{-1} is estimated from recent PFG-NMR (Gendron et al. 2008) and dual-focus FCS (Muller et al. 2008) data. The diffusion coefficients are given for 25°C.

2.4. Data Analysis.

Full titration series of FCS curves measured at different host concentrations were analyzed by global "target" analysis. This global analysis adjusts a model function to the full series of FCS curves over the full time interval including the diffusion, the triplet and the reaction terms according to a common dynamic-equilibrium model (Al-Soufi et al. 2005; Novo et al. 2007), as given in equation 1 (see Chapters I and II for a detailed explanation).

$$G(\tau) = \frac{1}{N}\left(1+\frac{\tau}{\bar{\tau}_D}\right)^{-1}\left(1+\left(\frac{\omega_{xy}}{\omega_z}\right)^2\frac{\tau}{\bar{\tau}_D}\right)^{-\frac{1}{2}}\left(1+A_R\,e^{-\tau/\tau_R}\right)\left(1+A_T\,e^{-\tau/\tau_T}\right)+b \qquad (1)$$

In order to perform the global "target" analysis we model the $[DNA]_0$-dependent parameters in eq. 1, such as the mean diffusion time, $\bar{\tau}_D$, the reaction time, τ_R, and the reaction term amplitude, A_R, as a function of $[DNA]_0$ of each sample as given in the following equations:

$$\bar{\tau}_D = \frac{\tau_f(1+K[DNA]_0)}{1+\frac{\tau_f}{\tau_b}K[DNA]_0} \qquad (2)$$

$$\tau_R = \left(k_-(1+K[DNA]_0)\right)^{-1} = (k_- + k_+[DNA]_0)^{-1} \qquad (3)$$

$$A_R = \frac{K[DNA]_0(1-q)^2}{(1+qK[DNA]_0)^2} \qquad (4)$$

The use of global fits reduces the number of fit parameters and, in consequence, also parameter correlation. As given in equations 2 to 4, the three relevant fit parameters $\bar{\tau}_D$, τ_R and A_R are determined as a function of a common fit parameter K, which is the association equilibrium constant. This way, the value of K obtained in the fit is the one which best describes both the diffusion and the reaction terms.

Other fit parameters can be shared among all curves: the diffusion times of free, τ_f, and bound binder, τ_b, the dissociation rate constant, k_-, the equilibrium constant, K, and the brightness ratio between bound and free binder, q. The relaxation time of the triplet, τ_T, and its amplitude, A_T, are considered non-dependent of $[DNA]_0$ and therefore are also shared parameters. The baseline, b, and the mean number of particles in the sample volume, N, are set as independent for each curve in order to compensate for possible impurities in the samples (note that scattering and impurities with low fluorescence have a strong effect on N).

In order to avoid parameter correlation, the diffusion time of the free binder, τ_f, was fixed to the experimental value obtained in the absence of DNA, and the diffusion time of the binder bound to DNA, τ_b, was fixed to the value obtained from the diffusion coefficients of the complexes estimated on the basis of reported experimental data (Tirado et al. 1984).

The factor (ω_{xy}/ω_z) is related to the sample volume geometry. It can suffer from slight variations due to the everyday fine adjustment of the equipment. Its value is fixed to that obtained for the calibration of the detection volume with Rhodamine 123 (see section 5.4 of Chapter I).

A modification was added to the model for the titrations with the binder with long linker, in order to consider the presence of a small amount of free OG488 in the stock of binder as a result of an incomplete purification after the synthesis. The new model considers the contribution of this free OG488 as an impurity.

$$
\begin{aligned}
G(\tau) &= r\, G_1(\tau) + (1-r)\, G_{\mathrm{imp}}(\tau) \\
G_1(\tau) &= \frac{1}{N}\left(1+\frac{\tau}{\bar{\tau}_D}\right)^{-1}\left(1+\left(\frac{\omega_{xy}}{\omega_z}\right)^2\frac{\tau}{\bar{\tau}_D}\right)^{-\frac{1}{2}}\left(1+A_R\, e^{-\tau/\tau_R}\right)\left(1+A_T\, e^{-\tau/\tau_T}\right) \\
G_{\mathrm{imp}}(\tau) &= \frac{1}{N}\left(1+\frac{\tau}{\tau_{\mathrm{imp}}}\right)^{-1}\left(1+\left(\frac{\omega_{xy}}{\omega_z}\right)^2\frac{\tau}{\tau_{\mathrm{imp}}}\right)^{-\frac{1}{2}}\left(1+A_{T,\mathrm{imp}}\, e^{-\tau/\tau_{T,\mathrm{imp}}}\right)
\end{aligned}
\tag{5}
$$

The following expressions for r and the apparent number of molecules, N, as well as the details of how to take into account the effect of impurities on FCS experiments are explained in the corresponding section of Chapter I.

$$
r = \frac{1}{1+\left(f_{Q,0}\left(\frac{1+K[DNA]}{1+qK[DNA]}\right)\right)^2 f_N} \tag{6}
$$

$$N = N_1 \frac{\left(1 + f_{Q,0}\, f_N \left(\frac{1 + K[\mathrm{DNA}]}{1 + q\, K[\mathrm{DNA}]}\right)\right)^2}{1 + f_N \left(f_{Q,0} \left(\frac{1 + K[\mathrm{DNA}]}{1 + q\, K[\mathrm{DNA}]}\right)\right)^2} \tag{5}$$

Global "target" analysis was programmed in OriginPro 8.0 (OriginLab Corporation, US). An empirical weighting function was used in order to take into account the strong variation of the noise in the FCS curves. All given uncertainties correspond to one standard deviation from the fits and do not include calibration errors.

3. Communication on DNA Binding Dynamics.

This section is the reproduction of the published work: *Single-Molecule Approach to DNA Minor-Groove Association Dynamics* (Bordello et al. 2012).

The Supporting Information at the end of the section includes supplementary figures of *FCS Titrations with DNA hairpins*; the explanation of the *Calculation of the Diffusional Rate Constants, k_d and k_d'*; and the detailed *Synthesis of BBA-OG* carried out by our collaborators from the Prof. José Luis Mascareñas Group (USC). To improve readability, some additional details from the original Supporting Information were moved to the section 2 of this Chapter *Materials and Methods*.

Numeration of Figures and Tables in the original manuscript has been changed by adding the section number to keep it consistent throughout the chapter.

Single-Molecule Approach to DNA Minor-Groove Association Dynamics

Jorge Bordello, M. I. Sánchez; M. E. Vázquez; J. L. Mascareñas, W. Al-Soufi and M. Novo

Angewandte Chemie International Edition (2012), 51, 7541–7544.

Chemists have long pursued the design and preparation of molecules that can recognize specific DNA sequences. The deciphering of the human genome and on-going efforts to sequence the genome of many other organisms have provided a wealth of information on DNA targets of both therapeutic and diagnostic interest, and therefore there is a renewed interest in the development of smart DNA minor-groove binders.[1,2] Despite the detailed structural and thermodynamic information available regarding the interaction of a number of minor-groove binders with the DNA, kinetic data are much more scarce. In addition, the very low dissociation rates typical of these agents result in very slow binding dynamics, which are experimentally not easily accessible.[3] Typically used stopped-flow methods can yield complex kinetics and artifacts arising from the relatively high binder concentrations often required in this technique. Moreover, the dissociation rates are usually obtained with indirect SDS sequestering techniques that only give apparent rates. Dynamic data of archetypical minor-groove binders such as Distamycin or Hoechst 33258 indicate that the association process is very fast and nearly diffusion limited, which is surprising given the severe geometric constraints imposed on the inclusion of a binder into the narrow minor groove.[4-7]

Cationic bis-benzamidines represent interesting platforms to target A/T-rich sequences preferentially over those containing G/C pairs. Prominent examples of this family, such as pentamidine or furamidine, have found clinical applications and are successfully used for the treatment of several major tropical diseases.[8] Nevertheless, the toxic side effects of these bis-benzamidines[9] have encouraged the search for new derivatives with improved efficacy, pharmacological properties and reduced adverse effects.[10] Bis-benzamidines bind short A/T-rich DNA sequences by insertion in the narrow minor groove. NMR and X-ray studies agree in the general picture of the interaction, in which the positively charged amidinium groups are situated deep in the groove, making both direct and indirect hydrogen bonds with the DNA bases and electrostatic contacts with the bottom of the groove.[11]

Recently we reported several rapid and practical synthetic approaches to bis-benzamidine DNA binders, some of which can be easily modified by conjugation to designed functionalities or fluorophores.[12] With this methodology at hand we decided to make the conjugate BBA-OG (Figure 3.1), featuring an Oregon green fluorophore attached to the DNA binder. We envisioned that the presence of a negative carboxylate charge in the fluorophore should increase the DNA dissociation rate, and thereby allow us to extract kinetic information using Fluorescence Correlation Spectroscopy (FCS). This technique provides a sensitive single-molecule approach to study fast kinetics of biomolecular interactions,[13] yielding accurate values for the binding equilibrium constant and the association and dissociation rate constants, as well as for the diffusion coefficients,[14,15] from which the diffusion-controlled rate constants can be estimated.[16] To the best of our knowledge this technique has not been previously used to analyze the dynamics of minor groove binders. The wide dynamic range of FCS makes it possible to identify the rate-limiting step in the association event by comparison of the dynamics of the association to DNA with different sequences and chain length, and thus to evaluate the importance of processes such as sliding or two-dimensional diffusion, which have been proposed as likely mechanisms for the binding of proteins to DNA.[16, 17]

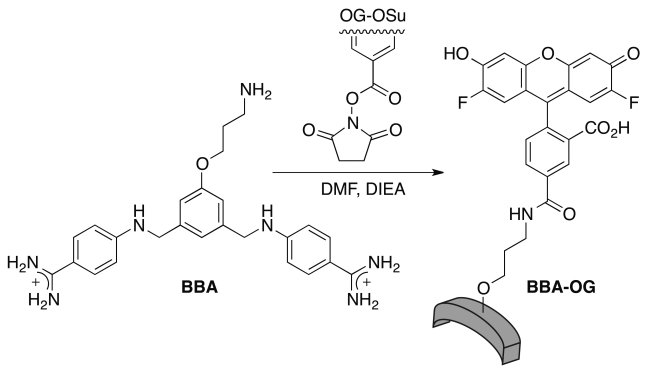

Figure 3.1. Synthesis of Oregon green-labeled bis-benzamidine BBA-OG.

FCS titrations of BBA-OG with three short hairpin oligonucleotides (12 bp + loop) containing as key target sequences AAATTT, AATTT and GGCCC and with a longer dsDNA (50 bp) containing one AAATTT site, were performed. For the AAATTT-hp an additional FCS titration at a higher salt concentration was measured. Figure 3.2 shows normalized fluorescence correlation curves of the binding of BBA-OG to the longer dsDNA. Without DNA only translational diffusion of the binder with correlation time τ_D is observed. Addition of DNA increases τ_D reflecting the slower diffusion of the dye bound to DNA. Additionally a new term appears with a shorter correlation time τ_R, which decreases as the concentration of DNA is increased (see insets in Figure 3.2). τ_R is the relaxation time of the

reversible binding process: $\tau_R = (k_+[\mathrm{DNA}]_0 + k_-)^{-1}$ with k_+ and k_- being the association and dissociation rate constants, respectively. The huge amplitude A_R of this term is due to the high increase in the brightness of bound BBA-OG.[18] The diffusion, and relaxation terms show the expected concentration dependence and are independent of the irradiance.[18,19] In order to reduce parameter correlation, the FCS titration series were analyzed by global target fits[14,15] with a common dynamic-equilibrium model of the diffusion, triplet and relaxation terms (Figure 3.2 and SI.1 to SI.4). The parameters that best fit the whole data set are given in Table 3.1 and Figure 3.3.

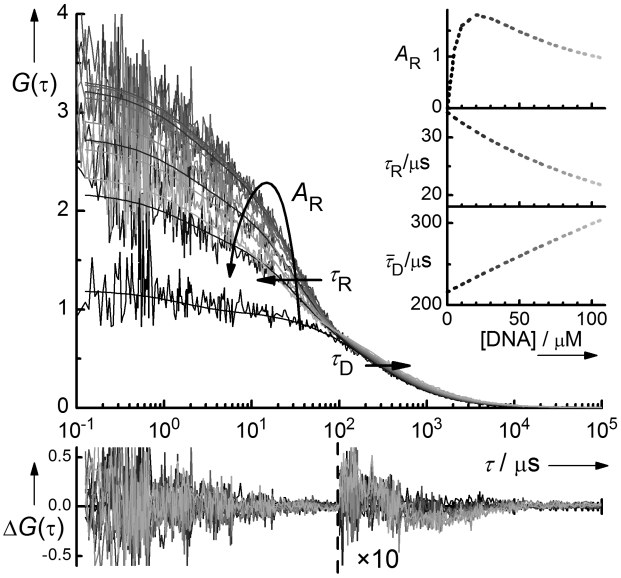

Figure 3.2. FCS curves of the titration of BBA-OG with **AAATTT-ds** and results of a global fit of the dynamic-equilibrium model, eqs. 1 to 4. Insets: variation of the mean diffusion time $\bar{\tau}_\mathrm{D}$, the relaxation time, τ_R and the relaxation amplitude A_R with [DNA] calculated from the fit parameters. Lower panel: Unweighted fit residuals. The small deviations at high DNA concentrations are due to minor fluorescent impurities in the DNA samples. Above 100 µs a factor of 10 was applied.

Table 3.1. Association (k_+) and dissociation (k_-) rate constants and binding equilibrium constant (K) of BBA-OG with DNA.

DNA[a]	k_+ /10^8 M^{-1} s^{-1}	k_- /10^4 s^{-1}	K /10^3 M^{-1}
AAATTT-hp[a]	1.36 ± 0.01	3.19 ± 0.02	4.27 ± 0.03
AATTT-hp[a]	0.95 ± 0.01	4.89 ± 0.05	1.95 ± 0.02
GGCCC-hp[a]	0.083 ± 0.003	14.0 ± 0.4	0.059 ± 0.001
AAATTT-ds[a]	1.56 ± 0.02	2.84 ± 0.02	5.47 ± 0.05
AAATTT-hp[b]	0.65 ± 0.03	4.63 ± 0.01	1.41 ± 0.03

[a] [NaCl]=0.1 M, [b] [NaCl]=1.0 M. See complete oligonucleotide sequences in section 2.2.

Figure 3.3 shows that the association rate constant decreases by more than one order of magnitude from the AT rich to GC containing sequences, whereas the dissociation rate constant increases 3-5 times. Both association and dissociation contribute to the specificity for the AT rich tracts, but the association has a higher effect. This is in agreement with reported results for the antibiotic Distamycin with different mismatched sites.[4] Moreover, the absolute values of k_+ for the AT sequences coincide well with those reported for other minor-groove binders [4-7] and show the small decrease with Na^+ concentration expected for groove binders,[20] suggesting analogous association mechanisms. Nevertheless, the dissociation rate constants are about 4 orders of magnitude higher than those of typical binders, resulting in much lower binding constants.

The above results indicate much weaker specific interactions of BBA-OG with the DNA minor groove, which is probably due to the electrostatic repulsion between the negatively charged OG moiety and DNA. The high binding constants of unlabeled bisbenzamidines supports this explanation.[12] On this basis we can consider BBA-OG as a valid model for the study of the association process to the minor groove of the DNA.

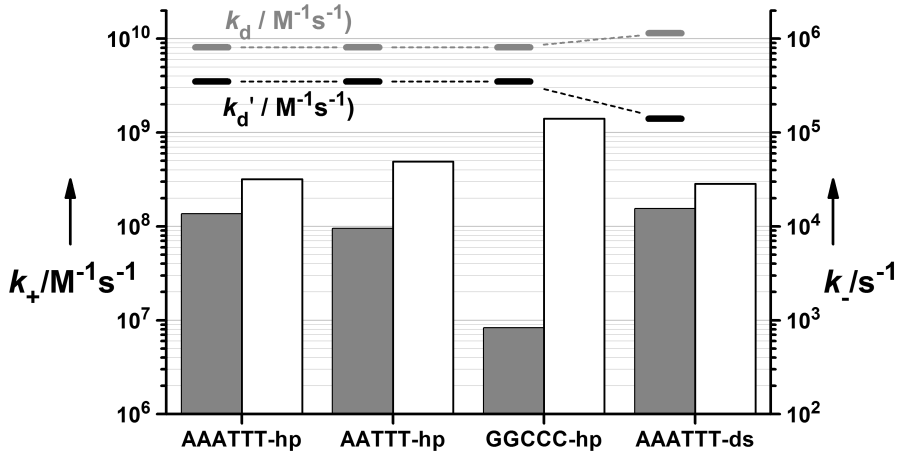

Figure 3.3. Association (grey, left scale) and dissociation (white, right scale) rate constants of BBA-OG with DNA obtained from FCS. Estimates of the diffusion-controlled association rate contants k_d and k_d' defined in Scheme 3.1 (see SI).

In order to determine the rate-limiting step for the association process we compare the dynamics of binding to the short DNA **AAATTT-hp** with that to the much longer **AAATTT-ds**, which has been designed avoiding other AT rich sites. Curiously, we don't find significant differences in the binding dynamics (Table 3.1, Figure 3.3). The similar dissociation (k_-) is readily explained in terms of similar specific interactions with the

AAATTT sequence. However, if diffusion plays an important role, the association dynamics should be affected by the increase of the DNA length.

For a more detailed analysis we propose a two-step mechanism like that previously used to describe other supramolecular binding processes (Scheme 3.1).[14,15] The first step is the formation of an encounter complex between DNA and binder, with a diffusion-controlled association rate which can be estimated based on the geometry of DNA and binder. The second step is the insertion of the binder into the minor-groove with a rate constant k_r, a process which conveys structural rearrangements or the breakdown and reconstitution of the water structure around the interacting species. The experimentally observed k_+ corresponds to the overall reaction described by a single relaxation time and is determined by the rate-limiting step. This mechanism is therefore different to the sequential model proposed for the binding of Hoechst 33258 to DNA[7] which involves two reactions with their corresponding two observed reaction times.

Assuming a rod-like structure of the DNA with a localized reactive site, we estimate lower bounds (see SI) of the diffusion-controlled association rate constants k_d and k_d' for the formation of unlocalized (U) and localized (L) encounter complexes, respectively, where the binder is either located arbitrarily at any position of the DNA (U) or already localized in the neighborhood of the reactive site (L) (Scheme 3.1).[16]

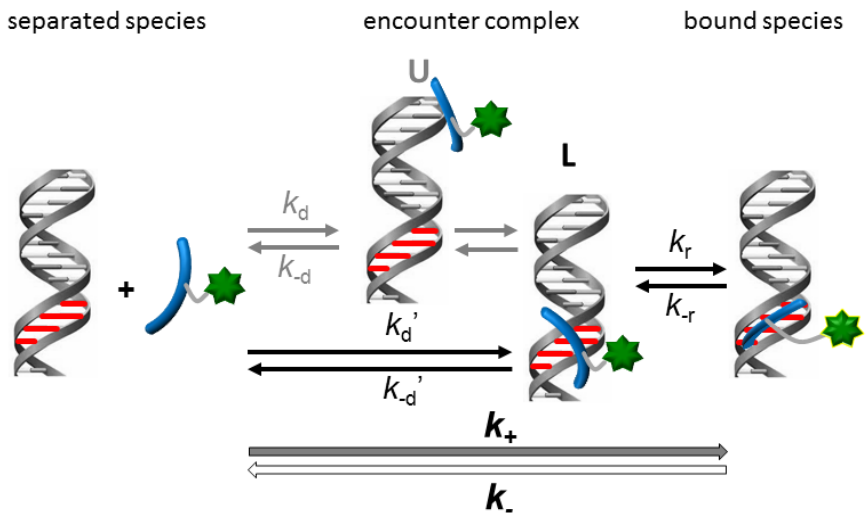

Scheme 3.1. Two-step mechanism proposed for the binding of BBA-OG with DNA involving the formation of an encounter complex, with the binder localised at the DNA reactive site (L) or unlocalised (U).

The estimated values of k_d' for the formation of localized complexes L are of course significantly lower than those of k_d corresponding to the formation of U, especially in the case of the long dsDNA (Figure 3.3, SI). Nevertheless, even for the most specific sequences, both k_d and k_d' are at least one order of magnitude higher than the observed overall rate constant k_+. This shows that the diffusion-controlled formation of the encounter complex is *not* the rate-limiting step, even if the binder is requested to be located near the reactive sequence. The encounter complexes U and L are in rapid pre-equilibrium with the separated species so that the overall rate of association between BBA-OG and DNA is not diffusion limited but determined by the next step of the process, namely the unimolecular inclusion into the minor groove. This step is probably essentially controlled by geometrical and orientational requirements, which depend on critical dimensions of both the binder and the minor groove. The presence of the exocyclic 2-amino group in GC tracts[21] may explain the much lower value of k_+ obtained for this sequence.

We can also conclude that processes that increase the rate of formation of localized encounter complexes, such as sliding or bi-dimensional diffusion along the DNA strand,[16, 17] do not play a key role in the association rate of BBA-OG, and probably also not for other minor groove binders.

In summary, our results indicate that the association process of BBA-OG to dsDNA is not controlled by diffusion, but by the rate-limiting insertion of the binder into the minor-groove. Moreover, we find that the association process has an important effect on the *specificity* to AT sites, whereas the differences in the binding *affinity* are mainly determined by the dissociation rate. This mechanism might constitute a general mechanism for small minor groove binders, but this should be confirmed with further studies on more typical minor groove agents. This information should be useful for the design of new DNA binders with optimized properties and for the future understanding of the behavior of these molecules in more complex cellular environments. This work has also shown the potential of FCS for the study DNA binding dynamics of minor-groove binders using labeled derivatives.

References.

[1] a) D. R. Boer, A. Canals, M. Coll, J. Chem. Soc., Dalton Trans. 2009, 3, 399-414; b) W. C. Tsee, D. L. Boger, Chem. Biol. 2004, 11, 1607-1617; c) E. Pazos, J. Mosquera, M. E. Vázquez, J. L. Mascareñas, ChemBioChem 2011, 12, 1958-1973. d) M. E. Vázquez, A. M. Caamaño and J. L. Mascareñas, Chem. Soc. Rev. 2003, 32, 338-349

[2] a) M. E. Vázquez, A. M. Caamaño, J. Martínez-Costas,L. Castedo, J. L. Mascareñas, Angew. Chem. Int. Ed. 2001, 40, 4723-4725; b) O. Vázquez, M. E. Vázquez, J. B. Blanco, L. Castedo, J. L. Mascareñas, Angew. Chem. Int. Ed. 2007, 46, 6886-6890.

[3] a) L. M. Wilhelmsson, P. Lincoln, B. Nordén in Sequence-Specific DNA Binding Agents (Ed:. M. Waring), The Royal Society of Chemistry 2006, pp. 69-95; b) T. C. S. Pace, C. Bohne, Adv. Phys. Org. Chem. 2007, 42, 167-223.

[4] R. Baliga, D. M. Crothers, J. Am. Chem. Soc. 2000, 122, 11751-11752.

[5] R. Baliga, D. M. Crothers, PNAS 2000, 97, 7814-7818.

[6] S. Y. Breusegem, S. Sadat-Ebrahimi, K. T. Douglas, R. M. Clegg, F. G. Loontiens, J. Mol. Biol. 2001, 308, 649-663.

[7] S. Y. Breusegem, R. M. Clegg, F. G. Loontiens, J. Mol. Biol. 2002, 315, 1049-1061.

[8] a) R. Balaña-Fouce, M. C. Redondo, Y. Pérez-Pertejo, R. Díaz-González, M. R. Reguera, Drug Discov. Today 2006, 11, 733-740; b) I. Midgley, K. Fitzpatrick, L. M. Taylor, T. L. Houchen, S. J. Henderson, S. J. Wright, Z. R. Cybulski, B. A. John, A. McBurney, D. W. Boykin, K. L. Trendler, Drug Metab. Dispos. 2007, 35, 955-967.

[9] a) W. D. Wilson, B. Nguyen, F. A. Tanious, A. Mathis, J. E. Hall, C. E. Stephens, D. W. Boykin, Curr. Med. Chem. Anticancer Agents 2005, 5, 389-408; b) A. H. Fairlamb, Trends Parasitol. 2003, 19, 488-494.

[10] R. R. Tidwell, D. W. Boykin in DNA and RNA Binders: From Small Molecules to Drugs (Eds.: M. Demeunynck, C. Bailly, W. D. Wilson), Wiley-VCH, Weinheim, Germany, 2003, pp. 414-460.

[11] C. M. Nunn, S. Neidle, J. Med. Chem. 1995, 38, 2317-2325.

[12] a) O. Vázquez, M. I. Sánchez, J. Martínez-Costas, M. E. Vázquez, J. L. Mascareñas, Org. Lett. 2010, 12, 216-219; b) O. Vázquez, M. I. Sánchez, J. L. Mascareñas, M. E. Vázquez, Chem. Commun. 2010, 46, 5518-5520; c) M. I. Sánchez, O. Vázquez, J. Martínez-Costas, M. E. Vázquez, J. L. Mascareñas, submitted.

[13] a) A. van Oijen, Curr. Opin. Biotechnol. 2011, 22, 75-80; b) D. Magde, E. L. Elson, W. W. Webb, Biopolymers 1974, 13, 29-61.

[14] W. Al-Soufi, B. Reija, M. Novo, S. Felekyan, R. Kühnemuth, C. A. M. Seidel, J. Am. Chem. Soc. 2005, 127, 8775-8784.

[15] W. Al-Soufi, B. Reija, S. Felekyan, C. A. Seidel, M. Novo, ChemPhysChem 2008, 9, 1819-1827.

[16] O. G. Berg, P. H. von Hippel, Annu. Rev. Biophys. Biophys. Chem. 1985, 14, 131-158.
[17] D. Vuzman, A. Azia, Y. Levy, J. Mol. Biol. 2010, 396, 674-684.
[18] J. Bordello, M. Novo, W. Al-Soufi, J. Colloid Interface Sci. 2010, 345, 369-376.
[19] M. Novo, D. Granadero, J. Bordello, W. Al-Soufi, J. Inclusion Phenom. Macrocyclic Chem. 2011, 1-10.
[20] (a) W. D. Wilson, F. A. Tanious, H.J. Barton, R.L. Jones, K. Fox, R.L. Wydra, L-Strekowski, Biochemistry 1990, 29, 8452-8461. (b) F. A. Tanious, J. M. Veal, H. Buczak, L. S. Ratmeyer, W. D. Wilson, Biochemistry 1992, 31, 3103-3112. (c) T. M. Lohman, CRC Crit. Rev. Biochem. 1986, 191-245.
[21] S. Neidle, Nat. Prod. Rep. 2001, 18, 291-309.
[22] D. Granadero, J. Bordello, M. J. Pérez-Alvite, M. Novo, W. Al-Soufi, Int. J. Mol. Sci. 2010, 11, 173-188.

Acknowledgments.

The authors thank the *Ministerio de Ciencia e Innovación* (CTQ2010-21369, SAF2007-61015, SAF2010-20822-C02, CTQ2009-14431/BQU, Consolider Ingenio 2010 CSD2007-00006) and the *Xunta de Galicia* (INCITE09262304PR, INCITE09E2R209064ES, IN845B-2010/094, INCITE09209084PR, GRC2010/12, PGIDIT08CSA-047209PR) for financial support. J.B. and M.I.S thank the *Ministerio de Ciencia e Innovación* for their research scholarships.

Supplementary Information.

FCS Titrations with DNA hairpins.

The following figures (S1 to S4) show the normalized fluorescence correlation curves measured for BBA-OG in the presence of different concentrations of DNA for the three sequences of hairpin DNA studied, together with the fitted curves and the residuals of the fits obtained from global target fits of the dynamic-equilibrium model, eq. SI.1-4. The values of individual fits to the FCS curves are consistent with the global fit results, but are strongly affected by parameter correlations. The values of the brightness ratio between bound and free binder, q, were between 9 and 12.

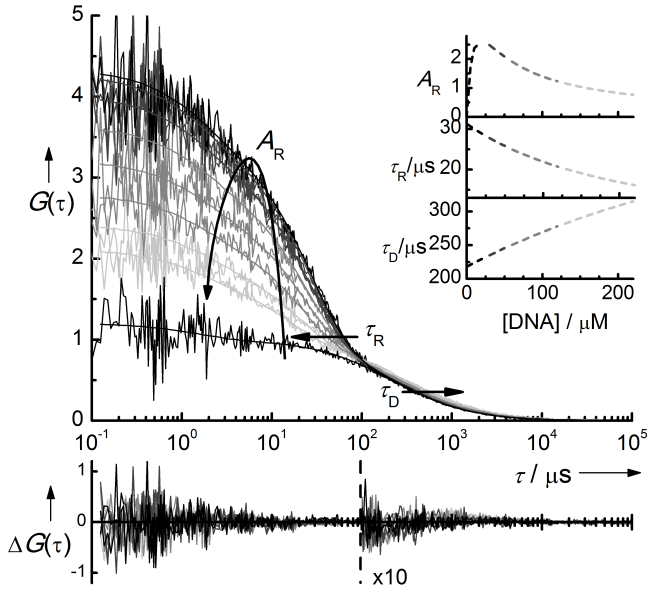

Figure SI.1. FCS curves for the titration of BBA-OG with **AAATTT-hp DNA** at [NaCl] = 0.1 M (experimental data and fitted curves using eq. 1 to 4). Insets: variation of the mean diffusion time $\bar{\tau}_D$, the relaxation time, τ_R and the relaxation amplitude A_R with [DNA] calculated from the fit parameters. The lower panel shows the fit residuals. Above 100 µs a factor of 10 was applied.

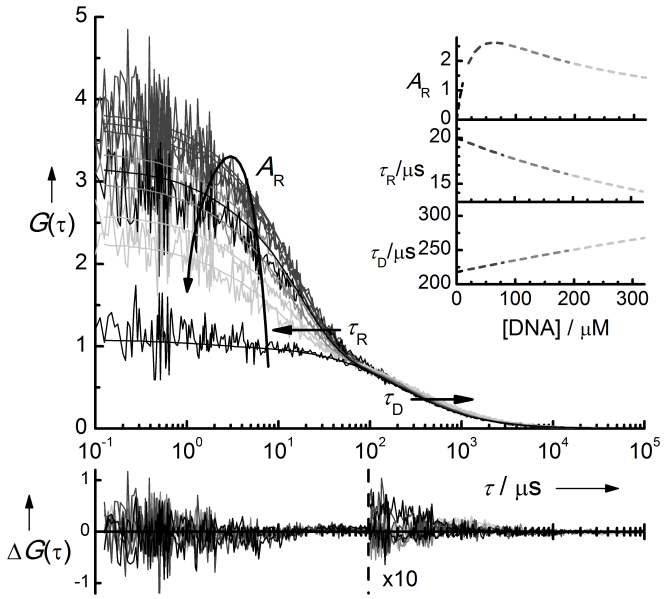

Figure SI.2. FCS curves for the titration of BBA-OG with **AATTT-hp DNA** at [NaCl] = 0.1 M (experimental data and fitted curves using eq. 1 to 4). Insets: variation of the mean diffusion time $\bar{\tau}_D$, the relaxation time, τ_R and the relaxation amplitude A_R with [DNA] calculated from the fit parameters. The lower panel shows the fit residuals. Above 100 µs a factor of 10 was applied.

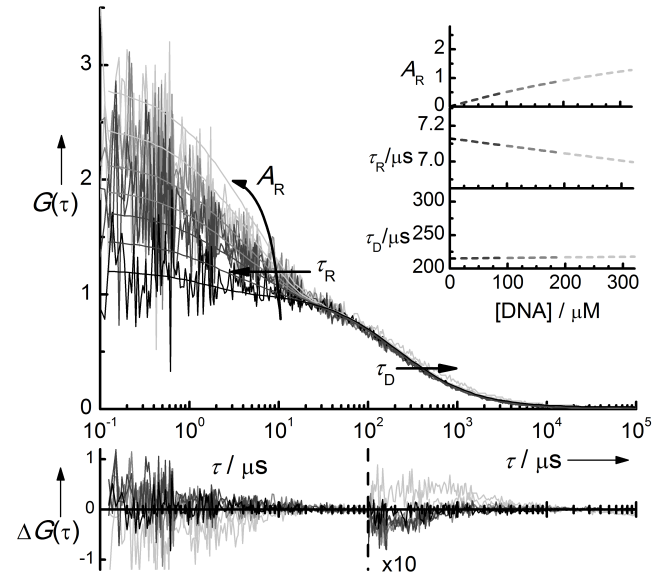

Figure SI.3. FCS curves for the titration of BBA-OG with **GGCCC-hp DNA** at [NaCl] = 0.1 M (experimental data and fitted curves using eq. 1 to 4). Insets: variation of the mean diffusion time $\bar{\tau}_D$, the relaxation time, τ_R and the relaxation amplitude A_R with [DNA] calculated from the fit parameters. The lower panel shows the fit residuals. Above 100 µs a factor of 10 was applied.

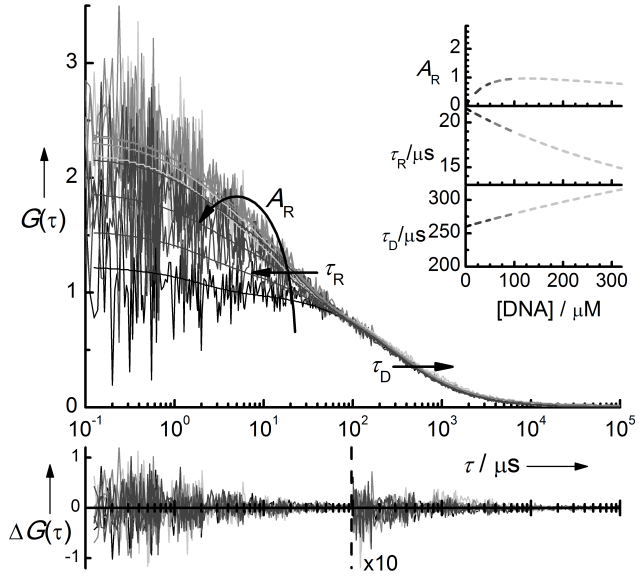

Figure SI.4. FCS curves for the titration of BBA-OG with **AAATTT-hp DNA at [NaCl] = 1.0 M** (experimental data and fitted curves using eq. 1 to 4). Insets: variation of the mean diffusion time $\bar{\tau}_D$, the relaxation time, τ_R and the relaxation amplitude A_R with [DNA] calculated from the fit parameters. The lower panel shows the fit residuals. Above 100 µs a factor of 10 was applied.

Calculation of the Diffusional Rate Constants, k_d and k_d'.

The diffusion-controlled rate constant of a bimolecular reaction can be calculated using the Smoluchowski equation for the case of two uniformly reactive homogeneous spheres (Berg and von Hippel 1985):

$$k_d = 4\,\pi\,D\,R \tag{S1}$$

$$k_d = 4\pi(D_A + D_B)(r_A + r_B) \tag{S2}$$

where D_A and D_B are the diffusion coefficients, and r_A and r_B the interaction radii of the two spheres.

The geometry of the DNA hairpin or strand used herein is not well described by a sphere, but has to be modeled as a rod or ellipsoid. Using this model the value for the DNA interaction radius can be estimated from the major and minor semi-axes (a and b, respectively) using the following expression (Berg and von Hippel 1985):

$$r_{DNA} \approx \frac{a}{ln\left(\frac{2a}{b}\right)} \tag{S3}$$

Using this expression for r_{DNA} we obtain a rate constant k_d which accounts for the diffusion-controlled formation of an encounter complex with the binder located arbitrarily at any position of the DNA (indicated as U in Scheme 3.1).

In cases where only a segment of the rod is reactive, one can define a second diffusional rate constant, k_d', which accounts for the diffusion step to yield an encounter complex where the binder is located in the neighborhood of the reactive base sequence with high affinity (indicated as L in Scheme 3.1). This diffusion-controlled rate constant can be estimated from k_d using the area ratio between the reactive segment and the whole DNA molecule. The area ratio can be estimated from the ratio between the length of the reactive site, l, and the total length of the molecule, $2a$.

$$k'_d = \frac{l}{2a} k_d \tag{S4}$$

These equations have been used to estimate the values for the diffusional component of the association constant in the interaction of BBA-OG with the two DNA molecules with the same specific sequence of base pairs (AAATTT) but different sizes: the hairpin (12 base pair + 5-base loop) and the 50-bp double stranded DNA. From the values of diffusion coefficients (derived from the diffusion times of the fits) and interaction radii (estimated with the rod model as explained above) we can establish lower limits for the diffusion-controlled association rate constants (see Table S1). Dimensions a, b and l of the DNAs used in this work were calculated from reported data (Fernandes et al. 2002):

Table S1. Diffusion coefficients (D_i), interaction radii (R), diffusional rate constants (k_d, k_d') and experimental association rate constants (k_+) for the interaction of the binder BBA-OG with the DNA-hp and DNA-ds used in this work. k_d' are the diff. rate constants referred to an interaction localized at the reactive site.

	D_i /10^{-10} m^2s^{-1}	R /Å	k_d /10^9 $M^{-1}s^{-1}$	k_d' /10^9 $M^{-1}s^{-1}$	k_+ /10^9 $M^{-1}s^{-1}$
BBA-OG	3.23				
DNA-hp	1.22	24.2	8.13	3.49	0.136
DNA-ds	0.67	39.0	11.5	1.38	0.156

The upper limit for the overall observed association rate constant k_+ is k_d, which considers the diffusional step till the binder comes into collision with any part of the DNA. In this case, the larger DNA (DNS-ds) has a higher value of k_d since the increase in the interaction radius compensates the decrease in the diffusion coefficient.

When we extend the diffusional step until the binder comes into collision with the segment of specific sequence in the DNA, we have to estimate the diffusion-controlled rate constant

through k_d'. In this case, the value of k_d' is lower for the longer DNA-ds than for the short DNA-hp, since the target zones are equal for both DNAs, but the diffusion coefficient is lower for the larger DNA (DNA-ds).

Although k_d' is much lower than k_d it is still about one order of magnitude higher than k_+, both for the short DNA-hp and the larger DNA-ds. This indicates that the association process of BBA-OG with DNA is not diffusion-controlled.

Synthesis of BBA-OG.

DMF and TFA were from *Scharlau*, CH_2Cl_2 from *Panreac*, CH_3CN from *Merck*. The rest of reagents were acquired from *Sigma-Aldrich* and *Invitrogen*. Some reactions were followed by analytical RP-HPLC with an Agilent 1100 series LC/MS using an Eclipse XDB-C18 (4.6 x 150 mm, 5 µm) analytical column. Standard conditions for analytical RP-HPLC consisted on an isocratic regime during the first 5 min, followed by a linear gradient from 5% to 95% of solvent B for 30 min at a flow rate of 1 mL/min (A: water with 0.1% TFA, B: acetonitrile with 0.1% TFA). Final products were purified on a *Büchi* Sepacore preparative system consisting on a pump manager C-615 with two pump modules C-605 for binary solvent gradients, a fraction collector C-660, and UV Photometer C-635. Purification was made using reverse phase linear gradients of $MeCN/H_2O$, with 0.1% TFA in 30 min with a flow rate of 30 mL/min, using a pre-packed preparative cartridge (150 × 40 mm) with reverse phase RP18ec silica gel (*Büchi* order number 54863). The fractions containing the products were freeze-dried, and their identity was confirmed by ESI-MS. All the bis-benzamidines were purified by HPLC and isolated as tris-TFA and bis-TFA salts.

Synthesis of BBA: Potassium tert-butoxide (36.4 mg, 0.324 mmol, 4 equiv) was added to a solution of the bis-amino benzamidine 1 (50 mg, 0.081 mmol) in dry DMSO (1.62 mL). After 30 min, 1-iodo-tert-butyl-2-aminopropylcarbamate (27.7 mg, 0.097 mol, 1.2 equiv) was added in portions. The reaction mixture was stirred under Ar at rt for 2 h. The crude reaction was directly purified by preparative reverse-phase chromatography (Büchi Sepacore) (gradient: 15% B, 5 min; 15% → 95 % B, 30 min.). The combined fractions were concentrated and freeze-dried.

The isolated Boc-protected compound was dissolved in CH2Cl2 (1 mL) and cooled to 0 °C. TFA (1 mL) was added drop wise and the resulting solution was stirred at 0 °C for 1h and at room temperature for other 2 h. The solvent was removed under reduced pressure, and the residual TFA was removed by co-distillation with CH2Cl2. The residue was purified by preparative reverse-phase chromatography (Büchi Sepacore) (gradient: 0% B, 5 min;

0% → 50 % B, 30 min.). The freeze-dried solid was identified as the desired product (BBA) (56.8 mg, 0.072 mmol, 89% overall yield for the 2-step process).

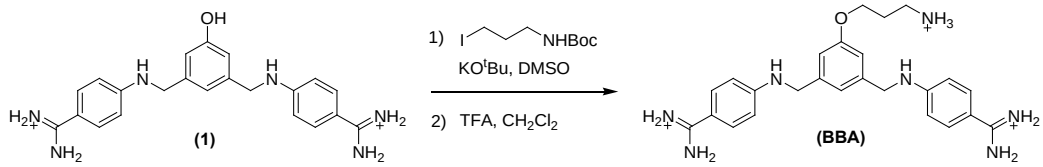

Figure SI.5. Reaction scheme for the synthesis of BBA.

Synthesis of BBA-OG: A solution of bis-amino benzamidine (BBA) (30.92 mg, 39.26 µmol, 4 equiv) in 98.15 µL of DMF/DIEA 0.2 M was added to (5 mg, 9.82 µmol) Oregon Green 488 succinimidyl ester and stirred for 2 h. The consumption of the starting material and the appearance of the desired product was confirmed by analytical RP-HPLC. The residue was purified by high pressure reverse-phase chromatography (gradient: 15% B, 5 min; 15%→95 % B, 30 min.). The appropriated fractions were collected, concentrated and freeze-dried to obtain the desired conjugate BBA-OG (6.5 mg, 5.80 µmol, 59 %).

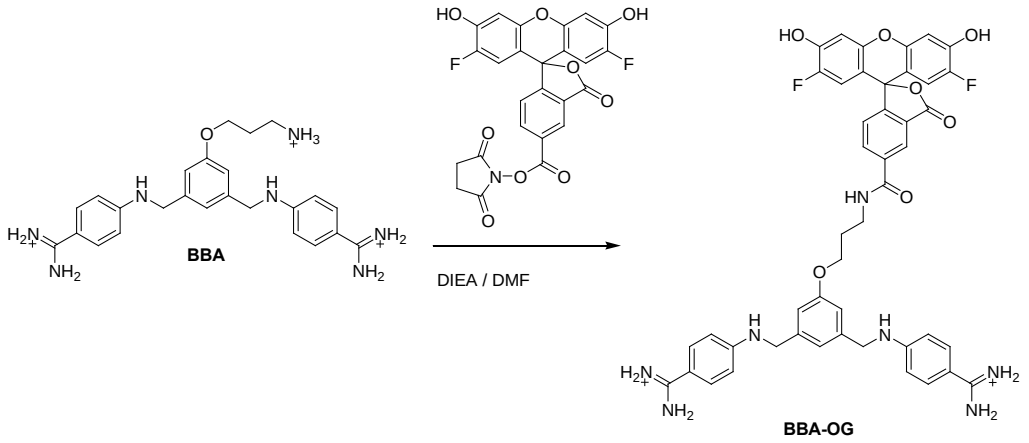

Figure SI.6. Reaction scheme for the synthesis of BBA-OG.

4. Influence of the Linker Length between the Binder and the attached Dye.

In this section the influence of the linker length between BBA and OG in the interaction of the binder with DNA was investigated. A new study of the dynamics was carried out using a binder in which the linker between BBA and the OG was lengthened to get the molecule labeled in Figure 1.3 as BBA-OG-long. FCS titrations were again performed for different sequences of DNA-hp at constant binder concentration (see Figures 4.1 and 4.2) similarly to the experiments with the previous binder BBA-OG.

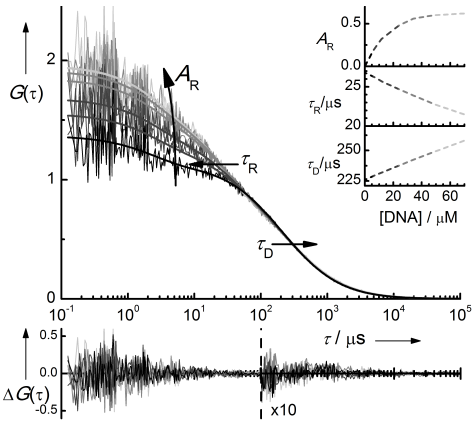

Figure 4.1. FCS curves for the titration of BBA-OG-long with AAATTT-hp DNA at [NaCl] = 0.1 M (experimental data and fitted curves). Insets: variation of the mean diffusion time $\bar{\tau}_D$, the relaxation time, τ_R and the relaxation amplitude A_R with [DNA] calculated from the fit parameters. The lower panel shows the fit residuals. Above 100 µs a factor of 10 was applied.

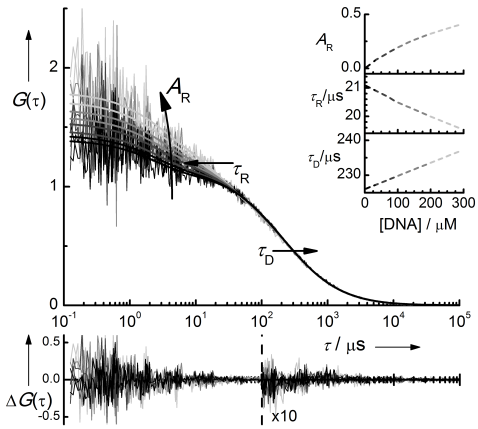

Figure 4.2. FCS curves for the titration of BBA-OG-long with GGCCC-hp DNA at [NaCl] = 0.1 M (experimental data and fitted curves). Insets: variation of the mean diffusion time $\bar{\tau}_D$, the relaxation time, τ_R and the relaxation amplitude A_R with [DNA] calculated from the fit parameters. The lower panel shows the fit residuals. Above 100 µs a factor of 10 was applied.

The correlation curves were analyzed globally for each titration with a similar model to that used for the binder with short linker (see details in section 2.4).

The fits are also shown in Figures 4.1 and 4.2 and the most important parameters obtained from them are collected in Table 4.1 and Figure 4.3.

Table 4.1. Association (k_+) and dissociation (k_-) rate constants, binding equilibrium constant (K) and brightness ratio of BBA-OG (binder with short linker) and BBA-OG-long (binder with long linker) with DNA-hp of two sequences AAATTT and GGCCC.

	k_+ /10^8 $M^{-1}s^{-1}$	k_- /$10^4 s^{-1}$	K /10^3 M^{-1}	q
AAATTT + BBA-OG	1.36 ± 0.01	3.19 ± 0.02	4.27 ± 0.03	12.4 ± 0.1
GGCCC + BBA-OG	0.083 ± 0.003	14.0 ± 0.4	0.059 ± 0.001	10.9 ± 0.1
AAATTT + BBA-OG-long	1.33 ± 0.04	3.7 ± 0.1	3.6 ± 0.1	4.2 ± 0.1
GGCCC + BBA-OG-long	0.13 ± 0.02	4.7 ± 0.3	0.28 ± 0.04	4.0 ± 0.2

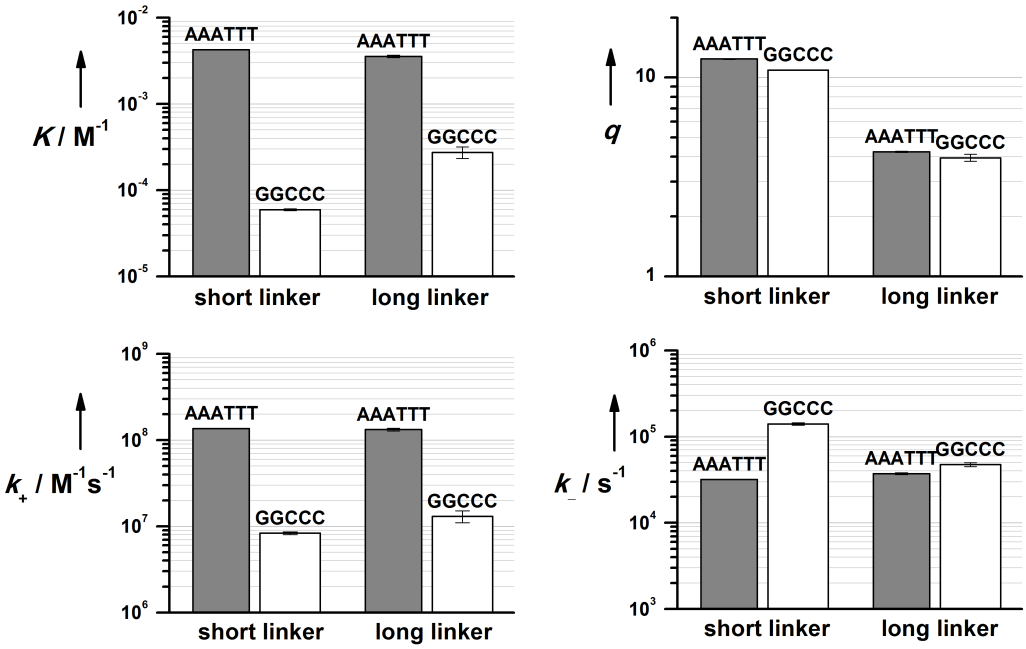

Figure 4.3. Equilibrium constant (upper left), brightness ratio (upper right), association and dissociation rate constants (bottom left and right respectively) for the interaction between BBA-OG binder and DNA-hp. Each pannel shows the results for the two binders (short and long linker) with AAATTT-hp (grey bar) and GGCCC-hp DNA (white bar)

The value for the association rate constant is still an order of magnitude higher for the sequence AAATTT than for the GGCCC. The values for the association rate constant, k_+, are very similar to those obtained for the binder with short linker, showing only a small difference in the case of the GGCCC sequence, which is not considered significant due to the high uncertainties.

In opposite to the binder with short linker, the values for the dissociation rate constant are very similar between the two sequences. The main change is observed with the sequence GGCCC, showing a 3-fold decrease in k_- when the values for the binder with short and long linker are compared. k_- values for the AAATTT sequence do not significantly change from one binder to the other.

According to the behavior of the rate constants, the values of the equilibrium constant, K, show again a higher affinity for the AAATTT sequence. However, the difference between both sequences is smaller than that observed for the binder with short linker, due to an increase in the affinity to the GGCCC sequence when lengthening the linker between BBA and OG.

The fact that the association rate constant, and very especially its relative values among the sequences, is barely affected by the length of the linker supports our premise that the association process for this type of binders is independent of the modifications performed to the binder. On the other hand, we know that the attachment of OG affects the dissociation process, with electrostatic and/or steric hindrance of the specific interactions between BBA and the minor groove, leading to an increase in the k_- values. As we can observe in the results for the short linker binder, the effect of the attachment of OG to the BBA is higher for the GGCCC region, showing a much higher value of k_-. This could explain the fact that in the GC region the groove is more sensitive to changes in the length of the linker between BBA and OG.

In relation with the dye response to the binding, for both titrations the brightness ratio remains constant in a level lower than half the value obtained for the titrations with the short-linker binder. This fact is related with the difference in brightness observed between both binders in absence of DNA. The photophysics of these molecules is discussed in the following section.

5. Photophysical Study of the Binder.

In order to explain the difference in the binder response among the two BBA derivatives, excitation and emission spectra were measured for both of them together with those for the BBA and OG (Figure 5.1). The minor-groove binder BBA absorbs in the UV range (315 nm) and has a weak emission at about 390 nm. On the contrary, the fluorescence marker OG presents its main absorption and emission bands in the visible range, although it shows an additional absorption band at 328 nm that overlaps with that of BBA. The coupling of these two molecules yields species BBA-OG and BBA-OG-long with absorption and emission spectra very similar to those of OG. Thus, the main emission band appears at 522 nm, independently of the excitation wavelength, although a residual emission is observed in BBA-OG and BBA-OG-long when exciting at 328 nm. Nevertheless, the fluorescence quantum yield of OG is much higher than those of the derivatives. For excitation at 488 nm, OG is 8.5 and 6.6 times brighter than BBA-OG and BBA-OG-long, respectively, as determined by FCS. The fluorescence decays of these species are triexponential in opposite to the monoexponential decay of OG (see Table 5.1). The longest lifetime is similar, but somewhat smaller than that of OG, and a new shorter lifetime is observed, which has the main contribution to fluorescence in the case of BBA-OG. The shortest lifetime is attributed to the effect of stray and Raman light.

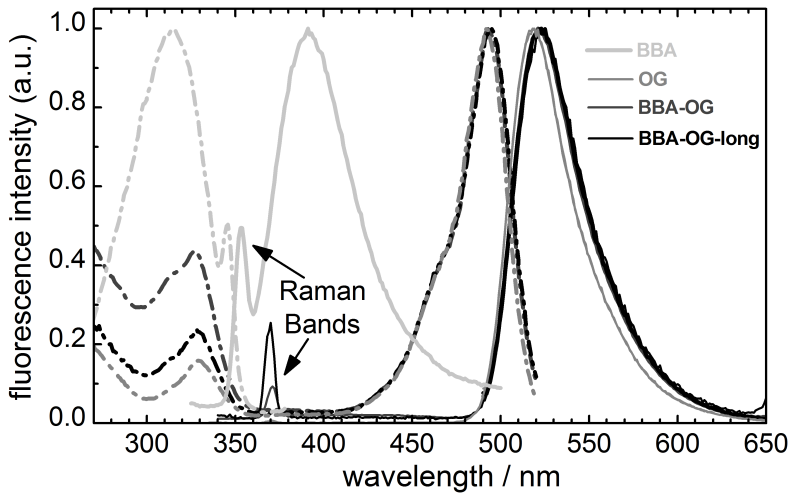

Figure 5.1. Fluorescence excitation (dashed dotted lines) and emission (solid lines) spectra of BBA (light grey), OG (grey), BBA-OG (dark grey) and BBA-OG-long (black). For BBA the spectra were measured at $\lambda_{em} = 391$ nm and $\lambda_{exc} = 315$ nm and for OG, BBA-OG and BBA-OG-long, at $\lambda_{em} = 525$ nm and $\lambda_{exc} = 328$ nm (thin lines), 488 nm (thick lines). The spectra were normalized at their maxima to facilitate comparison.

These results indicate that the derivatives BBA-OG and BBA-OG-long have the photophysical properties of OG instead of those of BBA, but they show a fluorescence quenching which leads to a much lower quantum yield and a shorter lifetime of the OG moiety in these derivatives. Moreover, the second lifetime observed in these species must be related to the quenching process. When comparing the two derivatives, it is observed that fluorescence quenching is more effective in BBA-OG, where the linker between BBA and OG is shorter. This suggests that the quenching process is due to the interaction between BBA and OG.

Table 5.1. Fit results of the fluorescence decays of OG and the binders BBA-OG and BBA-OG-long without and with DNA. B_2/B_3 is the ratio between the preexponential factors of lifetimes τ_2 and τ_3. Emission monitored at 520 ± 10 nm with excitation at 470 nm. DNA concentrations: (a) 305 μM; (b) 260 μM; (c) 306 μM; (d) 299 μM.

	τ_1 /ns	τ_2 /ns	τ_3 /ns	B_2/B_3	χ^2
OG	0.011 ± 0.009		4.158 ± 0.001		1.36
BBA-OG	0.05 (f)	1.54 ± 0.02	3.40 ± 0.06	5.1	1.14
[a]BBA-OG + DNA AAATTT-hp	0.04 ± 0.01	2.1 ± 0.2	4.35 ± 0.02	0.18	1.06
[b]BBA-OG + DNA GGCCC-hp	0.066 ± 0.007	1.72 ± 0.03	4.28 ± 0.03	1.6	1.16
BBA-OG-long	0.254 ± 0.007	1.59 ± 0.03	4.00 ± 0.02	1.3	1.10
[c]BBA-OG-long + DNA AAATTT-hp	0.28 ± 0.01	1.83 ± 0.06	4.26 ± 0.01	0.44	1.08
[d]BBA-OG-long + DNA GGCCC-hp	0.308 ± 0.009	1.86 ± 0.04	4.19 ± 0.02	0.92	1.06

In order to prove this hypothesis we have measured the fluorescence emission spectra and decays of OG in the presence of different concentrations of BBA (Figure 5.2 and Table 5.2). A dramatic decrease of the fluorescence intensity with the addition of BBA is observed, being the corresponding Stern-Volmer plot clearly non-linear. This indicates that both static and dynamic quenching take place. In fact, the decrease of the longer lifetime (τ_3), associated to OG, as the concentration of BBA is increased (Table 5.2), with a Stern-Volmer slope of 16.6 ± 0.3 mol^{-1} dm^3, evidences a collisional quenching. Nevertheless, a second shorter lifetime appears at about [BBA] = 2 mM, whose value decreases as the concentration of BBA is increased. The amplitude of this lifetime is small but positive and increases with BBA concentration. These are evidences of another process in the excited state reverse process to the collisional quenching.

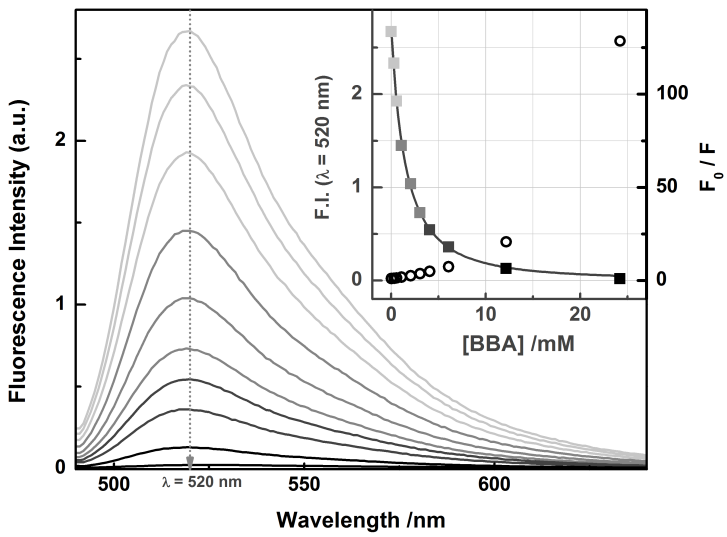

Figure 5.2. Fluorescence emission spectra of OG with different concentrations of BBA up to 25 mM. Inset: Fluorescence intensity at 520 nm against BBA concentration (filled squares, left scale) and fitted curve with the model described in text. Stern-Volmer plot for the fluorescence intensity measured at 520 nm (open circles, right scale). Excitation wavelength: 488 nm.

Table 5.2. Fit results of the fluorescence decays of OG in the presence of different concentrations of BBA. Triexponential fits with $\tau_1 = 0.03 \pm 0.02$ ns^{-1}. B_2/B_3 is the ratio between the preexponential factors of lifetimes τ_2 and τ_3. Emission monitored at 520 ± 10 nm with excitation at 470 nm.

[BBA] /mM	τ_2 /ns	τ_3 /ns	B_2/B_3	χ^2
0		4.158 ± 0.001		1.36
0.293		4.139 ± 0.001		1.27
0.554		4.116 ± 0.002		1.18
1.07		4.085 ± 0.002		1.08
2.05	2.6 ± 0.9	4.04 ± 0.03	0.042	1.16
3.04	2.9 ± 1.2	3.99 ± 0.09	0.075	1.14
4.05	1.7 ± 0.5	3.89 ± 0.01	0.027	1.05
6.06	1.6 ± 0.3	3.79 ± 0.02	0.061	1.08
12.1	1.2 ± 0.1	3.47 ± 0.02	0.15	0.96
24.2	1.0 ± 0.2	2.8 ± 0.2	0.17	0.97

On the basis of these results, a mechanism is proposed for the interaction of OG with BBA (Scheme 5.1) that includes the formation of a complex between OG and BBA in the ground state (K, equilibrium constant) and both the dynamic quenching of OG by BBA (k_1, bimolecular rate constant) and the reverse process (k_2, unimolecular rate constant) in the excited state. Electrostatic forces between the two molecules with charges of opposite sign favor the formation of an ion-pair complex and suggest that the quenching is due to photoinduced electron transfer (PET), as shown in Scheme 5.1. This process with rate constant k_E is very effective in the excited complex since the distance between charge donor and acceptor is very small and PET is known to drop rapidly with distance (Lakowicz 2006). There is also a collisional quenching, but this is expected to be less effective because the two molecules have to diffuse together, so that it is observed at relative high concentrations of BBA. When OG transfers an electron to BBA it undergoes a structural change similar to protonation and, as in the protonated species of OG, the fluorescence quantum yield decreases significantly. Therefore, the charge-transfer complex is expected to be no fluorescent.

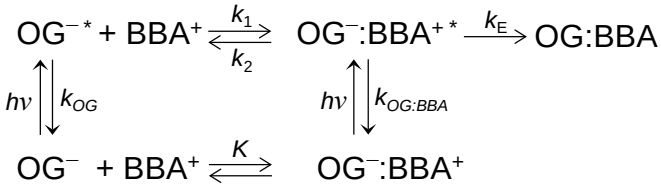

Scheme 5.1. Mechanism proposed for the interaction of OG with BBA including the formation of a complex between OG and BBA in the ground state (K, equilibrium constant) and reversible processes in the excited state with the rate constants k_1 (quenching) and k_2 (reverse process). k_E is the rate constant for the photoinduced electron transfer process.

Under experimental conditions of excess of BBA with respect to OG, the mechanism in Scheme 5.1 leads to equation 8 for the steady-state fluorescence intensity at a certain emission wavelength λ, $F(\lambda)$, as a function of the total BBA concentration, [BBA]. $F_{OG}(\lambda)$ and $F_{OG:BBA}(\lambda)$ are the fluorescence intensities at the emission wavelength λ of free OG and complex $OG^-:BBA^+$, respectively, and ε_{OG} and $\varepsilon_{OG:BBA}$ are their molar absorptivities at the excitation wavelength.

$$
\begin{aligned}
&F(\lambda) = F_1(\lambda) + F_2(\lambda)\\
&F_1(\lambda) = \frac{F_{OG}(\lambda)\,(1 + (R_2/R_\varepsilon)\,K\,[\mathrm{BBA}])}{(1 + K[\mathrm{BBA}])(1 + R_1(1 - R_2)[\mathrm{BBA}])}\\
&F_2(\lambda) = \frac{F_{OG:BBA}(\lambda)\,(1 - R_2 - R_E)}{(1 + K[\mathrm{BBA}])(1 + R_1(1 - R_2)[\mathrm{BBA}])}(R_1 R_\varepsilon[\mathrm{BBA}] + (1 + R_1[\mathrm{BBA}])K[\mathrm{BBA}])\\
&R_\varepsilon = \varepsilon_{OG}/\varepsilon_{OG:BBA};\ R_1 = k_1/k_{OG};\ R_2 = k_2/(k_2 + k_E + k_{OG:BBA});\ R_E = k_E/(k_2 + k_E + k_{OG:BBA})
\end{aligned}
\tag{8}
$$

The resolution of the corresponding differential equations leads to biexponential functions for the fluorescence decays of OG in the presence of different concentrations of BBA. Nevertheless, the two lifetimes cannot be assigned to each excited species and show complex dependencies on the rate constants defined in Scheme 5.1 (equation 9), as well as their amplitudes. Analysis of these equations shows that τ_A varies between the lifetime of OG* and that of the complex OG^-:BBA^{+*}, whereas τ_B is related to the relaxation time k_1 [BBA]+ k_2 in the excited state. The amplitude of τ_A is always positive and decreases as the concentration of BBA is increased. On the contrary, the amplitude of τ_B is only positive when excited-state quenching is more effective than that of the ground state ($k_1/k_2 > K$) and show very different dependencies on [BBA] for small changes in the values of the rate constants.

$$\tau_{A,B} = 2/\left(k_1[\mathrm{BBA}]+k_{OG} + k_2 + k_E + k_{OG:BBA} \pm \sqrt{\alpha}\right)$$
$$\alpha = (k_1[\mathrm{BBA}]+k_{OG} + k_2 + k_E + k_{OG:BBA})^2 - 4\left(k_{OG}\, k_2 + (k_1[\mathrm{BBA}] + k_{OG})(k_E + k_{OG:BBA})\right) \quad (9)$$

Taking this into account, the experimental lifetime τ_3 must be assigned to τ_A whereas τ_2 corresponds to τ_B. The small but positive amplitude of τ_2 indicates that the ratio between k_1 and k_2 is higher than the equilibrium constant K.

In order to prove the validity of the mechanism and estimate the rate constants involved, a first simple analysis of the lifetimes is performed. It can be easily deduced that the sum (S) and the product (P) of the inverses of the two lifetimes should vary linearly with the concentration of BBA, as given by equations 10 and 11. Figure 5.3 shows the plots of the values of S and P calculated from the experimental lifetimes (Table 5.2) and their corresponding linear fits. Good correlations are obtained and, in spite of the high uncertainties of the experimental values, the rate constants can be estimated (Table 5.3). The values obtained have acceptable errors of around 20% except for that of k_2 that is poorly estimated due to its very low value. Attempts to obtain better values of the rate constants involved in the proposed mechanism through global fit of equation 9 to the experimental values of τ_2 and τ_3 were not successful due to very strong correlations among the fit parameters.

$$S = \tau_A^{-1} + \tau_B^{-1} = k_{OG} + k_2 + k_E + k_{OG:BBA} + k_1[\mathrm{BBA}] \quad (10)$$

$$P = \tau_A^{-1}\, \tau_B^{-1} = k_{OG}(k_2 + k_E + k_{OG:BBA}) + k_1(k_E + k_{OG:BBA})[\mathrm{BBA}] \quad (11)$$

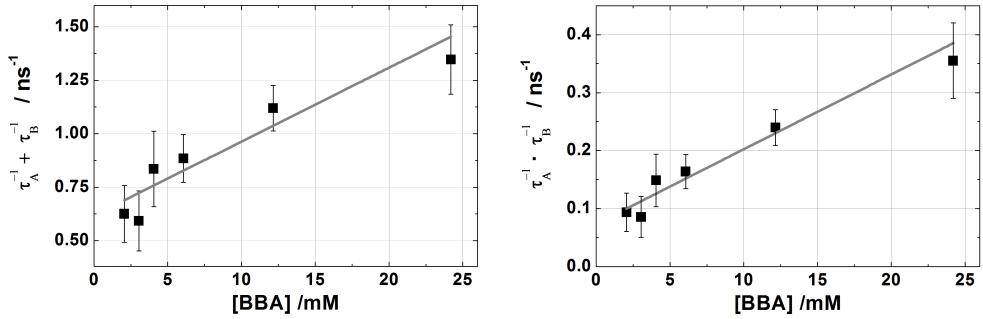

Figure 5.3. Weighted linear fits of sum S and product P of the inverse lifetimes τ_2 and τ_3 against BBA concentration (data of Table 2).

The estimation of the rate constants from fits of equations 10 and 11 (Figure 5.3 and Table 5.3) are now used to fit the steady-state fluorescence intensity at 520 nm for the interaction between OG and BBA using equation 8. As shown in Figure 5.2 inset this equation perfectly fits the data of fluorescence emission and yields a value for the equilibrium constant K of 540 M^{-1}, which is of the order of magnitude expected for the formation of such ion pairs (Freire et al. 2010). In the fit the complex OG^-:BBA^+ results to be non fluorescent, as it was already proposed.

Table 5.3. Values of the rate constants and the equilibrium constant K involved in the mechanism proposed for the interaction between OG and BBA (Scheme 5.1) obtained with different fits. Parameters with (f) were fixed in the fit.

Parameter	Linear fit of inverse lifetimes	Fit of steady-state fluorescence
K / 10^3 mol^{-1} dm^3		0.54 ± 0.04
k_{OG} / 10^9 s^{-1}	0.24050 ± 0.0008	0.24050 (f)
$k_{OG:BBA} + k_E$ / 10^9 s^{-1}	0.37 ± 0.08	0.37 (f)
k_1 / 10^9 s^{-1} mol^{-1} dm^3	35 ± 6	34.5 (f)
k_2 / 10^9 s^{-1}	0.004 ± 0.1	0.004 (f)

Once studied the interaction between BBA and OG we can conclude that is a quenching process of electron transfer nature the responsible for the decrease in brightness of the OG488 when this dye is attached to the BBA. The disappearance of this quenching effect when the BBA is bound to the DNA minor groove is what leads to the increase observed in the binder brightness.

The difference in the brightness ratio q observed for the titrations of BBA-OG and BBA-OG-long can be attributed to the different quenching efficiencies in both cases, since the electron transfer process between the two charged molecules OG and BBA is expected to be highly dependent on the distance. The high efficiency of this quenching, 0.88 and 0.85 for

BBA-OG and BBA-OG-long respectively, makes that small differences in this value become important when comparing the intensity of the quenched molecule between the two binders. Moreover, in the presence of DNA the value of the lifetime τ_3 is higher than that of OG (see Table 5.1), suggesting that the binder bound to DNA would be even brighter than OG itself.

6. Conclusions.

A novel approach through the synthesis of a new fluorescently labeled derivative from the cationic bis-benzamidines family of DNA binders allowed us to perform the first study of the minor groove binding dynamics by FCS. Our results indicate that the association process of minor-groove binders to DNA is not diffusion controlled, but the insertion of the binder into the minor-groove is the rate-limiting step. *Specificity* of these binders to AT sites seems to be mainly determined by the association process, whereas the binding *affinity* depends strongly on the dissociation rate.

Two are the main characteristics of this binder that makes possible the study of this dynamics by FCS. On the one hand, the labeling of a typical DNA minor-groove binder with a dye suitable for SM studies. After a photophysical study of the BBA-OG binder, the cationic BBA was proved to induce a quenching in the fluorescence of the negatively charged OG dye. The fact that this quenching disappears upon complexation between binder and DNA leads to an increase in brightness. This allows the determination of the dissociation rate constant from the analysis to the titration of FCS curves. On the other hand, the binder must present a relatively fast dissociation to fit the dynamic range of observation of FCS, which does not happen with most of the minor-groove DNA binder. By using a binder with a longer linker between the BBA part and the OG488 molecule, we demonstrate that both, the efficiency of the quenching and the dissociation rate constant, can be tuned by modifying the length of the linker.

Chapter V

Folding Dynamics of Riboswitches studied by Single-Molecule FRET and TIRF

Contents:

1. Introduction.

Various regulation mechanisms that control gene expression by modulating transcription, translation, splicing or mRNA stability according to a feedback mechanism are based on the formation of stable RNA-ligand complexes between specific metabolites and certain RNA elements, called riboswitches (Montange and Batey 2008; Roth and Breaker 2009). Riboswitches are RNA elements built into mRNA that can sense the concentration of a particular metabolite and turn gene expression on or off in response. Since its discovery, riboswitches have a central importance in RNA research as a bridge between genomics and proteomics.

The emerging field of riboswitches is becoming a very promising ground to develop anti-bacterial drugs that target essential metabolic pathways in bacteria and fungi (Blouin et al. 2009), since these organisms are lately becoming more resistant to existing antibiotics. Therefore, the results obtained from this kind of studies (Kuzmenkina et al. 2005) not only will improve the existing knowledge on RNA folding and riboswitch gene regulation mechanisms but also could be very valuable in the development of a new generation of new antimicrobial drugs targeting riboswitches for use as antibiotics.

The objective of studying these riboswitches is to analyze the molecular mechanisms involved in ligand- and ion-assisted folding and understand how their highly dynamic nature is used to trigger gene expression modulation.

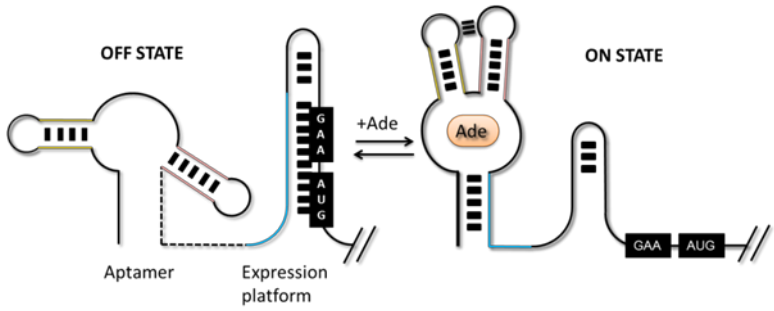

Figure 1. Schematic showing control of gene expression by the *V. vulnificus add* riboswitch at the translational level upon adenine (Ade) binding. Conformational rearrangements in the riboswitch structure induced by ligand binding expose the Shine-Dalgarno (GAA) and AUG sequences in the ON state.

These regulatory elements are typically positioned within in the 5'-untranslated region of messenger RNA (mRNA) and control the expression of genes that are located downstream of the mRNA sequence but also at more remote locations (Blouin et al. 2009; Schwalbe et al. 2007). Riboswitches are typically composed of two domains: a highly conserved

metabolite-sensor region known as the *aptamer domain* and the *expression* platform (Figure 1). The secondary structure of the expression platform, which can adopt two mutually exclusive conformations depending on whether the aptamer domain has the targeted metabolite bound or not, determines de outcome of the regulation process (Figure 1). The X-ray crystal structures available for purine riboswitches in the bound state have shown that the ligand is completely buried inside the RNA binding pocket (Batey et al. 2004; Pikovskaya et al. 2011; Serganov et al. 2004) (Figure 2a).

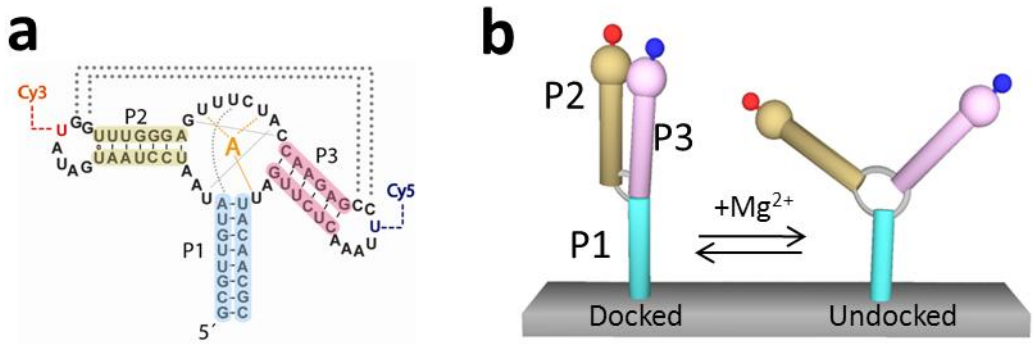

Figure 2. (a) Schematic showing the network of interactions within the aptamer core involved in ligand recognition (orange) and in the stabilization of the native state (grey). Base-pair contacts responsible to the P2-P3 loop-loop interaction are also shown. Nucleotides carrying the donor (Cy3) and acceptor (Cy5) FRET pair are also indicated. **(b)** Folding of the adenine aptamer induced by divalent metal ions promotes the docking of the P2 and P3 helical stems by stabilizing the loop-loop interaction.

It has already been shown that in the absence of the ligand, divalent metal ions are sufficient to promote the interaction between the P2 and P3 stem loops leading to an RNA structure that is peripherally pre-organized in a similar way to the bound-state but with the binding pocket remaining largely disordered (Lemay et al. 2006). It has been also shown by chemical probing (Lemay and Lafontaine 2007), NMR-spectra(Buck et al. 2007; Lee et al. 2010) and thermodynamic measurements (Gilbert et al. 2006) that ligand binding induces a transition from this unstructured "open" state to a locally organized conformation and this has led to the notion of ligand binding via an 'induced fit' mechanism (Noeske et al. 2007).

The *add* riboswitch from *Vibrio vulnificus* has been shown to operate at translational level and very likely under thermodynamic control (Lemay et al. 2011). Moreover, it appears based on biochemical data that it can bind the ligand after transcription of the expression platform, suggesting that *add* can reversibly switch between the quasi-energetic ON and OFF gene-regulation states at equilibrium.

Although chemical denaturation methods are commonly used in single-molecule studies of protein folding (Kuzmenkina et al. 2005), its translation into the single-molecule RNA field has remained surprisingly unexplored. On the other hand, several reports using a variety of ensemble-averaging techniques have already demonstrated how the effect of chemical-induced denaturation on the folding rates of large RNAs can be used to characterize the presence of kinetic traps and to provide evidences regarding the nature of the rate-limiting folding step (Pan et al. 1997; Shelton et al. 1999; Sosnick and Pan 2003).

The Mg^{2+}-induced folding pathway has been widely used in single molecule FRET studies of RNA (Heppell et al. 2011; Lemay et al. 2006; Lemay et al. 2009)(Figure 2b). In this work, we will study the denaturant-induced unfolding route, much more common in the investigation of single proteins (Kuzmenkina et al. 2005).

The combination of single-molecule FRET and chemical denaturation provides not only a more powerful framework to uncover the underlying folding kinetics but also a novel tool to investigate the stability of RNA-ligand complexes complementary to optical-tweezing methods (Lin and Thirumalai 2008).

Only very recently, a systematic study has appeared using sm-FRET and urea as a chemical denaturant for RNA or RNA-ligand complexes (Dalgarno et al. 2013). Given the potential advantages arising from this approach, here we explore the behavior of other potential denaturing agents (Lambert and Draper 2007) as an alternative to the previously used urea.

In this study we performed at single-molecule level a comparative characterization of the folding kinetics of the ligand-free state in presence of proline, betaine and formamide as denaturants to provide a preliminary analysis of their feasibility in single molecule chemical denaturation studies of riboswitches folding. We also studied the response of the *add* aptamer domain at different concentrations of ligand, monovalent cations and divalent metal ions in presence of the denaturant formamide.

2. Theory.

2.1. Single-Molecule FRET.

Förster resonance energy transfer (FRET) occurs between a donor (D) molecule in the excited state and an acceptor (A) molecule in the ground state. The donor molecules typically emit at shorter wavelengths that overlap with the absorption spectrum of the acceptor. Energy transfer occurs without the appearance of a photon and is the result of long range dipole–dipole interaction between the donor and acceptor (Lakowicz 2006).

The rate of energy transfer depends upon the extent of spectral overlap of the emission spectrum of the donor with the absorption spectrum of the acceptor, the quantum yield of the donor, the relative orientation of the donor and acceptor transition dipoles, and the distance between the donor and acceptor molecules. The distance dependence of FRET allows measurement of the distances between donors and acceptors (Lakowicz 2006; Roy et al. 2008). The efficiency of energy transfer, E, is the ratio of acceptor intensity to total emission intensity and is given as

$$E = \frac{1}{1 + (r/R_0)^6} \tag{1}$$

where r is the inter-dye distance, and R_0 is the Förster radius at which the FRET efficiency equals 50%. R_0 takes values between 2 and 7 nm for common pairs of fluorophores, therefore both fluorophores should be in a close proximity (<10nm) for the FRET to occur (Hinterdorfer and Oijen 2009).

The most common application of FRET is to measure the distances between two sites on a macromolecule. When we have a D–A pair covalently linked to a biopolymer, and a range of D–A distances is possible for the individual molecules, FRET can be used to study the conformational distributions. The relative number of donor and acceptor photons can be used to calculate FRET efficiency. Single molecule detection (SMD) is possible under favorable optical conditions for high-quantum-yield fluorophores. And these bursts were counted to obtain a histogram of FRET efficiencies.

Conformational dynamics of single molecules can also be observed in real time by tracking FRET changes. smFRET time trajectories are most commonly acquired by imaging surface immobilized molecules with the aid of wide-field total-internal reflection (TIR) microscopy that allows high-throughput data sampling (Roy et al. 2008).

The most popular single-molecule fluorophores are small organic dyes. Common FRET pairs with absorbance from 500–700 nm are Cyanine (Cy3 and Cy5; donor and acceptor, respectively), Alexa and Atto dyes (Kapanidis and Weiss 2002).

Apparent FRET efficiency is calculated as

$$E_{\text{app}} = \frac{I_{\text{A}}}{I_{\text{A}} + I_{\text{D}}} \tag{2}$$

where I_{A} and I_{D} represent acceptor and donor intensities, respectively. E_{app} provides only an approximate indicator of the inter-dye distance because of uncertainty in the orientation

factor. Nevertheless, apparent FRET is usually a monotonic function of distance (Roy et al. 2008). To determine actual FRET efficiency, one has to determine the correction factor, γ, which accounts for the differences in quantum yield and detection efficiency between the donor and the acceptor. γ is calculated as the ratio of change in the acceptor intensity, ΔI_A, to change in the donor intensity, ΔI_D, upon acceptor photobleaching ($\gamma = \Delta I_A/\Delta I_D$). Corrected FRET efficiency is then calculated using the expression (Ha et al. 1999):

$$E = \left(1 + \gamma \frac{I_D}{I_A}\right)^{-1} \tag{3}$$

Note that in order to calculate accurate FRET efficiencies, I_D and I_A signals should be estimated by removing donor leakage to acceptor channel and acceptor leakage to donor signal as well as background.

2.2. Total Internal Reflection Fluorescence.

Total Internal Reflection Fluorescence (TIRF) is an optical technique used in single-molecule microscopy. It employs the phenomenon of total internal reflection, which occurs when a beam of light in a high-refractive index medium (e.g., glass or quartz) hits the interface with a lower refractive index medium (e.g. aqueous solution), and the angle of incidence exceeds the critical angle, θ_C, for total reflection (Lakowicz 2006).

The refractive behavior of the propagating light when it encounters an interface between two media with different refractive index is governed by Snell's Law**:**

$$n_1 \sin\theta_1 = n_2 \sin\theta_2 \tag{4}$$

where n_1 is the higher refractive index and n_2 is the lower refractive index. The angle of the incident beam, with respect to the normal to the interface, is represented by θ_1, while the refracted beam angle within the lower-index medium is given by θ_2.

At total internal reflection conditions (i.e., $\alpha_2 \geq 90°$), the excitation beam reflects back into glass and generates at the interface with water an electromagnetic field, called the evanescent wave. The angle of incidence has to be greater than the critical angle, θ_C, given by the following equation:

$$\theta_C = \sin^{-1}(n_2/n_1) \qquad \text{where } n_1 > n_2 \tag{5}$$

For the transition from the quartz slide ($n_1 = 1.54$) into an aqueous solution ($n_2 = 1.33$), a critical angle of 60° results.

The evanescent wave has maximum of intensity at the surface and exponentially decays with the distance from the interface (Hinterdorfer and Oijen 2009):

$$I_z = I_0\, e^{-z/d} \tag{6}$$

where Iz is the intensity at a perpendicular distance z from the interface, and I_0 is the intensity at the interface.

The penetration depth, d, is dependent upon the wavelength of the incident illumination λ, the angle of incidence, θ, and the refractive indices of the media at the interface, according to the equation:

$$d = \frac{\lambda}{4\,\pi\sqrt{{n_1}^2 \sin^2\theta_1 - {n_2}^2}} \tag{7}$$

Only molecules that are at the TIRF surface are excited and fluoresce, while molecules in the bulk of solution, at the distances larger than 100-200 nm are not excited and do not fluoresce. TIRF efficiently rejects background signal from the bulk of solution and allows single molecule detection experiments.

The levels of fluorescence from a single fluorophore are extremely low (hundreds to thousands of photons per second). We will observe this fluorescence using an electron-multiplying (EM) charge-coupled device (CCD) camera which will produce an image, in which labeled RNA bound to the quartz slide will appear as bright spots. The time resolution of ultra-sensitive EM CCD cameras is limited to the CCD readout time, which is on the order of few milliseconds (Hinterdorfer and Oijen 2009).

In contrast to traditional techniques that detect only end-point results, TIRF measures the entire course of interactions, allowing the determination of k_+ and k_- rate constants.

There are two basic approaches to configuring an instrument for TIRF microscopy (Moerner and Fromm 2003). In this work we use the prism method (Figure 3), where the excitation path is independent of the objective and consists of a focused laser beam which is introduced into the microscope coverslip by means of a prism attached to its surface, and the beam incidence angle is adjusted to the critical angle. The setup with prism is easily accomplished, since it requires only the microscope, prism, and laser. The drawback for this setup is the requirement that the specimen be positioned between the prism and the microscope objective, therefore making difficult to place additional elements such as temperature control and real-time injection devices. Another disadvantage of the prism technique is that in most configurations based on inverted microscope designs, the illumination is introduced on the

specimen side opposite the objective optics, requiring imaging of the evanescent field region through the bulk of the specimen. However, the prism-type configuration by uncoupling the excitation and emission pathways provides a SNR higher than objective type systems. The other common approach is the objective lens technique, which is sometimes referred to as through the lens illumination, where a high numerical aperture objective is employed to introduce the laser to the coverslip-specimen interface.

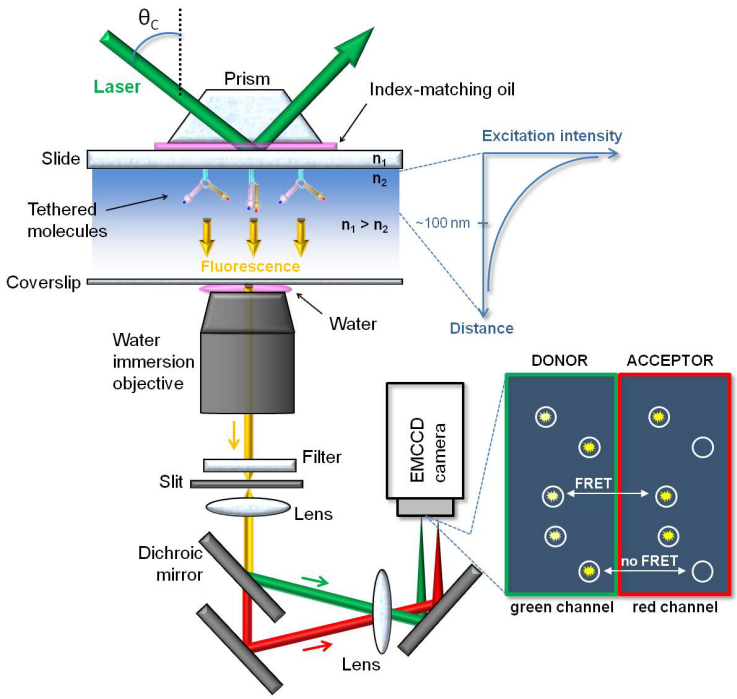

Figure 3. Instrumentation for TIR excitation and single-molecule FRET detection. single molecules immobilized on a quartz slide surface are excited by PTIR. The laser beam focused at a large incident angle ($\theta_C > 65°$) on the prism placed on the top of the sample creates an evanescent field at the quartz-water interface on the slide that penetrates into water in the sample chamber and decays exponentially along the z axis, therefore exciting only a few hundred nanometers from the interface. Fluorescence is collected using a high NA water-immersion objective because of its higher penetration depth, and the slit generates a final imaging area that is half of the CCD imaging area. The collimated image is split into the donor and acceptor emissions and imaged side by side on the CCD camera (camera image in inset). If the molecule of interest is only labeled with a donor, no fluorescence will be visible in the red detection channel of the CCD camera.

As in most single-molecule techniques, background light is one of the main problems with TIRF microscopy. In order to reduce the light at the excitation wavelength we will use an interference filter with high absorption at the excitation wavelength and high transmission for the desired emission light. Another important source of background, particularly for prism style TIRF, is microscope slides. Ordinary glass microscope slides are remarkably fluorescent,

due to impurities in the glass, so we have to use quartz microscope slides (also required to be able to make the channel with injection points).

Two important problems regarding the photophysics of the fluorescent probes used in single-molecule fluorescence experiments are photobleaching and blinking (Ha and Tinnefeld 2012). Especially in single-molecule FRET, where the fluctuations in FRET efficiency due to these processes can be hard to distinguish from those caused by the biophysical events under study such as conformational changes. A fluorophore is said to blink when its intensity repeatedly drops to zero and then comes back to normal. In contrast, photobleaching is an irreversible switching-off event, due to the interaction of the fluorophore in its excited state with molecular oxygen or other surrounding molecules.

All organic fluorophores eventually photobleach, permanently losing their fluorescence properties (Johnson-Buck et al. 2013). Although this is useful, since a single step photobleaching in a movie is evidence that the fluorescence originates indeed from a single molecule, it also reduces the time window of observation. For this reason is desirable to delay hotobleaching as much as possible. Apart from reducing the excitation intensity, photobleaching can be minimized by removing free oxygen from the solution using oxygen-scavenging enzymes (i.e., catalase and glucose oxidase mixture) (Rasnik et al. 2006). Oxygen collides with the molecule in its excited state and undergoes a chemical reaction with the dye, resulting in permanent photobleaching. So-called oxygen scavenging systems reduce the concentration of oxygen in solution by catalyzing its reaction with substrates other than the FRET donor and acceptor. Oxygen scavengers make it possible to watch a single organic dye on the order of 10 sec. (Hinterdorfer and Oijen 2009).

A related problem is blinking, it occurs when the molecules undergo intersystem crossing to the triplet state (approximately once every 1000 excitations). These molecules remain dark until they return to the ground singlet state. The lifetime of the triplet state is on a time scale usually ranging from milliseconds to seconds, resulting in a temporary blinking of the dye (Lakowicz 2006). When molecular oxygen is removed from solution other additives (Trolox, 2-mercaptoethanol) are used as alternative quenchers to reduce blinking (Roy et al. 2008).

Blinking as a reversible switching off can be misinterpreted as a large conformational change to a state with very low FRET (for example, macromolecular unfolding). As a general guideline, when FRET efficiency drops instantaneously to the level of donor only ($E_{\mathrm{app}} = 0$), this should be considered as blinking, unless this effect persists even in the presence of blinking suppressants, a direct excitation of acceptor confirms its activity and it does not depend on excitation intensity (Roy et al. 2008).

3. Materials and Methods.

3.1. Labeling and Purification of RNA Oligonucleotides.

Amino-modified oligonucleotides were purchased from Integrated DNA Technologies (IDT Inc.) and labeled using succinimidyl ester derivatives of Cy3 and Cy5 fluorophores following the protocol provided by the manufacturer (Invitrogen).

The add aptamer domain was assembled from oligonucleotides of the following sequences (all written in the 5' to 3' direction):

5' STRAND: biotin- CGCCGAGCGUUGUAUAAUCCUAAUGAUAUGGUUUGGGAGU.

3' STRAND: UUCUACCAAGAGCCUUAAACUCUUGAUUACAAACGCUCGCGC.

Fluorescently-labeled oligonucleotides were purified as described previously1. Purified RNA strands were annealed by heating a 1:1 mixture to 80°C in 10 mM HEPES (pH 8.0), 50 mM NaCl, and slow cooling to room temperature. T4 RNA ligase (New England Biolabs) was then added to the reaction and the sample was incubated at 37°C for 4 hours. Full length ligated RNA molecules were purified by gel electrophoresis (20% polyacrylamide gel electrophoresis containing 7 M urea), electroeluted into 8 M ammonium acetate and ethanol precipitated.

3.2. Denaturing Agents.

Formamide, betaine, urea and proline were purchased from Sigma. Stocks at highest concentration used containing 6% glucose were prepared for each of them and kept in the dark.

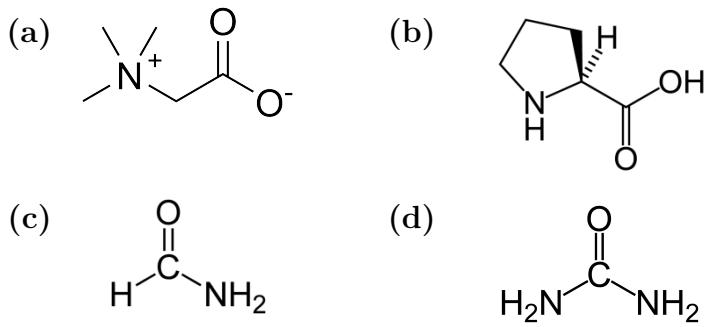

Figure 4. Molecular structure of the different osmolytes used as denaturing agents in this work: (a) Betaine; (b) Proline; (c) Formamide; (d) Urea.

3.3. Equipment Setup and Calibration.

Equipment Setup: Single-molecule FRET experiments were performed as previously reported (Brenner et al. 2010; Heppell et al. 2011). FRET trajectories were acquired from immobilized single-molecules using a prism-type total-internal reflection setup that includes an inverted microscope (Olympus IX71) coupled to a CW 532-nm laser (Crystalaser, USA) and a back illuminated Ixon EMCCD camera (Andor Technology, UK). Donor and acceptor fluorescence emissions were separated using dichroic mirrors (DCRLP, Chroma Technology) and imaged onto the left (donor) and right (acceptor) half-chip of the EMCCD. This setup allowed us to monitor the Cy3 and the Cy5 signals simultaneously.

Calibration: To ensure an accurate correspondence between the donor and acceptor images, an overlap map is created every day with an image of surface-tethered fluorescent microspheres (FluoSpheres 200 nm diameter, Invitrogen) with substantial emission in all detection channels. Specifically, we manually select 3 to 4 fluorescence peaks in the donor image and their corresponding peaks in the acceptor image of the fluorescent microspheres, and an automated algorithm generates a linear transformation between the two images that corrects for offset, rotation, rescaling and distortion.

3.4. Passivation and Surface-Immobilization Methods.

An air-tight sample chamber (Roy et al. 2008) is created by sandwiching double-sided tape between a precleaned slide and a coverslip and by applying epoxy as necessary. Simple pipetting or pumping through two holes pre-drilled in the slide allows exchange of solution without drying.

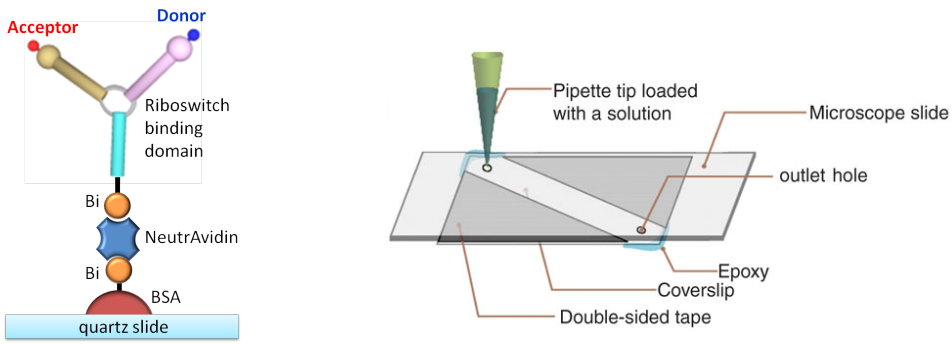

Figure 5. Left: Slides are passivated with biotinylated BSA protein which bounds nonspecifically to the surface. Biotinylated RNA is immobilized using NeutrAvidin. Right: A micro-channel slide is made by sandwiching a microscope slide and a coverslip with double-sided tape and by sealing with epoxy. Partially reproduced from Roy et al. (Roy et al. 2008).

Microscope slides were successively treated with biotinylated BSA (1 mg/mL) and neutravidin (0.2 mg/mL), and 20-200 pM dual labeled aptamer molecules carrying a biotin group at the 5' end were added to the slide. The imaging buffer contained 50 mM Tris-HCl (pH 8.0), 50 mM NaCl, 6% glucose (w/w), 0.02 mg/mL glucose catalase (Roche), 0.1 mg/mL glucose oxidase (Sigma), 1% 2-mercaptoethanol (triplet-state quencher) and the specified concentrations of $MgCl_2$ and urea, formamide, betaine or proline. Stocks at the maximum concentrations used for each denaturant containing 6% glucose were prepared and kept in the dark. All measurements were performed at room temperature (20°C) using integration times of 50 ms, unless stated otherwise.

3.5. Data Analysis.

Single-molecule FRET efficiency after background correction was approximated by $(I_A/[I_A+I_D])$, where I_A and I_D are the fluorescence intensities of the acceptor and donor, respectively. Because the quantum yields and detection efficiencies of Cy3 and Cy5 are very close, E_{app} closely matches the true efficiency of energy transfer. Data analysis was carried out by using laboratory-written analysis routines developed in MATLAB 7. Single-molecule FRET histograms were obtained by averaging the first 10 frames of each FRET trace for every individual molecule after manually filtering photobleaching and blinking effects. States were identified from E_{app} histograms, and dwell times were analyzed if the time resolution allowed the clear observation of transitions. Rapidly fluctuating molecules undergo more transitions than slowly fluctuating ones, and thus in order to avoid bias toward fast rates, dwell time histograms were obtained by using a weighting factor inversely proportional to the number of transitions observed for each molecule. These dwell time histograms were then fitted to a single-exponential function to obtain the lifetimes of each state, the inverse of the rate of conversion. For the heterogeneity analysis, the average of the dwell times was calculated for each state for each individual molecule.

4. Results.

4.1. Single Molecule Chemical Denaturation: Induced unfolding of docked ligand-free Adenine aptamers.

It has been previously shown that Förster resonance energy transfer (FRET) between Cy3 and Cy5 dyes located in the loops of the P2 and P3 stems of the *add* adenine aptamer can be used to monitor the docking and undocking dynamics corresponding to the formation of the loop-loop interaction (Lemay et al. 2006). Single aptamers were immobilized on a quartz-slide via biotin-streptavidin interactions. Single-molecule histograms at saturating Mg^{2+} concentration showed almost exclusively a single Gaussian peak centered at an apparent

FRET efficiency $E_{app} \sim 0.9$. As previously reported, this high-FRET value can be assigned to a Mg^{2+}-induced docked state (D) characterized by the formation of long-range tertiary contacts between P2 and P3 loops. We first check the system using urea, the most commonly used RNA denaturing agent (Dalgarno et al. 2013). After injection of 5 M concentration of urea, while maintaining the background concentration of mono- (50 mM NaCl) and divalent metal ions (4 mM Mg^{2+}), the single-molecule histogram shifted to a $E_{app} \sim 0.35$ (Figure 6). This low-FRET value matches that obtained in previous studies in the absence of Mg^{2+} ions, where it is demonstrated the adenine aptamer adopts a Y-shape undocked state lacking the loop-loop interaction (UD) (Lemay et al. 2006).

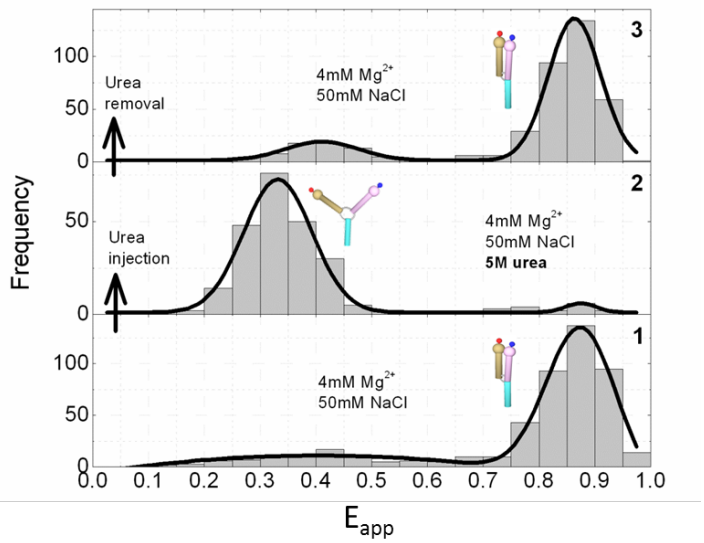

Figure 6. Single-molecule histograms at 4 mM Mg^{2+} and 50 mM NaCl (panel 1) showed most of the aptamer molecules in the docked conformation (D). In this state, the formation of the loop-loop interaction brings the donor in close proximity to the acceptor resulting in a high FRET state ($E_{app} \sim 0.9$). Injection of urea to the same surface-immobilized aptamers (panel 2) while maintaining the concentration of mono- and divalent metal ions shifted the single-molecule histogram to a low FRET state ($E_{app} \sim 0.4$) corresponding to the undocked state (UD). An additional cycle of urea removal (panel 3) shifted back the single-molecule histogram to the high FRET docked state (D).

By removing the ions at 5 M urea we proceed to the unfolding of the secondary structure, which we can also perform reversibly. The unfolded RNA corresponds to a peak centered at $E_{app} \sim 0.24$ (Figure 7), which is near the observed value obtained for a single-strand non-self-complementary DNA strand as observed by Murphy et al. (Murphy et al. 2004).

To examine the effect that chemical melting has on the relative equilibrium populations of the ligand-free state, we performed three titrations with different denaturing agents (Lambert and Draper 2007) (proline, betaine and formamide) at a fixed 4 mM concentration of divalent

metal ions. This concentration of Mg^{2+} ions was chosen to ensure that the RNA aptamer is mostly on a docked configuration before the addition of the denaturant.

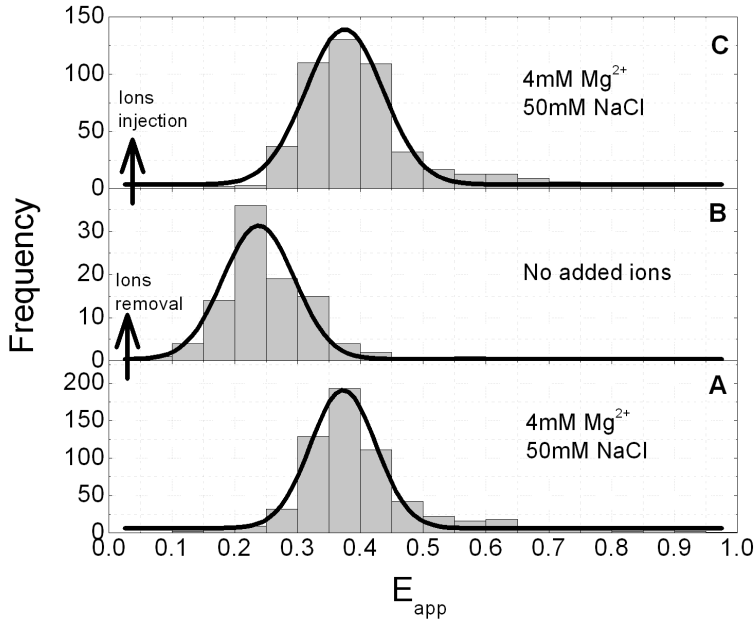

Figure 7. Single-molecule histograms at 5 M urea, 4 mM Mg^{2+} and 50 mM NaCl (panel A and C) showed most of the aptamer molecules in the undocked conformation (UD), $E_{app} \sim 0.38$. By removing the ions we can unfold the secondary structure of the RNA, resulting in a lower FRET state (panel B, $E_{app} \sim 0.24$) whose reversibility is shown by an additional cycle of ions addition shifting back the single-molecule histogram to the FRET undocked state (UD).

The immobilized molecules were first subjected to unfolding-refolding cycles, removing the urea by injecting a solution containing a folding buffer (4 mM Mg^{2+}, 50 mM NaCl). Under these conditions, we find again that the single-molecule histograms come back to the situation with a single Gaussian peak centered at the FRET value corresponding to the docked state $E_{app} \sim 0.9$, thus confirming that chemical-induced denaturation can be performed reversibly at the single-molecule level (see Figure 6 for the example with urea). In the experiments for the betaine, proline and formamide, a decrease in the density of immobilized aptamers was observed after addition of proline and betaine above certain concentrations, 2 M and 4 M for betaine and proline respectively, suggesting that these denaturing agents disrupt RNA immobilization, affecting streptavidin-biotin interactions. For the urea and formamide, concentrations above 5 M and 10 M respectively induce a significant change in the refraction index that introduces distortions in the evanescence wave generated at the quartz-water interface. Because of this, we kept these upper limits for their concentrations.

To examine the effect that chemical melting has on the relative equilibrium populations of the ligand-free state, we performed titrations for the different denaturing agents (proline, betaine and formamide) at a fixed 4 mM concentration of divalent metal ions (Figure 8). As we increased the denaturant concentration we observed a progressive decrease in the relative contribution of the Gaussian peak corresponding to the docked state D ($E_{app} \sim 0.9$) and a concomitant increase in the contribution of a Gaussian peak at a lower FRET (Figure 8).

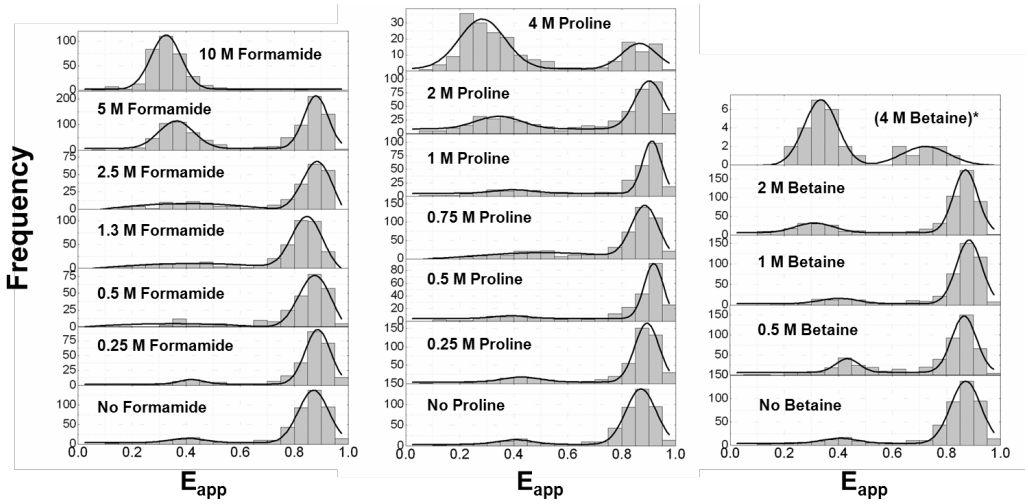

Figure 8. Single-molecule histograms of FRET efficiency as a function of denaturant concentration. Increasing the concentration of denaturant results in a progressive increase in the relative contribution of the single-molecule FRET histogram corresponding to the undocked state (UD). At 4 M concentration of Betaine, the surface attachment is disrupted and there was no enough spots to properly build a histogram.

At formamide concentration of 10 M, the single-molecule histogram showed almost exclusively a single Gaussian centered at a low-FRET value that can be assigned to the undocked state UD, as previously reported for the urea (Dalgarno et al. 2013). For the betaine and proline the RNA immobilization is disrupted before reaching the situation with a single population in the undocked state.

Corresponding anti-correlated donor and acceptor trajectories for some of the formamide concentrations studied can be found in Figure 9. In the absence of denaturant, the aptamer is mostly in the docked state D with occasional fast fluctuations to the undocked state UD until photobleaching occurs. As the formamide concentration is increased, transitions between the two FRET states become more frequent with the aptamer progressively remaining in the undocked state for longer periods. At formamide concentration of 10 M the aptamer is almost exclusively in the undocked state with occasional transitions to the docked conformation, where it remained for very short periods of time.

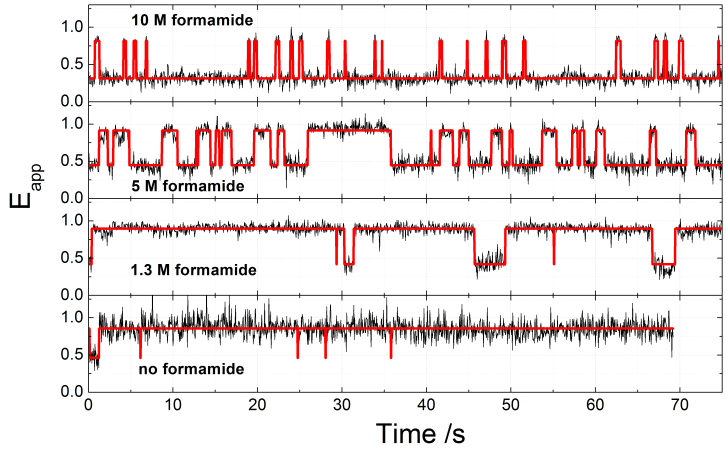

Figure 9. Single-molecule FRET trajectories obtained with 50 ms integration time at the indicated concentrations of formamide showing fast fluctuations between the D and UD states.

Dwell time histograms were plotted for the UD and D states at different denaturant concentrations (Figure 10 to Figure 12) and fitted to single exponential decays to extract the docking (k_{dock}) and undocking (k_{undock}) rates (Table 1), for the three denaturing agents.

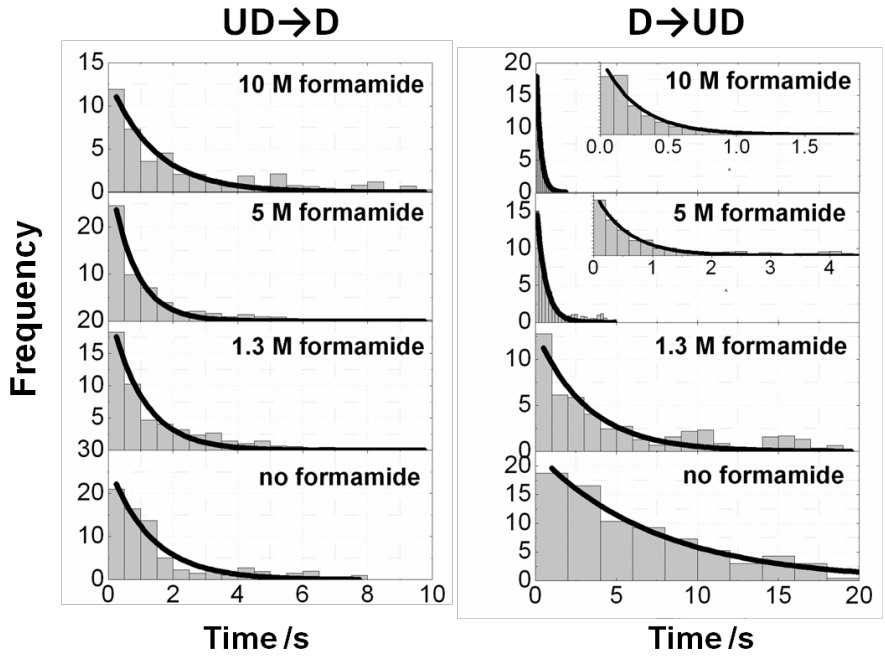

Figure 10. Dwell time histograms of the UD (left panels) and D (right panels) at the indicated formamide concentrations. The data have been fitted to single exponential decay functions to give the rates of docking (k_{dock}) and undocking (k_{undock}), respectively.

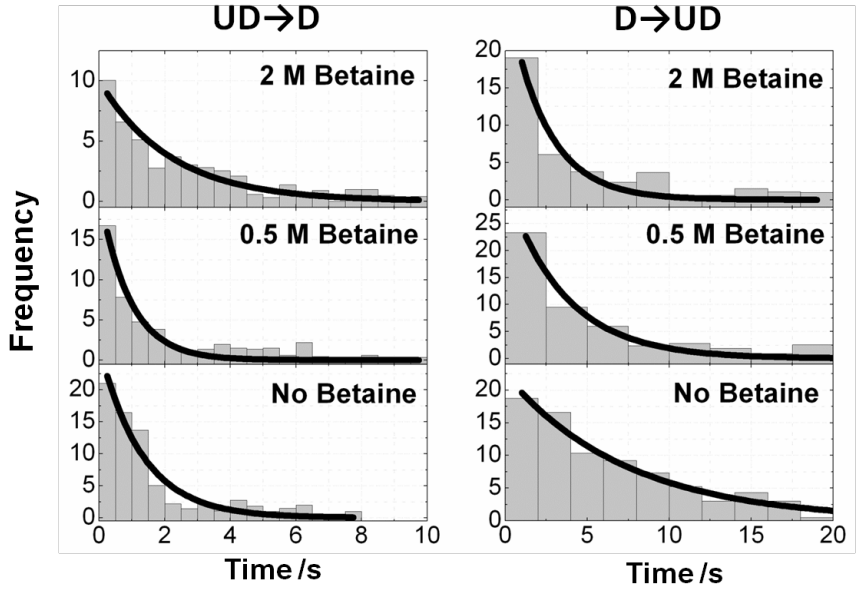

Figure 11. Dwell time histograms of the UD (left panels) and D (right panels) at the indicated betaine concentrations. The data have been fitted to single exponential decay functions to give the rates of docking (k_{dock}) and undocking (k_{undock}), respectively.

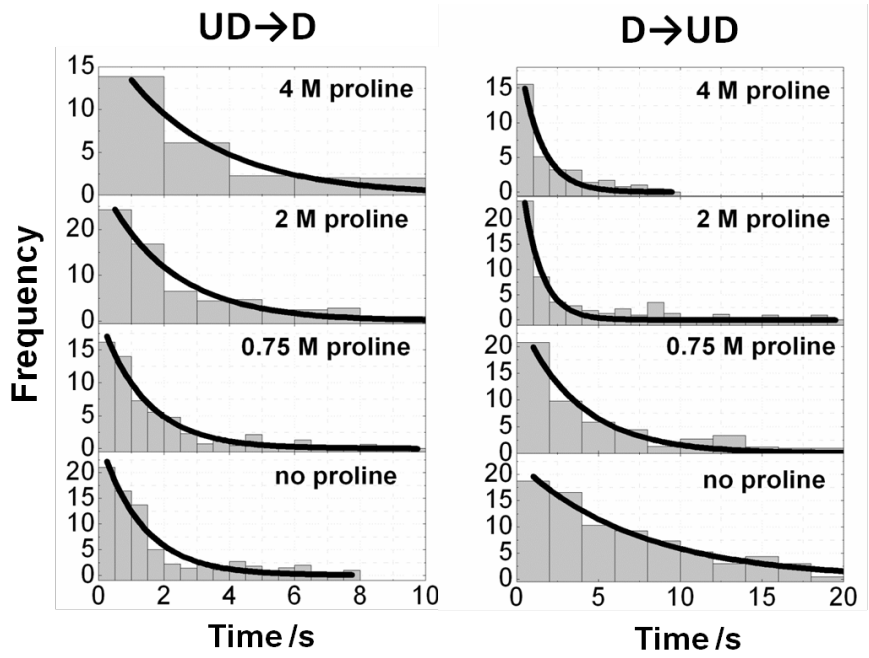

Figure 12. Dwell time histograms of the UD (left panels) and D (right panels) at the indicated proline concentrations. The data have been fitted to single exponential decay functions to give the rates of docking (k_{dock}) and undocking (k_{undock}), respectively.

Only for the formamide we can get a single population in the UD state. Analysis of its effect on k_{dock} and k_{undock} (Table 1) for the situations of UD and D states reveals a substantial increase in the rate of undocking (~ 37-fold) in the undocking rate from 0.13 s^{-1} with no formamide to a value of 4.9 s^{-1} at 10 M. In contrast, the docking rate practically remains constant with slight variations in the range of 0.7 to 1.3 s^{-1}. The equilibrium constant for the folding process, calculated from the k_{dock} and k_{undock} values, is reduced by a factor of ~ 30-fold between the limiting denaturant conditions.

As is frequently done in protein (Myers et al. 1995), and recently also RNA (Fang et al. 1999), folding studies, in order to further quantify these effects and allow the comparison among the different denaturing agents, we extracted the m-values by fitting the kinetic rates and equilibrium constants to the linear relationship ΔG(denaturant) = ΔG^{H2O}–m [denaturant], where ΔG^{H2O} is the free energy of folding in absence of denaturant and m is the denaturant response parameter, which represents the dependence of ΔG on denaturant concentration (Figure 13). Data measured in the research group for the urea titration were introduced in the plot in order to allow comparison. From the slope of [denaturant] versus lnK we obtained an $m(K)$ equal to 0.4 M^{-1} for the formamide and about 0.7 M^{-1} for the other three, confirming that all of them substantially destabilize the docked conformation. The corresponding value for the undocking rate $m(k_{undock})$ was very similar among all the denaturing agents around -0.5 M^{-1}, while little effect was obtained for the docking rate with a value of $m(k_{dock})$ = –0.1 for the formamide and ~ 0.2 for the rest.

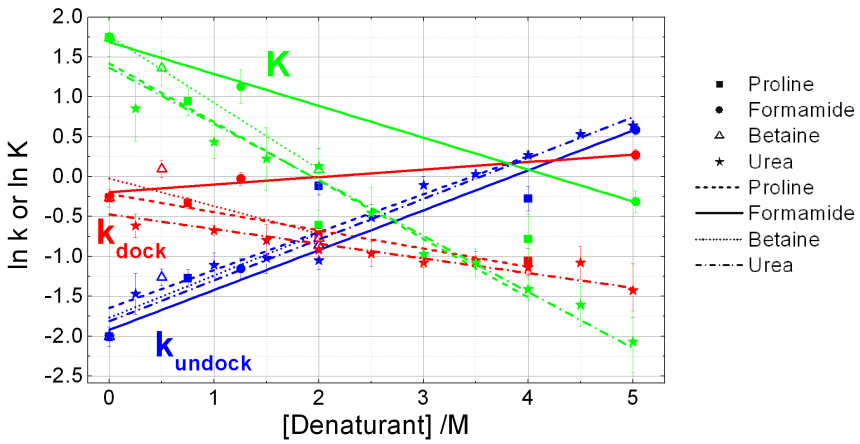

Figure 13. Effect of different denaturing agents (Proline (■), formamide (●), betaine (△) and urea(★)) on the equilibrium constant and docking and undocking kinetics of ligand-free aptamers at 4 mM saturating concentrations of Mg^{2+} ions. k_{dock} (red) and k_{undock} (blue) were obtained from the fits of the dwell time data as described in Figure 10 and K (green) is obtained from k_{dock} divided by k_{undock}. Lines correspond to the best linear regression fit to the logarithmic plot shown according to the equation: $lnk = -\Delta G^{H2O}/RT + m$ [denaturant]. Values specific rate constants and the resulting slopes are listed in Table 1.

Table 1. Effect of the different denaturants on the docking, undocking and equilibrium constants extracted from the single-molecule dwell time histograms at the indicated concentrations of denaturing agent in a background of 4 mM Mg^{2+} ions concentration. The errors associated to each value correspond to those obtained from the non-linear squares fitting of the dwell time histogram to a monoexponential decay function. Values of $m(k_{dock})$, $m(k_{undock})$ and $m(K)$ in M^{-1} obtained from the slope of the plots of lnK, lnk_{dock} or lnk_{undock} versus denaturant concentration. The number of significant figures for these values reflects the uncertainties obtained from the fits.

Denaturant	**Conc.** /M	k_{undock} /s^{-1}	k_{dock} /s^{-1}	K	m / M^{-1}		
	0	0.13 ± 0.02	0.77 ± 0.09	5.7 ± 1.3	k_{undock}	k_{dock}	K
	1.3	0.32 ± 0.04	0.97 ± 0.08	3.1 ± 0.6			
Formamide	5.0	1.8 ± 0.1	1.31 ± 0.09	0.73 ± 0.10	-0.50	-0.09	0.40
	10	4.9 ± 0.3	0.71 ± 0.08	0.15 ± 0.03			
	0.75	0.28 ± 0.03	0.72 ± 0.05	2.6 ± 0.5			
Proline	2	0.89 ± 0.10	0.48 ± 0.04	0.54 ± 0.10	-0.5[a]	0.23	0.7
	4	0.76 ± 0.11	0.35 ± 0.06	0.46 ± 0.14			
Betaine	0.5	0.28 ± 0.03	1.1 ± 0.1	3.9 ± 0.8	-0.5	0.3[1]	0.83
	2	0.42 ± 0.07	0.46 ± 0.04	1.1 ± 0.3			
Urea[b]					-0.51	0.19	0.70

[a] low R-square, [b] Data from Dalgarno et al. (Dalgarno et al. 2013).

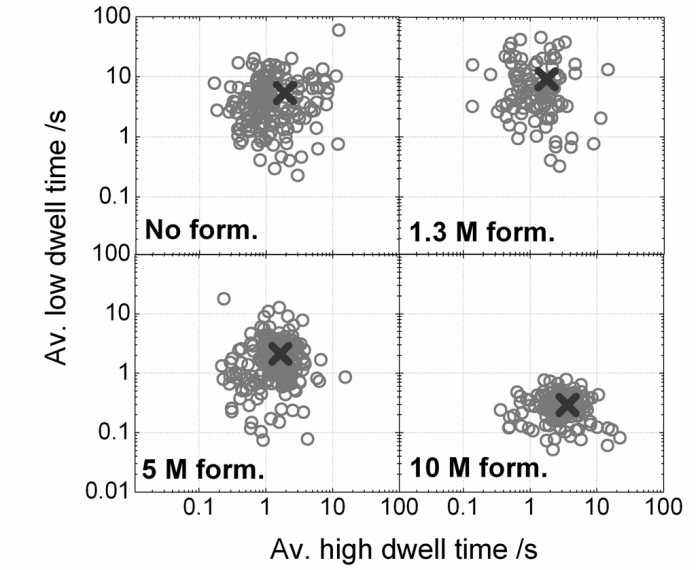

Figure 14. Contour plots of average dwell times in the D and UD states obtained from > 200 molecules as a function of formamide concentration. Red crosses mark the position of the average value at each formamide concentration. While the level of dynamic heterogeneity remains mostly unaltered, increasing concentrations of formamide progressively shift the average dwell time in the dock and undocked states by ~ 20- and ~ 2-fold, respectively.

Analysis of the dwell time histograms does not provide insights into whether or not a denaturing agent could additionally modulate the level of kinetic heterogeneity from molecule to molecule. To evaluate this, we measured the average times remaining on the D and UD states for >200 molecules as a function of formamide concentration (Figure 14), obtaining similar results than those for the urea (Dalgarno et al. 2013). The two-dimensional contour plots of the mean dwell times show a very similar low level of dynamic heterogeneity (< 10-fold) across the entire range of formamide concentrations. The 2D-contour plots also showed a variation in the average dwell times as a function of formamide concentration following a similar pattern to that previously detected by analyzing the transition-based single- molecule histograms.

4.2. RNA-ligand Interactions: Stabilization of the docked state against chemically-induced unfolding.

At 5 M formamide, the relative contribution of the Gaussian peak corresponding to the docked state (D) is similar to that of the undocked state (UD). Single-molecule FRET trajectories at these experimental conditions also revealed a higher frequency of fluctuations between the D and UD states when compared to the trajectories without formamide (Figure 9), with aptamer remaining in the docked state for periods 10-fold shorter. We performed a single-molecule FRET investigation of the add adenine aptamer in the presence of 5 M formamide at increasing concentrations of ligand up to 500 µM and in a similar 4 mM background of divalent metal ions as that used to characterize the ligand-free state.

Upon addition of adenine ligand, the relative population of the D ($E_{app} \sim 0.9$) and UD ($E_{app} \sim 0.34$) states changed, with the contribution of the undocked conformation decreasing from ~ 40% in the absence of ligand to a value of ~ 6% at 500 µM adenine ligand concentration (Figure 15).

In the presence of 10 µM adenine, we observed an indication of an additional state with an E_{app} of ~ 0.55. The existence of an intermediate state in the folding process of the loop-loop interaction structure of the adenine riboswitch has been reported before at low magnesium ion concentrations (Lemay et al. 2006) (e.g. 20 µM Mg^{2+} and below).

A comparison of the time traces obtained for the docked conformation at 5 M formamide concentration in the presence and absence of adenine ligand (Figure 9 and Figure 16) revealed a substantial difference in dynamic behavior, with the dwell times of the docked state in the presence of ligand being in average more than one order of magnitude longer than in the absence of ligand.

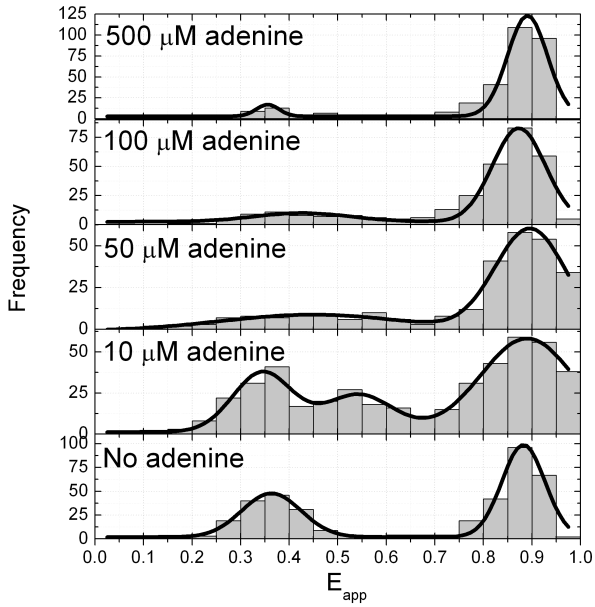

Figure 15. Single-molecule histograms of FRET efficiency in the presence of 5 M formamide and 4 mM Mg^{2+} showing the variation in the relative populations of the D and UD states as a function of increasing concentrations of adenine ligand.

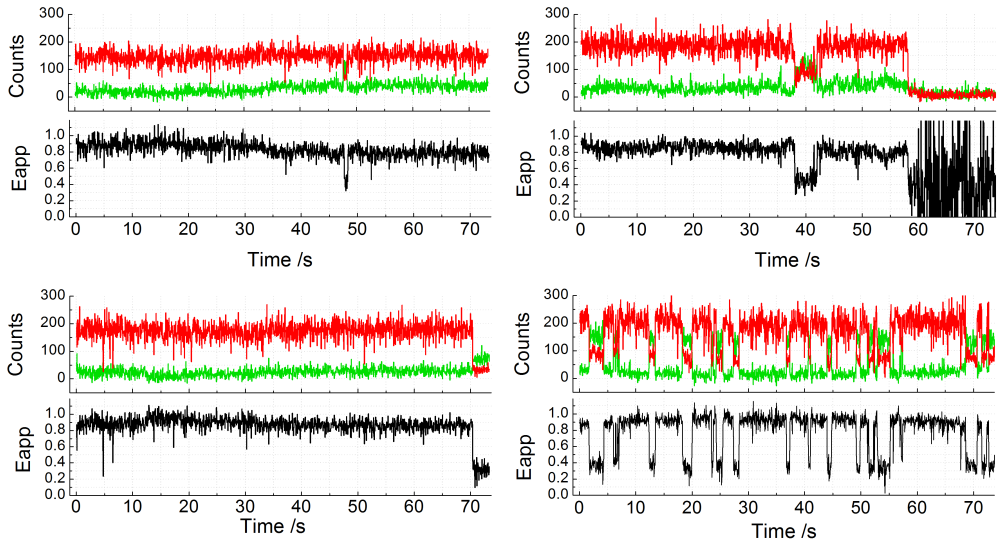

Figure 16. Representative anti-correlated donor-acceptor intensity traces and single-molecule FRET trajectories obtained at 4 mM Mg^{2+} and 5 M formamide in the presence of 100 μM adenine ligand.

At adenine ligand concentration of 100 µM, the majority of aptamers reverted to a docked state conformation as reflected by the ~ 85% contribution of the Gaussian centered at $E_{app} \sim 0.9$; we interpreted this result from an increased population of aptamer-ligand complexes and the subsequent protection of the docked state against formamide unfolding. The frequency of fluctuations between the D and UD states is much lower that under similar concentration of Mg^{2+} ions and formamide but in the absence of adenine ligand. At these conditions most time traces showed an extremely long-lived docked state lasting for several tens of seconds with occasional fluctuations to the undocked state (Figure 16).

For this reason, it is not possible to calculate the k_{undock}, being necessary longer traces at lower intensity to avoid photobleaching. However, the inspection of the anti-correlated donor and acceptor traces and the associated FRET trajectories obtained revealed a remarkably slower undocking dynamics in presence of the ligand with respect to the conditions of 5 M formamide or even those without formamide. Interestingly, the docking rate constant (0.73 s^{-1}, Figure 17) is almost identical to that obtained in the absence of adenine ligand at the same formamide concentration (Table 1), showing a clear ligand-induced deceleration of the undocking process.

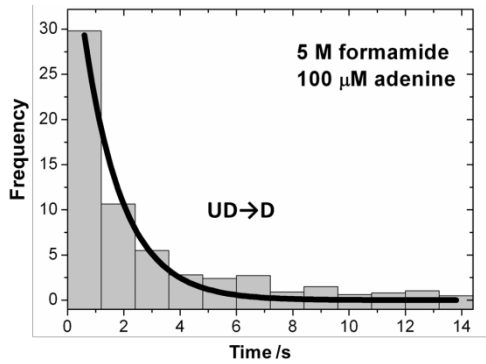

Figure 17. Single-molecule dwell time histogram and corresponding fitting to mono-exponential decay function (solid line) obtained for the docking process of the adenine aptamer at 4 mM Mg^{2+} and 5 M formamide in the presence of 100 µM adenine ligand. At these conditions single-molecule trajectories are not long enough to perform a quantitative estimation of the undocking rate.

4.3. Effect of Divalent Cations in presence of Formamide.

To further characterize the effect of formamide on the docking dynamics of the adenine aptamer, we next performed a formamide titration at different concentrations of divalent metal ions.

The effect of 5 M concentration of formamide in the relative equilibrium populations of the docked and undocked states at different concentrations of Mg^{2+} ions are shown in the set of single-molecule FRET histograms in Figure 18. Representative anti-correlated donor and acceptor trajectories and corresponding apparent FRET efficiency traces are also shown. As expected, increasing the concentration of Mg^{2+} at a fixed 5 M concentration of formamide shifted the equilibrium towards the docked state from a neglectable contribution at 0.5 mM Mg^{2+} to a > 90% at 20 mM Mg^{2+}. Single-molecule FRET traces obtained at these conditions showed a significant increase in the dwell time of the docked state at Mg^{2+} concentrations above 6 mM compared to those obtained at 0.5 mM Mg^{2+} (Figure 18).

Observing the data in Figure 18 we can confirm that the presence of formamide always shifts the equilibrium towards the undocked state in comparison with the situation at the same magnesium concentrations without formamide (Lemay and Lafontaine 2007).

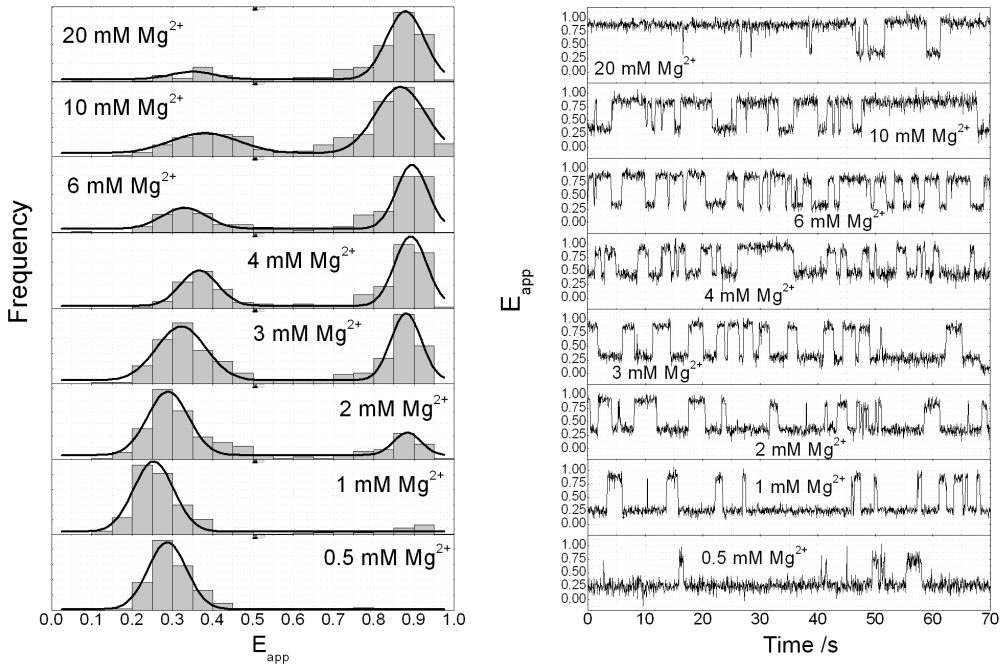

Figure 18. Left: Set of single-molecule FRET histograms at 5 M concentration of formamide and different concentrations of Mg^{2+} ions. Right: Representative for each Mg^{2+} concentration.

4.4. Monovalent Cations also protect the Folding State.

Chemical unfolding can also be counteracted by increasing the concentration of monovalent cations. The effect of different concentrations of NaCl in the relative equilibrium populations of the docked and undocked states without Mg^{2+} is shown in the set of single-molecule FRET histograms in Figure 19 for three situations: without denaturing agent, and at saturating concentrations of formamide and urea, 10 M and 5 M respectively.

As expected, increasing the concentration of Na^+ shifted the equilibrium towards the docked state in the three cases. However in presence of urea or formamide a single population of D state is not reached even at concentrations of Na^+ as high as 1 M.

Dynamics at high Na^+ concentrations and without Mg^{2+} are too fast to perform a rate analysis for both the formamide and the urea case (Figure 20). As an example, FRET histograms and representative anti-correlated donor and acceptor trajectories and corresponding apparent FRET efficiency traces are shown for the situation at 5 M urea and 1 M NaCl at two integrations times of 16 and 50 ms (Figure 21). We can see that even at the shorter integration time the dynamics are too fast for the camera time resolution.

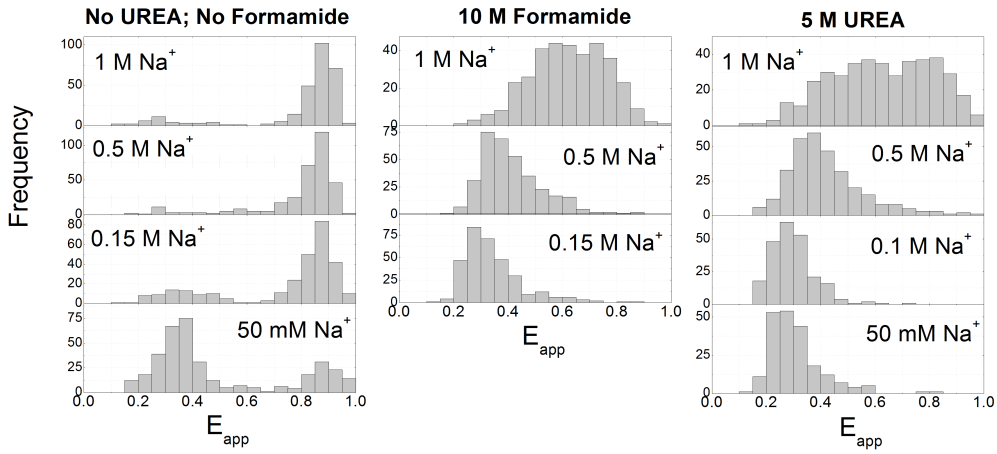

Figure 19. Single-molecule histograms of FRET efficiency as a function of Na^+ concentration. Increasing the concentration of monovalent cations results in a progressive increase in the relative contribution of the single-molecule FRET histogram corresponding to the docked state (D). Both histograms at 1 M of Na^+, at 10 M of formamide and 5 M of urea, show a very broad peaks as a result of the very fast dynamics between U and UD states. In these cases FRET efficiencies of 0.5 to 0.7 correspond actually to the average between U and UD states that interconvert at a time scale faster than the 0.5 s interval uses to calculate the FRET efficiency.

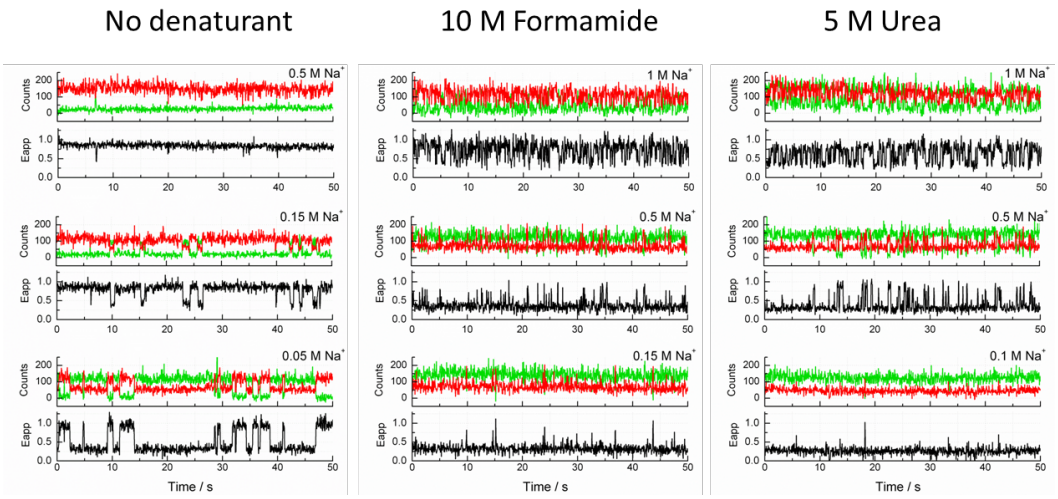

Figure 20. Representative anti-correlated donor and acceptor trajectories with the corresponding apparent FRET efficiency traces at different NaCl concentrations.

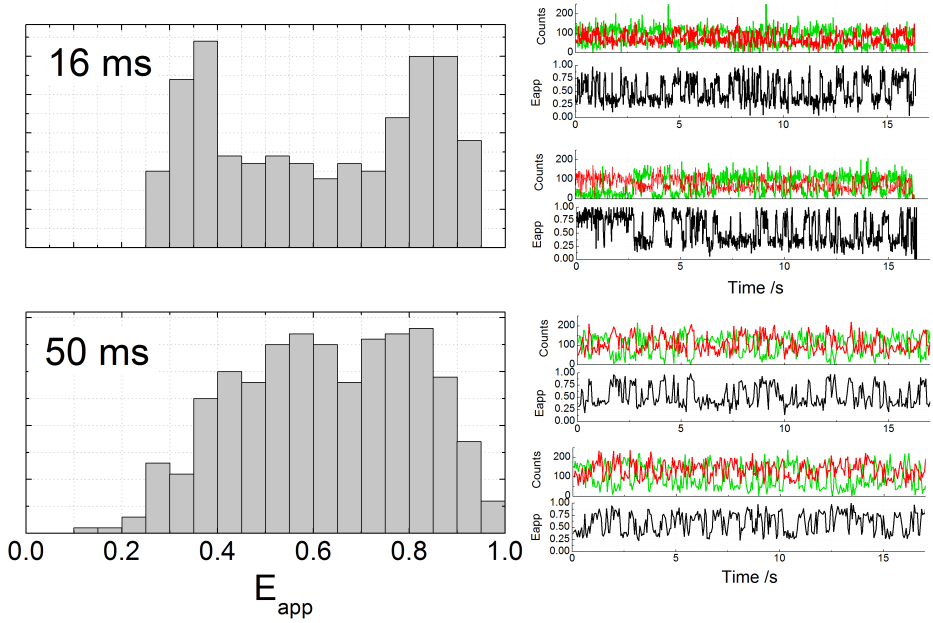

Figure 21. Single-molecule histograms of FRET efficiency and representative anti-correlated donor and acceptor trajectories with the corresponding apparent FRET efficiency traces at 5 M urea and 1 M NaCl. Histogram and traces at the top half panels were performed using an integration time of 16 ms while for the bottom half histogram and traces an integration time of 50 ms was used. Both FRET histograms were obtained by averaging the first 10 frames of each FRET trace for every individual molecule. Even at the shorter integration time the dynamics are too fast to completely separate D and UD populations.

The effect of urea and formamide in the populations of D and UD states can be quantified by the average FRET for each situation which is independent of the integration time. In Figure 22 we can see that both urea and formamide decrease the average FRET in comparison with the situation without denaturing agent, with the effect of 5 M of urea being equivalent to 10 M of formamide.

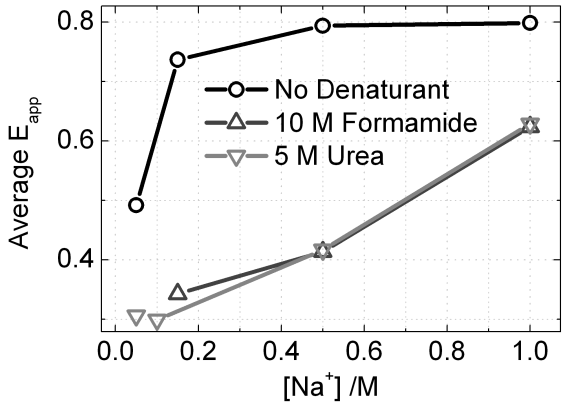

Figure 22. Average FRET efficiency as a function of Na^+ concentration. Increasing the concentration of monovalent cations results in a progressive increase in the average FRET value. An average FRET of 0.3 corresponds to a single population in the UD state, while a value of 0.9 corresponds to the docked state (D). Upward blue triangle represent measurements at 10 M concentration of formamide, downward green triangle at 5 M of urea, and black circles represent measurements without denaturing agent.

5. Discussion.

In this study we used the combination of single-molecule FRET and chemical denaturation to comparatively evaluate the docking dynamics and stability of the ligand-free form of the aptamer domain of the *add* riboswitch using three different denaturants.

First, we proved the compatibility of the three different denaturing agents first time used in single molecule FRET with the surface immobilization and passivation protocols normally employed in single-molecule studies of RNA function based on streptavidin-biotin interactions. For the formamide we could increase the concentration up to 10 M until reaching a single population of UD state in presence of 4 mM Mg^{2+} and 50 mM of Na^+, just before the induced change in the refraction index introduces significant distortions in the evanescence wave generated at the quartz-water interface. In the proline and betaine cases, at concentrations ≥ 4 M the surface attachment starts being disrupted before the equilibrium completely shifted to the UD state.

We confirmed that chemical melting can be tailored to target exclusively the tertiary interactions of the RNA structure (Figure 6, Figure 8), being also possible to reversibly unfold the secondary structure when we remove the ions in presence of denaturant (Figure 7). The assignment of the efficiencies of energy transfer of ~ 0.35 and 0.9 in the presence and absence denaturant to the ligand-free undock and dock states of the tertiary structure is supported by the similar values obtained for the different denaturants at the different Mg^{2+} concentrations investigated and the coincidence with those published previously (Dalgarno et al. 2013). We have also shown that single RNA molecules can undergo sequential cycles of folding and refolding and still preserve intact their ability to adopt the native docked conformation (Figure 6).

We studied the effect on tertiary structure for three denaturing agents: proline, betaine and formamide and perform a comparison with previously measured data for urea (Dalgarno et al. 2013). Although the exact nature of the interactions between the RNA and those denaturants are still not well understood (Lambert and Draper 2007), acceleration of RNA folding by urea is emerging as a signature of kinetic traps as the rate-limiting step in large RNAs (Pan et al. 1997; Sosnick and Pan 2003). For the *add* riboswitch aptamer, the absence of significative acceleration of the docking rate using any denaturant supports a trap-free rate-limiting step for the formation of the ligand-free state (Figure 13). Moreover, at saturating concentrations of divalent metal ions, the 37-fold increase of the undocking rate in the range 0 to 10 M formamide indicates that the global effect of these denaturants on the ligand-free aptamer takes place mostly via destabilization of the docked state. This is also reflected by the slope of lnk_{undock} versus denaturant concentration, or $m(k_{undock})$-*value*, equal to ~ 0.5 M^{-1} consistent for all the denaturants studied (Figure 13). Interestingly, the docking rate also shows a moderate but significant decrease (~2-fold) with increasing concentrations of proline and betaine, which by extrapolation coincides with that observed for urea (Dalgarno et al. 2013). Taken together, this data are consistent with a conformational search model, where the rate-limiting step for ligand-free docking involves the formation of stable tertiary contacts between the loops located at the end of the P2 and P3 stems and the addition of denaturant makes the formation of these native interactions less favorable.

The slope of the plot *lnK* versus denaturant concentration, the *m(K)-value*, is 0.4 M^{-1} for formamide and almost double for the urea, proline and betaine. These represent the dependence of the folding free energy on denaturant concentration and indicate that formamide is twice less effective as a denaturant than urea, proline or betaine.

Focusing on the formamide, we can conclude that the reduction in the docking equilibrium induced by its interaction with the mRNA aptamer is based on a substantial acceleration of the undocking process, while the docking rate is very little affected, presenting a low level of

dynamic heterogeneity across the entire range of formamide concentrations (Figure 14), similar to that observed for urea (Dalgarno et al. 2013).

Next, we probed directly the influence of adenine ligand in the stability of the docked state (D) and the corresponding dynamics of the docking process in presence of formamide. Our single-molecule denaturation measurements reveal that increasing the ligand concentration at constant formamide induces a pronounced increase in the dwell times of the docked state (Figure 16) while docking rate constant is almost identical to that obtained in the absence of adenine ligand (Figure 17). Therefore, higher concentrations of formamide are required in the presence of ligand to induce a similar shift in the relative equilibrium populations of the D and UD states to that observed for the ligand-free form. The decrease for the undocking rate of the add aptamer-ligand complex compared to the ligand-free form (see traces for 5 M of formamide in Figure 9 and Figure 16) is in agreement with recent values extracted from force-based mechanical unfolding (Lin and Thirumalai 2008).

The observed dependence of these effects with the concentration of adenine ligand clearly indicates that those are caused by the formation of the aptamer-ligand complex and the subsequent protection of the ligand-bound docked state against denaturation.

In the apparent FRET efficiency histogram at 10 µM adenine, we observed indications of the intermediate state at E_{app} ~0.55 previously reported for the Mg-induced folding pathway of the adenine riboswitch (Lemay et al. 2006). Although, at the high magnesium ion concentrations used here (4 mM Mg^{2+}) the interconversion between the UD state and this intermediate state is too fast to be resolved, the existence of this discrete intermediate state confirms that the addition of adenine promotes the formation of an intermediate structure, providing further evidence for assistance by the binding ligand.

The effect of monovalent and divalent cations in presence of formamide were also preliminary studied. During the magnesium titration in presence of 5 M of formamide, the relative duration between the low and high FRET states exhibits a strong dependence on magnesium ion concentration especially in the range from 0.5 to 4 mM Mg^{2+}. This is in agreement with the results already published without formamide, although in this case we have to go above 10 mM magnesium ions to neutralize the effect of the formamide and reach the situation in which the aptamer molecules exist mostly in the high-FRET state until fluorophore photobleaching occurs. This dependence of the effect of the formamide on the magnesium concentration opens the door to future studies using single-molecule chemical denaturation to reveal the mechanistic role of the Mg^{2+} ions by measuring the formamide-induced effect at subsaturating concentrations of Mg^{2+}. Concentrations of monovalent ions above 150 mM were proved to induce a total shift to the folding state in absence of magnesium. However in

presence of 10 M formamide or 5 M urea a single population of D state is not reached even at concentrations of Na^+ as high as 1 M, showing a too fast interconversion between the D and UD states to be resolved by our TIRF microscope at its highest resolution of 16 ms (Figure 21). Using the average FRET we can conclude than the effect at 10 M of formamide on the response to Na^+ concentration is equivalent to that of 5 M urea. The dwell times observed for the traces at 10 M formamide in presence of high concentrations of Na^+ without magnesium are much shorter than those observed for the traces with similar average FRET efficiency from the formamide titration at 4 mM Mg^{2+} or the magnesium titration at 5 M formamide, showing that for the same equilibrium populations of the D and UD states, the dynamic behavior can be very different depending on the conditions. Contrarily to what happen with denaturant or magnesium-induced changes in K, the increase in Na^+ concentration at saturating concentrations of denaturant affects mainly to the dwell time of the UD state, as shown in the FRET efficient trajectories. It means that the main influence is on k_{dock} instead of k_{undock}, suggesting that the stability of the docked state in presence of denaturant is limited by the absence of divalent metal ions. Although not proven at this stage, it is tempting to speculate that the different behaviour observed between mono- and divalent metal ions might reflect the different nature of the stabilization process induced by both ions. It is know from the crystal structure of the add aptamer riboswitch that stabilization of the folded state requires specifically bound divalent metal ions, therefore Mg^{2+} offers and additional interaction beyond the charge screening provided by monovalent metal ions. The absence of this specific interaction may explain the faster dynamics (most likely faster unfolding) observed in Na^+ compared to Mg^{2+}. However, in order to firmly support this conclusion, further data has to be taken in order to obtain quantitative values for the rate constants.

Summarizing Discussion and Conclusions

In this thesis stability and dynamics of different chemical and biological systems were successfully studied through single-molecule fluorescence (SMF) techniques.

Fluorescence Correlation Spectroscopy (FCS) was proved to be a powerful single molecule technique for the study of the stability and the association dynamics of supramolecular systems and, in particular, of host-guest inclusion complexes.

Throughout the study of different systems, FCS technique was optimized especially for the determination of host-guest binding dynamics. Some practical aspects of relevant importance were discussed in **Chapter I**, particularly those regarding calibration, sample preparation or the influence of cover-slide thickness. The most reliable value in the literature for an absolute value of the diffusion coefficient of a standard was found to be that given by Muller (Muller, Loman et al. 2008) for the Rhodamine 6G determined at 25°C using dual focus FCS (2fFCS). This value together with the ratios of Gendron (Gendron, Avaltroni et al. 2008) for other rhodamines allowed us to establish a common reference point to calculate absolute diffusion coefficients for both excitation wavelengths used in this work (405 and 488 nm). Regarding the cover-slide thickness influence in FCS measurements, an important variability in thickness was discovered among the cover-slides. This variability has significant influence on the results, increasing the diffusion time values when its effect is not corrected by adjusting the correction collar at the right position at each measurement. The problem was avoid by using well plates, which allowed one to perform a whole titration in the same well following a careful protocol of sample preparation.

The effect of impurities on FCS results was investigated and also collected in an extensive section in **Chapter I**. We performed a deep discussion deducing equations to relate impurities more important characteristics (concentration and brightness) with their influence on parameters obtained from the fit to the FCS correlation curves. Three ratios (in intensity, f_I; number, f_N; and brightness, f_Q.) were defined to express the contribution of the impurity relative to the main fluorophore of the sample. This allowed the deduction of general expressions and plots to predict the effect of impurities on the different parameters.

Impurities were found to have a strong influence on the apparent number of molecules, *N*. The effect on *N* can be calculated through the impurities contribution to the intensity signal. The maximum influence is given by a situation with a highly concentrated impurity with very low brightness. In cases in which the impurity are molecules that are much less bright than the fluorophore we are interested in (less than 1%) but with huge contributions to the intensity (up to a 50%), the influence on the number of molecules will be very high, but neglectable on the diffusion time. The scattered light coming from the solvent is a clear example of this situation.

On the contrary to what happens with the number of molecules, the diffusion time will be much more affected by impurities with high brightness. Also, the more different in size are the fluorophore and the impurity the bigger will be the influence on the diffusion time.

The influence of impurities on the apparent number of molecules, *N*, during titrations in host-guest complexations was also studied in this chapter. Experimental data of titrations with unexpected increases in *N* (at constant concentration of fluorophore) were collected for different host-guest systems. Two different models were developed in order to establish in which cases theses changes in *N* could be explained on the basis of the impurities present either in the stock of fluorophore or in the stock of host. In the case of an impurity in the stock of guest, this will lead to a change in the apparent number of molecules during a titration, only when the brightness ratio between guest and impurity depends on the concentration of added host. In any case, the knowledge of two of the three ratios f_I, f_N and f_Q together with the equations we have proposed allow one to predict the influence on the number molecules and on the diffusion time. It helps to interpret correctly the data in FCS, and distinguish between those effects caused by the impurity and those due to the interaction between host and guest. Calculations and analysis discussed in this chapter make it possible to study systems with certain levels of impurities even when the effects of the interaction between host and guest are weak.

The study on the interaction between adamantane and cyclodextrin collected in **Chapter II** shows how using FCS host-guest binding equilibrium constant can be determined analyzing the variation in the diffusion coefficient of the fluorescent guest or host with no need for a change in the photophysical properties of the fluorescent probe. Following this strategy, FCS can target the study of almost any host guest systems as long as host or guest is labeled with a fluorophore. However, the use of standard UV/Vis absorption and fluorescence spectroscopy requires a change in the absorption or emission spectra of the dye upon complexation as it happens in the association of PY and PB with γCD studied in other of the papers included in **Chapter II**. In this work, the analysis of the variation in the spectra allowed us to make

interesting conclusions regarding the different behavior between the two pyronines and the stabilities of the pyronine dimers and 1:1 and 2:1 complexes with γCD.

FCS gives also access to the association/dissociation rate constants of the host-guest inclusion providing that the fluorescence intensity of host or guest changes upon complexation. The comparison of the rate constants with that of a diffusion-controlled process estimated from the same FCS experiment allows a better understanding of the association dynamics. Results for different host-guest systems were collected in the third contribution included in **Chapter II**, showing that cyclodextrin cavities act as "hard" cages which put geometric and orientational restrictions on the inclusion of a hydrophobic guest, whereas micelles behave as "soft" cages without geometrical requirements.

The study of hydrophobic interactions in ionic colloidal systems by FCS requires neutral fluorescent probes, which typically present a lower brightness, worse photostability and mostly need an excitation at lower wavelength as compared to the charged dyes mostly used in FCS. It has been shown in **Chapter III** that the dynamics of the host-guest association of a neutral hydrophobic dye to micelles can be studied by FCS in spite of the low quantum yield, low saturation threshold and higher energetic excitation of the dye. The careful selection of the experimental conditions made it possible to obtain the dynamic and diffusional properties with reasonable precision. It was also discussed that the contrast in the brightness of free and bound dye (brightness ratio q) has a strong influence on the sensitivity of the FCS experiment to the association dynamics. The simulations in this chapter show how a strong contrast $q > 1$ leads to high amplitudes of the reaction term already at low micelle concentrations, which means that the most suitable measurements to determine the rate constant under these conditions will be those at low surfactant concentration.

As a relevant example of positive-contrast dye, the interaction between the surfactant Triton X-100 and the fluorophore Coumarine 152 was studied. The selection of the measurement conditions according to the contrast of the dye allowed us to satisfactorily obtain the kinetic constants of the system, confirming that micelles act as a *soft cage* which allows a diffusion-limited entry of the dye into the micelle. Being the association rate constant diffusion-limited, both the binding equilibrium constant and the overall exchange (relaxation) rate of different micellar systems will be determined mainly by the exit rate constant, which shows a strong dependence on the specific interactions between dye and micelle. This leads to a broad dynamic range of the exchange in micellar systems, which can be well covered by FCS.

The use of both neutral and charged dyes opens the way to systematic studies of the dynamics of matter exchange in series of neutral and ionic colloidal systems and to evaluate the role of electrostatic as compared to other weak interactions.

In **Chapter IV**, a novel fluorescently labeled derivative from the cationic bis-benzamidines (BBA) family of minor groove binders labeled with the negatively charged Oregon Green (OG) was used to study for the first time by FCS the binding dynamics of a minor groove binder to both high and low affinity DNA sequences. As a result of using this modified binder the dissociation dynamics of BBA-OG is faster than that of more typical minor-groove binders, making it accessible by a highly sensitive single-molecule technique as FCS.

This study yielded values for the binding equilibrium constant, the association and dissociation rate constants, and also the diffusion coefficients, which were necessary to estimate the diffusion-controlled rate constants. The comparison of the dynamics of the association of BBA-OG to different DNA sequences and to DNA of different length allowed us to identify the rate-limiting step in this process and evaluate the importance of mechanisms such as sliding or two dimensional diffusion found for the binding of proteins to DNA. FCS revealed that the dynamics of the association process of the bisbenzamidine minor-groove binder BBA-OG to dsDNA is not controlled by diffusion, but by the insertion of the binder into the groove at the specific site, as shown by the rate constants for each step of the binding event. Specificity of these binders to AT sites seems to be mainly determined by the association process, whereas the binding affinity depends strongly on the dissociation rate.

It was also confirmed that the association rates obtained for the binder under study are very similar to those reported for typical minor-groove binders. Consequently, this mechanism might constitute a general mechanism for small minor groove binders, however this should be confirmed with further studies on more typical minor groove agents.

After a photophysical study of the BBA-OG binder, the cationic bis-benzamidine (BBA) was proved to induce a quenching in the fluorescence of the OG dye. The disappearance of this quenching upon complexation with DNA leads to the flickering in the fluorescence intensity of the binder required to yield the entry and exit rate constants by Fluorescence Correlation Spectroscopy.

By using a binder with a longer linker between the BBA part and the OG488 molecule, we demonstrate that both, the efficiency of the quenching and the dissociation rate constant, can be tuned by changing the length of the linker.

In **Chapter V** a combination of single-molecule FRET and chemical denaturation was used to comparatively evaluate the docking dynamics and stability of the ligand-free form of the aptamer domain of the add riboswitch using three different denaturants: proline, betaine and formamide.

The compatibility of the three different denaturing agents first time used in single molecule FRET with the surface immobilization and passivation protocols was tested. For the formamide the concentration could be increased until reaching a single population of UD state in presence of magnesium and sodium ions, just before the induced change in the refraction index introduces significant distortions in the evanescence wave generated at the quartz-water interface. In the proline and betaine cases, at concentrations lower concentrations the surface attachment starts being disrupted before the equilibrium completely shifted to the UD state.

It was confirmed that chemical melting can be tailored to target exclusively the tertiary interactions of the RNA structure being also possible to reversibly unfold the secondary structure when we remove the ions in presence of denaturant. It was also shown that single RNA molecules can undergo sequential cycles of folding and refolding and still preserve intact their ability to adopt the native docked conformation.

The effect on the tertiary structure was also studied for the three mentioned denaturing agents and a comparison with previously measured data for urea was performed. The results indicate that the global effect of these denaturants on the ligand-free aptamer takes place mostly via destabilization of the docked state. The results are consistent with a conformational search model, where the rate-limiting step for ligand-free docking involves the formation of stable tertiary contacts between the loops located at the end of the P2 and P3 stems and the addition of denaturant makes the formation of these native interactions less favorable.

Experiments in presence of ligand for using formamide indicate that the formation of the aptamer-ligand complex protects the ligand-bound docked state against denaturation.

The effect of monovalent and divalent cations in presence of formamide was also preliminary studied, showing that the effect of this denaturant can be neutralized by increasing the concentration of magnesium ions. This observed dependence of the effect of the formamide on the magnesium concentration opens the door to future studies using single-molecule chemical denaturation to reveal the mechanistic role of the magnesium ions. Contrarily to what happen with denaturant or magnesium-induce changes in K, the main influence of the increase in Na^+ concentration at saturating concentrations of denaturant is on k_{dock} instead of k_{undock}, suggesting that the stability of the docked state in presence of denaturant is limited by the absence of divalent metal ions. However, in order to firmly support this conclusion, further data has to be taken in order to obtain quantitative values for the rate constants.

As a **conclusion**, the objectives fulfilled in this thesis can be briefly summarized as follows:

Most of the content in this work was dedicated to Fluorescence Correlation Spectroscopy (FCS) technique. In-depth studies on the dynamic behavior of different host-guest systems were carried out, such as the interaction between different types of fluorescent dyes and surfactants or the interaction between a DNA minor groove binder and different DNA sequences. In all cases, the results discussed here led to significant contributions for a better understanding of the mechanisms involved in this type of supramolecular associations.

The potential and limitations of FCS, as well as the influence of important factors such as the contrast in the brightness of free and bound dye (brightness ratio) or the fluorescent impurities present in the samples were analyzed in detail, providing through different plots and equations very useful guidance for the use of FCS to study a broad range of supramolecular host-guest systems.

Additionally, single-molecule FRET in combination with total internal reflection fluorescence (TIRF) microscopy was used to investigate RNA folding kinetics, since conformational changes of biomolecules typically present too slow dynamics to be measured by a free-diffusion-molecule technique as FCS. The chemical denaturation approach was tested in order to study the response of the add aptamer domain of the Adenine riboswitch at different concentrations of ligand, monovalent cations and divalent metal ions, opening the door to further studies to unveil their role in the folding mechanism.

Resumen

Esta tesis se basa en la aplicación de técnicas de detección de fluorescencia de moléculas individuales (SMF, por sus siglas en inglés) al estudio a nivel molecular y supramolecular de la estabilidad y el comportamiento dinámico de distintos sistemas químicos y bioquímicos.

La mayor parte del contenido se dedica a la optimización y aplicación de la técnica SMF de *Espectroscopia de Correlación de Fluorescencia* (FCS) (Gell et al. 2006; Rigler and Elson 2001; Sauer et al. 2011; Selvin and Ha 2008; Thompson 1991; Zander et al. 2002). Esta técnica estudia las moléculas mientras difunden libremente en disolución, de manera que el tiempo de observación de una molécula está, por tanto, limitado a su tránsito a través del volumen de excitación y detección dados por la óptica de un microscopio confocal, por lo que se utiliza para estudiar procesos con dinámicas rápidas (escalas temporales inferiores a 1 ms).

Para estudiar procesos más lentos se hace necesaria la inmovilización de moléculas sobre una superficie permitiendo observarlas durante tiempos más largos. Esta es la estrategia seguida en la segunda de las técnicas SMF utilizadas en esta tesis, la *Transmisión de Energía de Resonancia* de moléculas individuales en un microscopio de *Fluorescencia de Reflexión Interna Total* (sm-FRET/TIRF) cuyos experimentos fueron llevados a cabo durante una estancia en el laboratorio del Dr. Carlos Penedo en la Universidad de St. Andrews, Escocia.

La aplicación de FCS se centró en sistemas anfitrión-huésped (*host-guest*), llevándose a cabo estudios de la interacción entre colorantes fluorescentes de distinta naturaleza o moléculas marcadas con fluoróforos y macromoléculas tales como ciclodextrinas, micelas o distintas cadenas de nucleótidos de ADN. En todos los casos los resultados discutidos han conducido a contribuciones significativas a la hora de avanzar en el entendimiento de los mecanismos involucrados en este tipo de asociaciones supramoleculares. A su vez se ha pretendido sentar las bases para la utilización de FCS como herramienta en el estudio de un amplio rango de sistemas supramoleculares de tipo *host-guest*.

También se incluye en esta tesis el estudio de los cambios conformacionales en aptámeros de ARNm. La dinámica de este tipo de sistemas es demasiado lenta para que su estudio pueda ser abordado mediante FCS, por lo que el sistema se investiga mediante inmovilización de las

moléculas sobre una superficie para estudiarlas mediante sm-FRET en combinación con microscopía TIRF.

Capítulo I: Detección de Fluorescencia de Moléculas Individuales (SMFD).

En el Capítulo I se hace una breve introducción a la detección de moléculas individuales mediante fluorescencia, llevando a cabo una descripción detallada de la técnica de FCS: componentes, montaje, principales ecuaciones en el análisis de datos, etc.

En la *Espectrocopia de Correlación de Fluorescencia* se analizan las fluctuaciones en la intensidad de fluorescencia, que pueden ser debidas principalmente a tres causas: la difusión de las moléculas entrando y saliendo del volumen de detección (unos pocos femtolitros en los que suele haber de 1 a 10 moléculas), reacciones químicas, cambios estructurales o cualquier otro tipo de proceso que afecte a señal de fluorescencia de las moléculas en torno a su valor de equilibrio. La escala temporal de cada uno de estos procesos puede obtenerse del análisis a la función de autocorrelación de la traza *intensidad vs. tiempo*, de modo que cada uno de los mismos aparece a un tiempo de correlación que corresponde a su escala temporal típica.

En este capítulo se recogen también algunos aspectos prácticos, fruto de la optimización de la técnica en su aplicación a los distintos sistemas estudiados. Se aportan soluciones al tema de la calibración del tamaño del foco, la preparación de muestras durante titraciones o la influencia del grosor del cubreobjetos sobre el que se coloca la muestra.

Para poder obtener un valor absoluto del coeficiente de difusión de una especie a partir de su tiempo de difusión determinado en FCS, es necesario calibrar el equipo ya que el tiempo de difusión viene dado por el tamaño del foco, que depende de cada equipo y además puede sufrir variaciones con los ajustes diarios que se realizan al sistema óptico. La solución pasa por medir cada día una especie de coeficiente de difusión conocido cuya relación con el tiempo de difusión se utilizará para transformar los demás tiempos de difusión a coeficientes de difusión. En este caso se tomó como referencia el coeficiente de difusión dado por Muller (Muller et al. 2008) para la rodamina 6G, que fue determinado utilizando FCS de dos focos, que permite obtener valores absolutos del coeficiente de difusión. A partir de este valor se utilizaron las relaciones dadas por Gendron et al. (2008) para obtener el valor para otras rodaminas lo que sirvió para establecer un punto de referencia común para calcular coeficientes de difusión absolutos para las dos longitudes de onda de excitación utilizadas en esta tesis (405 y 488 nm).

La influencia del grosor del cubreobjetos en las medidas de FCS ya fue descrita anteriormente en la bibliografía (Enderlein et al. 2005). Sin embargo, se hace necesario comprobar la sensibilidad de cada equipo a este factor. Al hacerlo se determinó una importante variabilidad

en el grosor entre los distintos cubreobjetos utilizados e incluso dentro del mismo. Se observó que esta desviación tiene una influencia significativa en los resultados, incrementando los valores del tiempo de difusión si el efecto no se corrige ajustando el collar de corrección del objetivo a la posición adecuada en cada medida. Finalmente el problema fue resuelto con la utilización de placas multipocillo. Siguiendo un cuidadoso protocolo de preparación de muestras por el método de dilución-extracción, estas placas permiten llevar a cabo todas las medidas de una misma serie en el mismo pocillo, evitando la influencia por las desviaciones en el grosor del cubreobjetos.

Por último, en este primer capítulo se dedica una amplia sección al efecto que impurezas fluorescentes tienen en las medidas de FCS. En este sentido, se llevó a cabo una profunda discusión en la cual se dedujeron ecuaciones y modelos para relacionar las características más importantes de una impureza (concentración y luminosidad) con su influencia en los parámetros obtenidos del ajuste a las curvas de FCS. Se definieron tres relaciones (en intensidad, f_{I}; número, f_{N}; y luminosidad, f_{Q}) para expresar la contribución de la impureza en relación al fluoróforo principal. Esto permitió la deducción de expresiones generales y gráficas para predecir el efecto de una impureza en los parámetros más importantes obtenidos del ajuste a una curva de FCS: el número de moléculas aparente, N, y tiempo de difusión, τ_{D}.

Se encontró que las impurezas tienen una gran influencia en el número de moléculas aparente, N. Este efecto puede ser determinado a partir de la contribución de las impurezas a la intensidad de señal. Para una misma contribución en la intensidad, el caso de máxima influencia se da en aquella situación con impurezas en gran concentración pero poca luminosidad. Así, en casos en los que la impureza es mucho menos luminosa que el fluoróforo de interés (menor al 1 %) pero con altas contribuciones en la intensidad de señal (hasta un 50 %), la influencia en el número de moléculas va ser muy grande, sin embargo, la influencia en el tiempo de difusión será despreciable. La luz dispersa que viene de disolvente es un claro ejemplo de esta situación. Al contrario de lo que ocurre con el numero de moléculas, el tiempo de difusión se va a ver mucho más afectado por la presencia de impurezas de alta luminosidad. También, cuanto mayor sea la diferencia en tamaño entre la impureza y el fluoróforo mayor será la influencia en el tiempo de difusión.

De manera particular se estudió el caso concreto de la influencia de impurezas fluorescentes en el número de moléculas aparente durante titraciones para el estudio de complejaciones *host-guest*. Ya que en varias ocasiones al estudiar distintos sistemas se obtuvieron series de curvas de FCS en donde se observaba un inesperado aumento en N, a pesar de mantener la concentración de fluoróforo constante durante toda la titración. A partir de las ecuaciones deducidas para la influencia de una impureza fluorescente se desarrollaron dos modelos para determinar si dicho aumento podía explicarse en base a la presencia de impurezas en alguno

de los dos stocks, *host* o *guest*, utilizados para preparar las distintas muestras. Se observa que en el caso de una impureza en el stock de la especie fluorescente (normalmente el *guest*), ésta sólo dará lugar a un amento en el número de moléculas si la relación de luminosidades entre el *guest* fluorescente y la impureza depende de la concentración de *host* añadido. Los modelos propuestos permiten que determinando de dos de las tres relaciones f_I, f_N y f_Q se pueda predecir la influencia tanto en el número de moléculas como en el tiempo de difusión. Todo ello ayuda a interpretar correctamente los resultados obtenidos en FCS, y distinguir entre aquellos efectos causados por una impureza y los debidos a la interacción entre *host* y *guest*. De este modo los cálculos y análisis discutidos en esta sección permiten el estudio de sistemas con cierto nivel de impurezas incluso cuando los efectos de la interacción entre *host* y *guest* son débiles, ya que hace posible el determinar si una determinada variación en un parámetro puede ser o no atribuida a la impureza.

Capítulo II: Interacciones *Host-Guest* estudiadas mediante Técnicas de Fluorescencia.

En el Capítulo II se recogen estudios sobre varios sistemas *host-guest*. A través de tres trabajos ya publicados se discuten los factores que controlan la estructura y la estabilidad de estos complejos supramoleculares.

En un primer trabajo se aborda el estudio fluorimétrico de la complejación de las pironinas Y y B con γ-ciclodextrina (γCD) (Bordello et al. 2009), como continuación de un trabajo anterior realizado en el grupo de investigación para la βCD (Reija et al. 2005) que presenta un tamaño menor de la cavidad. El efecto de la complejación con γCD sobre los espectros de absorción y de emisión de las pironinas es similar al observado con βCD, con una importante disminución en el rendimiento cuántico de fluorescencia y sólo un ligero desplazamiento de los espectros. No obstante, aparecen cambios adicionales muy significativos en los espectros de absorción que se atribuyen a la formación de dímeros de pironina favorecida por la presencia de la ciclodextrina con mayor tamaño de cavidad. En este trabajo se estudiaron los equilibrios de complejación y dimerización y se determinaron las constantes de equilibrio y los espectros puros de las especies implicadas. Se discutió también el diferente comportamiento de ambas pironinas y la estabilidad de sus dineros, y los complejos 1:1 y 2:1 con γCD.

En un segundo trabajo incluido en este capítulo se recoge el estudio de la interacción entre el Adamantano y la β-ciclodextrina (Granadero et al. 2010). A través de este estudio se muestra como utilizando FCS, la constante de equilibrio para sistemas *host-guest* puede ser determinada analizando la variación en el coeficiente de difusión de la especie fluorescente (ya sea *host* o *guest*) sin necesidad de un cambio en las propiedades fotofísicas de la sonda fluorescente, lo cual contrasta con el uso de las técnicas más estándar de *Absorción UV/Vis* y

Espectroscopia de Fluorescencia en donde se requiere de un cambio en el espectro de absorción o emisión como resultado de la complejación para que el equilibrio pueda ser estudiado. Siguiendo la estrategia indicada en este trabajo, utilizando FCS se puede abordar el estudio de casi cualquier sistema *host-guest*, con el único requisito de que una de las dos especies esté marcada con un fluoróforo.

Sin embargo, el mayor potencial de la técnica de FCS reside en su capacidad para determinar constantes cinéticas de asociación o disociación en este tipo de sistemas, siempre que la intensidad de fluorescencia de una de las dos especies cambie al producirse la complejación. Además FCS permite la comparación de las constantes cinéticas obtenidas para un determinado sistema con aquellas de un proceso controlado por difusión, de modo que este estudio de la dinámica de asociación conduce a un mejor entendimiento del mecanismo seguido en cada caso. En el tercer trabajo incluido en este capítulo (Novo et al. 2011) se recogen resultados para la dinámica de distintos sistemas *host-guest*, y se compara mecanísticamente el comportamiento de las ciclodextrinas con *hosts* de distinta naturaleza como son las micelas. Se concluye que las ciclodextrinas actúan como *cuerpos rígidos*, con importantes restricciones geométricas y de orientación ante la inclusión de un *guest* hidrofóbico, mientras que la naturaleza multimérica de las micelas hace que se comporten como *cuerpos blandos* sin restricciones geométricas a la asociación.

Capítulo III: Estudio de la Dinámica de Intercambio de un Colorante Hidrofóbico Neutro en Disoluciones Micelares mediante FCS.

El Capítulo III se basa también en un trabajo ya publicado. En éste se discute el papel de la relación de luminosidades del fluoróforo durante el proceso de asociación para aumentar la sensibilidad de la técnica de FCS en la determinación de las constantes cinéticas en la formación de complejos de inclusión. En este capítulo se estudia la dinámica de intercambio del colorante cumarina 152 (C152) entre las micelas del surfactante neutro Triton X-100 (TX100) y la fase acuosa. Estos resultados se comparan con resultados previos para colorantes catiónicos, como la rodamina 123, que típicamente muestran una variación inversa en la relación de luminosidades.

El estudio de interacciones de tipo hidrofóbico en sistemas coloidales mediante FCS requiere de sondas fluorescentes neutras, que típicamente presentan menor luminosidad, peor fotoestabilidad y, por lo general, necesitan de una longitud de onda de excitación menor en comparación con los colorantes cargados que se suelen utilizar en FCS. En este trabajo, se discute que la dinámica de asociación para un sistema *host-guest* puede ser estudiada mediante FCS utilizando un colorante hidrofóbico a pesar de las numerosas desventajas que éste presenta. Con el estudio de la interacción entre la C152 y el TX100 se demuestra que

una selección de las condiciones de medida teniendo en cuenta el contraste del colorante hace posible obtener las propiedades difusionales y dinámicas con una precisión razonable. La discusión sobre la influencia del contraste en la luminosidad entre el colorante libre y asociado a las micelas (relación de luminosidades, q) concluye que éste tiene un gran efecto sobre la sensibilidad del experimento para determinar la dinámica de asociación. Las simulaciones incluidas en este capítulo muestran como un alto contraste, $q > 1$, lleva a que se alcancen valores elevados de la amplitud del término de reacción a bajas concentraciones de micelas, lo cual significa que las medidas idóneas para determinar la constante cinética en dichas condiciones serán a bajas concentraciones de surfactante.

Los valores obtenidos para las constantes cinéticas del sistema confirman que las micelas de TX100 permiten una asociación del colorante C152 limitada por difusión. Esto hace que la constante de equilibrio y la constante de relajación del sistema vengan dadas principalmente por la constante cinética de disociación, que muestra una fuerte dependencia de las interacciones especificas entre colorante y micela.

A la vista de los resultados, se puede concluir que FCS permite el uso de ambos tipos de colorantes, neutros y cargados, abriendo el camino a estudios sistemáticos de la dinámica de intercambio de materia en series de sistemas coloidales neutros e iónicos, y así evaluar el papel de las fuerzas de naturaleza electrostática en comparación con otras interacciones más débiles.

Capítulo IV: Estudio de la Dinámica de un ligando del surco menor del ADN mediante FCS.

En el Capítulo IV se utilizó la técnica de FCS para investigar la afinidad y la dinámica de asociación de ligandos sintéticos a distintas secuencias de ADN. Parte de los resultados más relevantes ya han sido publicados en una comunicación (Bordello et al. 2012).

Para posibilitar por primera vez el estudio mediante FCS de la dinámica de asociación de un ligando del surco menor a secuencias de ADN de distintas afinidades, se estableció una colaboración con el grupo de los profesores José Luis Mascareñas y Eugenio Vázquez Sentís (USC) desde donde se realizó la síntesis de un nuevo derivado de la familia de las bis-benzamidinas (ligandos catiónicos que se unen al surco menor del ADN) marcado con Oregon Green (fluoróforo aniónico).

La utilización de este ligando modificado lleva a una dinámica de disociación más rápida que la típica de ligandos del surco menor, haciendo el estudio de la asociación accesible a una técnica SMF de alta sensibilidad como es FCS.

En este trabajo se obtuvieron valores para la constante de equilibrio, las constantes cinéticas de asociación y disociación, y también los coeficientes de difusión, que son necesarios para estimar las constantes cinéticas que marcan el control por difusión del proceso. La comparación de la dinámica de asociación de este ligando a diferentes secuencias de ADN de distinta longitud permitió identificar el paso limitante de la velocidad del proceso y evaluar la importancia de mecanismos como el deslizamiento o la difusión en dos dimensiones comunes en la asociación de determinados ligandos a proteínas. FCS reveló que la dinámica de asociación del proceso del ligando estudiado al ADN de doble cadena no está controlada por difusión, sino por la inserción del ligando en el lugar específico del surco, como muestran las constantes cinéticas de cada una de las etapas del proceso de asociación. La especificidad de estos ligandos a secuencias de alta afinidad (ricas en bases AT), parece estar determinado principalmente por el proceso de asociación, mientras que la afinidad de la unión depende fuertemente de la velocidad de disociación.

Las constantes cinéticas de asociación obtenidas para este ligando fueron muy similares a las existentes en la bibliografía para ligandos típicos del surco menor. En consecuencia, el mecanismo propuesto podría constituir un mecanismo general para ligandos del surco menor de pequeño tamaño, aunque esta afirmación tendrá que ser confirmada en futuros estudios con otros ligandos típicos del surco menor.

A través de un estudio de la fotofísica de este ligando se probó que la bis-benzamidina induce una desactivación (*quenching*) sobre el Oregon Green. Este *quenching* desaparece al complejarse el ligando con el ADN, de modo que este cambio en la luminosidad permite la obtención de las constantes cinéticas de asociación y disociación mediante FCS.

La modificación de este ligando aumentando el número de enlaces en la unión entre la bis-benzamidina y el Oregon Green permitió demostrar que, tanto la eficiencia del *quenching* como los valores de la constante cinética de disociación con el ADN, pueden ser modificados variando la longitud de la unión entre ambas moléculas.

Capítulo V: Estudio de la Dinámica de Plegamiento de Riboswitches mediante FRET de Moléculas Individuales y TIRF.

Como se comentó anteriormente, por estudiar moléculas en difusión libre, FCS está restringida al estudio de sistemas que presentan dinámicas rápidas, y por tanto no es útil para estudiar la cinética en otros tantos procesos biológicos que ocurren a escalas temporales significativamente más largas que el tiempo de difusión de una molécula a través del volumen de detección.

El estudio de estos sistemas también se puede abarcar por medio de técnicas de detección SMF, aunque requieren de una estrategia diferente a la utilizada en FCS, que consiste en la inmovilización de las moléculas sobre una superficie, permitiendo tiempos de observación mucho más largos que aquellos que se dan en montajes en las que éstas se encuentran difundiendo libremente.

En el Capítulo V de esta tesis se recogen los resultados obtenidos durante una estancia en el Laboratorio de Biofísica y Dinámica Biomolecular del Dr. Penedo, en la Universidad de St. Andrews (Escocia). En este estudio se aplica dicha estrategia de inmovilización para estudiar el plegamiento de aptámeros de ARN, utilizando la *microscopia de Fluorescencia de Reflexión Interna Total* (TIRF) en combinación con la *Transmisión de Energía de Resonancia* de moléculas individuales (smFRET) para identificar transiciones en el cambio de conformación y caracterizar estos cambios en la ruta de desnaturalización química de un *riboswitch* (ARNm), a la vez que se proporciona información sobre la cinética del proceso.

Un *riboswitch* es un fragmento de ARNm que es capaz de unirse específicamente a un metabolito (ligando). La parte de la secuencia de ARN donde se da esta unión se denomina aptámero, como resultado éste cambia su conformación (estructura terciaria) afectando a una segundo dominio denominado plataforma de expresión responsable de la regulación de la expresión génica. El aptámero puede encontrarse en distintas conformaciones, plegado o desplegado, siendo también sensible a la presencia de cationes monovalentes y divalentes.

Concretamente la combinación de smFRET y la desnaturalización química fue utilizada para evaluar comparativamente la dinámica de plegamiento y la estabilidad de la forma sin ligando del aptámero del *add riboswitch* utilizando tres agentes desnaturalizantes: prolina, betaína y formamida. Se comprobó la compatibilidad de estos tres agentes desnaturalizantes, que se utilizan por primera vez en sm-FRET, con los protocolos de pasivado de la superficie e inmovilización de las moléculas.

Los resultados mostraron que para la formamida la concentración podía incrementarse hasta alcanzar una única población de aptámeros en estado desplegado en presencia de cationes magnesio y sodio. Se observó que a mayores concentraciones de formamida se induce un cambio en el índice de refracción que introduce distorsiones significativas en la onda evanescente generada en la interfase cuarzo-agua. Tanto para la prolina como para la betaína, ya a menores concentraciones el anclaje de las cadenas de ARN a la superficie empieza a romperse antes de que el equilibrio se mueva completamente al estado desplegado.

También se demuestra que la desnaturalización química puede ajustarse de tal modo que afecte únicamente a las interacciones terciarias de la estructura del ARN, siendo posible

romper también la estructura secundaria cuando eliminamos del medio los cationes en presencia del agente desnaturalizante. Se demostró también que aptámeros individuales pueden someterse a ciclos secuenciales de plegamientos y desplegamientos y preservar intacta su capacidad de adoptar la conformación nativa plegada.

El efecto en la estructura terciaria se estudió para los tres agentes desnaturalizantes antes mencionados, llevando a cabo también una comparación con datos medidos previamente para un agente desnaturalizante típico como es la urea. Los resultados indican que el efecto global de estos agentes desnaturalizantes sobre la forma libre (sin ligando) del aptámero tiene lugar principalmente mediante la desestabilización del estado plegado. Este hecho es consistente con el modelo de *búsqueda conformacional*, donde el paso limitante de la velocidad para el plegamiento de la forma libre del aptámero conlleva la formación de contactos estables a nivel terciario y que la adición de agente desnaturalizante hace la formación de estas interacciones de la conformación nativa menos favorables.

Experimentos en presencia de ligando utilizando formamida indica que la formación del aptámero complejado (con el ligando) protege el estado plegado contra la desnaturalización.

El efecto de cationes monovalentes y divalentes en presencia de formamida también fue estudiado de manera preliminar, mostrando que el efecto de este agente desnaturalizante puede ser neutralizado incrementando la concentración de iones magnesio. La dependencia de la concentración de magnesio observada sobre el efecto de la formamida abre la puerta a futuros estudios utilizando desnaturalización química de moléculas individuales para desvelar el papel mecanístico que juegan los cationes divalentes. Contrariamente a lo que ocurre con cambios en la constante de equilibrio entre los estados plegado y desplegado inducidos por agentes desnaturalizantes o por el magnesio, el incremento de iones sodio afecta principalmente a la constante cinética de plegamiento en lugar de a la de desplegamiento, sugiriendo que la estabilidad de estado plegado en presencia de agente desnaturalizante es limitada por la ausencia de iones metálicos divalentes. Sin embargo, para poder realizar esta afirmación de manera concluyente, se han de tomar nuevos datos para obtener valores cuantitativos para las constantes cinéticas.

References

Al-Soufi, W., Reija, B., Novo, M., Felekyan, S., Kühnemuth, R. and Seidel, C.A.M. 2005, "Fluorescence Correlation Spectroscopy, a Tool to investigate Supramolecular Dynamics: Inclusion Complexes of Pyronines with Cyclodextrin", *Journal of the American Chemical Society,* vol. 127, no. 24, pp. 8775-8784.

Al-Soufi, W., Reija, B., Felekyan, S., Seidel, C.A. and Novo, M. 2008, "Dynamics of supramolecular association monitored by fluorescence correlation spectroscopy", *Chemphyschem: a European journal of chemical physics and physical chemistry,* vol. 9, no. 13, pp. 1819-1827.

Baliga, R. and Crothers, D.M. 2000a, "The Kinetic Basis for Sequence Discrimination by Distamycin A", *Journal of the American Chemical Society,* vol. 122, no. 47, pp. 11751-11752.

Baliga, R. and Crothers, D.M. 2000b, "On the kinetics of distamycin binding to its target sites on duplex DNA", *Proceedings of the National Academy of Sciences,* vol. 97, no. 14, pp. 7814-7818.

Barbas, C.F., Burton, D.R., Scott, J.K. and Silverman, G.J. 2007, "Quantitation of DNA and RNA", *Cold Spring Harbor Protocols,* vol. 2007, no. 11, pp. pdb.ip47.

Batey, R.T., Gilbert, S.D. and Montange, R.K. 2004, "Structure of a natural guanine-responsive riboswitch complexed with the metabolite hypoxanthine", *Nature,* vol. 432, no. 7015, pp. 411-415.

Bell, C.A., Hall, J.E., Kyle, D.E., Grogl, M., Ohemeng, K.A., Allen, M.A. and Tidwell, R.R. 1990, "Structure-activity relationships of analogs of pentamidine against Plasmodium falciparum and Leishmania mexicana amazonensis.", *Antimicrobial Agents and Chemotherapy,* vol. 34, no. 7, pp. 1381-1386.

Berg, O.G. and von Hippel, P.H. 1985, "Diffusion-controlled macromolecular interactions", *Annual Review of Biophysics and Biophysical Chemistry,* vol. 14, no. 1, pp. 131-158.

Blouin, S., Mulhbacher, J., Penedo, J.C. and Lafontaine, D.A. 2009, "Riboswitches: ancient and promising genetic regulators", *ChemBioChem,* vol. 10, no. 3.

Böhmer, M. and Enderlein, J. 2003, "Fluorescence Spectroscopy of Single Molecules under Ambient Conditions: Methodology and Technology", *ChemPhysChem,* vol. 4, no. 8, pp. 792-808.

Bohne, C. 2006, "Supramolecular Dynamics Studied Using Photophysics", *Langmuir,* vol. 22, no. 22, pp. 9100-9111.

Bordello, J., Reija, B., Al-Soufi, W. and Novo, M. 2009, "Host-assisted guest self-assembly: enhancement of the dimerization of pyronines Y and B by gamma-cyclodextrin", *Chemphyschem : a European journal of chemical physics and physical chemistry,* vol. 10, no. 6, pp. 931-939.

Bordello, J., Novo, M. and Al-Soufi, W. 2010, "Exchange-Dynamics of a Neutral Hydrophobic Dye in Micellar Solutions Studied by Fluorescence Correlation Spectroscopy", *Journal of Colloid And Interface Science,* vol. 345, pp. 369-376.

Bordello, J., Sánchez, M.I., Vázquez, M.E., Mascareñas, J.L., Al-Soufi, W. and Novo, M. 2012, "Single-Molecule Approach to DNA Minor-Groove Association Dynamics", *Angewandte Chemie International Edition,* vol. 51, no. 30, pp. 7541-7544.

Brenner, M.D., Scanlan, M.S., Nahas, M.K., Ha, T. and Silverman, S.K. 2010, "Multivector Fluorescence Analysis of the xpt Guanine Riboswitch Aptamer Domain and the Conformational Role of Guanine", *Biochemistry,* vol. 49, no. 8, pp. 1596-1605.

Breusegem, S.Y., Sadat-Ebrahimi, S., Douglas, K.T., Clegg, R.M. and Loontiens, F.G. 2001, "Increased stability and lifetime of the complex formed between DNA and meta-phenyl-substituted hoechst dyes as studied by fluorescence titrations and stopped-flow kinetics", *Journal of Molecular Biology,* vol. 308, no. 4, pp. 649-663.

Breusegem, S.Y., Clegg, R.M. and Loontiens, F.G. 2002, "Base-sequence specificity of Hoechst 33258 and DAPI binding to five (A/T)4 DNA sites with kinetic evidence for more than one high-affinity Hoechst 33258-AATT complex", *Journal of Molecular Biology,* vol. 315, no. 5, pp. 1049-1061.

Buck, J., Fürtig, B., Noeske, J., Wöhnert, J. and Schwalbe, H. 2007, "Time-resolved NMR methods resolving ligand-induced RNA folding at atomic resolution", *Proceedings of the National Academy of Sciences,* vol. 104, no. 40, pp. 15699-15704.

Cao, Y. and Li, H. 2011, "Dynamics of Protein Folding and Cofactor Binding Monitored by Single-Molecule Force Spectroscopy", *Biophysical journal,* vol. 101, no. 8, pp. 2009-2017.

Cecconi, C., Shank, E.A., Marqusee, S. and Bustamante, C.J. 2007, "Studying protein folding with laser tweezers", *Proceedings of the International School of Physics "Enrico Fermi",* vol. 165th, pp. 145-160.

Chen, Y., Muller, J.D., So, P.T.C. and Gratton, E. 1999, "The Photon Counting Histogram in Fluorescence Fluctuation Spectroscopy", *Biophysical journal,* vol. 77, no. 1, pp. 553-567.

Dalgarno, P.A., Bordello, J., Morris, R., St-Pierre, P., Dubé, A., Samuel, I.D.W., Lafontaine, D.A. and Penedo, J.C. 2013, "Single-molecule chemical denaturation of riboswitches", *Nucleic acids research.*

Del Poeta, M., Schell, W.A., Dykstra, C.C., Jones, S., Tidwell, R.R., Czarny, A., Bajic, M., Bajic, M., Kumar, A., Boykin, D. and Perfect, J.R. 1998, "Structure-In Vitro Activity Relationships of Pentamidine Analogues and Dication-Substituted Bis-Benzimidazoles as New Antifungal Agents", *Antimicrobial Agents and Chemotherapy,* vol. 42, no. 10, pp. 2495-2502.

Demchenko, A.P. 2009, *Introduction to Fluorescence Sensing,* Introduction to Fluorescence Sensing, Springer.

Eggeling, C., Widengren, J., Rigler, R. and Seidel, C.A.M. 1998, "Photobleaching of fluorescent dyes under conditions used for single-molecule detection: evidence of two-step photolysis", *Analytical Chemistry,* vol. 70, no. 13, pp. 2651-2659.

Elson, E.L. and Magde, D. 1974, "Fluorescence correlation spectroscopy. I. Conceptual basis and theory", *Biopolymers,* vol. 13, no. 1, pp. 1-27.

Elson, E. 2011, *Fluorescence Correlation Spectroscopy: Past, Present, Future*, Cell Press.

Enderlein, J., Gregor, I., Patra, D., Dertinger, T. and Kaupp, U.B. 2005, "Performance of Fluorescence Correlation Spectroscopy for Measuring Diffusion and Concentration", *Chemphyschem,* vol. 6, no. 11, pp. 2324-2336.

Eriksson, M., Karlsson, H.J., Westman, G. and Åkerman, B. 2003, "Groove-binding unsymmetrical cyanine dyes for staining of DNA: dissociation rates in free solution and electrophoresis gels", *Nucleic acids research,* vol. 31, no. 21, pp. 6235-6242.

Eriksson, M., Westerlund, F., Mehmedovic, M., Lincoln, P., Westman, G., Larsson, A. and Åkerman, B. 2006, "Comparing mono- and divalent DNA groove binding cyanine dyes - Binding geometries, dissociation rates, and fluorescence properties", *Biophysical chemistry,* vol. 122, no. 3, pp. 195-205.

Fang, X., Pan, T. and Sosnick, T.R. 1999, "Thermodynamic Framework and Cooperativity in the Tertiary Folding of a Mg^{2+}-Dependent Ribozyme", *Biochemistry,* vol. 38, no. 51, pp. 16840-16846.

Fernandes, M., Ortega, A., Lopez Martinez, M. and García De La Torre, J. 2002, "Calculation of hydrodynamic properties of small nucleic acids from their atomic structure", *Nucleic acids research,* vol. 30, no. 8, pp. 1782.

Freire, S., Bordello, J., Granadero, D., Al Soufi, W. and Novo, M. 2010, "Role of Electrostatic and Hydrophobic Forces in the Interaction of Ionic Dyes with Charged Micelles", *Photochemical & Photobiological Sciences,* vol. 9, pp. 687-696.

Gell, C., Brockwell, D. and Smith, A. 2006, *Handbook of Single Molecule Fluorescence Spectroscopy,* Oxford University Press, USA.

Gendron, P.O., Avaltroni, F. and Wilkinson, K.J. 2008, "Diffusion coefficients of several rhodamine derivatives as determined by pulsed field gradient-nuclear magnetic resonance and fluorescence correlation spectroscopy", *Journal of Fluorescence,* vol. 18, no. 6, pp. 1093-1101.

Gilbert, S.D., Stoddard, C.D., Wise, S.J. and Batey, R.T. 2006, "Thermodynamic and Kinetic Characterization of Ligand Binding to the Purine Riboswitch Aptamer Domain", *Journal of Molecular Biology,* vol. 359, no. 3, pp. 754-768.

Granadero, D., Bordello, J., Pérez-Alvite, M.J., Novo, M. and Al-Soufi, W. 2010b, "Host-Guest Complexation Studied by Fluorescence Correlation Spectroscopy: Adamantane-Cyclodextrin Inclusion", *International Journal of Molecular Sciences,* vol. 11, no. 1, pp. 173-188.

Ha, T., Ting, A.Y., Liang, J., Caldwell, W.B., Deniz, A.A., Chemla, D.S., Schultz, P.G. and Weiss, S. 1999, "Single-molecule fluorescence spectroscopy of enzyme conformational dynamics and cleavage mechanism", *Proceedings of the National Academy of Sciences,* vol. 96, no. 3, pp. 893-898.

Ha, T. and Tinnefeld, P. 2012, "Photophysics of Fluorescent Probes for Single-Molecule Biophysics and Super-Resolution Imaging", *Annual Review of Physical Chemistry,* vol. 63, no. 1, pp. 595-617.

Haq, I., Ladbury, J.E., Chowdhry, B.Z., Jenkins, T.C. and Chaires, J.B. 1997, "Specific binding of hoechst 33258 to the d(CGCAAATTTGCG)2 duplex: calorimetric and spectroscopic studies", *Journal of Molecular Biology,* vol. 271, no. 2, pp. 244-257.

Haran, G. 2003, "Single-molecule fluorescence spectroscopy of biomolecular folding", *Journal of Physics: Condensed Matter,* vol. 15, no. 32, pp. R1291-R1317.

Haustein, E. and Schwille, P. 2004, "Single-molecule spectroscopic methods", *Current opinion in structural biology,* vol. 14, no. 5, pp. 531-540.

Heppell, B., Blouin, S., Dussault, A., Mulhbacher, J., Ennifar, E., Penedo, J.C. and Lafontaine, D.A. 2011, "Molecular insights into the ligand-controlled organization of the SAM-I riboswitch", *Nat Chem Biol,* vol. 7, no. 6, pp. 384-392.

Hinterdorfer, P. and Oijen, A. 2009, *Handbook of Single-Molecule Biophysics,* Springer, New York.

Johnson-Buck, A., Blanco, M. and Walter, N. 2013, "Single-Molecule Fluorescence Resonance Energy Transfer" in , ed. G.K. Roberts, Springer Berlin Heidelberg, pp. 2329-2335.

Kapanidis, A. and Weiss, S. 2002, "Fluorescent probes and bioconjugation chemistries for single-molecule fluorescence analysis of biomolecules", *The Journal of chemical physics,* vol. 117, no. 24, pp. 10953-10964.

Kapusta, P. 2010, "Absolute Diffusion Coefficients: Compilation of Reference Data for FCS Calibration" Picoquant Application Notes.

Kask, P., Palo, K., Ullmann, D. and Gall, K. 1999, "Fluorescence-Intensity Distribution Analysis and Its Application in Biomolecular Detection Technology", *Proceedings of the National Academy of Sciences of the United States of America,* vol. 96, no. 24, pp. 13756-13761.

Kawakami, M., Byrne, K., Brockwell, D.J., Radford, S.E. and Smith, D.A. 2006, "Viscoelastic Study of the Mechanical Unfolding of a Protein by AFM", *Biophysical journal,* vol. 91, no. 2, pp. L16-L18.

Krichevsky, O. and Bonnet, G. 2002, "Fluorescence correlation spectroscopy: the technique and its applications", *Reports on Progress in Physics,* vol. 65, pp. 251-297.

Kühnemuth, R. and Seidel, C.A.M. 2001, "Principles of single molecule multiparameter fluorescence spectroscopy", *Single Molecules,* vol. 2, no. 4, pp. 251-254.

Kuzmenkina, E.V., Heyes, C.D. and Nienhaus, G.U. 2005, "Single-molecule Förster resonance energy transfer study of protein dynamics under denaturing conditions", *Proceedings of the National Academy of Sciences of the United States of America,* vol.102, no.43, pp.15471-15476.

Lakowicz, J.R. 2006, *Principles of Fluorescence Spectroscopy,* Springer, USA.

Lambert, D. and Draper, D.E. 2007, "Effects of Osmolytes on RNA Secondary and Tertiary Structure Stabilities and RNA-Mg2+ Interactions", *Journal of Molecular Biology,* vol. 370, no. 5, pp. 993-1005.

Laughton, C. and Luisi, B. 1999, "The mechanics of minor groove width variation in DNA, and its implications for the accommodation of ligands", *Journal of Molecular Biology,* vol. 288, no. 5, pp. 953-963.

Lee, M., Gal, M., Frydman, L. and Varani, G. 2010, "Real-time multidimensional NMR follows RNA folding with second resolution", *Proceedings of the National Academy of Sciences.*

Lemay, J., Desnoyers, G., Blouin, S., Heppell, B., Bastet, L., St-Pierre, P., MassÃ©, E. and Lafontaine, D.A. 2011, "Comparative Study between Transcriptionally- and Translationally-Acting Adenine Riboswitches Reveals Key Differences in Riboswitch Regulatory Mechanisms", *PLoS Genet,* vol. 7, no. 1, pp. e1001278.

Lemay, J., Penedo, J.C., Tremblay, R., Lilley, D.M.J. and Lafontaine, D.A. 2006, "Folding of the Adenine Riboswitch", *Chemistry & biology,* vol. 13, no. 8, pp. 857-868.

Lemay, J., Penedo, J.C., Mulhbacher, J. and Lafontaine, D.A. 2009, "Molecular Basis of RNA-Mediated Gene Regulation on the Adenine Riboswitch by Single-Molecule Approaches; Riboswitches" in , ed. A. Serganov, Humana Press, pp. 65-76.

Lemay, J. and Lafontaine, D.A. 2007, "Core requirements of the adenine riboswitch aptamer for ligand binding", *RNA,* vol. 13, no. 3, pp. 339-350.

Lin, J. and Thirumalai, D. 2008, "Relative Stability of Helices Determines the Folding Landscape of Adenine Riboswitch Aptamers", *Journal of the American Chemical Society,* vol. 130, no. 43, pp. 14080-14081.

Margittai, M., Widengren, J., Schweinberger, E., Schroeder, G.F., Felekyan, S., Haustein, E., Koenig, M., Fasshauer, D., Grubmueller, H., Jahn, R. and Seidel, C.A.M. 2003, "Single-molecule fluorescence resonance energy transfer reveals a dynamic equilibrium between closed and open conformations of syntaxin 1", *Proceedings of the National Academy of Sciences of the United States of America,* vol. 100, no. 26, pp. 15516-15521.

Michalet, X., Kapanidis, A.N., Laurence, T., Pinaud, F., Doose, S., Pflughoefft, M. and Weiss, S. 2003, "The power and prospects of fluorescence microscopies and spectroscopies", *Annual Review of Biophysics and Biomolecular Structure,* vol. 32, no. 1, pp. 161-182.

Michalet, X., Weiss, S. and Jäger, M. 2006, "Single-Molecule Fluorescence Studies of Protein Folding and Conformational Dynamics", *Chemical reviews,* vol. 106, no. 5, pp. 1785-1813.

Moerner, W.E. and Fromm, D. 2003, "Methods of single-molecule fluorescence spectroscopy and microscopy", *Review of Scientific Instruments,* vol. 74, no. 8, pp. 3597-3619.

Montange, R.K. and Batey, R.T. 2008, "Riboswitches: Emerging Themes in RNA Structure and Function", *Annual Review of Biophysics,* vol. 37, no. 1, pp. 117-133.

Muller, C., Loman, A., Pacheco, V., Koberling, F., Willbold, D. and Richtering, W. 2008a, "Precise measurement of diffusion by multi-color dual-focus fluorescence correlation spectroscopy", *Europhysics Letters,* vol. 83, no. 4.

Muller, C.B., Loman, A., Richtering, W. and Enderlein, J. 2008b, "Dual-Focus Fluorescence Correlation Spectroscopy of Colloidal Solutions: Influence of Particle Size", *Journal of Physical Chemistry B,* vol. 112, no. 28, pp. 8236-8240.

Murphy, M.C., Rasnik, I., Cheng, W., Lohman, T.M. and Ha, T. 2004, "Probing Single-Stranded DNA Conformational Flexibility Using Fluorescence Spectroscopy", *Biophysical journal,* vol. 86, no. 4, pp. 2530-2537.

Myers, J.K., Nick Pace, C. and Martin Scholtz, J. 1995, "Denaturant m values and heat capacity changes: Relation to changes in accessible surface areas of protein unfolding", *Protein Science,* vol. 4, no. 10, pp. 2138-2148.

Neidle, S. 2001, "DNA minor-groove recognition by small molecules", *Natural product reports,* vol. 18, no. 3, pp. 291-309.

Neidle, S. 2008, "Principles of Small Molecule-DNA Recognition" in *Principles of Nucleic Acid Structure* Academic Press, New York, pp. 132-203.

Noeske, J., Buck, J., Fürtig, B., Nasiri, H.R., Schwalbe, H. and Wöhnert, J. 2007, "Interplay of 'induced fit' and preorganization in the ligand induced folding of the aptamer domain of the guanine binding riboswitch", *Nucleic acids research,* vol. 35, no. 2, pp. 572-583.

Novo, M., Felekyan, S., Seidel, C.A.M. and Al-Soufi, W. 2007, "Dye-Exchange Dynamics in Micellar Solutions Studied by Fluorescence Correlation Spectroscopy", *Journal of Physical Chemistry B,* vol. 111, no. 14, pp. 3614-3624.

Novo, M., Granadero, D., Bordello, J. and Al-Soufi, W. 2011, "Host–guest association studied by fluorescence correlation spectroscopy", *Journal of Inclusion Phenomena and Macrocyclic Chemistry,* pp. 1-10.

Pace, T.C.S. and Bohne, C. 2008, "Dynamics of Guest Binding to Supramolecular Systems: Techniques and Selected Examples", *Advances in Physical Organic Chemistry,* vol. 42, pp. 167-223.

Pan, J., Thirumalai, D. and Woodson, S.A. 1997, "Folding of RNA involves parallel pathways", *Journal of Molecular Biology,* vol. 273, no. 1, pp. 7-13.

Peng, Q. and Li, H. 2008, "Atomic force microscopy reveals parallel mechanical unfolding pathways of T4 lysozyme: Evidence for a kinetic partitioning mechanism", *Proceedings of the National Academy of Sciences,* vol. 105, no. 6, pp. 1885-1890.

Pikovskaya, O., Polonskaia, A., Patel, D.J. and Serganov, A. 2011, "Structural principles of nucleoside selectivity in a 2'-deoxyguanosine riboswitch", *Nat Chem Biol,* vol. 7, no. 10, pp. 748-755.

Rasnik, I., McKinney, S.A. and Ha, T. 2006, "Nonblinking and long-lasting single-molecule fluorescence imaging", *Nat Meth,* vol. 3, no. 11, pp. 891-893.

Reija, B., Al-Soufi, W., Novo, M. and Vázquez Tato, J. 2005, "Specific interactions in the inclusion complexes of Pyronines Y and B with beta-cyclodextrin", *Journal of Physical Chemistry B,* vol. 109, no. 4, pp. 1364-1370.

Rigler, R. and Elson, E.S. 2001, *Fluorescence correlation spectroscopy: theory and applications,* Springer Verlag, Berlin.

Roth, A. and Breaker, R.R. 2009, "The structural and functional diversity of metabolite-binding riboswitches", *Annual Review of Biochemistry,* vol. 78, pp. 305-334.

Roy, R., Hohng, S. and Ha, T. 2008, "A practical guide to single-molecule FRET", *Nature methods,* vol. 5, no. 6, pp. 507-516.

Rüttinger, S., Buschmann, V., Krämer, B., Erdmann, R., Macdonald, R. and Koberling, F. 2008, "Comparison and accuracy of methods to determine the confocal volume for quantitative fluorescence correlation spectroscopy", *Journal of microscopy,* vol. 232, no. 2, pp. 343-352.

Sauer, M., Hofkens, J. and Enderlein, J. 2011, "Fluorescence Correlation Spectroscopy" in *Handbook of Fluorescence Spectroscopy and Imaging* Wiley-VCH Verlag GmbH & Co. KGaA, pp. 93-146.

Schwalbe, H., Buck, J., Fürtig, B., Noeske, J. and Wöhnert, J. 2007, "Structures of RNA Switches: Insight into Molecular Recognition and Tertiary Structure", *Angewandte Chemie International Edition,* vol. 46, no. 8, pp. 1212-1219.

Selvin, P.R. 2000, "The renaissance of fluorescence resonance energy transfer", *Nature structural biology,* vol. 7, no. 9, pp. 730-734.

Selvin, P.R. and Ha, T. 2008, *Single-molecule techniques: a laboratory manual,* Cold Spring Harbor, N.Y.: Cold Spring Harbor Laboratory Press, c2008.

Serganov, A., Yuan, Y., Pikovskaya, O., Polonskaia, A., Malinina, L., Phan, A.T., Hobartner, C., Micura, R., Breaker, R.R. and Patel, D.J. 2004, "Structural Basis for Discriminative Regulation of Gene Expression by Adenine- and Guanine-Sensing mRNAs", *Chemistry & biology,* vol. 11, no. 12, pp. 1729-1741.

Shelton, V.M., Sosnick, T.R. and Pan, T. 1999, "Applicability of Urea in the Thermodynamic Analysis of Secondary and Tertiary RNA Folding†", *Biochemistry,* vol. 38, no. 51, pp. 16831-16839.

Sosnick, T.R. and Pan, T. 2003, "RNA folding: models and perspectives", *Current opinion in structural biology,* vol. 13, no. 3, pp. 309-316.

Tanious, F.A., Veal, J.M., Buczak, H., Ratmeyer, L.S. and Wilson, W.D. 1992, "DAPI (4',6-diamidino-2-phenylindole) binds differently to DNA and RNA: minor-groove binding at AT sites and intercalation at AU sites", *Biochemistry,* vol. 31, no. 12, pp. 3103-3112.

Thompson, N.L. 1991, "Fluorescence Correlation Spectroscopy" in *Topics in Fluorescence Spectroscopy. Techniques*, ed. J.R. Lakowicz, Plenum Press, New York, pp. 337-378.

Tinoco, I. and Gonzalez, R.L. 2011, *Biological mechanisms, one molecule at a time.*

Tirado, M.M., Martínez, C.L. and de la Torre, J.G. 1984, "Comparison of theories for the translational and rotational diffusion coefficients of rod-like macromolecules. Application to short DNA fragments", *The Journal of chemical physics,* vol. 81, pp. 2047.

Valeur, B. 2002, *Molecular Fluorescence: Principles and Applications,* Wiley-VCH, Germany.

Vazquez, O., Sanchez, M.I., Martinez-Costas, J., Vazquez, M.E. and Mascarenas, J.L. 2010, "Bis-4-aminobenzamidines: versatile, fluorogenic A/T-selective dsDNA binders", *Organic letters,* vol. 12, no. 2, pp. 216-219.

Vuzman, D., Azia, A. and Levy, Y. 2010, "Searching DNA via a "Monkey Bar" mechanism: the significance of disordered tails", *Journal of Molecular Biology,* vol. 396, no. 3, pp. 674-684.

Walter, N.G., Huang, C.Y., Manzo, A.J. and Sobhy, M.A. 2008, "Do-it-yourself guide: how to use the modern single-molecule toolkit", *Nature Methods,* vol. 5, no. 6, pp. 475-489.

Waring, M.J. 2006, *Sequence-specific DNA binding agents,* Royal Society of Chemistry.

Weiss, S. 2000, "Measuring Conformational Dynamics of Biomolecules by Single Molecule Fluorescence Spectroscopy", *Nature structural biology,* vol. 7, no. 9, pp. 724-729.

Wilson, W.D., Tanious, F.A., Barton, H.J., Jones, R.L., Fox, K., Wydra, R.L. and Strekowski, L. 1990, "DNA sequence dependent binding modes of 4',6-diamidino-2-phenylindole (DAPI)", *Biochemistry,* vol. 29, no. 36, pp. 8452-8461.

Zander, C., Enderlein, J. and Keller, R.A. 2002, *Single-Molecule Detection in Solution-Methods and Applications,* VCH-Wiley, Berlin/New York.

List of Publications and Contributions to Conferences

Papers:

Bordello, Jorge; Reija, Belén; Al-Soufi, Wajih; Novo, Mercedes. *Host-Assisted Guest Self-Assembly: Enhancement of the Dimerization of Pyronines Y and B by γ-Cyclodextrin.* ChemPhysChem (2009), 10(6), 931-939.

Freire, Sonia; **Bordello, Jorge**; Granadero, Daniel; Al-Soufi, Wajih; Novo, Mercedes. *Role of Electrostatic and Hydrophobic Forces in the Interaction of Ionic Dyes with Charged Micelles.* Photochemical & Photobiological Sciences (2010), 9(5), 687-696.

Granadero, Daniel; **Bordello, Jorge**; Pérez-Alvite, María Jesús; Novo, Mercedes; Al-Soufi, Wajih. *Host-Guest Complexation studied by FCS: Adamantane-Cyclodextrin Inclusion.* International Journal of Molecular Sciences (2010), 11, 173-188.

Bordello, Jorge; Novo, Mercedes; Al-Soufi, Wajih. *Exchange-Dynamics of a Neutral Hydrophobic Dye in Micellar Solutions studied by Fluorescence Correlation Spectroscopy.* Journal of Colloid and Interface Science (2010), 345(2), 369-376.

Novo, Mercedes; Granadero, Daniel; **Bordello, Jorge**; Al-Soufi, Wajih. *Host-Guest Association studied by FCS.* Journal of Inclusion Phenomena and Macrocyclic Chemistry (2011), 70(3-4), 259-268.

Bordello, Jorge; Sánchez, Mateo I.; Vázquez, M. Eugenio; Mascareñas, José L.; Al-Soufi, Wajih and Novo, Mercedes. *Single-Molecule Approach to DNA Minor-Groove Association Dynamics.* Angewandte Chemie International Edition (2012), 51, 7541–7544.

Dalgarno, Paul A.; **Bordello, Jorge;** Morris, Rhodri; St-Pierre, Patrick; Dubé, Audrey; Samuel, Ifor D.W.; Lafontaine, Daniel A. and Penedo, J. Carlos. *Single-Molecule Chemical Denaturation of Riboswitches.* Nucleic Acids Research (2013), vol 41, no. 7, pp. 4253-4265.

Piñeiro, Lucas; Freire, Sonia; **Bordello, Jorge**; Novo, Mercedes and Al-Soufi, Wajih. *Dye Exchange in Micellar Solutions. Quantitative Analysis of Bulk and Single Molecule Fluorescence Titrations.* Submitted.

Conference proceedings:

Novo, Mercedes; **Bordello, Jorge**; Granadero, Daniel; Freire, Sonia; Al-Soufi, Wajih. *Supramolecular Host-Guest Complexes between Coumarin 460 and Cyclodextrins: A Matter of Size.* Proceedings of ECSOC-12, The Twelfth International Electronic Conference on Synthetic Organic Chemistry, November 1-30, 2008. Editor: Julio A. Seijas & M. Pilar Vázquez Tato. CD-ROM edition. ISBN 3-906980-20-0. Published in 2008 by MDPI, Basel, Switzerland.

Granadero, Daniel; **Bordello, Jorge**; Novo, Mercedes; Al-Soufi, Wajih. *Complexation of Synthetic Organic Dye Dapoxyl with Cyclodextrins studied by Fluorescence Spectroscopy.* Proceedings of ECSOC-13, The Thirteenth International Electronic Conference on Synthetic Organic Chemistry, November 1-30, 2009. Editor: Julio A. Seijas & M. Pilar Vázquez-Tato. CD-ROM edition. ISBN: 3-906980-23-5. Published in 2009 by MDPI, Basel, Switzerland.

Al-Soufi, Wajih; Granadero, Daniel; **Bordello, Jorge**; Freire, Sonia; Pineiro, Lucas; Novo, Mercedes. *Evidence of Cyclodextrin Aggregation obtained with FCS.* Proceedings of ECSOC-14, The Fourteenth International Electronic Conference on Synthetic Organic Chemistry, November 1-30, 2010. Editor: Julio A. Seijas & M. Pilar Vázquez-Tato. CD-ROM edition. ISBN 3-906980-24-3. Published in 2010 by MDPI, Basel, Switzerland.

Conferences contributions:

Mercedes Novo, **Jorge Bordello**, Belén Reija, Wajih Al-Soufi. *Estudio Fluorimétrico de la Complejación de Pironinas con γ-Ciclodextrina.* VII Congreso de Fotoquímica. Logroño (Spain). June 22-24, 2005.

Jorge Bordello, Mercedes Novo, Sonia Freire, Belén Reija and Wajih Al-Soufi. *Enhanced-Sensitivity Probes for the Study of Dye-Exchange Dynamics in Micellar Solutions by FCS.* XIX IUPAC Conference on Physical Organic Chemistry. Santiago de Compostela (Spain). Jul. 13-18, 2008.

Sonia Freire, Wajih Al-Soufi, **Jorge Bordello**, Belén Reija and Mercedes Novo. *Interactions between Rhodamine 123 and Surfactant Micelles.* XIX IUPAC Conference on Physical Organic Chemistry. Santiago de Compostela, Spain. July 13-18, 2008.

Ramos-Cabrer, P.; Argibay, Bárbara; Agulla, Jesús; **Bordello, Jorge**; Granadero, Daniel; Al-Soufi, Wajih; Brea, David; Sobrino, T.; Castillo, José. *Towards the Optimization of Gd-doped Liposomes for their use in Stroke Therapies.* 4th European Molecular Imaging Meeting of the European Society for Molecular Imaging ESMI. Barcelona (Spain). May 27-30, 2009.

Jorge Bordello, Daniel Granadero, Mercedes Novo y Wajih Al-Soufi. *The Influence of Hydrophobic Fluorescence Probes on Surfactant Premicellization studied by FCS.* 11th International Conference on Methods and Applications of Fluorescence (MAF11). Budapest (Hungary). Sep. 6-9, 2009.

Wajih Al-Soufi, **Jorge Bordello**, Daniel Granadero y Mercedes Novo. *Supramolecular Association studied by FCS.* 11th International Conference on Methods and Applications of Fluorescence (MAF11). Budapest (Hungary). Sep. 6-9, 2009.

Daniel Granadero, **Jorge Bordello**, Mercedes Novo y Wajih Al-Soufi. *Size-Selective Complexation of Dapoxyl by Cyclodextrins studied by Fluorescence Spectroscopy.* 11th International Conference on Methods and Applications of Fluorescence (MAF11). Budapest (Hungary). Sep. 6-9, 2009.

Jorge Bordello, Daniel Granadero, Mercedes Novo y Wajih Al-Soufi. *Fluorescence Correlation Spectroscopy as a Tool to study the Interaction Dye-Surfactant during the Micellization Process.* IX Congreso de Fotoquímica. Bilbao (Spain). Sep. 21-23, 2009.

Daniel Granadero, **Jorge Bordello**, Mercedes Novo y Wajih Al-Soufi. *Estudio Fluorescente de la Complejación del Dapoxyl por Ciclodextrinas: Efecto del tamaño de la cavidad en el tipo y fortaleza de los complejos.* IX Congreso de Fotoquímica. Bilbao (Spain). Sep. 21-23, 2009.

Mercedes Novo, Sonia Freire, D. Granadero, **Jorge Bordello** y Wajih Al-Soufi. *Papel de las Fuerzas Electrostáticas e Hidrofóbicas en las Interacciones entre Rodamina 123 y diferentes tipos de Tensioactivos.* IX Congreso de Fotoquímica. Bilbao (Spain). Sep. 21-23, 2009.

Sonia Freire, **Jorge Bordello**, Lucas Piñeiro, Wajih Al-Soufi, and Mercedes Novo. *Potential Fluorescence Markers for Early beta-Amyloid Aggregates.* XXV International Conference on Photochemistry (ICP2011). Beijing, August 7-12, 2011.

Wajih Al-Soufi, **Jorge Bordello**, Mateo I. Sánchez, M. Eugenio Vázquez, José L. Mascareñas, and Mercedes Novo. *Supramolecular Association Dynamics studied by FCS.* International Bunsen Discussion Meeting "Förster Resonance Energy transfer in Life Sciences". Göttingen, March 27-30, 2011.

Jorge Bordello, Mateo I. Sánchez, M. Eugenio Vázquez, José L. Mascareñas, Wajih Al-Soufi, and Mercedes Novo. *Association Dynamics of DNA Minor Groove Binders.* III Jornadas Ibéricas de Fotoquímica. Granada, 4th-7th September, 2011.

Curriculum Vitae

I was born on August 1984, in Ferrol (Spain), where I grew up and completed my secondary education, graduated in 2002.

After studying Industrial Engineering for three years at the University of Santiago de Compostela in Lugo, I was awarded with the First Prize in the Final-Year Project Competition for a work on the interaction between Ciclodextrines and Pironines by fluorescence spectroscopy, and got the national End-of-Degree Award in 2005. That year, I enrolled to study a degree in Chemistry at the same university, which I would finish two years later.

In 2006, I was granted with a Collaboration Scholarship of the Regional Government (Xunta de Galicia) for Research Initiation at the Physical Chemistry Department of the USC.

In 2007, I visited the Biomedical NMR group of Professor Klaas Nicolay at the Eindhoven University of Technology where I learned how to prepare and characterize liposomes, suitable as fluorescence and MR contrast agents. This together with an advanced course on magnetic resonance by the Spanish Royal Society of Chemistry I attended in Jaca (Spain) allowed me to participate in a collaboration project with the Clinical Neuroscience Research Laboratory (Hospital Clínico Universitario, Santiago de Compostela) to develop several lipid-based nanoparticles for molecular imaging with MRI and optical techniques.

In 2008, I won a FPU predoctoral fellowship from the Spanish Government. In 2009, I obtained my Diploma of Advanced Studies in the area of Physical Chemistry after finishing the inter-university PhD program on *Science and Technology of Colloids and Interfaces*. As a part of these doctoral studies, in 2008 I attended a one-month course hosted by the University Pablo de Olavide in Sevilla, and completed my background on fluorescence techniques going to the Fluorescence Foundation summer school in Genoa, Italy.

In the period from 2009 to 2012 I focused on the study of the dynamics in different host-guest systems, such as micelles and DNA binders, by Fluorescence Correlation Spectroscopy, which would represent the core of this doctoral dissertation at the Biophysical Chemistry, Photophysics and Spectroscopy Group of the USC. The more interesting results during these years were reported in several conferences and publications.

In 2010, I spent 4 months at the Biophysics and Biomolecular Dynamics Lab of Dr. Carlos Penedo at the University of St. Andrews (Scotland), where I worked on the study of RNA folding dynamics by single molecule FRET.

During the years 2010 to 2011, I also collaborated in the teaching activity of the Department of Physical Chemistry at the USC in different subjects from the degrees in Industrial Chemical Processes Engineering and Chemistry.

Appendix. Thesis by Series of Published Papers

This thesis is presented in the style of a series of published papers. The publications included as part of the thesis are listed below. This appendix collects an original reprint of each one of them.

PAPER 1:

Jorge Bordello; Belén Reija; Wajih Al-Soufi and Mercedes Novo.
Host-Assisted Guest Self-Assembly: Enhancement of the Dimerization of Pyronines Y and B by γ-Cyclodextrin. ChemPhysChem (2009), 10(6), 931-939.

PAPER 2:

Daniel Granadero; **Jorge Bordello**; M.J. Perez-Alvite; M. Novo and Wajih Al-Soufi.
Host-Guest Complexation studied by Fluorescence Correlation Spectroscopy: Adamantane-Cyclodextrin Inclusion. International Journal of Molecular Sciences (2010), 11, 173-188.

PAPER 3:

Mercedes Novo; Daniel Granadero; **Jorge Bordello** and Wajih Al-Soufi.
Host-Guest Association studied by Fluorescence Correlation Spectroscopy. Journal of Inclusion Phenomena and Macrocyclic Chemistry (2011), 70(3-4), 259-268.

PAPER 4:

Jorge Bordello; Mercedes Novo and Wajih Al-Soufi.
Exchange-Dynamics of a Neutral Hydrophobic Dye in Micellar Solutions studied by Fluorescence Correlation Spectroscopy. Journal of Colloid and Interface Science (2010), 345(2), 369-376.

PAPER 5:

J. Bordello; M.I. Sánchez; M.E. Vázquez; J.L. Mascareñas; W. Al-Soufi and M. Novo.
Single-Molecule Approach to DNA Minor-Groove Association Dynamics. Angewandte Chemie International Edition (2012), 51, 7541–7544.

DOI: 10.1002/cphc.200800776

Host-Assisted Guest Self-Assembly: Enhancement of the Dimerization of Pyronines Y and B by γ-Cyclodextrin

Jorge Bordello, Belén Reija, Wajih Al-Soufi,* and Mercedes Novo*[a]

The role of small variations in the structural properties of host and guest molecules on the stoichiometry and strength of supramolecular associations is analyzed. Earlier we found that a change in substituents from pyronine B to pyronine Y has a dramatic effect on both the stability and the dynamics of the association of these guests with β-cyclodextrin as host. Now we study the association between these two pyronines and a cyclodextrin with a bigger cavity (γ-cyclodextrin) using UV/Vis absorption and fluorescence spectroscopy. The absorption spectra of the pyronines show complex variations with cyclodextrin concentration indicating that pyronine dimerization is strongly enhanced inside the cavity of the cyclodextrin. A full model is proposed and the equilibrium constants of the involved processes and the absorption and emission spectra of the different species are estimated. The equilibrium constants of the formation of complexed dimers are much higher than those for free dimerization or for the inclusion of a single guest. The γ-cyclodextrin host acts like a belt to assist the guest self-assembly. The differences in the stability of pyronine B and pyronine Y dimers are explained on the basis of their structure and geometry.

1. Introduction

Knowledge of the structural factors controlling non-covalent host–guest interactions is fundamental for the understanding of molecular recognition phenomena in biological systems, and it is also of great importance for the design of functional supramolecular systems with a wide range of applications. Structure and stability of supramolecular host–guest assemblies depend sensitively on the properties of host and guest molecules. Analysis of the dynamics of supramolecular association by fluorescence correlation spectroscopy (FCS) has shown the important interplay between geometrical requirements and specific interactions between host and guest.[1,2] The overall stability of the assembly depends on the balance between the geometric and orientational requirements limiting the association rate constant and the strength of specific interactions controlling the dissociation process. Subtle changes in the geometry or electronic structure of host or guest can have a big influence on this balance and may lead to big changes in the stability or even on the type of the supramolecular species formed.

Cyclodextrin inclusion complexes are simple and useful models for the study of this kind of intermolecular host–guest interactions. Cyclodextrins (CDs) are toroidally shaped polysaccharides with a highly hydrophobic central cavity that allows them to form inclusion complexes with many organic substrates.

Earlier we studied the host–guest interactions between the pyronines Y (PY) and B (PB) and β-cyclodextrin (βCD).[1,3] It was found that these two xanthene dyes (Figure 1) form inclusion complexes of stoichiometry 1:1 with βCD. The values of the corresponding stability constants show that the complex PB:βCD is about five times more stable than the complex PY:βCD. Specific interactions between the xanthene moiety and the electron-rich oxygens of the cyclodextrin cavity were suggested to be responsible for the stability of the complexes, as well as for their different photophysical properties with respect to free pyronines in aqueous solution. Dynamic studies performed by FCS yielded the individual rate constants of the association and dissociation processes.[1] The association rate constants of the two pyronines with βCD are similar, but much lower than that of a diffusion-controlled collision process, which is attributed to geometrical and orientational require-

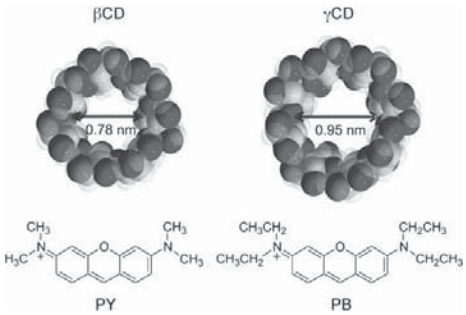

Figure 1. Structures and cavity sizes of βCD and γCD and structures of pyronines Y and B.

[a] J. Bordello, Dr. B. Reija, Prof. Dr. W. Al-Soufi, Prof. Dr. M. Novo
Grupo de Fotofísica e Fotoquímica Molecular
Departamento de Química Física, Facultade de Ciencias
Universidade de Santiago de Compostela
27002 Lugo (Spain)
Fax: (+34) 982-285-872
E-mail: wajih.al-soufi@usc.es
m.novo@usc.es

Supporting information for this article is available on the WWW under http://dx.doi.org/10.1002/cphc.200800776.

ments during the inclusion. The dissociation rate constant of the complex PB:βCD is, however, significantly smaller than that of PY:βCD. These results confirmed that the different stability of the two complexes is due to the specific host–guest interactions controlling the dissociation rate and not because of the guest geometry itself.

In order to understand better the factors controlling the stability of cyclodextrin complexes, further studies were performed with the same pyronines and a cyclodextrin of wider cavity, the γ-cyclodextrin (γCD). γCD is built up from eight glucopyranose units instead of the seven units of βCD so that the diameter of its inner cavity is about 20% larger than that of βCD (Figure 1).[4] FCS studies yielded values of the association rate constants of the pyronines with γCD that are significantly larger than with βCD, as expected due to the lower geometrical restrictions imposed by the bigger cavity during inclusion of the guest.[2] Nevertheless, the dissociation rate constants increase even more due to weaker specific interactions between guest and host in the bigger cavity of γCD, so that the overall stability of the pyronine:γCD complexes is much lower than that of the pyronine:βCD complexes.

Apart from the differences in the association dynamics, the increase of the cavity size from βCD to γCD leads to further interesting changes in the complexation behaviour of the pyronines, which are analyzed herein. The association equilibria between the pyronines and γCD are studied by means of absorption and fluorescence spectroscopy in order to determine the stoichiometries of the complexes formed, to obtain their corresponding stability constants and to characterize their structures on the basis of their photophysical properties.

The formation of inclusion complexes between pyronines PB and PY and the three natural cyclodextrins was studied earlier by Schiller et al. using equilibrium and temperature-jump visible spectrophotometry.[5–7] Nevertheless, the experimental conditions used (low CD concentrations and presence of 1.0 mol dm^{-3} NaCl in the aqueous solutions) and the strong approximations applied in the data analysis make their results unreliable. It is known that high ionic strengths have a great influence on the dye aggregation processes, which are important in the systems under study.[8]

2. Results

Series of absorption spectra (about fifteen spectra in each series) of each pyronine in the presence of different concentrations of γCD were measured. Figure 2 shows some of the spectra for each series. As the concentration of γCD is increased, a decrease in the apparent molar absorptivity at the pyronine absorption maximum is first observed together with an increase of the absorptivity at the shoulder (see insets in Figure 2). At higher γCD concentrations the molar absorptivity at the shoulder decreases again and, in the case of PB, an increase in molar absorptivity is also observed at the pyronine absorption maximum. There are no clear isosbestic points for the entire range of γCD concentrations.

The possible aggregation of PY and PB in aqueous solution was studied by measuring series of absorption spectra of solutions with increasing pyronine concentrations (20 to 30 spectra in each series). Those absorption spectra are represented in Figure 3 in terms of the apparent molar absorptivity, which allows a better appreciation of the spectral changes as the concentration of pyronine is increased.

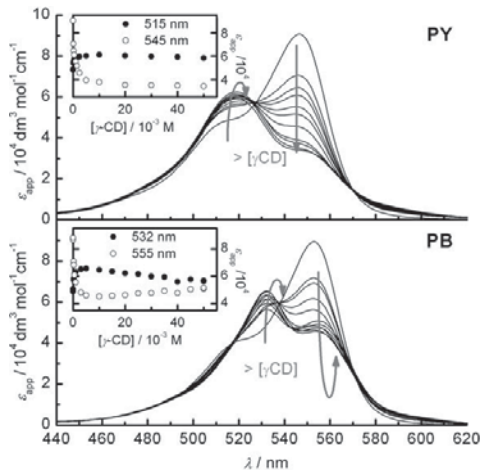

Figure 2. Absorption spectra of PY and PB in aqueous solution in the presence of different concentrations of γCD (0 to 0.050 mol dm^{-3}) at fixed pyronine concentrations (3.6×10^{-5} mol dm^{-3} for PY and 6.6×10^{-5} mol dm^{-3} for PB). Insets: Plots of the apparent molar absorptivity (in dm^3 mol^{-1} cm^{-1}) at two selected wavelengths versus γCD concentration.

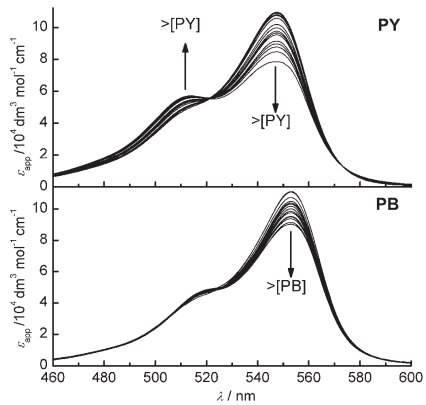

Figure 3. Absorption spectra of PY and PB in aqueous solution as a function of pyronine concentration, varying from 8×10^{-6} to 1.1×10^{-4} mol dm^{-3} for PY and from 3×10^{-6} to 1.0×10^{-4} mol dm^{-3} for PB.

A systematic decrease of the apparent molar absorptivity at the pyronine absorption maxima with increasing pyronine concentrations is observed, together with an increase of the absorption at the shoulder in the case of PY. Clear isosbestic points are observed for both pyronines. In accordance, the plots of absorbance versus pyronine concentration show clear

deviations from linearity at concentrations higher than 2×10^{-5} mol dm^{-3}. Stray light effects were ruled out as the experimental conditions were chosen to be within the linear range of the spectrophotometer, but a small contribution of the pyronine fluorescence emission was detected at the highest concentrations in the wavelength range where absorption and emission spectra overlap.

Series of emission spectra of the two pyronines in the presence of different concentrations of γCD were measured (Figure 4). In both cases a decrease in the fluorescence intensity is observed as the concentration of γCD is increased, together with a slight shift of the emission spectrum to higher wavelengths. The plots of the fluorescence intensity versus γCD concentration (insets in Figure 4) show that the decrease is steeper for PB than for PY.

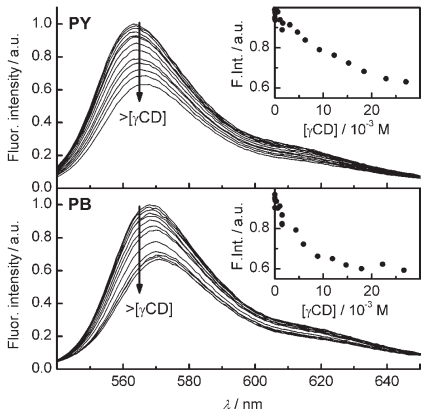

Figure 4. Corrected emission spectra of PY and PB in aqueous solution in the presence of different concentrations of γCD (0 to 0.027 mol dm^{-3}) at fixed pyronine concentration (2.0×10^{-7} mol dm^{-3} for both PY and PB). Insets: Plots of fluorescence intensity at 565 nm versus γCD concentration.

Time-resolved fluorescence measurements were performed for solutions of the pyronines at different concentrations of γCD. Table 1 gives the fluorescence lifetimes and amplitudes obtained in the fits of a multiexponential model to the fluorescence decays. In the absence of γCD and at low concentrations the decays are monoexponential for PY and biexponential for PB, although in the latter the second lifetime has a minor contribution that is independent of the γCD concentration. At a γCD concentration of 0.050 mol dm^{-3} and larger, a shorter lifetime is detected whose amplitude seems to increase slightly with the concentration of γCD. Since all the lifetimes are short for the time resolution of the instrument used, it was necessary to fix one of the lifetime values in some of the fits to avoid parameter correlation. This might have some effect on the amplitude values, which are highly dependent on slight changes of the lifetime values.

Table 1. Fluorescence lifetimes, amplitudes and chi square values obtained in the individual fits of a multiexponentional model to the fluorescence decays of PY and PB in the presence of different concentrations of γCD (pyronine concentration = 1.0×10^{-6} mol dm^{-3}). The sum of the amplitudes (A_i) is normalized to 100 to facilitate comparison.

[γCD] [mol dm^{-3}]	τ_1 [ns] (A_1)	τ_2 [ns] (A_2)	τ_3 [ns] (A_3)	χ^2
PY + γCD				
0		1.687 ± 0.004 (100)		1.10
0.00025		1.689 ± 0.004 (100)		1.01
0.0015		1.689 ± 0.004 (100)		1.16
0.0050	1.2 ± 0.2 (30)	1.81 ± 0.06 (70)		1.09
0.0100	1.09 ± 0.05 (30)	1.8 (fixed) (70)		1.07
0.0300	1.07 ± 0.05 (30)	1.8 (fixed) (70)		1.13
0.0500	1.1 ± 0.1 (36)	1.85 ± 0.04 (64)		1.13
PB + γCD				
0		1.07 ± 0.02 (97)	2.3 ± 0.4 (3)	1.08
0.00025		1.08 ± 0.02 (97)	2.6 ± 0.6 (3)	1.11
0.00075		1.049 ± 0.006 (97)	2.5 (fixed) (3)	1.13
0.0015		1.03 ± 0.02 (97)	2.1 ± 0.4 (3)	1.18
0.0050	0.75 ± 0.09 (30)	1.2 (fixed) (67)	4 ± 1 (1)	1.21
0.0100	0.79 ± 0.08 (44)	1.2 (fixed) (53)	3.2 ± 0.7 (3)	0.98
0.0300	0.76 ± 0.08 (44)	1.2 (fixed) (53)	3.0 ± 0.5 (3)	1.04
0.0500	0.55 ± 0.08 (30)	1.2 (fixed) (68)	2.9 ± 0.3 (3)	1.16

3. Discussion

3.1. Stoichiometry and Model Determination

The variations in the absorption spectra of PY and PB in the presence of different concentrations of γCD (Figure 2) cannot be explained by a simple 1:1 association as in the case of βCD.[3] The lack of clear isosbestic points and the nonmonotonic dependence of the apparent molar absorptivity with the γCD concentration (see insets in Figure 2) show that there must be more than two absorbing species in equilibrium. Moreover, analysis of the series of absorption spectra with PCA yield three to four structural components contributing to the experimental spectra for both pyronines (Figures 1S and 2S, Supporting Information). Therefore, formation of complexes of higher stoichiometries must be considered. Taking into account the tendency of xanthene dyes to aggregate in aqueous solutions[8] and the bigger cavity of γCD compared to βCD, pyronine dimers and/or inclusion complexes of the dimers (2:1 pyronine:CD complexes) are possible species contributing to the observed absorption spectra. As mentioned above, formation of 2:1 and even 2:2 complexes of these pyronines with γCD has been reported in the literature, but formation of pyro-

nine dimers was not taken into account.[5–7] However, the experimental conditions used therein were very different to ours and the models proposed were not satisfactorily justified.

In order to investigate the dimerization of the pyronines in aqueous solution, absorption measurements were performed with varying pyronine concentrations in the absence of γCD (Figure 3). Experimental absorption spectra show systematic variations in the apparent molar absorptivity with clear isosbestic points as the concentration of pyronine is increased, suggesting formation of dimers. This is confirmed by the results of the PCA analysis of these series of absorption spectra up to pyronine concentrations of $(6–8)\times10^{-5}$ mol dm^{-3}, that yield two structural components which are attributed to pyronine monomers and dimers (Figures 3S and 4S, Supporting Information). It must be noted that, if the spectra of the solutions with even higher pyronine concentrations are included in the PCA analysis, a third component is observed due to the contribution of fluorescence emission at long wavelengths.

Taking into account all these experimental findings, a general mechanism is proposed for the association of the pyronines with γCD, where 1:1 and 2:1 pyronine:γCD inclusion complexes are included (P:γCD and P_2:γCD, respectively, in Scheme 1). Formation of the 2:1 complexes can take place by

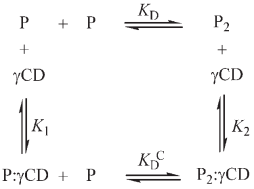

Scheme 1. Mechanism proposed to explain the association of PY and PB with γCD in aqueous solution including four absorbing species: pyronine monomer (P), pyronine dimer (P_2), 1:1 complex (P:γCD) and 2:1 complex (P_2:γCD). These species are interconnected through four equilibria characterized by their corresponding equilibrium constants K_D, K_1, K_2 and K_D^C.

association of a second pyronine molecule with a 1:1 complex as well as by inclusion of a pyronine dimer (P_2) into the γCD cavity. Thus, the proposed mechanism is cyclic with four species present in equilibrium. If the concentration of pyronine is too low to yield dimers, the 2:1 complexes can anyhow be formed from the 1:1 complexes.

The equilibrium constants in Scheme 1 are functions of the equilibrium concentrations of the different species as given by Equations (1)–(4):

$$K_1 = \frac{[\mathrm{P}:\gamma\mathrm{CD}]}{[\mathrm{P}][\gamma\mathrm{CD}]} \quad (1)$$

$$K_2 = \frac{[\mathrm{P_2}:\gamma\mathrm{CD}]}{[\mathrm{P_2}][\gamma\mathrm{CD}]} \quad (2)$$

$$K_D = \frac{[\mathrm{P_2}]}{[\mathrm{P}][\mathrm{P}]} \quad (3)$$

$$K_D^C = \frac{[\mathrm{P_2}:\gamma\mathrm{CD}]}{[\mathrm{P}][\mathrm{P}:\gamma\mathrm{CD}]} \quad (4)$$

From the definitions of the equilibrium constants it is easily deduced that only three of them are independent, with the fourth being combination of the others, as shown in Equation (5):

$$K_D^C = \frac{K_D K_2}{K_1} \quad (5)$$

The mechanism proposed in Scheme 1 must also be in agreement with the results of fluorescence measurements. The series of emission spectra with varying γCD concentrations (Figure 4) are very similar to those obtained with βCD, where only free pyronine and the 1:1 complex were observed.[3] As in that case, analysis with PCA yields only two structural components contributing to the experimental emission spectra (see Figures 5S and 6S in the Supporting Information). This seems to be in disagreement with the proposed mechanism but, taking into account that the pyronine concentration used in fluorescence measurements is much lower than in absorption measurements, the equilibrium concentrations of pyronine dimers should be negligible and insignificant concentrations of the 2:1 complex are also expected to be present. Moreover, the dimers of xanthene dyes are typically non-fluorescent[8] so that even if some small amounts of those species were present, they would not be detected in the fluorescence measurements. Therefore, only two fluorescence species, free pyronine P and 1:1 complex P:γCD are considered to contribute to the emission spectra of the pyronines with varying γCD concentrations.

The results of the time-resolved fluorescence measurements are in perfect agreement with our interpretation. Single-fluorescence lifetimes corresponding to those of the free pyronines are obtained in the absence of γCD and at low concentrations of γCD, whereas second shorter lifetimes are observed at higher γCD concentrations. As in the case of βCD, the shorter lifetimes are attributed to the 1:1 complexes of the pyronines with γCD.[3] The equilibrium concentrations of these complexes increase with γCD concentration and therefore the amplitudes corresponding to those lifetimes increase, whereas the amplitudes of the pyronine lifetimes decrease. In the case of PB, the third residual lifetime is attributed to a hydrolysis product of this pyronine, which was also observed in the measurements with βCD.

3.2. Quantitative analysis

A quantitative analysis of the experimental data is necessary in order to check the validity of the proposed mechanism and to determine the spectra of the different species present and the equilibrium constants involved. However, resolving such a complex mechanism makes it necessary to follow a systematic

analysis procedure. In a first step, the dimerization of the pyronines in the absence of γCD is analyzed in order to determine the corresponding equilibrium constants K_D and the absorption spectra of the dimers. The second step is the analysis of the series of emission spectra to obtain information about the 1:1 complexation process, specially the association equilibrium constants K_1. Using all this information, the series of absorption spectra of the pyronines with different concentrations of γCD are analyzed on the basis of the complete mechanism to obtain the equilibrium constants K_2 and the absorption spectra of the 1:1 and 2:1 complexes.

In the absence of γCD, only the dimerization process in Scheme 1 needs to be considered, as shown in Scheme 2.

$$P + P \overset{K_D}{\rightleftharpoons} P_2$$

Scheme 2. Dimerization of PY and PB in absence of γCD.

Taking into account the definition of K_D [Eq. (3)], the equilibrium concentrations of the pyronine monomers and dimers are related to the total pyronine concentration $[P]_0$ as shown in Equations (6) and (7):

$$[P] = \frac{-1 + \sqrt{1 + 8K_D[P]_0}}{4K_D} \quad (6)$$

$$[P_2] = \frac{[P]_0}{2} + \frac{1 - \sqrt{1 + 8K_D[P]_0}}{8K_D} \quad (7)$$

and the apparent molar absorptivity at a wavelength λ is the sum of contributions of these two species [Eq. (8)]:

$$\varepsilon_{app}(\lambda) = \varepsilon_P(\lambda)\frac{[P]}{[P]_0} + \varepsilon_{P_2}(\lambda)\frac{[P_2]}{[P]_0} \quad (8)$$

where $\varepsilon_X(\lambda)$ denotes the molar absorptivity of species X at λ.

Equation (8) can now be used as fit function in the global analysis of the series of absorption spectra with varying pyronine concentrations (Figure 3). Nevertheless, for these fits to be correct, the distorting effect of fluorescence emission on the absorption spectra detected at high pyronine concentrations and long wavelengths should be eliminated. This implies that either the concentration range or the wavelength range of the analysis must be limited. For the determination of the dimerization equilibrium constants, the whole concentration range should be used in order to increase the contribution of the dimer to absorption. Therefore, fits of Equation (8) were performed using the whole concentration dataset, but only in the short-wavelength range (440–525 nm for PY and 440–540 nm for PB). In these fits, the values of K_D listed in Table 2 were obtained. The order of magnitude of these values is typical for xanthene dyes,[8] but they are somewhat higher than those reported for these pyronines in aqueous solution.[9] Afterwards the complete absorption spectra of the pyronines monomer and dimer were determined in further fits using the whole wavelength range but a limited concentration range (up to 5–6×10^{-5} mol dm^{-3}) and fixing K_D to the value obtained before (Figure 5). The spectra of the monomers coincide perfectly with the experimental absorption spectra of PY and PB at the lowest concentrations, validating the analysis procedure. The spectra of the dimers are slightly dependent on the concentration range and/or the value of K_D used. However, absorption maximum and band splitting are not significantly affected (see Figure 7S in the Supporting Information). These spectra coincide very well with those published before,[9,10] except for the absolute values of the molar absorptivities reported for the dimers which are only half of the true values due to an error in the dimer concentrations that these authors used.

Table 2. Values of the equilibrium constants defined in Scheme 1 for PY and PB with γCD. The values of K_D and K_2 were obtained in the fits of absorption data and those of K_1 in the fits of emission data, except for the value given in parenthesis which results from the analysis of absorption data (see text). The values of K_D^C were calculated using Equation (5).

	PY + γCD	PB + γCD
K_D [10^3 mol^{-1} dm^3]	3.0 ± 0.5	5.0 ± 0.8
K_1 [10^3 mol^{-1} dm^3]	0.04 ± 0.01 (≈0.07)	0.19 ± 0.04
K_2 [10^3 mol^{-1} dm^3]	26 ± 4	8.3 ± 0.5
K_D^C [10^3 mol^{-1} dm^3]	(2.0±0.7)×10^3	(2.2±0.6)×10^2

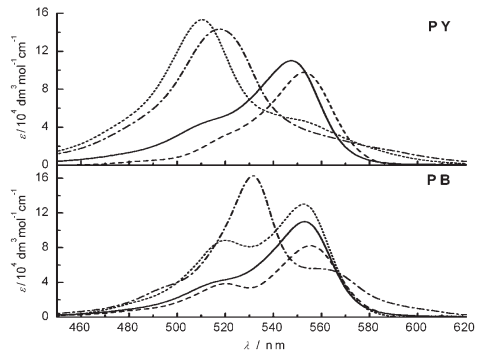

Figure 5. Absorption spectra of the different species present in equilibrium in aqueous solutions of the pyronines PY and PB in the presence of γCD: free pyronine monomer P (——), pyronine dimer P_2 (•••••), P:γCD complex (- - - -) and P_2:γCD complex (–•–•).

The next step is the analysis of the series of emission spectra. Also in this case the mechanism in Scheme 1 can be simplified, since the only fluorescent species present are the free pyronines and their 1:1 complexes linked by the equilibrium given in Scheme 3:

Under the assumption that no interconversion processes take place in the excited state (since the association and dissociation rates cannot compete with the deactivation rates of the excited species[1,2]) and that the cyclodextrin equilibrium concentration coincides with its initial concentra-

$$P + \gamma CD \overset{K_1}{\rightleftharpoons} P{:}\gamma CD$$

Scheme 3. Equilibrium of 1:1 association between pyronines PY and PB and γCD.

tion (excess of γCD compared to pyronine), Equation (9) is obtained for the dependence of the fluorescence intensity at a certain wavelength, $F(\lambda)$, with γCD concentration:

$$F(\lambda) = \frac{F_P(\lambda) + F_{P:\gamma CD}(\lambda) K_1 [\gamma CD]_0}{1 + K_1 [\gamma CD]_0} \quad (9)$$

where $F_P(\lambda)$ and $F_{P:\gamma CD}(\lambda)$ are the fluorescence intensities at wavelength λ when all the pyronine were free and complexed, respectively.

Using Equation (9) as a fit function, a global analysis was performed for the series of emission spectra of the two pyronines with γCD. The fits were very satisfactory and gave the values of the 1:1 association equilibrium constants K1 listed in Table 2 and the emission spectra of species P and P:γCD (Figure 6). The uncertainties in the K_1 values reflect the differences found among several series of data. The spectra of the free pyronines obtained from our fits coincide with those measured experimentally in the absence of cyclodextrin, again validating the proposed model. The emission spectra calculated for the complexes P:γCD are similar to those of the complexes P:βCD,[3] as shown in Figure 6. The good fits and the satisfactory spectra of the species involved confirm that there is no contribution of the pyronine aggregates to the emission, as was also observed for the aggregates of these pyronines in colloidal solutions.[11]

The results of time-resolved fluorescence measurements (Table 1) are in agreement with the analysis above. For each pyronine, two lifetimes whose values do not vary with the concentration of γCD are observed, indicating that the association process in the excited state does not compete with the deactivation process. The shorter lifetime, which is attributed to the complex P:γCD, is not observed at the lowest γCD concentrations, since the equilibrium constants K_1 are relatively low (Table 2) and therefore the concentration of complex is small at those concentrations. Moreover, it must be noted that both the lifetimes of the free pyronines and those of their complexes are short for the time resolution of our system, so that it is difficult to obtain accurate values of these lifetimes. This problem also affects the preexponential factors, which approximately show the expected tendencies (the amplitude of the free-pyronine lifetime decreases with the concentration of γCD and that corresponding to the complex increases) but are too inaccurate to be quantitatively analyzed as it was done in the case of βCD.[3]

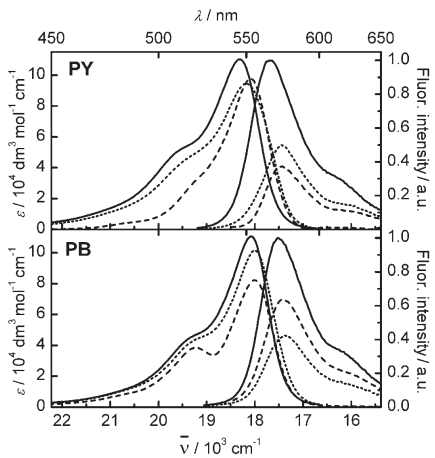

Figure 6. Absorption and emission spectra of PY and PB as free monomers in aqueous solution (——) and forming 1:1 complexes with βCD[3] (•••••) and with γCD (-----).

Finally, we deal with the analysis of the series of absorption spectra of the pyronines in the presence of different concentrations of γCD (Figure 2). As proposed above, these spectra are contributed by the four species in equilibrium shown in Scheme 1. Taking into account the definitions of the equilibrium constants [Eqs. (1)–(4)] and the matter balances for γCD and for the pyronines, Equations (10)–(13) are obtained for the equilibrium concentrations of the four species under conditions of excess of γCD ($[\gamma CD]_0 \gg [P]_0$):

$$[P] = \frac{-(1 + K_1[\gamma CD]_0) + \sqrt{(1 + K_1[\gamma CD]_0)^2 + 8K_D(1 + K_2[\gamma CD]_0)[P]_0}}{4K_D(1 + K_2[\gamma CD]_0)} \quad (10)$$

$$[P_2] = K_D[P]^2 \quad (11)$$

$$[P:\gamma CD] = K_1[\gamma CD]_0[P] \quad (12)$$

$$[P_2:\gamma CD] = K_D K_2 [\gamma CD]_0 [P]^2 \quad (13)$$

The apparent molar absorptivity measured at a certain wavelength λ is the sum of the contributions of the four species, as shown in Equation (14):

$$\varepsilon_{app}(\lambda) = \frac{1}{[P]_0}(\varepsilon_P(\lambda)[P] + \varepsilon_{P_2}(\lambda)[P_2] + \varepsilon_{P:\gamma CD}(\lambda)[P:\gamma CD] + \varepsilon_{P_2:\gamma CD}(\lambda)[P_2:\gamma CD]) \quad (14)$$

This equation was used as fit function in the global analysis of the series of absorption spectra of the pyronines with fixed pyronine concentrations and varying concentrations of γCD (Figure 2) applying principal components gobal analysis (PCGA). The global nonlinear fit parameters are the three equilibrium constants (K_1, K_2 and K_D). The molar absorptivities of the four contributing species, which make up their characteristic absorption spectra, were fitted as linear global parameters. Nevertheless, in order to minimize statistical correlation among these parameters, K_1 and K_D were fixed at the values obtained in the analysis above (Table 2) as well as the molar absorptivities of monomer and dimer of each pyronine (absorption spectra shown in Figure 5). In the case of PB the fits are straightforward and very satisfactory and yield the value of K_2 listed in Table 2 and the spectra of the complexes PB:γCD and PB_2:γCD shown in Figure 5. Varying the value of K_1 within its uncertainty interval leads to small changes in the fitted spectrum of PB:γCD, but has a negligible effect on the absorption spectrum of PB_2:γCD (see Figure 8S in the Supporting Information). Nevertheless, in the case of PY, there is a strong correlation among

the fit parameters K_2 and the molar absorptivities of the complexes PY:γCD and PY_2:γCD that must be controlled to get a satisfactory fit. For this purpose, a preliminary spectrum for PY_2:γCD was determined using only the experimental data at concentrations of γCD higher than 1.5×10^{-3} mol dm^{-3}, at which the contribution of the dimer PY_2 can be neglected. Then the whole data set was analyzed in an iterative process looking for the chi-square minimum where either the spectrum of PY_2:γCD or the value of K_1 was fixed as well as K_D and the spectra of PY and PY_2. The best fit was achieved for the values of K_1 and K_2 given in Table 2 and for the spectra shown in Figure 5 of the complexes PY:γCD and PY_2:γCD. The value of K_1 is higher than that obtained from emission measurements, but of the same order of magnitude. Lower values of K_1 provoked significant distortions of the PY:γCD spectrum at the low-wavelength range, but the value of K_2 (Table 2) and the spectral properties of PY_2:γCD were not significantly affected (see Figure 8S in the Supporting Information).

The values obtained for K_2 are in good agreement with the values reported in the literature for PY and PB, although in that work the experiments were performed in aqueous solutions of 1.0 mol dm^{-3} NaCl and at 25 °C.[5,6] Also absorption spectra for the P_2:γCD complexes were estimated in that work, which have similar properties as our spectra. Nevertheless, in those estimations it was assumed that the spectra of the P:γCD complexes were the same as the spectra of the monomers, which is a very strong assumption. Our analysis shows that the absorption spectra of the P:γCD complexes are quite different to those of the free monomers (Figure 5) and that they have a strong influence on the spectra determined for the P_2:γCD complexes.

3.3. Discussion of Results

On the basis of the results presented so far we first discuss the properties of P:CD (1:1) complexes, then the formation of complexed dimers P_2:γCD and finally the relative orientation of the guests in the dimers.

As already determined in dynamic studies of these systems, the increase in cavity size in γCD with respect to βCD has a great effect on the stability of the P:CD complexes.[1,2] The values obtained for the 1:1 association equilibrium constant of the pyronines with γCD (K_1 in Table 2) are one order of magnitude smaller than those determined with βCD,[3] a result that has been explained on the basis of the association dynamics of these systems studied by FCS. Moreover, the complexes PB:CD are about five times more stable than those formed by PY both with βCD and γCD. This is due to the stronger interaction of PB with the interior of the CD cavity that is reflected in the smaller dissociation rate constants.[2] Nevertheless, P:γCD and P:βCD complexes show very similar photophysical properties, as shown in Figure 6. Both the absorption and the emission spectra of these complexes are slightly red-shifted with respect to the spectra of the corresponding free pyronines. Fluorescence quantum yield decreases in the complexes with respect to free pyronines as well as fluorescence lifetime, due to the increase of the nonradiative deactivation rate constant (see Table 3). This increase is smaller in the complexes P:γCD, again reflecting the weaker specific interactions of the pyronines with the CD having a bigger cavity.

Table 3. Fluorescence lifetimes, fluorescence quantum yields, radiative deactivation rate constants and nonradiative deactivation rate constants of PY and PB in aqueous solution and their 1:1 complexes with βCD and with γCD.

	τ [ns]	ϕ	k_r [10^9 s^{-1}]	k_{nr} [10^9 s^{-1}]
PY[3]	1.76	0.47	0.27	0.30
PY:βCD[3]	1.08	0.27	0.25	0.68
PY:γCD	1.1	0.33	0.30	0.61
PB[3]	1.20	0.36	0.31	0.56
PB:βCD[3]	0.50	0.19	0.38	1.6
PB:γCD	0.75	0.27	0.36	0.97

However, the larger cavity size of γCD with respect to βCD has another important effect on the complexation behaviour of these systems, namely the efficient formation of P_2:γCD complexes that are highly stabilized through cooperative interactions. These complexed pyronine dimers are already observed at low pyronine concentrations where formation of free dimers is negligible. The addition of γCD thus causes a strong enhancement of pyronine dimerization. This effect illustrates the great potential of CDs as molecular reactors and catalyzers[12,13] and as a tool to assist guest self-assembly. The different complexation stoichiometries lead to a complicated mechanism for the interaction of the pyronines with γCD (Scheme 1), where pyronine dimerization is included as a second pathway for the formation of P_2:γCD complexes. For the interaction of these pyronines with βCD the mechanism is much simpler, since the cavity size is too small for the formation of 2:1 complexes and, at the concentrations used in those measurements, pyronine dimerization needs not to be taken into account.[3]

The values of the equilibrium constants given in Table 2 allow us to calculate the equilibrium concentrations of each species present as functions of γCD concentration using Equations (10) to (13). As expected, the relative concentrations of P_2 and P_2:γCD are highly dependent on the total pyronine concentration, being negligible at the concentrations used for emission measurements. This supports the assumption made for the analysis of the series of emission spectra. The concentration of P_2 decreases rapidly when adding γCD, whereas that of P_2:γCD increases at low γCD concentrations and decreases afterwards. In spite of the low values of K_1 and the high values of K_D^C, P:γCD concentration increases as the concentration of γCD is increased and it is the predominant species at high γCD concentrations, except in the case of high dye concentrations. This can be understood since in our studies the total pyronine concentration is much lower than that of γCD, so that a P:γCD complex has a very low probability to find a second free pyronine molecule to form a P_2:γCD complex. This would not be the case if the dye and γCD concentrations were comparable.

The capacity of γCD to enhance pyronine dimerization can be quantified by comparing the equilibrium constant K_D with the product $K_1 K_D^C$ (see Scheme 1 and Table 2). Their values indicate that dimer formation inside the γCD cavity is 8 and 26

times enhanced for PB and PY respectively, relative to the aqueous solution. Although no dynamic information is available for the dimer formation, the high value of K_D^C suggests the importance of cooperative effects during the formation of the P_2:γCD complexes and that hydrophobic interactions play an important role in the stability of the pyronine dimers, as already proposed for other dyes.[8] Comparing the two pyronines, the dimerization enhancement is significantly larger for PY than for PB, as reflected in the higher stability constant K_2 of the complex PY_2:γCD compared to PB_2:γCD (see Table 2). This difference may be attributed to the better fit of two PY molecules inside the γCD cavity in comparison to the bulkier PB, but the necessary reorientation of the PB dimers could also play an important role, as discussed herein.

The absorption spectra of species P_2 and P_2:γCD obtained by global analysis of the experimental data (Figure 5) provide interesting information about the geometries of the dimers of the two pyronines by applying exciton theory.[14,15] For both pyronines the absorption spectra of the P_2:γCD complexes show single bands which are blue-shifted with respect to the spectra of the monomers, indicating a parallel geometry (H-type or "sandwich") in both cases. On the contrary, the free dimers of PY and PB have different spectral properties. The spectrum of PY_2 shows a single blue-shifted absorption band typical of a "sandwich" H-type aggregate, whereas the spectrum of PB_2 has two bands, indicating a geometry somewhere between a parallel dimer and a head-to-tail dimer (J-type). In order to obtain more quantitative information about the geometries of the dimers, their absorption spectra were decomposed in several Gaussian curves and the oscillator strength ratios between the blue and the red bands were calculated. For PY_2 and the two complexed dimers, PY_2:γCD and PB_2:γCD, these ratios are higher than 1.3, confirming that they are H-type (see Figure 7).[16] In the case of PB_2, the ratio of oscillator strengths corresponds to an oblique head-to-tail dimer with an angle between the monomer units of about 100°, as represented in Figure 7. These results suggest that PB_2 has to undergo a great geometrical change when it is included inside the γCD cavity, which should reduce the association rate constant and may explain the lower stability of the complex PB_2:γCD in comparison to PY_2:γCD.

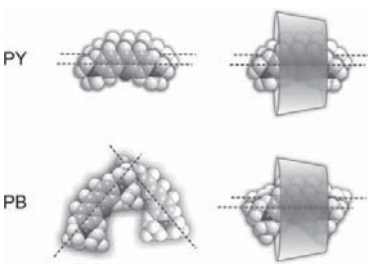

Figure 7. Approximate geometries of the free dimers PY_2 and PB_2 and of the complexed dimers PY_2:γCD and PB_2:γCD as derived from their absorption spectra.

The results obtained herein again give evidence of the important differences in the aggregation and complexation behaviour of the two pyronines derived from the simple substitution of the methyl groups by ethyl groups. In the case of the P:CD complexes, the stability is determined by the strength of the specific interactions between the xanthene moiety and the interior of the CD cavity, with potential steric effects of the side groups being negligible. On the contrary, the bulkier ethyl groups of PB hinder parallel dimerization in the free dimers and decrease the stability of the complexed dimer. The γCD cavity is like a belt, assisting the self-assembly of the pyronine dimers, which do not significantly form on their own.

Experimental Section

Materials: PY was purchased from Sigma (51% dye content) and PB from Aldrich (57% dye content). The main impurities of these materials are not water-soluble, so that they can be separated by filtration of the aqueous solutions.[6] γCD (Sigma–Aldrich) was used as delivered. The pH of the solutions was controlled by addition of $HClO_4$ (Merck, p.a.). Water was purified with a Milli-Q system.

Sample Preparation: Stock solutions of PY and PB were prepared as reported before and were stable for 2–3 days when kept protected from light.[3] The absence of fluorescence impurities in these stocks was checked by comparing the excitation and the emission fluorescence spectra of diluted aqueous solutions monitored at different emission and excitation wavelengths, respectively. The concentrations of the stocks were estimated using the literature value of $\varepsilon = 1.1\times10^5\ mol^{-1}\,dm^3\,cm^{-1}$ for the molar absorptivity of both PY[17] and PB[5] at their respective absorption maxima. Very dilute samples were used for this estimation to avoid the effect of pyronine aggregation. The inaccuracy of these concentrations, inferred from the disagreement of the reported molar absorptivity values, has a direct effect on the absolute values obtained for the equilibrium constants but has not been taken into account for the estimation of their errors.

Aqueous solutions for measurements were freshly prepared by dilution of the stocks, with pyronine concentrations in the range $(0.03–1)\times10^{-4}\ mol\,dm^{-3}$ for absorption and $(0.2–1)\times10^{-6}\ mol\,dm^{-3}$ for fluorescence. Dilution was made using $HClO_4$ solutions of pH 4.0 ± 0.5 instead of water in order to minimize the hydrolysis of the pyronines. Samples of varying CD concentration were prepared by addition of different volumes of a γCD stock solution (concentration about $0.050\ mol\,dm^{-3}$). Adsorption of the pyronines on glass surfaces caused poor reproducibility of fluorescence intensity, especially in the case of PB. In order to minimize this problem the glass flasks were rinsed several times with pyronine solutions of the desired concentration and small amounts of γCD were added to the PB stocks for the titration experiments. Also quartz cells were used, since the adsorption on this material was negligible. No deoxygenation of the samples for time-resolved measurements was necessary since these pyronines have short fluorescence lifetimes.

Absorption Measurements: Absorption spectra were recorded in a Varian–Cary 300 spectrometer using quartz cells. Baselines of 0% and 100% transmittance were recorded with water in both sample and reference cells. Cells of 10.0 mm and 4.0 mm path length (ℓ) were used to cover a wide range of concentrations in each series assuring that the absorbance values were within the linear range of the spectrometer. The linear range of the spectrometer was checked to be up to an absorbance of 4.25, as determined with

solutions of different concentrations of methyl orange. These solutions were also measured with the two cells of different path lengths in order to obtain the exact conversion factor. The absorption spectra are shown in units of apparent molar absorptivity ε_{app} (i.e. $A/\ell C_0$) to eliminate the effect of the different path lengths and dye concentrations on the measured absorbances. The optical effect of the cyclodextrin on the absorption spectra was corrected using a γCD solution with the same concentration as the sample solution as reference. Temperature was kept constant at $20\pm1\,^{\circ}C$ during the measurements.

Fluorescence measurements: Both steady-state and time-resolved fluorescence measurements were performed with an Edinburgh Instruments F900 spectrofluorimeter, equipped with a Xenon lamp of 450 W as excitation source for steady-state measurements and a hydrogen-filled nanosecond flashlamp for lifetime measurements using the time-correlated single-photon counting technique. Excitation wavelengths were 515 nm for steady-state emission spectra and 310 nm in time-resolved measurements. Fluorescence decays were measured at 565 nm with a TAC resolution of 0.053 ns, but were limited by the pulse width (typical half width 1.5 ns). All decays were measured up to 10000 counts at maximum. Emission spectra were corrected for the wavelength dependence of the detection system. All experiments were carried out at $20\pm1\,^{\circ}C$.
Absolute quantum yields were determined using rhodamine B in basic ethanol as the standard, with a reported value of 0.70 for its fluorescence quantum yield.[18]

Data analysis: The series of absorption and emission spectra obtained in the titrations with γCD were analyzed using PCGA.[19] This method can be applied to series of spectra which vary with an external parameter, as the γCD concentration or the pyronine concentration in our case. The first step of PCGA is a principal components analysis (PCA), where the minimal number of spectral components responsible for the observed variations is obtained. This information helps to draw up a theoretical model that is used in the second step as a fit function for a nonlinear least-squares global analysis using the whole spectra as a dataset. The results of this global fit are the values of the physicochemical parameters involved in the model and the individual spectra of the components. Individual fits of fluorescence decays were performed with the software package from Edinburgh Instruments using deconvolution of the lamp pulse. The series of decays at different γCD concentrations were also analyzed with the above-described PCGA using a modified procedure that allows deconvolution of the lamp pulses.

Acknowledgements

B.R. and J.B. thank the Ministerio de Ciencia e Innovación for research scholarships. M.N. and W.A.S. thank the Ministerio de Ciencia e Innovación and Xunta de Galicia for financial support (projects CTQ2007-68057-CO2-O2, INCITE07PXI209034ES, INCITE08E1R209060ES, Network 2006/124).

Keywords: cyclodextrins · host–guest systems · pyronines · supramolecular chemistry · UV/Vis spectroscopy

[1] W. Al-Soufi, B. Reija, M. Novo, S. Felekyan, R. Kühnemuth, C. A. M. Seidel, *J. Am. Chem. Soc.* **2005**, *127*, 8775.
[2] W. Al-Soufi, B. Reija, S. Felekyan, C. A. M. Seidel, M. Novo, *ChemPhysChem* **2008**, *9*, 1819.
[3] B. Reija, W. Al-Soufi, M. Novo, J. Vázquez Tato, *J. Phys. Chem. B* **2005**, *109*, 1364.
[4] J. Szejtli, *Chem. Rev.* **1998**, *98*, 1743.
[5] R. L. Schiller, S. F. Lincoln, J. H. Coates, *J. Chem. Soc. Faraday Trans. 1* **1986**, *82*, 2123.
[6] R. L. Schiller, S. F. Lincoln, J. H. Coates, *J. Chem. Soc. Faraday Trans. 1* **1987**, *83*, 3237.
[7] R. L. Schiller, S. F. Lincoln, J. H. Coates, *J. Incl. Phenom.* **1987**, *5*, 59.
[8] Ó. Valdés-Aguilera, D. C. Neckers, *Acc. Chem. Res.* **1989**, *22*, 171.
[9] L. P. Gianneschi , T. Kurucsev, *J. Chem. Soc. Faraday Trans. 2* **1974**, *70*, 1334.
[10] L. P. Gianneschi, A. Cant, T. Kurucsev, *J. Chem. Soc. Faraday Trans. 2* **1977**, *73*, 664.
[11] M. Arık, Y. Onganer, *Chem. Phys. Lett.* **2003**, *375*, 126.
[12] K. Takahashi, *Chem. Rev.* **1998**, *98*, 2013.
[13] L. Barr, P. Dumanski, C. Easton, J. Harper, K. Lee, S. Lincoln, A. Meyer, J. Simpson, *J. Inclusion Phenom. Macrocyclic Chem.* **2004**, *50*, 19.
[14] E. G. McRae, M. Kasha in *Physical Process in Radiation Biology*, Academic Press, New York, **1964**, p. 23.
[15] M. Kasha, R. Rawls, M. Ashraf, *Pure Appl. Chem.* **1965**, *11*, 371.
[16] V. Martínez Martínez, F. López Arbeloa, J. Prieto Bańuelos, T. López Arbeloa, I. López Arbeloa, *J. Phys. Chem. B* **2004**, *108*, 20030.
[17] M. El Baraka, M. Deumie, P. Viallet, T. J. Lampidis, *J. Photochem. Photobiol. A* **1991**, *56*, 295.
[18] F. López Arbeloa, T. López Arbeloa, M. J. Tapia Estévez, I. López Arbeloa, *J. Phys. Chem.* **1991**, *95*, 2203.
[19] W. Al-Soufi, M. Novo, M. Mosquera, *Appl. Spectrosc.* **2001**, *55*, 630.

Received: November 20, 2008
Published online on March 17, 2009

Int. J. Mol. Sci. **2010**, *11*, 173-188; doi:10.3390/ijms11010173

OPEN ACCESS

International Journal of
Molecular Sciences
ISSN 1422-0067
www.mdpi.com/journal/ijms

Article

Host-Guest Complexation Studied by Fluorescence Correlation Spectroscopy: Adamantane–Cyclodextrin Inclusion

Daniel Granadero [1], Jorge Bordello [1], Maria Jesus Pérez-Alvite [2], Mercedes Novo [1] and Wajih Al-Soufi [1,*]

[1] Departamento de Química Física, Facultade de Ciencias, Universidade de Santiago de Compostela, E-27002 Lugo, Spain; E-Mails: daniel.granadero@usc.es (D.G.); jorge.bordello@usc.es (J.B.); m.novo@usc.es (M.N.)

[2] Departamento de Química Orgánica, Facultade de Química, Universidade de Santiago de Compostela, E-15782 Santiago de Compostela, Spain; E-Mail: mj.perez.alvite@usc.es (M.J.P-A.)

* Author to whom correspondence should be addressed; E-Mail: wajih.al-soufi@usc.es; Tel.: +34-982-285-900; Fax: +34-982-285-872.

Received: *1 December 2009; in revised form: 31 December 2009 / Accepted*: *4 January 2010 / Published*: *12 January 2010*

Abstract: The host-guest complexation between an Alexa 488 labelled adamantane derivative and β-cyclodextrin is studied by Fluorescence Correlation Spectroscopy (FCS). A 1:1 complex stoichiometry and a high association equilibrium constant of $K = 5.2 \times 10^4$ M^{-1} are obtained in aqueous solution at 25 °C and pH = 6. The necessary experimental conditions are discussed. FCS proves to be an excellent method for the determination of stoichiometry and association equilibrium constant of this type of complexes, where both host and guest are nonfluorescent and which are therefore not easily amenable to standard fluorescence spectroscopic methods.

Keywords: fluorescence correlation spectroscopy; host-guest chemistry; adamantane; cyclodextrin

1. Introduction

Supramolecular host-guest chemistry describes the formation of molecular complexes composed of small molecules (guests) noncovalently bound to larger molecules (hosts) in a unique structural relationship [1]. Host-guest complexes are of great technological importance and have been extensively studied [2]. Several techniques such as calorimetry, conductivity, pH potentiometry, capillary electrophoresis, and absorption or fluorescence spectroscopy are used to determine their stoichiometry and stability. Among these, fluorescence spectroscopy is widely used, because it is a sensitive and relatively straightforward technique. Standard fluorescence spectroscopy analyzes the variation of a spectroscopic property (quantum yield, spectral shift, lifetime, or anisotropy) of a fluorescent guest or host due to the complexation. A significant variation of any of these parameters requires an intimate participation of the fluorophore in the complexation process, which limits the use of this technique to cases where the fluorophore itself is included as guest (Figure 1a) or is expulsed from the interior of the host by a nonfluorescent guest in a competitive process or where some specific interactions take place. Most technologically interesting host-guest complexes are themselves nonfluorescent and the attachment of a fluorescent label in order to use them in standard fluorescence spectroscopy leads to a dilemma: on one hand, the fluorophore should not interfere in the host-guest complexation under study, but on the other hand a sufficiently strong interaction between fluorophore and host or guest is necessary in order to detect a change in the spectral properties upon complexation. Although many specific solutions have been found, the study of fluorescently labelled host-guest systems by standard fluorescence spectroscopy is still challenging.

Figure 1. Fluorescent labelling of a host-guest complex (a) inclusion of a fluorescent guest (b) guest with attached fluorophore (c) host with attached fluorophore.

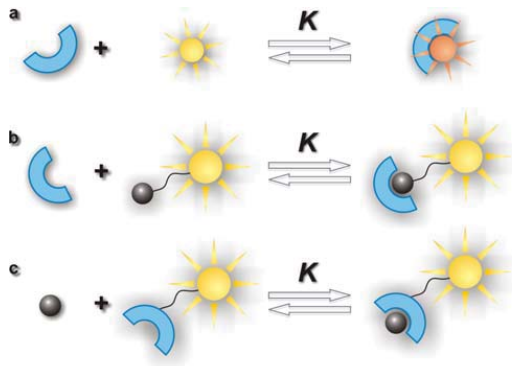

Fluorescence Correlation Spectroscopy (FCS) can solve the described problem in a more general way. Instead of the change in the spectral properties FCS analyses the variation in the diffusion coefficient of a fluorophore attached to guest or host due to the increase in the molecular weight upon complexation (see Figures 1b,c) The fluorophore itself need not to interact directly with the host-guest complex except for a common diffusive movement. This relaxes the conditions imposed on the

fluorophore which can be selected independently of the specific host-guest system, so that bright and photostable dyes can be attached at convenient positions in guest or host.

FCS is a well established fluctuation correlation method that extracts information about the dynamics of molecular processes from the small changes in molecular concentration or chemical states that arise from spontaneous fluctuations around equilibrium [3]. FCS allows one to study dynamic and photophysical processes that take place in a wide time scale in one and the same experiment. It is a single molecule technique which uses very small sample volumes determined by a confocal setup and nanomolar fluorophore concentrations. FCS is used in a wide range of fields, but surprisingly few applications to the study of host-guest complexation can be found. We studied recently by FCS host-guest dynamics and determined the fast entry/exit rate constants of fluorescent dyes within cyclodextrins [4,5]. In this contribution we will study by FCS the stoichiometry and the stability of the inclusion complex formed between the host β-cyclodextrin (βCD) and the nonfluorescent guest adamantane labelled with Alexa 488 as fluorescent probe (see Figure 2).

Figure 2. (a) Structure of Ada-A488 (b) Structure of βCD. (c) Sketch of an adamantane-βCD inclusion complex.

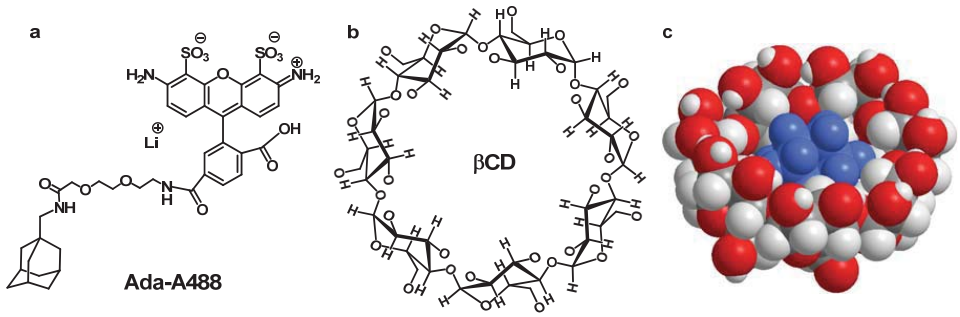

Cyclodextrins (CD) are naturally occurring water-soluble toroidally shaped polysaccharides with a highly hydrophobic central cavity that have the ability to form inclusion complexes with a variety of organic and inorganic substrates [6-12]. The three major natural cyclodextrins are α–, β– and γ–CD built up from 6, 7 and 8 glucopyranose units, respectively. CDs are often found as building blocks of supramolecular systems, self-assemblies or chemical sensors [13–18]. The ability of CDs to form inclusion complexes, in which the physicochemical properties of the guest molecules change with respect to the free molecules, has led to a variety of applications [19–25].

Adamantane (tricyclo[3.3.1.1(3,7)]decane, $C_{10}H_{16}$) is formed by four cyclohexanes fused to each other in chair conformations achieving a strain free and highly symmetrical stable structure. The adamantyl group is a spherical group with a diameter of 7 Å which perfectly matches the cavity diameter of βCD. Adamantane derivatives form therefore 1:1 inclusion complexes with βCD with high values of the association equilibrium constant, typically between 10^4–10^5 M^{-1} [26–31]. Due to their high stability βCD-adamantane complexes have found several important applications both in supramolecular chemistry and in biomedical applications, such as hydrogels [32], affinity biosensors [33], surface-mediated gene delivery [34], cyclodextrin polymer-based particles [35, or supramolecular polymers [36,37].

In this work we demonstrate how FCS can be used to study the inclusion complex formation between βCD and adamantane labelled with the fluorescent probe Alexa 488 (Ada-A488 as shown in Figure 2). We discuss the necessary experimental conditions, determine the stoichiometry and the equilibrium constant and compare the results with those published for similar guests obtained with other methods.

2. Theory

2.1. Mechanism

The association of the fluorescent guest A and the nonfluorescent host H yielding a fluorescent complex B is treated as a reversible chemical reaction with (association) equilibrium constant *K*:

$$\mathrm{A+H} \underset{}{\overset{K}{\rightleftharpoons}} \mathrm{B} \tag{1}$$

The equilibrium constant *K* is related to the entry (association) (k_+) and exit (dissociation) (k_-) rate constants as follows:

$$K = \frac{k_+}{k_-} \tag{2}$$

Under conditions where the host concentration [H] is always much higher than that of the fluorescent guest, this concentration coincides with the initial host concentration $[\mathrm{H}]_0$, and the complexation "reaction" is pseudo-first-order with the relaxation ("reaction") time τ_R given by:

$$\tau_\mathrm{R} = (k_+[\mathrm{H}]_0 + k_-)^{-1} \tag{3}$$

2.2. FCS

FCS analyzes the fluorescence intensity fluctuations that are caused by the spontaneous variations in the number of fluorescent molecules in the confocal sample volume due to translational diffusion [5,38–40]. The observed fluorescence intensity fluctuates at a time scale given by the mean residence time of a fluorophore in the sample volume. The intensity fluctuations $\delta F(t) = F(t) - \langle F \rangle$ are analyzed by the normalized temporal autocorrelation function $G(t)$ as function of the correlation time τ as given in Equation (4):

$$G(\tau) = \frac{\left\langle \delta F(t) \cdot \delta F(t+\tau) \right\rangle}{\left\langle F(t) \right\rangle^2} \tag{4}$$

The time dependent part of the correlation function describing pure translational diffusion of a single fluorescent species in and out of a sample volume G_D is given in Equation (5):

$$G_\mathrm{D}(\tau) = \frac{1}{N}\left(1+\frac{\tau}{\tau_\mathrm{D}}\right)^{-1}\left(1+\left(\frac{w_\mathrm{xy}}{w_\mathrm{z}}\right)^2\frac{\tau}{\tau_\mathrm{D}}\right)^{-\frac{1}{2}} \tag{5}$$

Here a three-dimensional Gaussian sample volume is assumed with radial and axial i/e^2 radii w_xy and w_z, respectively. *N* is the mean number of fluorescent molecules within the sample volume and τ_D is

the translational diffusion (transit) time of the molecules across the sample volume, which is related to the translational diffusion coefficient D by Equation (6) [3,41]. The radius of the sampling volume, w_{xy}, is determined from a calibration measurement with a reference dye with known diffusion coefficient (in this case rhodamine 123) as described in the Experimental section.

$$D = \frac{w_{xy}^2}{4\tau_D} \tag{6}$$

At higher excitation power the dark triplet state of the dye may be significantly populated and a superimposed fast flickering of the fluorescence intensity may be observed with amplitude A_T and a time constant τ_T given by the triplet lifetime of the fluorophore. This leads to an additional exponential term in the correlation function as described in Equation (7):

$$G_{DT}(\tau) = G_D(\tau) \cdot \left(1 + A_T\, e^{-\tau/\tau_T}\right) \tag{7}$$

In the case that the exchange of the fluorophore between free and bound states is much faster than the typical transit time of the fluorophore across the sample volume ($\tau_R << \tau_D$) these states of the fluorophore will not be seen by FCS as two distinct species, but as a single one with a mean diffusion time $\overline{\tau}_D$. The value of $\overline{\tau}_D$ depends then on the individual diffusion coefficients D_f and D_b of free and bound fluorophore and on the molar fractions $X_x = N_x/(N_f + N_b)$ of these species:

$$\overline{\tau}_D = \frac{w_{xy}^2}{4(X_f D_f + X_b D_b)} = \left(X_f(\tau_f)^{-1} + X_b(\tau_b)^{-1}\right)^{-1} \tag{8}$$

The full correlation curve describing translational diffusion of two fluorescent species in fast exchange and a common triplet term is given in Equation (9) where the diffusion term is defined by the mean diffusion time $\overline{\tau}_D$:

$$G_{DT}(\tau) = \frac{1}{N}\left(1 + \frac{\tau}{\overline{\tau}_D}\right)^{-1}\left(1 + \left(\frac{w_{xy}}{w_z}\right)^2 \frac{\tau}{\overline{\tau}_D}\right)^{-\frac{1}{2}} \cdot \left(1 + A_T\, e^{-\tau/\tau_T}\right) \tag{9}$$

In the case of a fluorescent guest, a 1:1 stoichiometry, and under the conditions that the free host concentration is always much higher than that of the guest, [A] << [H], the mean diffusion time $\overline{\tau}_D$ can be expressed as function of the total host concentration $[H]_0$, the equilibrium association constant K and the limiting values of the diffusion times of free and bound dye, τ_f and τ_b, respectively:

$$\overline{\tau}_D = \frac{\tau_f(1 + K[M]_0)}{1 + \frac{\tau_f}{\tau_b} K[M]_0} \tag{10}$$

The equilibrium association constant K can then be determined from a fit to a series of mean diffusion times measured at different host concentrations or directly from a global fit to the series of correlation curves.

3. Results and Discussion

The determination of absolute diffusion coefficients with standard FCS can be affected by several experimental errors [42]. For the determination of the equilibrium constant and the stoichiometry of

the complexation only relative values of the diffusion times are needed, but even these may be distorted at high excitation irradiance due to saturation or photodestruction of the fluorophore. The residence time of the complex in the focal volume is longer than that of the free fluorophore, which may increase the photobleaching probability and thus shorten the apparent diffusion times. This in turn flattens the titration curve and leads to an underestimation of the equilibrium constant. Therefore, as a first step the irradiance dependence of the fluorescence count rate and of the diffusion coefficient of free and complexed Ada-A488 has been studied. Figure 3 shows that the registered fluorescence count rate per Ada-A488 molecule (the molecular brightness) (filled black squares) increases linearly at low irradiance but levels off slightly at higher values. The presence of βCD ([βCD] = 6.4×10^{-3} mol dm^{-3}) has only small influence on the brightness of the fluorophore, with a reduction of about 5% at low and about 25% at highest irradiance. This change may be due to different photobleaching probabilities of free and complexed dye, to polarisation effects in the detection optics, to a change of the refractive index of the solution, or to increased scattering, but it may also be due to some direct interaction between the Alexa 488 chromophore and the adamantane-cyclodextrin complex. However, the Alexa 488 fluorophore is too big to be included into the βCD cavity and no efficient competition with the adamantane inclusion is to be expected.

The diffusion time of Ada-A488 (open squares in Figure 3), increases significantly on the addition of βCD (open circles). At highest irradiance a very similar slight decrease of the diffusion times (of about 5%) is observed in both cases, probably due to some saturation effect. For the titration measurements an irradiance of $I_0/2 = 27$ kW cm^{-2} was chosen, which is at the upper end of the linear increase of the brightness.

Figure 3. Power series of the FCS signal of Ada-A488 in aqueous solution (squares, $[\beta CD]_0 = 0$ mol dm^{-3}) and at high concentration of βCD (circles, $[\beta CD]_0 = 6.4 \times 10^{-3}$ mol dm^{-3}). [Ada-A488] ≈ 10^{-9} mol dm^{-3}). Left scale, filled symbols: count rate per single Ada-A488 molecule. Right scale, open symbols: diffusion time of Ada-A488. All data obtained from FCS correlation curves similar to those shown in Figure 4 at different excitation irradiances. Counts per molecule (cpm) is the total detected fluorescence count rate divided by the mean number of molecules in the focus ***N***.

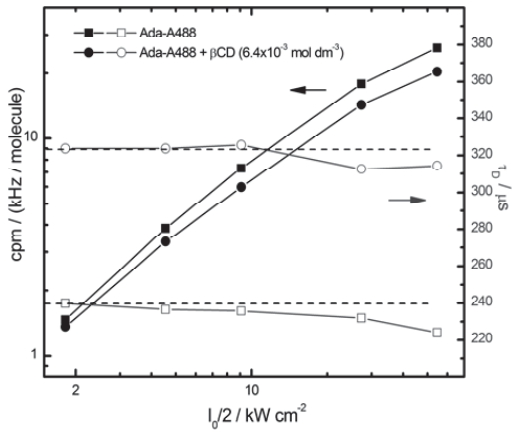

Figure 4. Fluorescence intensity correlation curves $G(\tau)$ of Ada-A488 in the presence of increasing concentrations of βCD ([βCD] = 0 mol dm^{-3} to 6.4 × 10^{-3} mol dm^{-3}) in aqueous solution. ([Ada-A488] ≈ 10^{-9} mol dm^{-3}). Panel a: normalized experimental correlation curves at increasing βCD concentration (grey curves) and two representative curves from the global fit of Equations. (9) and (10) at [βCD] = 0 mol dm^{-3} (red curve) and [βCD] = 6.4 × 10^{-3} mol dm^{-3} (blue curve) to the correlation curves. The intermediate fit curves are not shown for clarity.Small vertical bars indicate the diffusion time obtained from the fit. Inset: mean diffusion times $\overline{\tau}_D$ as function of βCD concentration determined from individual fits of the Equation (9) to the correlation curves. The highest concentrations are not shown. See also Figure 5. Panel b: stacked representation of the same correlation curves as in panel a. Panel c: weighted residuals from the global fit (vertical scale is arbitrary).

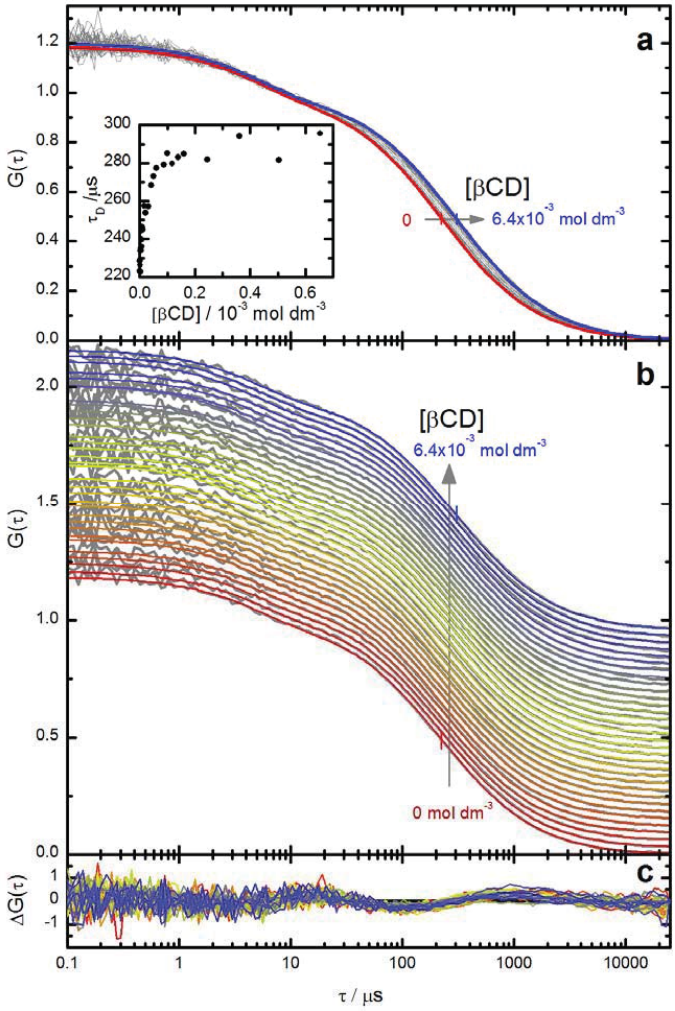

The normalized fluorescence intensity correlation curves $G(\tau)$ of Ada-A488 in water at different βCD concentrations are shown as grey lines in Figure 4. The detected fluorescence intensity is strongly correlated at very short correlation times, but then two decorrelation terms are observed at around 5 μs and 200 μs. The amplitude of the first term increases strongly at higher irradiance (not shown) but is independent of the βCD concentration. It can therefore be safely assigned to the population of the triplet state of Alexa 488. The second term shifts to longer correlation times at increasing βCD concentration and is assigned to the diffusion of the fluorophore in and out of the sample volume. All correlation curves can be well fitted with correlation function G_{DT} [Equation (9)] yielding the diffusion times τ_D shown in the inset of Figure 4a.

The strong increase of τ_D already at very low βCD concentration can not be explained by an increase of the solvent viscosity, which is not significant at these low cyclodextrin concentrations [43]. We interpret these values of τ_D as mean diffusion times $\overline{\tau}_D$ of the fluorophore in fast exchange between free and bound states as described by Equations (8)–(10). The fit of these mean diffusion times $\overline{\tau}_D$ by the model of a complexation with stoichiometry 1:1 [Equation (10)] is very satisfactory as shown in Figure 5. More precise values of the parameters are obtained by a direct global target fit of the correlation curves by Equations (9) and (10) as shown in Figure 4. The results of this global fit are listed in Table 1, together with calculated values of the diffusion coefficients and the hydrodynamic radii of free dye and the complex.

Figure 5. Upper panel: Mean diffusion times $\overline{\tau}_D$ as function of βCD concentration determined from individual fits of correlation function G_{DT} [Equation (9)] to the normalized correlation curves of Figure 4. Parameter of the fit as given in the text. The black curve represents the best fit of Equation (10) to $\overline{\tau}_D$ with the parameter $\tau_f = 225 \pm 2$ μs, $\tau_b = 297 \pm 2$ μs, and $K = (48 \pm 7) \times 10^3$ mol^{-1}dm^3. Note that due to the logarithmic concentration scale the values at [βCD] = 0 M are not visible in the figure, although they are included in the fit. Lower panel: residuals of the fit.

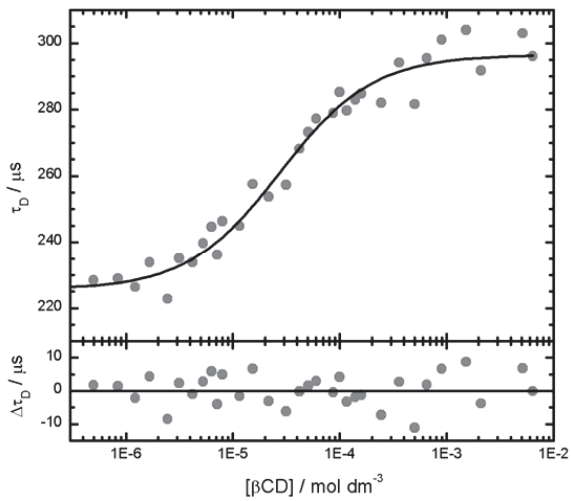

Table 1. Results of the global target fit of Equations (9) and (10) to the correlation curves shown in Figure 4 and calculated values. All values at 25.0 ± 0.5 °C.

	Ada-A488 + βCD
K /10^3 M^{-1}	52 ± 2
τ_f /ms	0.222 ± 0.002
τ_b /ms	0.300 ± 0.002
A_T	0.20
τ_T /μs	4.8
D_f /10^{-10} m^2s^{-1}	3.15 ± 0.30
D_b /10^{-10} m^2s^{-1}	2.33 ± 0.20
$R_{h,f}$ /Å	7.8 ± 0.7
$R_{h,b}$ /Å	10.5 ± 0.9

The limiting diffusion times obtained from the fits to the series of correlation curves were converted to translational diffusion coefficients D using Equation (6) with the radial $1/e^2$ radius of the sample volume obtained from a calibration with Rhodamine 123 as reference (see experimental section). The uncertainty in this calibration and other systematic errors are not included in the indicated standard deviations. The hydrodynamic radii R_h of free Ada-A488 and of the complex Ada-A488:βCD were estimated applying the Stokes-Einstein relation [Equation (11)] with the viscosity of water η (25 ºC) = 0.8905 cP:

$$R_h = \frac{kT}{6\pi\eta D} \tag{11}$$

As expected, the free guest Ada-A488 has a higher diffusion coefficient than the complex Ada-A488:βCD. The diffusion coefficient of homogeneous spherical particles is expected to change with the inverse of the cubic root of their molar mass $D \sim R_h^{-1} \sim M^{-1/3}$. As shown previously this is well fulfilled for small globular molecules and for inclusion complexes of different cyclodextrins [4]. In this case the ratio between the diffusion coefficients $D_b/D_f = 0.74$ coincides perfectly with that expected from the ratio of their molar masses $(M_b/M_f)^{-1/3} = (2.37)^{-1/3} = 0.75$. The absolute values of the diffusion coefficients compare very well with those obtained before for complexes between pyronines and βCD and γCD [4,5].

As can be deduced from the residuals in Figure 5, the precision in the measurement of the diffusion times in these experiments is about $\sigma(\tau_D)/\tau_D \approx 2\%$. This translates to a minimal detectable relative change of the molar mass of the fluorophore from this data of about 20%.

The very high value of the association equilibrium constant $K = 5.2 \times 10^4$ M^{-1} agrees well with that given in the literature for the inclusion of different adamantane derivatives into βCD with values of $K = 1–10 \times 10^4$ M^{-1} [26–31,44].

Finally, the fact that in spite of the high association equilibrium constant a fast exchange of Ada-A488 between free and complexed state is observed indicates that the association rate constant must be similar or even slightly higher than that observed for the dynamics of the association of

pyronines to βCD [4,5]. An additional correlation term due to the exchange itself is not observed as the fluorophore does not change its brightness upon complexation.

4. Experimental Section

4.1. Materials

βCD (Sigma-Aldrich) (M = 1134.98 g mol^{-1}) was used as delivered. βCD was checked for fluorescence impurities and was found to be clean enough for classical fluorescence measurements and for FCS experiments. Water was purified with a Milli-Q system. The synthesis of the Ada-A488 compound (M = 825.88 g mol^{-1}) is described in Section 4.4.

4.2. Sample Preparation

Stock aqueous solutions of βCD were freshly prepared with a concentration of about 8×10^{-3} mol dm^{-3}. Stock solutions of Ada-A488 were prepared as follows: the solid compound Ada-A488 was first dissolved in ethanol in order to facilitate its solubilisation. Then, an aliquot of this solution was diluted 1,000 times in 0.1 mol dm^{-3} phosphate buffer to adjust the pH at 6. The concentrations of Ada-A488 in these stock solutions were still 25-fold higher than that necessary for the FCS measurements (approximately 10^{-9} mol dm^{-3}). The FCS samples were finally prepared by dilution of a constant volume of the corresponding Ada-A488 stock together with different volumes of the βCD stock solution and addition of water to adjust to a certain total volume. All these volumes were weighed so that concentration corrections could be performed. Special care was taken in order to avoid any possible contamination of the samples with fluorescent impurities. At the highest βCD concentrations a slight turbidity was observed in the samples, which explains an additional small very slow term in the correlation curves.

4.3. FCS Measurements

The confocal epi-illuminated setup used for the FCS measurements is similar to that described elsewhere [4,45]. A 40 μL drop of each sample was deposited on a borosilicate coverslip (Menzel Gläser, NO. 1 DE). The samples were excited by the continuous linearly polarized light of a 489 nm laser diode (Becker&Hickl, BDL-485-SMC, DE) coupled to a monomode optical fiber (Point-Source, kineFLEX-P-1-S-405-0.7, UK). The light output of the fiber was collimated (Schäfter&Kirchhoff, 60FC-4-6,2-01-DI, DE), spectrally cleaned (Semrock, Brightline HC 482/18, US), redirected by a dichroic mirror (Semrock, Brightline BS R488, US) and focused into the sample by a high aperture microscope objective (Olympus, UPLSAPO 60xW/1.20, water immersion) mounted in an inverted microscope (Olympus, IX-71). The fluorescence was collected by the same objective and then refocused through the dichroic mirror onto a pinhole (Thorlabs, ∅ = 50 μm, US) in the image plane. The light passing the pinhole was collimated, then split into two beams by a nonpolarizing beamsplitter cube (Newport, 05BC17MB.1, US) and each focused onto avalanche photodiodes (MPD50CTC APD, ∅ = 50 μm, MPD, Italy). Band-pass filters (Semrock, Brightline HC 525/45, US) in front of the detectors discriminated fluorescence from scattered laser light. Both output signals were processed and stored by TCSPC-modules (SPC 132, Becker & Hickl GmbH, Berlin, Germany).

Correlation curves were calculated with a fast home-built routine that runs under LabVIEW (National Instruments) [45]. Typically 20 million photons were collected for each correlation curve with count rates around 50 kHz. All measurements were made at stabilized temperature, 25.0 ± 0.5 °C. The excitation power as measured in the focus of the microscope objective by a power meter (Thorlabs, PM30-120, US) was typically 240 µW, corresponding to a mean irradiance of $I_0/2 = P/(\pi \cdot \omega_{xy}^2) = 27$ kW cm^{-2}, assuming a Gaussian intensity distribution along the optical axis. P is the excitation power in the sample) [46].

The focal area and the detection volume were calibrated with Rhodamine 123 in aqueous solution at low irradiance yielding a radial $1/e^2$ radius of $\omega_{xy} = 0.53$ µm. The value of $D_{R123} = (4.6 \pm 0.4) \times 10^{-10}$ m^{2}s^{-1} is estimated from recent PFG-NMR [47] and dual-focus FCS [48] data. The diffusion coefficients are given for 25 °C. All given uncertainties correspond to one standard deviation from the fits and do not include calibration errors.

Series of FCS curves measured at different host concentrations were analyzed by global "target" analysis programmed in OriginPro 8.0 (OriginLab Corporation, US). An empirical weighting function was used in order to take into account the strong variation of the noise in the FCS curves.

4.4. Synthesis of the Ada-A488 Compound

Preparation of compound 1 (see Scheme 1)

1-adamantanemethylamine (85.8 mg, 0.52 mmols) was dissolved in dry DCM (10.4 mL) and Fmoc 8-amino-3,6-dioxaoctanoic acid (200mg, 0.52 mmols), HATU (217 mg, 0.57 mmols) and DIEA (546 mL, 3.12 mmols) were successively added.

After 1 h stirring at rt, the solution was poured into a separation funnel and washed with HCl (5%) and $NaHCO_3$ (sat). The organic layers were dried over Na2SO4, filtered and concentrated under reduce pressure, providing a yellow oil that when purified by flash chromatography (2–4% MeOH in DCM) gave (**1**, 222 mg) of the compound as a white foam [80%, Rf = 0.5 (5% MeOH in DCM)].

Scheme 1. Synthesis of the Ada-A488 compound (4).

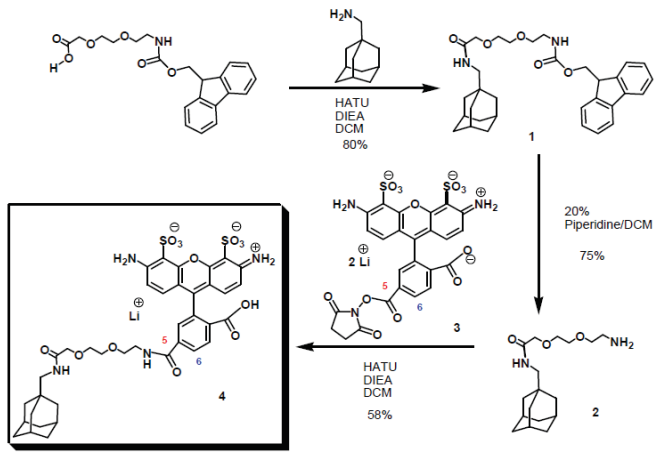

Preparation of compound 2

A solution of Fmoc 8-amino-3,6-dioxaocta-methyladamantane amide (**1**, 25 mg, 0.047 mmols) in piperidine-DCM mixture (1:4, 0.5 mL) was stirred at rt for 20 min, the solvent was removed *in vacuo*, and the residue was dissolved in DCM . This solution was washed with NaOH (1M). The organic phase was concentrated and dissolved in H2O. The resulted solution was centrifugated and the supernatant was liofilized giving 8-amino-3,6-dioxaocta-methyladamantane amide (**2**, 11 mg) as a yellow oil which was used without further purification [75%, Rt = 15.3 min (Eclipse Inertsil analitic column, 50–80 % MeOH 0.1%TFA in H2O 0.1%TFA in 19 min)].

^{1}**H NMR** (CD_3CN, 250.13 MHz, d): 7.04–6.85 (m, 2H, NH_2), 3.9 (s, 2H, CH_2 ester), 3.65–3.52 (m, 6H, CH_2 ether), 3.01–2.89 (bs, 2H, CH_2 amine), 2.83 (d, J = 6.57 Hz, 2H, CH_2 amide), 1.72–1.47 (m, 7H, CH and CH_2 Ad), 1.4 (s, 6H, CH_2 Ad).

Preparation of compound 4

8-amino-3,6-dioxaocta-methyladamantane amide (**2**, 0.35 mg, 1.12 mmols) and Alexa Fluor 488 carboxylic acid succinimidyl ester (mixed isomers) (**3**, 0.2 mg, 0.31 mmols) were dissolved in dry DCM (500 mL) and dry DMF (20 mL), DIEA (1 mL, 5.5 mmols) was added and the mixture was stirred under argon for 1 h. The crude was purified by HPLC, affording (**4**, 0.15 mg) of compound as a pink solid [58%, Rt = 15 min and 16min for 2 isomers (Eclipse Inertsil analitic column, 50–80% MeOH 0.1%TFA in H_2O 0.1%TFA in 19 min)].

MS (MALDI-TOF) [m/z (%)]: 825 ([M^-], 100), 779.4 (8), 604.2 (16).

Abbreviations Used

CD_3CN: Deuterated acetonitrile; DCM: Dichloromethane; DIEA: Diisopropylethylamine; DMF: dimethylformamide; Fmoc: Fluorenylmethoxycarbonyl; HATU:O-(7-azabenzotriazol-1-yl)-1,1,3,3-tetramethyluronium hexafluorophosphate; ^{1}H NMR: Proton nuclear magnetic resonance; HPLC: High Performance Liquid Chromatography; MALDI-TOF: Mass Spectrometry of Laser Desorption/Ionization-Time of Flight; bs: broad singlet; d: doublet; m: multiplet; s: singlet; rt: room temperature.

Suppliers

Fmoc 8-amino-3,6-dioxaoctanoic acid: Commercially available from Bachem; Alexa Fluor 488 carboxylic acid succinimidyl ester (mixed isomers): Commercially available from Molecular Probes.

5. Conclusions

Fluorescence correlation spectroscopy has been proved to be an excellent method for the determination of the stoichiometry and the association equilibrium constant of host-guest complexes with fluorescently labelled guests. FCS requires only that guest or host can be fluorescently labelled and that the complexation increases sufficiently the molar mass of the fluorescent species. FCS needs only minimal amounts of host and guest, is fast and relatively straightforward, as long as the

experimental conditions are carefully selected. All commercially available systems allow this type of measurements.

A very high value of the association equilibrium constant between Ada-A488 and βCD was determined, which agrees well with that given in the literature for the inclusion of similar adamantane derivatives into βCD.

Acknowledgements

J.B. thanks the Ministerio de Ciencia e Innovación for a research scholarship. M.J.P.A thanks the Spanish MICINN for her FPI Fellowship. M.N. and W.A. thank the Ministerio de Ciencia e Innovación and the Xunta de Galicia for financial support (CTQ2004-07683-C02-02, INCITE07PXI209034ES, INCITE08E1R209060ES).

References and Notes

1. Turro, N.J. Supramolecular structure and dynamics special feature: Molecular structure as a blueprint for supramolecular structure chemistry in confined spaces. *Proc. Nat. Acad. Sci. USA* **2005**, *102*, 10766–10770.
2. Dodziuk, H. *Introduction to Supramolecular Chemistry*; Springer: Dordrecht, The Netherlands, 2002.
3. Rigler, R.; Elson, E.S. *Fluorescence Correlation Spectroscopy*: *Theory and Applications*; Springer: Berlin, Germany, 2001.
4. Al-Soufi, W.; Reija, B.; Novo, M.; Felekyan, S.; Kühnemuth, R.; Seidel, C.A.M. Fluorescence correlation spectroscopy, a tool to investigate supramolecular dynamics: Inclusion complexes of pyronines with cyclodextrin. *J. Am. Chem. Soc.* **2005**, *127*, 8775–8784.
5. Al-Soufi, W.; Reija, B.; Felekyan, S.; Seidel, C.A.; Novo, M. Dynamics of supramolecular association monitored by fluorescence correlation spectroscopy. *Chemphyschem* **2008**, *9*, 1819–1827.
6. Cramer, F.; Hettler, H. Inclusion compounds of cyclodextrins. *Naturwissenschaften* **1967**, *54*, 625–32.
7. Szejtli, J. Introduction and general overview of cyclodextrin chemistry. *Chem. Rev.* **1998**, *98*, 1743–1754.
8. Dodziuk, H. *Cyclodextrins and Their Complexes*: *Chemistry, Analytical Methods, Applications*; Wiley: Weinheim, Germany, 2006.
9. Carrazana, J.; Reija, B.; Ramos Cabrer, P.; Al-Soufi, W.; Novo, M.; Vázquez Tato, J. Complexation of methyl orange with beta-cyclodextrin: Detailed analysis and application to quantification of polymer-bound cyclodextrin. *Supramol. Chem.* **2004**, *16*, 549–559.
10. Bordello, J.; Reija, B.; Al-Soufi, W.; Novo, M. Host-assisted guest self-assembly: Enhancement of the dimerization of pyronines Y and B by gamma-cyclodextrin. *Chemphyschem* **2009**, *10*, 931–939.
11. Reija, B.; Al-Soufi, W.; Novo, M.; Vázquez Tato, J. Specific interactions in the inclusion complexes of Pyronines Y and B with beta-cyclodextrin. *J. Phys. Chem. B* **2005**, *109*, 1364–1370.

12. Bohne, C. Supramolecular dynamics of guest complexation to cyclodextrins. *Spectrum* **2000**, *13*, 14–19.
13. Harada, A.; Li, J.; Kamachi, M. Synthesis of a tubular polymer from threaded cyclodextrins. *Nature* **1993**, *364*, p. 516.
14. Lehn, J.M. *Supramolecular Chemistry*; VCH: Weinheim, Germany, 1995.
15. Nepogodiev, S.A.; Stoddart, J.F. Cyclodextrin-based catenanes and rotaxanes. *Chem. Rev.* **1998**, *98*, 1959–1976.
16. Alvarez Parrilla, E.; Ramos Cabrer, P.; Al-Soufi, W.; Meijide del Río, F.; Rodríguez Núñez, E.A.; Vázquez Tato, J. Dendritic growth of a supramolecular complex. *Angew. Chem. Int. Ed. Engl.* **2000**, *39*, 2856–2858.
17. Ogoshi, T.; Harada, A. Chemical sensors based on cyclodextrin derivatives. *Sensors* **2008**, *8*, 4961–4982.
18. Hennig, A.; Bakirci, H.; Nau, W.M. Label-free continuous enzyme assays with macrocycle-fluorescent dye complexes. *Nat. Methods* **2007**, *4*, 629–632.
19. Breslow, R.; Belvedere, S.; Gershell, L.; Leung, D. The chelate effect in binding, catalysis, and chemotherapy. *Pure Appl. Chem.* **2000**, *72*, 333–342.
20. Loftsson, T.; Brewster, M.E. Pharmaceutical applications of cyclodextrins. 1. Drug solubilization and stabilization. *J. Pharm. Sci.* **1996**, *85*, 1017–1025.
21. Uekama, K.; Hirayama, F.; Irie, T. Cyclodextrin drug carrier systems. *Chem. Rev.* **1998**, *98*, 2045–2076.
22. Hirayama, F.; Uekama, K. Cyclodextrin-based controlled drug release system. *Adv. Drug Deliv. Rev.* **1999**, *36*, 125–141.
23. Lezcano, M.; Al-Soufi, W.; Novo, M.; Rodríguez-Núñez, E.; Vázquez Tato, J. Complexation of several benzimidazole-type fungicides with alpha- and beta-cyclodextrins. *J. Agric. Food Chem.* **2002**, *50*, 108–112.
24. Ritter, H.; Tabatabai, M. Cyclodextrin in polymer synthesis: A green way to polymers. *Progr. Polym. Sci.* **2002**, *27*, 1713–1720.
25. Davis, M.E.; Brewster, M.E. Cyclodextrin-based pharmaceutics: Past, present and future. *Nat. Rev. Drug Discov.* **2004**, *3*, 1023–1035.
26. Eftink, M.R.; Andy, M.L.; Bystrom, K.; Perlmutter, H.D.; Kristol, D.S.J. Cyclodextrin inclusion complexes: Studies of the variation in the size of alicyclic guests. *J. Am. Chem. Soc.* **1989**, *111*, 6765–6772.
27. Cromwell, W.C.; Bystrom, K.; Eftink, M.R. Cyclodextrin-adamantanecarboxylate inclusion complexes: Studies of the variation in cavity size. *J. Phys. Chem.* **1985**, *89*, 326–332.
28. Gelb, R.I.; Schwartz, L.M. Complexation of admantane-ammonium substrates by beta-cyclodextrin and its O-methylated derivatives. *J. Incl. Phenom. Mol. Recogn. Chem.* **1989**, *7*, 537–543.
29. Palepu, R.; Reinsborough, V.C. β-cyclodextrin inclusion of adamantane derivatives in solution. *Aust. J. Chem.* **1990**, *43*, 2119–2123.
30. Kwak, E.S.; Gomez, F.A. Determination of the binding of β-cyclodextrin derivatives to adamantane carboxylic acids using capillary electrophoresis. *Chromatographia* **1996**, *43*, 659–662.

31. Harries, D.; Rau, D.C.; Parsegian, V.A. Solutes probe hydration in specific association of cyclodextrin and adamantane. *J. Am. Chem. Soc.* **2005**, *127*, 2184–2190.
32. Koopmans, C.; Ritter, H. Formation of physical hydrogels *via* host-guest interactions of b-cyclodextrin polymers and copolymers bearing adamantyl groups. *Macromolecules* **2008**, *41*, 7418–7422.
33. Holzinger, M.; Bouffier, L.; Villalonga, R.; Cosnier, S. Adamantane/β-cyclodextrin affinity biosensors based on single-walled carbon nanotubes. *Biosens. Bioelectron.* **2009**, *24*, 1128–1134.
34. Park, I.; von Recum, H.A.; Jiang, S.; Pun, S.H. Spatially-controlled delivery of cyclodextrin-based polyplexes from solid surfaces. *Mol. Ther.* **2006**, *13*, S67–S67.
35. Bellocq, N.C.; Pun, S.H.; Jensen, G.S.; Davis, M.E. Transferrin-containing, cyclodextrin polymer-based particles for tumor-targeted gene delivery. *Bioconjug. Chem.* **2003**, *14*, 1122–1132.
36. Munteanu, M.; Choi, S.; Ritter, H. Cyclodextrin-click-cucurbit[6]uril: Combi-receptor for supramolecular polymer systems in water. *Macromolecules* **2009**, *42*, 3887–3891.
37. Soto Tellini, V.H.; Jover, A.; Carrazana Garcia, J.; Galantini, L.; Meijide, F.; Vázquez Tato, J. Thermodynamics of formation of host-guest supramolecular polymers. *J. Am. Chem. Soc.* **2006**, *128*, 5728–5734.
38. Widengren, J.; Rigler, R. Fluorescence correlation spectroscopy as a tool to investigate chemical reactions in solutions and on cell surfaces. *Cell Mol. Biol.* **1998**, *44*, 857–879.
39. Widengren, J. *Photophysical aspects of FCS Measurements*; Rigler, R., Elson, E.S., Eds.; Springer Verlag: Berlin, Germany, 2001; p. 276.
40. Haustein, E.; Schwille, P. In *Fluorescence Correlation Spectroscopy in Vitro and in Vivo*; Selvin, P. R., Ha, T., Eds.; Cold Spring Harbor Laboratory Press: New York, NY, USA, 2008; p. 259.
41. Elson, E.L.; Magde, D. Fluorescence correlation spectroscopy. I. Conceptual basis and theory. *Biopolymers* **1974**, *13*, 1–27.
42. Enderlein, J.; Gregor, I.; Patra, D.; Dertinger, T.; Kaupp, U.B. Performance of fluorescence correlation spectroscopy for measuring diffusion and concentration. *Chemphyschem* **2005**, *6*, 2324–2336.
43. Alcor, D.; Allemand, J.F.; Cogne-Laage, E.; Croquette, V.; Ferrage, F.; Jullien, L.; Kononov, A.; Lemarchand, A. Stochastic resonance to control diffusive motion in chemistry. *J. Phys. Chem. B* **2005**, *109*, 1318–1328.
44. Carrazana, J.; Jover, A.; Meijide, F.; Soto, V.H.; Vázquez Tato, J. Complexation of adamantyl compounds by beta-cyclodextrin and monoaminoderivatives. *J. Phys. Chem. B* **2005**, *109*, 9719–9726.
45. Felekyan, S.; Kuhnemuth, R.; Kudryavtsev, V.; Sandhagen, C.; Becker, W.; Seidel, C.A.M. Full correlation from picoseconds to seconds by time-resolved and time-correlated single photon detection. *Rev. Sci. Instrum.* **2005**, *76*, 083104:1–083104:14.
46. Eggeling, C.; Widengren, J.; Rigler, R.; Seidel, C.A.M. Photobleaching of fluorescent dyes under conditions used for single-molecule detection: Evidence of two-step photolysis. *Anal. Chem.* **1998**, *70*, 2651–2659.
47. Gendron, P.O.; Avaltroni, F.; Wilkinson, K.J. Diffusion coefficients of several rhodamine derivatives as determined by pulsed field gradient-nuclear magnetic resonance and fluorescence correlation spectroscopy. *J. Fluoresc.* **2008**, *18*, 1093–1101.

48. Muller, C.; Loman, A.; Pacheco, V.; Koberling, F.; Willbold, D.; Richtering, W. Precise measurement of diffusion by multi-color dual-focus fluorescence correlation spectroscopy. *Europhys. Lett.* **2008**, *83*, 46001:1–46001:6.

J Incl Phenom Macrocycl Chem (2011) 70:259–268
DOI 10.1007/s10847-010-9859-4

ORIGINAL ARTICLE

Host–guest association studied by fluorescence correlation spectroscopy

Mercedes Novo · Daniel Granadero · Jorge Bordello · Wajih Al-Soufi

Received: 26 June 2010 / Accepted: 5 September 2010 / Published online: 28 September 2010

Abstract Fluorescence Correlation Spectroscopy (FCS) is a powerful single molecule technique for the study of the stability and the association dynamics of supramolecular systems and, in particular, of host–guest inclusion complexes. With FCS the host–guest binding equilibrium constant is determined analysing the variation in the diffusion coefficient of the fluorescent guest or host with no need for a change in the photophysical properties of the fluorescent probe. FCS gives also access to the association/dissociation rate constants of the host–guest inclusion providing that the fluorescence intensity of host or guest changes upon complexation. These rate constants can be compared with that of a diffusion-controlled process estimated from the same FCS experiment allowing for a better understanding of the association dynamics. The results show that cyclodextrin cavities act as "hard" cages which put geometric and orientational restrictions on the inclusion of a hydrophobic guest, whereas micelles behave as "soft" cages without geometrical requirements.

In our contribution to this special issue we review briefly the application of FCS to the study of host–guest inclusion complexes with an emphasis on practical aspects and relevant bibliographic references.

Keywords Cyclodextrins · Micelles · Fluorescence correlation spectroscopy · Supramolecular association · Supramolecular dynamics

Introduction

Host–Guest complexes are supramolecular aggregates stabilized by non-covalent bonds and are ubiquitous in biochemical, pharmaceutical, environmental, cosmetic, food, and other chemical systems and applications [1]. Different approaches are necessary to fully understand a supramolecular system: structural studies yield stoichiometry, geometry, association sites and heterogeneity, thermodynamic studies provide information about stability, equilibrium constants and reversibility, and finally dynamic studies are necessary to describe the association/dissociation dynamics, diffusional properties or conformational dynamics. Most published studies focus on structure and thermodynamics of supramolecular association, which, however, give very few information about the dynamics of the system. As pointed out by Bohne "Dynamic studies are necessary to provide the 'movie' in addition to the 'snapshots' taken from structural and thermodynamic measurements" [2].

In this contribution we briefly summarize how to use Fluorescence Correlation Spectroscopy (FCS) for the study of supramolecular association and, more specifically, of the stability and the binding[1] dynamics in host–guest systems. We show how knowledge about the dynamics gives valuable information about the association mechanism, which is directly related to the structure of the host and the guest. For details we refer to relevant bibliography.

M. Novo (✉) · D. Granadero · J. Bordello · W. Al-Soufi
Department of Physical Chemistry, University of Santiago de Compostela, Biophysical Chemistry, Photophysics and Spectroscopy Group, 27002 Lugo, Spain
e-mail: m.novo@usc.es

[1] As usual we use "binding" as a general term for an attractive noncovalent interaction. In the context of "host–guest" systems it refers to a "complexation" or more specifically to "inclusion".

Association dynamics

Host–Guest complexes are typically formed by the association of host H with guest G to give a 1:1 complex HG (see Fig. 1). The association rate (on-rate) $v_+ = k_+ [H] [G]$ is described by the bimolecular association rate constant k_+, whereas the dissociation rate (off-rate) $v_- = k_- [HG]$ is defined by the unimolecular dissociation rate constant k_-. Both processes, association and dissociation, are rate-limited by molecular diffusion and thus upper limits are given by diffusion-controlled rate constants: i.e. $k_+ < 10^{10}$ M^{-1} s^{-1}, $k_- < 10^9$ s^{-1} in aqueous solution.

At equilibrium both rates are equal, $v_+ = v_-$, and the binding equilibrium constant K is derived as ratio of the association and dissociation rate constants as given in Eq. (1).

$$K = \frac{[HG]_{eq}}{[H]_{eq}\,[G]_{eq}} = \frac{k_+}{k_-} \tag{1}$$

Dynamic studies give information on how fast the complex associates or dissociates. For a 1:1 complexation the corresponding rate law [Eq. (2)] and the typical condition of excess host concentration[2] ($[H]_0 \gg [G]_0$) lead to a pseudo-first order association rate and to kinetics which are mono-exponential with an observed relaxation rate constant k_R as given in Eq. (3).[3]

$$\frac{d[HG]}{dt} = k_+ [H]\,[G] - k_- [HG] \tag{2}$$

$$[G](t) \sim e^{-k_R t}, \quad [HG]\,(t) \sim 1 - e^{-k_R t}, \quad k_R = k_+ [H]_0 + k_- \tag{3}$$

The relaxation rate constant k_R depends on the two rate constants, k_+ and k_-. The contribution of the association process can be modulated by varying the host concentration $[H]_0$, but not that of the dissociation [3, 4].

Can we infer information about the relaxation rate constant k_R of the binding equilibrium from the corresponding equilibrium constant K? In other words: does knowledge about the stability (thermodynamics) of a complex give information about the dynamics of the host guest association? The answer is "not so much"; systems with similar values of their stability constant K may present very different values of their association and dissociation rate constants. For example, for a typical intermediate stability constant, $K = 1000$ M^{-1}, the association rate constant can fall in a very wide interval, between very low values, e.g. $k_+ = 10^3$ M^{-1} s^{-1} or very high ones, only limited by diffusion ($k_+ = 10^{10}$ M^{-1} s^{-1}), with the corresponding values of the dissociation rate constants as indicated in Fig. 2.

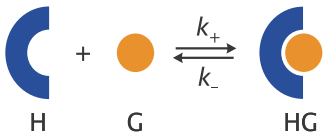

Fig. 1 Host H and guest G form complex HG with association rate constant k_+ and separate with dissociation rate constant k_-

That host–guest complexes with similar stability can present very different dynamics, had already been demonstrated by the classical work of Cramer et al. [5] for the inclusion of different azoderivatives by α-cyclodextrin (α-CD) studied by the temperature-jump technique. Substitution of the azoderivatives with ethyl or methyl side groups changes only very slightly the stability of the α-CD inclusion complex but decreases the association and dissociation rate constants by several orders of magnitude.

How fast is the association/dissociation process? The time scale of this process is given by the relaxation time $\tau_R = k_R^{-1}$ which is the inverse of the relaxation rate constant k_R [Eq. (3)]. Again, as an example, for $K = 1000$ M^{-1}, we can analyse the two above-mentioned cases as depicted in Fig. 3, right panel: slow dynamics with $k_+ = 10^3$ M^{-1} s^{-1}, $k_- = 1$ s^{-1} (upper red curve) correspond to long relaxation times of $\tau_R = 1$ s. Fast, diffusion-controlled dynamics with $k_+ = 10^{10}$ M^{-1} s^{-1}, $k_- = 10^7$ s^{-1} (lower, blue curve) lead to short relaxation times of $\tau_R = 100$ ns or faster. These

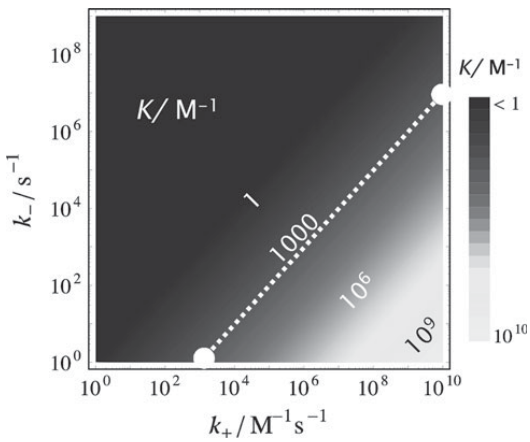

Fig. 2 Very different values of the association rate constant k_+ and the dissociation rate constant k_- can lead to the same value of the binding equilibrium constant K

[2] Here we assume that the guest acts as fluorescent probe. Being FCS a single molecule technique, the total concentration of the fluorescent probe is very low, of the order of $[G]_0 \approx 10^{-8}$ M. Thus, the condition ($[H]_0 \gg [G]_0$) is fulfilled even for hosts of low solubility or high affinity systems.

[3] Don't confuse the time dependence of the guest concentration [G](t) with the autocorrelation of the intensity fluctuations $G(\tau)$ defined in Eq. (4).

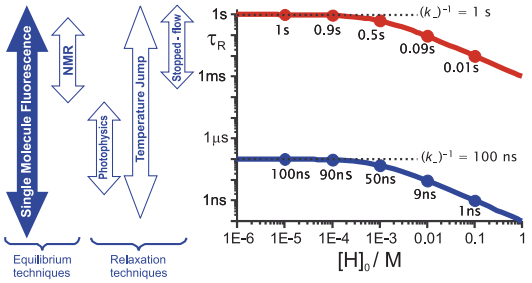

Fig. 3 *Right panel*: For the same typical intermediate binding equilibrium constant, $K = 1000\ M^{-1}$, the relaxation time $\tau_R = k_R^{-1}$ of the equilibrium can vary in a very wide time interval from seconds to nanoseconds. *Upper curve*: slow dynamics with $k_+ = 10^3\ M^{-1}\ s^{-1}$, $k_- = 1\ s^{-1}$, and $\tau_R < 1$ s. *Lower curve*: fast dynamics with $k_+ = 10^{10}\ M^{-1}\ s^{-1}$, $k_- = 10^7\ s^{-1}$, and $\tau_R < 100$ ns. *Left panel*: Dynamic range covered by some frequently used fast techniques for the determination of the rate constants of supramolecular association/dissociation

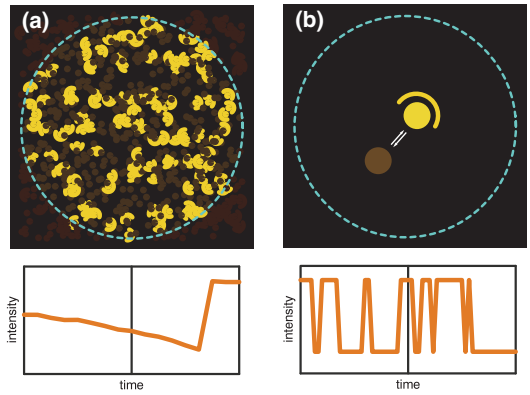

Fig. 4 Simulated kinetic experiments for the study the dynamics of a reversible (association) reaction assuming that the guest increases its fluorescence intensity upon complexation. *Upper panels*: scheme of the sample volume (*dashed circle*) with *bright* complex and *dark* free guest. *Lower panels*: observed total fluorescence intensity as function of time (time increases to the left). **a** Standard "bulk" measurement: the ensemble relaxes back to equilibrium after an external perturbation. The relaxation time is determined from the exponential change in the "bulk" fluorescence intensity. **b** Single molecule measurement: the system is at equilibrium and the reversible process is followed directly from the change in fluorescence intensity provoked by the reaction. Depending on the single molecule technique the rate constants k_+ and k_- are determined directly from the time the system stays in each of the two states (free, bound) or the relaxation time τ_R is determined from the characteristic time of the fluorescence fluctuations

relaxation rates correspond to conditions of very low host concentration where the dissociation process controls the relaxation rate. In both cases the observed relaxation time is shortened with increasing host concentration. As can be seen, binding dynamics cover a very wide time range and the upper limit corresponds to very fast reactions experimentally not easily accessible.

Frequently used fast techniques for the determination of the rate constants of supramolecular association/dissociation are temperature-jump (T-Jump), time-resolved fluorescence (TRF), laser flash photolysis (LFP), ultrasonic relaxation and stopped-flow (see Fig. 3, left panel) [2, 6–8]. These methods analyze the relaxation of the system back to equilibrium after a perturbation. TRF and LFP rely on the photophysics of chromophores with fluorescent excited states or long lived triplet states and/or on the presence of a quenching molecule. Ultrasonic relaxation needs no chromophore but requires detailed knowledge about the molecular process being disturbed. Laser T-Jump covers a wide time range from nanoseconds to seconds, whereas TRF, LFP and ultrasonic relaxation are limited to dynamics of nano- to microseconds. Stopped-flow techniques can only be used to study slow dynamics. There are other techniques that allow dynamic study of systems at thermodynamic equilibrium. The most known is NMR, which is, however, limited to slow dynamics.

Single molecule fluorescence

The study of supramolecular dynamics require methodologies which cover a very wide range of time scales, ideally within the same experiment. It is also preferred not to rely on unique photophysical properties of the host guest system and to avoid perturbation of the system. Techniques which analyze the fluorescence of single molecules have the potential to cover these needs. They analyze variations in the fluorescence intensity of a molecular system due to spontaneous fluctuations around the equilibrium, without the need for an external perturbation and they can cover a very wide dynamic range [9, 10].

Although standard "bulk" fluorescence experiments already use low dye concentrations of about 10^{-6} mol/L and small detection volumes around 1 mm^3, the observed fluorescence is still an average of the light emitted by about 10^{11} dye molecules! This huge number average hides any static and temporal heterogeneities in the molecular ensemble and, more important for our case, makes it practically impossible to follow directly the dynamics of the unsynchronized molecular processes. Kinetic measurements at these "bulk" concentrations require therefore some external perturbation which synchronizes the molecular processes, so that their relaxation back to equilibrium can be followed as a macroscopic variation of the ensemble properties (Fig. 4a).

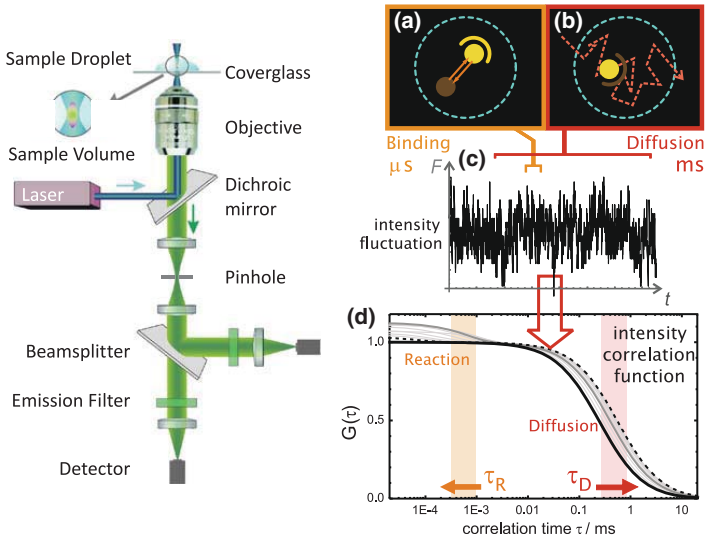

Fig. 5 Principles of Fluorescence Correlation Spectroscopy. *Left panel*: epi-illuminated confocal microscope used to create a microscopic sample volume. *Right panel*: scheme of the data analysis. **a**, **b** The *dashed circles* indicate the border of the sample volume. The *dots* represent dye molecules undergoing a reversible association (**a**), and moving randomly through the solution due to Brownian motion (**b**). Detected fluorescence intensity (**c**), and autocorrelation function of the intensity fluctuations (**d**)

Single molecule fluorescence techniques observe a very small number or even a single molecule at a time (Fig. 4b) and avoid thus the loss of information due to averaging. Observing a few molecules allows one to follow directly the dynamics of the reversible association process as significant fluctuations in the fluorescence intensity, provided that the association affects the brightness[4] of the fluorescent guest (or host).

In order to detect fluorescence from single fluorophores it is not sufficient to reduce the concentration of the observed dye but it is also necessary to suppress the background signal (Raman scattering, impurities) by reducing the sample volume itself. Different techniques are used for this aim. For slow dynamics one of the reaction partners is typically immobilized on a glass surface and the fluorescence is excited only within a very thin layer above this surface by means of special illumination techniques (e.g. total internal reflection, TIR). The fluorescence from this layer can then be detected with highly sensitive CCD cameras [9]. Dynamics in the microsecond to hour range can be observed, limited mainly by the photostability of the dyes at the long end and the time resolution of the detection at short times.

Faster dynamics are typically observed with molecules which diffuse freely through a very small open detection volume defined by the focus of an epi-illuminated confocal microscope (see Fig. 5). During the transit through the sample volume the fluorophore is repeatedly excited and the change in fluorescence intensity due to the reversible reaction is detected. Here the dynamic range is limited by the fluorescence lifetime of some nanoseconds of the dye itself and the mean transit time of the fluorophore through the sample volume, typically in the millisecond range. The fluorescence intensity fluctuations can be analyzed by different techniques, and we will present in the following FCS as one of the most widely used.

For all Single Molecule Fluorescence techniques several conditions have to be fulfilled. One needs very bright and photostable dyes, very efficient excitation and detection setups, very low dye concentrations and highly purified solvents and solutes. In order to observe the dynamics one also relies on a highly fluorescent probe molecule which undergoes some change in its photophysical properties during the association/dissociation process.

Fluorescence correlation spectroscopy

Principles

FCS analyzes the spontaneous temporal fluctuations of the fluorescence intensity emitted by a few (1–10) molecules in a small open sample volume. These intensity fluctuations may be due to various processes at the molecular level: changes in the singlet or triplet excited-state population, changes in the local concentration due to translational motion of the fluorophores in and out of the sample volume or changes in their physicochemical properties, for example due to a chemical reaction or, as in our case, supramolecular association. Each of these processes modulates

[4] The species dependent *brightness* is given by the product of the extinction coefficient, fluorescence quantum yield and detection efficiency and is a measure for the detected fluorescence count rate from each species.

the fluorescence intensity at a characteristic timescale which can in principle be derived from the autocorrelation function of the intensity trace. Several excellent reviews [11–15], monographs [9, 16–19], and textbooks [20, 21] present FCS theory for different applications. We will point out briefly the most important aspects.

In FCS the molecules under study diffuse freely freely within a small sample droplet and eventually pass through the focus of a confocal epi-illuminated fluorescence microscope (Fig. 5, left). The focus defines an open microscopic effective detection volume of some femtoliter (10^{-15} L). If the concentration of the dye molecules in the droplet is low (nanomolar, 10^{-9} mol/L) then only very few molecules are observed at a time. The molecules are excited by laser light through the microscope objective and their fluorescence is collected by the same objective and focused through a pinhole and filters onto detectors with single photon sensitivity. The molecules move randomly through the solution due to Brownian motion (Fig. 5b) and at the same time undergo a fast reversible reaction (Fig. 5a). Both processes introduce fluctuations at characteristic time scales in the detected total fluorescence intensity $F(t)$ (Fig. 5c). The characteristic time of the fluctuations is determined from the autocorrelation curve $G(\tau)$ of the intensity fluctuations $\delta F(t)$ (Fig. 5d) given by Eq. (4) with correlation time τ [3, 4].

$$G(\tau) = \frac{\langle \delta F\,(t) \cdot \delta F\,(t+\tau)\rangle}{\langle F\,(t)\rangle^2} \tag{4}$$

Under the conditions discussed in the following sections the full correlation function for translational diffusion and a fast reversible (association) reaction is given by Eq. (5) with the mean diffusion (transit) time $\bar{\tau}_D$, the mean number of fluorescent molecules in the sample volume N, the ratio between radial and axial radii of the sample volume w_{xy}/w_z, and the amplitude A_R of the reaction term.

$$G_{\mathrm{DR}}(\tau) = \frac{1}{N}\left(1+\frac{\tau}{\bar{\tau}_{\mathrm{D}}}\right)^{-1}\left(1+\left(\frac{w_{\mathrm{xy}}}{w_{\mathrm{z}}}\right)^2\frac{\tau}{\bar{\tau}_{\mathrm{D}}}\right)^{-\frac{1}{2}}\left(1+A_{\mathrm{R}}\,e^{-k_{\mathrm{R}}\tau}\right) \tag{5}$$

Translational diffusion

On the millisecond time scale the observed fluorescence intensity depends on the number of dye molecules present in the open sample volume, a number which fluctuates due to the entry and exit of dyes under Brownian motion. The characteristic time of these fluctuations reflects the mean transit (or diffusion) time τ_{D} of the fluorescent species through the sample volume, which depends on the translational diffusion coefficient of the fluorophore and on the size of the sample volume. A calibration of this size with a reference dye allows one then to determine the diffusion coefficient of the fluorophore from measurements of τ_{D}. The translational diffusion coefficient D is inversely proportional to the diffusion time τ_{D} according to Eq. (6), with w_{xy} being the radial radius of the sample volume. The diffusion coefficient D is also related to the hydrodynamic radius R_h as given for homogeneous spheres by the Stokes–Einstein relation on the right hand in Eq. (6), where k is the Boltzmann constant and η the viscosity of the solvent.

$$D = \frac{w_{xy}^2}{4\tau_D} = \frac{kT}{6\pi\eta R_h} \tag{6}$$

The amplitude of the correlation function [Eq. (5)] is inversely proportional to the number of fluorophores in the detection volume (N), which is a peculiarity of the technique: the lower the concentration of dye the higher the amplitude of the fluctuations and, consequently, of the correlation function.

Binding equilibrium constant

The diffusion coefficient of a fluorescent guest decreases when it binds to a host. The association of the guest to the host introduces a variation in the observed diffusion coefficient (or diffusion time) of the guest which depends on the third root of the molar mass ratio, as given by Eq. (7) for homogeneous compact spheres.

$$\frac{D_{HG}}{D_G} = \frac{\tau_G}{\tau_{HG}} \approx \frac{R_{h,G}}{R_{h,HG}} \approx \sqrt[3]{\frac{M_G}{M_{HG}}} \tag{7}$$

FCS is used here for binding dynamics that are much faster than the mean diffusion time of the fluorophore through the detection volume (fast exchange). In this case the fluorescent guests will associate and dissociate many times during their transit, changing rapidly between free (G) and bound (HG) state. The observed mean diffusion time $\bar{\tau}_D$ depends then on the fraction of the time that the fluorescent guests spent in the free or in the bound state. This can be expressed by the number-weighted mean diffusion coefficient $\bar{D}$ obtained from the individual coefficients D_G and D_{HG} of free and bound dye and the number fractions $X_x = N_x/(N_G + N_{HG})$as given in Eq. (8).

$$\bar{\tau}_D = \frac{w_{xy}^2}{4\bar{D}} \quad \bar{D} = X_G D_G + X_{HG} D_{HG} \tag{8}$$

In the case of the equilibrium of Fig. 1 and Eq. (1) the fractions can be expressed by the equilibrium constant K and the host concentration $[\mathrm{H}]_0$ which leads to Eq. (9).

$$\bar{\tau}_D([\mathrm{H}]) = \frac{\tau_G(1+K[\mathrm{H}]_0)}{1+\frac{\tau_G}{\tau_{HG}}K[\mathrm{H}]_0} \tag{9}$$

Titrations of this mean diffusion time at different host concentrations $[\mathrm{H}]_0$ allows one to determine the binding

equilibrium constant K and the limiting diffusion coefficients of free and bound guest [4].

The binding equilibrium constant K can be determined solely from the change in the hydrodynamic properties of the guest upon complexation. For the determination of K it is therefore not necessary (but allowed) that the fluorophore changes its brightness during the binding. This makes it possible to study nonfluorescent hosts labelled with a fluorophore which does not need to interact itself with the host. This is an advantage of FCS over other fluorescence techniques which rely on a significant change of some fluorescence properties of the guest in order to detect its binding.

An example is the inclusion of the nonfluorescent guest adamantane by β-CD [22]. The fluorescent label (Alexa 488) attached to the adamantane presents no change in its fluorescent properties due to the inclusion of the adamantane moiety by β-CD. The inclusion equilibrium is therefore not easily accessible by standard fluorescence techniques. A FCS titration, however, shows immediately a systematic increase of the diffusion time of the fluorescently labelled adamantane ($M_G = 826$ g mol^{-1}) on the addition of β-CD ($M_H = 1135$ g mol^{-1}), as shown in Fig. 6.

The experimentally determined ratio of the limiting values $D_{HG}/D_G = \tau_G/\tau_{HG} = 0.74$ coincides perfectly with the expected value $(M_G/M_{HG})^{1/3} = (0.422)^{1/3} = 0.75$ [see Eq. (7)] [22]. The equilibrium constant obtained from these FCS titrations is in good agreement with that obtained by other techniques.

In order to follow with FCS the relatively small variations in the diffusion coefficient D_{HG}/D_G observed with small hosts such as cyclodextrins great care has to be taken during the experiments and artefacts introduced by triplet-state population, saturation and photobleaching, background signal, variation in solvent viscosity, sample temperature and deformations of the effective detection volume (due, for example, to very small variations in the cover slide thickness) have to be taken into account [22–24].

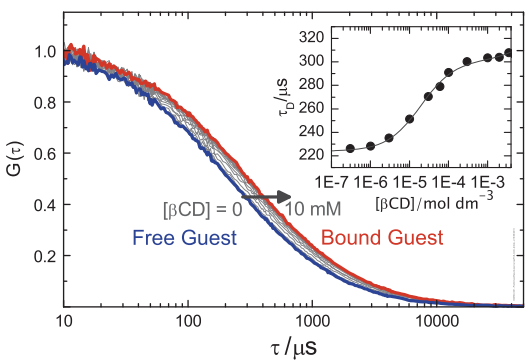

Fig. 6 Inclusion equilibrium between β-CD and adamantane labeled with Alexa 488 dye studied by FCS. Main panel: the diffusion term of the correlation curves shifts to longer times on the addition of increasing amounts of β-CD due to the increase in the mean diffusion time $\bar{\tau}_D$ of the guest. *Inset*: Plot of $\bar{\tau}_D$versus $[\beta\text{-CD}]_0$ (note the logarithmic concentration scale). Fitting of $\bar{\tau}_D$ with Eq. (9) yields the high equilibrium constant $K = (52 \pm 2)\ 10^3$ M^{-1} [22]

For an accurate determination of the binding equilibrium constant it is very important to make sure that the observed diffusion time is not affected by saturation and photobleaching of the fluorophore due to too high excitation irradiance. The diffusion time has to be independent of the excitation power, both at zero and at high host concentrations, which has to be checked experimentally for each host–guest combination. Too high irradiance shortens the observed diffusion time as a function of the host concentration and leads to strongly erroneous results for the equilibrium constant.

Binding dynamics

Binding dynamics can be observed when the fluorescence brightness of the guest changes between its free and bound states. Binding leads then to fluorescence blinking which can be analysed by FCS. To be detectable in FCS the blinking must be much faster than the transit through the sample volume, that is the relaxation time τ_R of the binding process (Eq. (2)) must be shorter than the diffusion time τ_D (fast exchange). The fluorescence intensity fluctuations due to the binding dynamics introduce then an additional term in the correlation function (Eq. (5)) at the relaxation time τ_R with an amplitude A_R which depends strongly on the brightness ratio $q = Q_{HG}/Q_G$ of bound and free fluorophore (Fig. 7, insets τ_R and A_R). Again both τ_R and A_R can be expressed as function of the host concentration and the binding constant as given in Eqs. (10) and (11). [3]

$$\tau_R\left([\mathrm{H}]\right) = \left(k_-\left(1 + K[\mathrm{H}]_0\right)\right)^{-1} \tag{10}$$

$$A_R = \frac{K[\mathrm{H}]_0(1-q)^2}{\left(1 + qK[\mathrm{H}]_0\right)^2} \tag{11}$$

The amplitude of the reaction term A_R is zero both at very low and at very high host concentrations when the guest is either totally free or fully bound (see Fig. 7). The highest amplitude A_R is reached at a host concentration $[\mathrm{H}]_{0,\max} = (K{\cdot}q)^{-1}$ which depends on the brightness ratio q. Fluorophores which increase strongly their brightness upon binding make it possible to detect the dynamics already at a very small degree of binding (low host concentrations) and at relatively long relaxation times [25].

From fits of the corresponding correlation function [Eqs. (5), (9), (10), (11)] to the experimental correlation curves one determines both the equilibrium constant K and the

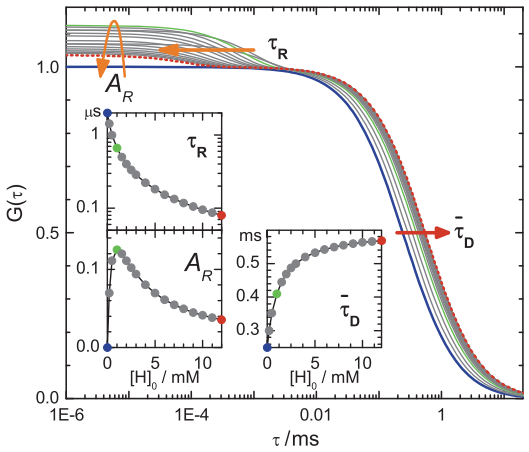

Fig. 7 *Main panel*: Correlation curves from simulated FCS experiments [Eq. (5)] of an inclusion equilibrium as depicted in Fig. 5. *Thick line*: free guest, $[H]_0 = 0$. *Thin grey lines*: intermediate host concentrations. *Dashed line*: highest host concentration $[H]_0 = 12$ mM. *Insets*: Dependence of the amplitude of the relaxation term A_R, of the relaxation time τ_R, and of the mean diffusion time $\bar{\tau}_D$ on $[H]_0$. (Parameters used for simulation: $N = 1$, $\tau_G = 0.25$ ms, $\tau_{HG} = 0.6$ ms, $q = 0.5$, $K = 2000$ M^{-1}, $k_+ = 10^9$ M^{-1} s^{-1}, $k_- = 5\ 10^5$ s^{-1})

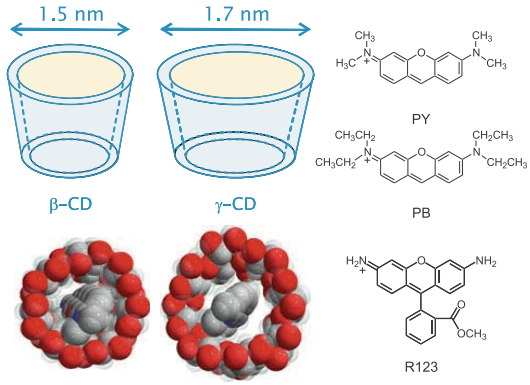

Fig. 8 Geometry of β-CD and γ-CD. Structures of the dyes PY, PB, and R123

dissociation rate constant k_-. From Eq. (1) also the association rate constant k_+ is obtained. [3]

Complications may arise when additional terms appear in the correlation curves, mainly due to excited-state dynamics of the fluorophore. Transitions in and out of the dark triplet state of the fluorophore introduce fluorescence fluctuations with the triplet lifetime of some microseconds [26]. The population of the triplet state is strongly dependent on the excitation power and can in principle be reduced working at low irradiance.

Influence of host–guest geometry on the dynamics

In order to study the influence of the geometry of host and guest on the binding dynamics we studied two parent cyclodextrins, β-CD and γ-CD, and two analogous guest molecules, pyronine Y (PY) and pyronine B (PB), which have the same xanthene skeleton but methyl and ethyl substituents, respectively, at the amino side groups (Fig. 8).

Electronic absorption and fluorescence spectroscopic studies showed that in all cases 1:1 pyronine:CD complexes are formed, although also 2:1 complexes with γ-CD are observed for both pyronines at dye concentrations much higher than those used in FCS [27, 28]. The values of the (1:1) association equilibrium constants, K, differ significantly between the four host–guest combinations (Table 1). In contrast to what may be expected, for each type of CD the binding constant is larger with PB than with PY in spite of the bulkier side groups of PB. Moreover, larger association equilibrium constants are obtained for the CD of smaller cavity.

The pure emission spectra of free and bound dyes allow one to estimate the brightness ratio q as given in Table 1. In the systems studied here, the brightness of the dyes decrease significantly when they are bound to the hosts.

As an example Fig. 9 shows a series of correlation curves obtained in titration experiments of PY with β-CD. Due to the fast exchange of the pyronine guest in and out of the CD complex only a single diffusion term with a mean diffusion time, $\bar{\tau}_D$, is observed which increases as the host concentration is increased (compare insets $\bar{\tau}_D$ in Figs. 7, 9). The second term in the correlation curves due to the association/dissociation dynamics is described by the relaxation time, τ_R, and an amplitude A_R that varies with the concentration of the host as expected (compare insets τ_R in Figs. 7, 9). In all cases it has to be checked that the relaxation time is in fact much shorter than the diffusion time, in order to allow for the separation of the two terms in the correlation function. The small contribution of the triplet-state formation to the correlation curves which appears at about the same correlation time as the reaction term must also be taken into account in the analysis.

Global target analysis of the FCS curves as a function of host concentration with the correlation function as given in Eq. (5) yields the association/dissociation rate constants [3]. The results of the fits for the systems under study are shown in Table 1. In most cases the value of K obtained from bulk fluorescence and absorption titrations was fixed in the fits of the correlation curves, in order to improve the accuracy of other fit parameters such as k_-. For the system PY:γ-CD it was not possible to determine the association and dissociation rate constants since the reaction term

Table 1 Results from Global target fits of series of FCS curves and derived values as explained in the text [3, 4]

	PB:β-CD	PY:β-CD	PB:γ-CD	PY:γ-CD	R123:TX100
$K/10^3$ M^{-1}	2.1 ± 0.2	0.40 ± 0.04	0.19 ± 0.03	0.04 ± 0.01	65 ± 3
q	0.49 ± 0.04	0.6 ± 0.2	0.67 ± 0.02	0.34 ± 0.02	0.42 ± 0.03
τ_A/ms	0.30 ± 0.02	0.25 ± 0.02	0.27 ± 0.02	0.23 ± 0.02	0.263 ± 0.002
τ_B/ms	0.40 ± 0.04	0.45 ± 0.06	0.46 ± 0.05	0.41 ± 0.05	1.66 ± 0.05
$k_+/10^9 M^{-1} s^{-1}$	**0.15 ± 0.05**	**0.2 ± 0.1**	**0.56 ± 0.11**	**>1**	**14 ± 1**
$k_-/10^4 s^{-1}$	7.6 ± 2.7	50 ± 30	300 ± 30	–	22 ± 1
$k_d/10^9 M^{-1} s^{-1}$	**7.7 ± 0.5**	**8.0 ± 0.5**	**8.0 ± 0.5**	**8.4 ± 0.3**	**16 ± 1**
$k_{-d}/10^9$ s^{-1}	2.0 ± 0.1	2.6 ± 0.2	2.1 ± 0.2	2.7 ± 0.1	0.11 ± 0.01
$k_r/10^9$ s^{-1}	0.04 ± 0.01	0.07 ± 0.03	0.16 ± 0.03	–	–
$k_{-r}/10^4$ s^{-1}	7.7 ± 2.7	50 ± 30	320 ± 100	–	–
$D_G/10^{-10} m^2$ s^{-1}	4.8 ± 0.4	5.8 ± 0.4	4.8 ± 0.4	5.8 ± 0.4	4.3 ± 0.4
$D_{HG}/10^{-10}$ m^2 s^{-1}	3.6 ± 0.4	3.2 ± 0.3	3.1 ± 0.4	3.5 ± 0.4	0.7 ± 0.1
R_G/R_{HG} (Å)	5.1/6.8	4.2/7.6	5.1/7.8	4.2/7.0	5.7/36
$M_{w,G}/M_{w,HG}$ (Da)	324/1459	267/1402	324/1621	267/1564	381/95000

The diffusion coefficients D and all derived values were recalculated for a new reference value for Rhodamine 6G, $D_{R6G}(25\ °C) = (4.0 \pm 0.3)\ 10^{-10}$ m^2 s^{-1} [29, 30]. The uncertainties represent one standard deviation as given by the fits and do not include the uncertainty in the reference value. All values given for 25 °C. The molar mass does not include that of the counterions of the charged dyes

As a guide for the eye the association rate constant and the diffusion controlled rate constant are set in bold

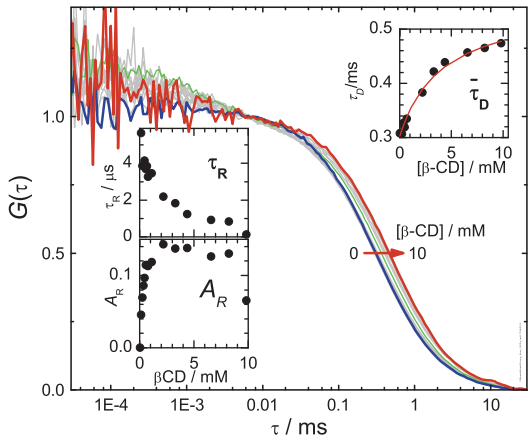

Fig. 9 *Main panel*: Experimental normalized correlation curves of PY in aqueous solution with increasing β-CD concentrations. *Insets*: Variation of the mean diffusion time τ_D, the relaxation time τ_R and the amplitude of the reaction term A_R with the concentration of β-CD as determined from individual fits of Eq. (5) [3]

appears at too short correlation times overlapping with the fluorescence lifetime of PY.

From the hydrodynamic properties of host and guest the collision rate constants k_d for a purely diffusion-controlled association process between two species can be estimated applying the Smoluchowski equation [Eq. (12)] as given in Table 1.

$$k_d = 4\pi\ (D_G + D_H)\ (R_G + R_H)\ N_0 \qquad (12)$$

(D_G, R_G and D_H, R_H are diffusion coefficients and hydrodynamic radii of guest G and host H, respectively, and N_0 is the Avogadro constant.) This diffusion limited rate constant k_d will be compared later with the rate constant k_+ of association between guest and host determined from the same FCS data. It is clearly an advantage of FCS to yield in the same measurement information about both diffusional and association dynamics.

Binding dynamics of "hard" and "soft" cages

The rate constants k_+ of association of the guests PY and PB to β-CD are both similar with a very high value of about $k_+ = 0.2 \times 10^9$ M^{-1} s^{-1} (Table 1). This is, however, still about 40 times lower than the estimated collision rate constant $k_d = 8 \times 10^9$ M^{-1} s^{-1}, with which host and guest collide due to Brownian motion in the solvent (Eq. (12), Table 1). The overall association (inclusion) is thus much slower than expected for a diffusion-controlled process. This can be understood on the basis of a two step process (see Fig. 10a) [3]. First host and guest collide with rate constant k_d and form an encounter complex within a common solvent cage. If no specific interactions are assumed a lifetime of the encounter complex of about 1 ns can be estimated. During this lifetime host and guest collide of the order of 100 times changing randomly their relative orientation. In most cases they separate again with rate constant k_{-d} without inclusion. Depending on the geometrical requirements for the inclusion of the guest into the host a small fraction of the relative orientations may be

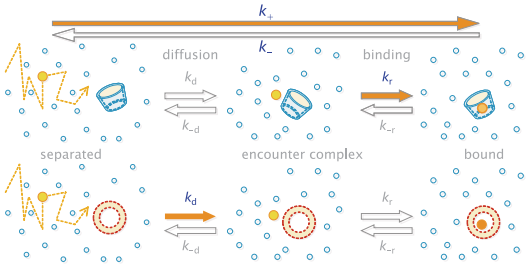

Fig. 10 Two step mechanism for supramolecular association involving the formation of an encounter complex, for a "hard" cage (cyclodextrin) (**a**) and a "soft" cage (micelles) (**b**)

favourable so that inclusion can occur with a rate constant of inclusion, k_r. The overall association rate is thus mostly controlled by this inclusion step.

Both guests, PY and PB, have similar association rate constants in spite of their different side groups. On one hand, simulations indicate that the side groups may not change significantly the critical dimension which determines the probability to enter the β-CD cavity [3] and, on the other hand, the high flexibility of the CD molecule probably allows for an induced fit compensating part of the difference in the guest geometry [31].

Another interesting result is the fact that the difference in the stability of these inclusion complexes is determined by their dissociation and not by the association process. The dissociation rate constants of PY and PB with β-CD (Table 1) differ in about one order of magnitude, reflecting the stronger interaction of PB than PY with the interior of the β-CD cavity, as already proposed on the basis of "bulk" fluorescence studies [32].

What happens if we increase the size of the host cavity? The data for the inclusion of PY and PB by γ-CD, a host with a 20 % bigger diameter of its cavity, show that the association rate constant, k_+, of the PB:γ-CD complex is about four times higher than in the case of PB:β-CD (Table 1). The wider γ-CD cavity increases the fraction of favourable relative orientations which lead to an inclusion, although the association process is still not diffusion controlled.

However, the wider cavity weakens also the specific interactions between host and included guest resulting in a strongly increased dissociation rate constant. The overall stability of the pyronine/γ-CD complexes is therefore much lower than that of the pyronine/β-CD complexes.

What do we expect for hosts without geometric restrictions? Micelles are themselves highly dynamic supramolecular self-assemblies of surfactants. Dyes such as the xanthene dye, rhodamine 123 (R123) exchange dynamically between the aqueous and the micellar pseudophase in a process similar to the inclusion described before. But, as opposed to the cyclodextrins, the micelle presents no geometric restrictions for the association of the dye; they act as "soft" hosts.

R123 is a typical probe for FCS, and is very suitable for dynamic studies in micellar systems since it presents a partition equilibrium between the aqueous phase and the micellar pseudophase formed by neutral micelles such as those formed by the aggregation of a well-known non-ionic surfactant, Triton X-100 (TX100) (Fig. 8). [4, 33, 34]. The 1:1 binding equilibrium constant for the partition equilibrium of the R123 with TX100 micelles is given in Table 1. Due to the low dye concentrations an occupancy number of more than one dye molecule per micelle is negligible.

A strong change in the brightness of R123 during the association process to TX100 micelles makes it possible to follow the association dynamics with FCS as described before (Table 1) [4, 25, 33]. As expected, the rate constant of the association of R123 to a TX100 micelle is as fast as the diffusion-controlled collision rate constant itself: $k_+ \approx k_d \approx 15 \times 10^9\ \mathrm{M}^{-1}\ \mathrm{s}^{-1}$. This shows that the association is diffusion controlled, in accordance with the picture of an unspecific association without orientational or geometrical requirements (see Fig. 10b). In this sense, the micelles may be seen as "soft" cages, as opposed to the cyclodextrin "hard" cages, which, although highly flexible, impose orientational restrictions to the inclusion.

Acknowledgments MN and WAS thank the Xunta de Galicia and the Ministerio de Educación y Ciencia for financial support (CTQ2007-68057-C02-02/BQU, INCITE09E2R209064ES, INCITE09262304PR, 2009/029). J. B. thanks the Ministerio de Educación y Ciencia for a research scholarship.

References

1. Dodziuk, H.: Introduction to Supramolecular Chemistry. Springer, Dordrecht (2002)
2. Bohne, C.: Supramolecular dynamics studied using photophysics. Langmuir. **22**, 9100–9111 (2006)
3. Al-Soufi, W., Reija, B., Novo, M., Felekyan, S., Kühnemuth, R., Seidel, C.A.M.: Fluorescence correlation spectroscopy, a tool to investigate supramolecular dynamics: inclusion complexes of pyronines with cyclodextrin. J. Am. Chem. Soc. **127**, 8775–8784 (2005)
4. Al-Soufi, W., Reija, B., Felekyan, S., Seidel, C.A., Novo, M.: Dynamics of supramolecular association monitored by fluorescence correlation spectroscopy. Chemphyschem. **9**, 1819–1827 (2008)
5. Cramer, F., Saenger, W., Spatz, H.C.: Inclusion compounds. XIX. The formation of inclusion compounds of alpha-cyclodextrin in aqueous solutions. Thermodynamics and kinetics. J. Am. Chem. Soc. **89**(1), 14–20 (1967). doi:10.1021/ja00977a003
6. Kleinman, M.H., Bohne, C.: Use of photophysical probes to study dynamic processes in supramolecular structures. In: Ramamurthy, V., Schanze, K.S. (eds.) Organic Photochemistry, p. 391. Marcel Dekker Inc, New York (1997)
7. Pace, T.C.S., Bohne, C.: Dynamics of guest binding to supramolecular systems: techniques and selected examples. Adv. Phys. Org. Chem. **42**, 167–223 (2008)

8. Zana, R.: Dynamics of Surfactant Self-Assemblies: Micelles, Microemulsions, Vesicles, and Lyotropic Phases. Taylor & Francis/CRC Press, Boca Raton (2005)
9. Selvin, P.R., Ha, T.: Single-Molecule Techniques: A Laboratory Manual. Cold Spring Harbor Laboratory Press, Cold Spring Harbor (2008)
10. Walter, N.G., Huang, C.Y., Manzo, A.J., Sobhy, M.A.: Do-it-yourself guide: how to use the modern single-molecule toolkit. Nat. Methods. **5**, 475–489 (2008)
11. Widengren, J., Rigler, R.: Fluorescence correlation spectroscopy as a tool to investigate chemical reactions in solutions and on cell surfaces. Cell. Mol. Biol. **44**, 857–879 (1998)
12. Van Craenenbroeck, E., Engelborghs, Y.: Fluorescence correlation spectroscopy: molecular recognition at the single molecule level. J. Mol. Recognit. **13**, 93–100 (2000)
13. Krichevsky, O., Bonnet, G.: Fluorescence correlation spectroscopy: the technique and its applications. Rep. Prog. Phys. **65**, 251–297 (2002)
14. Hess, S.T., Huang, S., Heikal, A.A., Webb, W.W.: Biological and chemical applications of fluorescence correlation spectroscopy: a review. Biochemistry. (N. Y.) **41**, 697–705 (2002)
15. Gösch, M., Rigler, R.: Fluorescence correlation spectroscopy of molecular motions and kinetics: advances in fluorescence imaging: opportunities for pharmaceutical science. Adv. Drug Deliv. Rev. **57**, 169–190 (2005)
16. Thompson, N.L.: Fluorescence correlation spectroscopy. In: Lakowicz, J.R. (ed.) Topics in Fluorescence Spectroscopy. Techniques, p. 337. Plenum Press, New York (1991)
17. Rigler, R., Elson, E.S.: Fluorescence Correlation Spectroscopy: Theory and Applications. Springer Verlag, Berlin (2001)
18. Zander, C., Enderlein, J., Keller, R.A.: Single-Molecule Detection in Solution—Methods and Applications. VCH-Wiley, Berlin (2002)
19. Gell, C., Brockwell, D., Smith, A.: Handbook of Single Molecule Fluorescence Spectroscopy. Oxford University Press, Oxford (2006)
20. Valeur, B.: Molecular Fluorescence: Principles and Applications. Wiley-VCH, Weinheim (2002)
21. Lakowicz, J.R.: Principles of Fluorescence Spectroscopy. Springer, New York (2006)
22. Granadero, D., Bordello, J., Pérez-Alvite, M.J., Novo, M., Al-Soufi, W.: Host-guest complexation studied by fluorescence correlation spectroscopy: adamantane–cyclodextrin inclusion. Int. J. Mol. Sci. **11**, 173–188 (2010)
23. Enderlein, J., Gregor, I., Patra, D., Fitter, J.: Art and artefacts of fluorescence correlation spectroscopy. Curr. Pharm. Biotechnol. **5**, 155–161 (2004)
24. Enderlein, J., Gregor, I., Patra, D., Dertinger, T., Kaupp, U.B.: Performance of fluorescence correlation spectroscopy for measuring diffusion and concentration. Chemphyschem. **6**, 2324–2336 (2005)
25. Bordello, J., Novo, M., Al-Soufi, W.: Exchange-dynamics of a neutral hydrophobic dye in micellar solutions studied by fluorescence correlation spectroscopy. J. Colloid Interface Sci. **345**, 369–376 (2010)
26. Widengren, J., Mets, U., Rigler, R.: Fluorescence correlation spectroscopy of triplet states in solution: a theoretical and experimental study. J. Phys. Chem. **99**, 13368–13379 (1995)
27. Reija, B., Al-Soufi, W., Novo, M., Vázquez Tato, J.: Specific interactions in the inclusion complexes of pyronines Y and B with beta-cyclodextrin. J. Phys. Chem. B **109**, 1364–1370 (2005)
28. Bordello, J., Reija, B., Al-Soufi, W., Novo, M.: Host-assisted guest self-assembly: enhancement of the dimerization of pyronines Y and B by gamma-cyclodextrin. Chemphyschem. **10**, 931–939 (2009)
29. Gendron, P.O., Avaltroni, F., Wilkinson, K.J.: Diffusion coefficients of several rhodamine derivatives as determined by pulsed field gradient-nuclear magnetic resonance and fluorescence correlation spectroscopy. J. Fluoresc. **18**, 1093–1101 (2008)
30. Müller, C.B., Eckert, T., Loman, A., Enderlein, J., Richtering, W.: Dual-focus fluorescence correlation spectroscopy: a robust tool for studying molecular crowding. Soft Matter. **5**, 1358–1366 (2009)
31. Dodziuk, H.: Rigidity versus flexibility. A review of experimental and theoretical studies pertaining to the cyclodextrin nonrigidity. J. Mol. Struct. **614**, 33–45 (2002)
32. Almgren, M., Wang, K., Asakawa, T.: Fluorescence quenching studies of micellization and solubilization in fluorocarbon-hydrocarbon surfactant mixtures. Langmuir. **13**, 4535–4544 (1997)
33. Novo, M., Felekyan, S., Seidel, C.A.M., Al-Soufi, W.: Dye-exchange dynamics in micellar solutions studied by fluorescence correlation spectroscopy. J. Phys. Chem. B **111**, 3614–3624 (2007)
34. Freire, S., Bordello, J., Granadero, D., Al Soufi, W., Novo, M.: Role of electrostatic and hydrophobic forces in the interaction of ionic dyes with charged micelles. Photochem. Photobiol. Sci. **9**, 687–696 (2010)

Journal of Colloid and Interface Science 345 (2010) 369–376

Contents lists available at ScienceDirect

Journal of Colloid and Interface Science

www.elsevier.com/locate/jcis

Exchange-dynamics of a neutral hydrophobic dye in micellar solutions studied by Fluorescence Correlation Spectroscopy

Jorge Bordello, Mercedes Novo, Wajih Al-Soufi *

Departamento de Química Física, Facultade de Ciencias, Universidade de Santiago de Compostela, E-27002 Lugo, Spain

ARTICLE INFO

Article history:
Received 21 November 2009
Accepted 22 January 2010
Available online 28 January 2010

Keywords:
Fluorescence Correlation Spectroscopy
Micelles
Dye exchange dynamics
Supramolecular dynamics
Coumarines
Triton X-100

ABSTRACT

The dynamics of the exchange of the moderately hydrophobic neutral dye Coumarine 152 between the aqueous phase and the phase formed by neutral Triton X-100 micelles is studied by Fluorescence Correlation Spectroscopy. The changes in the photophysical properties of the dye in presence of the micelles are discussed. The low quantum yield, the low saturation threshold and the necessary high energetic excitation of this dye requires a careful selection of the experimental conditions in order to obtain dynamic and diffusional properties with reasonable precision. It is shown that the contrast between the brightness of free and bound dye has a strong influence on the sensitivity of the FCS experiment. The entry rate constant of the dye to the micelles, $k_+ = (0.8 \pm 0.3) \times 10^{10}\ M^{-1}\ s^{-1}$, is very near to the diffusion controlled limit. The high association equilibrium constant of $K = (129 \pm 3) \times 10^3\ M^{-1}$ is mainly determined by the low exit rate constant, $k_- = (0.6 \pm 0.2) \times 10^5\ s^{-1}$.

1. Introduction

Micelles are highly cooperative, dynamically organized molecular assemblies, stabilized mainly by hydrophobic interactions. Both surfactants and solubilized molecules are constantly exchanged between the micelles and the surrounding aqueous solution. The study of the dynamics of the exchange processes of solubilizates and surfactant molecules is of critical importance for the characterization of a micellar system and also essential for a more detailed theoretical understanding of their formation [1]. Micellar exchange dynamics have significant influence on the performance of a given surfactant solution in technological processes, such as detergency, foaming, solubilisation, emulsification or wetting [2].

Recently we have shown how the typically very fast dye exchange dynamics can be conveniently studied with Fluorescence Correlation Spectroscopy (FCS), using micelles as membrane mimetic systems and a typical mitochondrial fluorescence marker, Rhodamine 123 (R123), as probe [3,4]. We also demonstrated the advantages of FCS to determine the association/dissociation rate constants of fluorescent dyes with cyclodextrins [5].

FCS is a fluctuation correlation method that extracts information about the dynamics of molecular processes from the small changes in molecular concentration or chemical states that arise from spontaneous fluctuations around equilibrium. Therefore FCS yields direct information about the dynamics of a fluorescent probe without the need for external disturbances. FCS allows one to study dynamic and photophysical processes that take place in a wide time scale in one and the same experiment. FCS is a single molecule technique, using very small sample volumes determined by a confocal setup and nanomolar fluorophore concentrations [6].

Fluorophores used in FCS are typically very bright and highly photostable dyes, such as Rhodamines or other Xanthene derivatives. Unfortunately, most of these dyes are charged molecules. This complicates the systematic study of the interaction of a hydrophobic dye with different micellar systems, many of the surfactants being themselves ionic species. The resulting strong electrostatic interactions between a charged dye, ionic surfactant and the counterions present in solution mask the weaker hydrophobic forces which control the exchange of neutral guests. A charged dye is not a good probe for the study of matter exchange in ionic micelles, except in the case that the electrostatic interactions themselves are the main interest.

Looking for neutral fluorophores one finds that most of them have less adequate properties for FCS. They typically present a lower brightness, worse photostability and mostly need an excitation at lower wavelength with the resulting increase in background signal. The use of these dyes requires a very careful selection of the experimental conditions. On the other hand some of these dyes compensate these disadvantages at least partially by the fact that they show a strong increase in their brightness upon association to a micelle, just opposite to the behaviour of typical FCS dyes. This is a big advantage as we will show in this contribution. It makes it much easier to detect even small amounts of associated dye and allows one to study the dynamics of the association at low surfactant

* Corresponding author. Fax: +34 982 285872.
E-mail address: wajih.al-soufi@usc.es (W. Al-Soufi).

0021-9797/$ - see front matter © 2010 Elsevier Inc. All rights reserved.
doi:10.1016/j.jcis.2010.01.064

concentration and in a time interval better accessible to standard FCS equipment.

As a representative example for this type of neutral hydrophobic probes we use coumarine 152 (C152). C152 partitions between the micellar pseudo-phase and the aqueous solution. 7-aminocoumarines have relatively low fluorescence quantum yields in aqueous solution and a poor photostability [7,8]. In addition, coumarines need a more energetic excitation at shorter wavelengths, which also excites more fluorescent impurities. However, in spite of these drawbacks, the neutral coumarines have certain advantages which make them interesting for the study presented here. They are characterized by two excited singlet states, an intramolecular charge transfer state (ICT) and a twisted intramolecular charge transfer state (TICT) [9]. It is known that the ICT states in 7-aminocoumarins are highly fluorescent whereas their TICT states are non fluorescent [10–12]. In the nonpolar and restrictive environment of micelles the formation of TICT states is suppressed, resulting in an appreciable enhancement and blue shift of the fluorescence of the dye within the micellar pseudo-phase (bound dye) as compared to that of the dye in the aqueous phase (free dye). The result is a strong increase in the detected molecular brightness of the 7-aminocoumarins as they associate to a micelle [13]. Additionally, coumarines generally show a much higher Stokes Shift than for example rhodamines, which make it easier to separate the dye fluorescence from the Raman signal of the excitation laser light.

We use the neutral surfactant Triton X-100 (TX100, t-Oct-C_6H_4-$(OCH_2CH_2)_{10}OH$, M_w = 646.85 g mol^{-1}), formed by a polar polyethylene glycol chain and a hydrophobic aromatic chain. Although this surfactant has been extensively studied, there is still some discrepancy about its properties regarding micelle formation. Recent studies reported significant variations of the aggregation number and the *cmc* depending on surfactant concentration, temperature and the technique used [14–16]. We use the following most cited values: critical micelle concentration $cmc = 2.6 \times 10^{-4}$ mol dm^{-3} and aggregation number N_{agg} = 143 [17]. The choice of these values has direct effect on the absolute values of our reported rate constants but does not affect the overall conclusions.

We first determine quantum yields, the brightness ratio, and the partition equilibrium constant from ensemble steady state absorption and fluorescence spectra. Then we discuss the experimental conditions in the FCS measurements with respect to the brightness contrast, saturation and photobleaching. Finally we present the diffusional properties and the exchange dynamics as determined from FCS.

2. Materials and methods

2.1. Materials

Coumarine 152 was purchased from Sigma–Aldrich and used as received. The surfactant TX100 (Fluka BioChemika) was checked for fluorescence impurities and was found to be clean enough for classical fluorescence measurements and for FCS experiments. Water was purified with a Milli-Q system.

2.2. Sample preparation

Stock aqueous solutions with concentrations of 15–35×10^{-3} mol dm^{-3} of the surfactant TX100 were prepared. Stock solutions of C152 were prepared with 10-fold higher concentrations than those necessary for the titrations (approximately 10^{-8}–10^{-9} mol dm^{-3} in FCS). The measuring samples were prepared by dilution of a constant volume of the corresponding C152 stock together with different volumes of the surfactant stock solution and addition of water to adjust a certain total volume. The accuracy of these volumes was checked by weighing, and concentration corrections were made. Utmost care had been taken not to contaminate the samples with fluorescent impurities.

Due to the low solubility of C152 in water aqueous solutions of C152 for the stock were stirred over night at room temperature and then filtered. The final concentration of C152 in the filtered solution was then determined from its absorption at 405 nm. The molar absorption coefficient of C152 in water at this wavelength ($\varepsilon^{405}_{water}$ = 2532 ± 10 mol^{-1} m^2) was once determined from the following procedure: first the molar absorption coefficient of C152 was determined in ethanol, in which C152 is well soluble (ε^{405}_{EtOH} = 2034.3 ± 9.0 mol^{-1} m^2). Then the concentration of a filtered aqueous solution of C152 of known absorbance was obtained by evaporating the water of a given volume, redissolving it in ethanol and measuring its absorbance in this solvent. With ε^{405}_{EtOH} the concentration and thus $\varepsilon^{405}_{water}$ can be calculated.

2.3. Equipment

Absorption spectra were measured with a Varian-Cary 300 spectrophotometer. Fluorescence emission spectra were recorded with a Edinburgh Instruments F900 spectrofluorimeter.

The setup used for the FCS measurements has been described elsewhere [18]. A 40 μL drop of each sample was deposited on borosilicate coverslips (Menzel Gläser, NO. 1 DE). The autofluorescence of these coverslips was sufficiently suppressed in the confocal setup. The samples were excited by the linearly polarized light of a 405 nm continuous wave laser diode (Becker & Hickl, BDM-405-SMC, DE) which was spectrally cleaned (Semrock, Maxdiode LD01-405/10, US), redirected by a dichroic mirror (AHF Analysentechnik, z405 RDC, DE) and focused into the sample by a microscope objective (Olympus, UPLSAPO 60 × W/1.20, water immersion) mounted in an inverted microscope (Olympus, IX-71). The fluorescence was focused onto a pinhole (Thorlabs, ∅ = 50 μm, US) and then split into two beams by a nonpolarizing beamsplitter cube (Newport, 05BC17 MB.1, US). Each beam was then focused onto an avalanche photodiode (MPD50CTC APD, ∅ = 50 μm, MPD, Italy). A band-pass filter (HQ550/100 M, AHF Analysentechnik, Tübingen, Germany) in front of the beamsplitter discriminated fluorescence from scattered light. The detector signals were processed and stored by two TCSPC-modules (SPC 132, Becker & Hickl GmbH, Berlin, Germany). Typically 20 million photons were collected for each correlation curve with count rates between 5 and 20 kHz. All measurements were made at stabilized temperature, 25.0 ± 0.5 °C. The excitation power as measured in the focus of the microscope objective by a power meter (Thorlabs, PM30-120, US) was typically 300 μW, corresponding to a mean irradiance of $I_0/2 = P/(\pi \cdot \omega^2_{xy})$ = 26 kW cm^{-2}, assuming a Gaussian intensity distribution along the optical axis. P is the excitation power in the sample [7].

The focal area and the detection volume have been calibrated with Rhodamine B (RB) in aqueous solutions at low irradiance. Recent PFG-NMR [19] and dual-focus FCS [20] measurements of the diffusion coefficients of typical rhodamine dyes determine much higher values than those used before in FCS. The diffusion coefficient of RB was estimated from these references to $D_{RB} = (4.4 \pm 0.4) \times 10^{-10}$ m^2 s^{-1}, yielding a radial $1/e^2$ radius of ω_{xy} = 0.50 μm. However, the very low absorption of RB at the excitation wavelength of 405 nm may introduce systematic errors in the calibration. All diffusion coefficients are corrected for temperature and viscosity effects and are given for 25 °C.

2.4. Data analysis

The series of absorption and emission spectra obtained in the titrations of C152 with the surfactant were analyzed using

principal components global analysis (PCGA) [21]. For FCS curves two levels of nonlinear data analysis have been applied: (1) Individual correlation curves were fitted by a fast home-built routine that runs under LABVIEW (National Instruments). (2) Series of correlation curves measured at different surfactant concentrations were analyzed by global "target" analysis programmed in OriginPro 8.0 (OriginLab Corporation, US) or in Matlab (The MathWorks, US).

3. Theory

The necessary theory has been described in more detail elsewhere and only a brief overview will be given here [3,4,18].

3.1. Mechanism

When a dye is added to a surfactant solution above the *cmc*, depending on the nature of the dye, it can either associate totally with the micelles or it can partition between the aqueous solution and the micellar pseudo-phase. In the latter case a partition equilibrium model is considered between free dye (D_f) and dye bound to the micelles (D_b):

$$D_f + M \overset{K}{\rightleftharpoons} D_b \tag{1}$$

where K is the equilibrium binding constant [17]. As for any other equilibrium process, absorption and fluorescence titrations with constant concentration of dye and varying concentrations of micelles (i.e., surfactant) allow for the determination of the binding constant.

The concentration of micelles $[M]$ can be obtained from the total surfactant concentration $[S]$ as follows:

$$[M] = \frac{[S] - cmc}{N_{agg}} \tag{2}$$

3.2. FCS

FCS analyzes spontaneous fluorescence intensity fluctuations that may be caused by various processes at the molecular level [4,22–24]. The normalized autocorrelation function $G(\tau)$ of the intensity fluctuations $\delta F(t) = F(t) - \langle F \rangle$ is given by:

$$G(\tau) = \frac{\langle \delta F(t) \cdot \delta F(t+\tau) \rangle}{\langle F(t) \rangle^2} \tag{3}$$

The correlation function for translational diffusion G_D is given by [6,25]:

$$G_D(\tau) = \frac{1}{N}\left(1+\frac{\tau}{\tau_D}\right)^{-1}\left(1+\left(\frac{w_{xy}}{w_z}\right)^2\frac{\tau}{\tau_D}\right)^{-\frac{1}{2}} \tag{4}$$

A three-dimensional Gaussian distribution of the detected fluorescence is assumed with radial and axial $1/e^2$ radii w_{xy} and w_z, respectively. N is the mean number of fluorescent molecules within the sample volume and τ_D is the translational diffusion time of the molecules across the sample volume, which is related to the translational diffusion coefficient D by:

$$D = \frac{w_{xy}^2}{4\tau_D} \tag{5}$$

3.3. Correlation function for the partition equilibrium

The correlation function taking into account the variation in the diffusion coefficient and in the brightness of a dye due to a chemical equilibrium reaction has been described previously [5]. The partition equilibrium (Eq. (1)) between free and bound dye is treated as a reversible chemical reaction with (partition) binding equilibrium constant $K = k_+/k_-$ defined by the entry (association) (k_+) and exit (dissociation) (k_-) rate constants.

Under conditions where the micelle concentration $[M]$ is always much higher than that of the dye, this concentration coincides with the initial micelle concentration $[M]_0$ ($[D_f] \ll [M] \approx [M]_0$), and the reaction is pseudo-first-order with the relaxation ("reaction") time τ_R given by:

$$\tau_R = (k_+[M]_0 + k_-)^{-1} \tag{6}$$

Applying the assumption that the relaxation time of the reaction is much shorter than the typical diffusion times of free, τ_f, and bound dye, τ_b, (i.e. fast exchange, $\tau_R \ll \tau_f, \tau_b$), the following correlation function for the diffusion and equilibrium reaction is obtained:

$$G_{DR}(\tau) = \frac{1}{N_f + N_b}\left(1+\frac{\tau}{\bar{\tau}_D}\right)^{-1}\left(1+\left(\frac{w_{xy}}{w_z}\right)^2\frac{\tau}{\bar{\tau}_D}\right)^{-\frac{1}{2}} \cdot \left(1 + A_R e^{-\tau/\tau_R}\right) \tag{7}$$

where the diffusion term is defined by a mean diffusion time $\bar{\tau}_D$ and an amplitude that depends on the mean numbers N_f and N_b of free and bound dye molecules in the sample volume. The reaction term has a relative amplitude A_R and a correlation time given by the reaction time τ_R.

The parameters $\bar{\tau}_D$, τ_R, and A_R can be expressed directly as function of $[M]_0$ and K:

$$\bar{\tau}_D = \frac{\tau_f(1+K[M]_0)}{1+\frac{\tau_f}{\tau_b}K[M]_0} \tag{8}$$

$$\tau_R = (k_-(1+K[M]_0))^{-1} \tag{9}$$

$$A_R = \frac{N_f N_b (Q_f - Q_b)^2}{(Q_f N_f + Q_b N_b)^2} = \frac{K[M]_0(1-q)^2}{(1+qK[M]_0)^2} \tag{10}$$

The reaction amplitude, A_R, depends on the brightness ratio $q = Q_b/Q_f$ of free and bound guest. The species-dependent brightness is defined by the product of the extinction coefficients, fluorescence quantum yield and detection efficiency $Q_x = \varepsilon_x \cdot \Phi_{(F)X} \cdot g_x$.

It is interesting to analyse the amplitude of the correlation function G_{DR} (Eq. (7)) at different correlation times. At very short times ($\tau \ll \tau_R$) the amplitude is exactly that of two non-interacting species weighted by their fractional intensities, as shown in Eq. (11). At these short times the dye exchange is frozen and the two species, free and bound dye, contribute independently to the total intensity.

$$\begin{aligned} G_{DR}(0) &= \frac{1}{N_f + N_b}\cdot(1+A_R) = \frac{Q_f^2 N_f + Q_b^2 N_b}{(Q_f N_f + Q_b N_b)^2} \\ &= \left(\frac{Q_f N_f}{Q_f N_f + Q_b N_b}\right)^2 \frac{1}{N_f} + \left(\frac{Q_b N_b}{Q_f N_f + Q_b N_b}\right)^2 \frac{1}{N_b} \end{aligned} \tag{11}$$

However, at an intermediate time range typical for the diffusion through the sample volume the fast exchange of the dye between free and bound states smears out their properties and the dye appears as one single diffusive species with a mean brightness and a mean diffusion time $\bar{\tau}_D$ (Eq. (8)). Therefore, as long as the exchange is much faster than the diffusion, $\tau_R \ll \tau_D$, only a single diffusional term is observed with an amplitude given by the inverse of the total number of dye molecules $G_{DR}(\tau_R \ll \tau \ll \tau_D) = (N_f + N_b)^{-1}$, independent of the individual brightness, just as expected for the single (mean) species.

3.4. Brightness ratio

We will analyze more generally the influence of the ratio between the brightness of free and bound dye, $q = Q_b/Q_f$, on the sensitivity of the FCS measurement to the dynamics of the dye exchange. The observations are also valid for other similar reversible reactions and other hosts. As explained before, the rate constants of the reaction are determined from series of reaction times, τ_R (Eq. (6)), which in turn are estimated from fits of Eq. (7) to series of FCS curves in a titration experiment with varying micelle concentrations. The reaction times are best determined from reaction terms which both have high amplitudes A_R and appear at long correlation times. The advantage of a high amplitude is directly the increase in the signal to noise ratio. Longer reaction times shift the reaction term away from the limited time resolution of the FCS equipment and towards regions of the correlation curve with lower noise. An upper limit for the value of the reaction time τ_R that can be conveniently determined is imposed by the assumptions of a fast exchange ($\tau_R \ll \tau_D$) in Eq. (7).

The dependence of the amplitude of the reaction term A_R on the micelle concentration (Eq. (10)) is illustrated in Fig. 1 for different values of the brightness ratio q. For convenience both the concentration ratio $K \cdot [M]_0 = N_b/N_f$ (upper nonlinear scale) and the molar fraction of bound dye ($X_b = K[M]_0/(1 + K[M]_0)$) (lower linear scale) are given as scales. The linear dependence of the reaction time $\tau_R k_- = 1 - X_b = (1 + K[M]_0)^{-1}$ (Eq. (9)) on the fraction of bound dye is also indicated in the figure (grey dashed line).

The micelle concentration $[M]_{0,max}$ and the molar fraction $X_{b,max}$ at which the reaction term amplitude A_R reaches its maximum, as well as the value of the maximum itself, $A_{R,max}$, depend only on the brightness ratio q:

$$K \cdot [M]_{0,max} = \frac{1}{q}; \quad X_{b,max} = \frac{1}{1+q};$$
$$A_{R,max} = \frac{(1-q)^2}{4q} = \frac{(Q_A - Q_B)^2}{4Q_A Q_B} \tag{12}$$

The reaction time which corresponds to this maximum amplitude is given by Eq. (13)

$$\tau_{R,max} = \frac{1}{k_-}\frac{q}{1+q} \tag{13}$$

High amplitudes A_R are obtained for high brightness contrasts, that is both for $q \gg 1$ and $q \ll 1$. However, in the case of dyes with lower brightness in the bound state, $q < 1$ ($q = 0.5$ and $q = 0.25$ in Fig. 1), high micelle concentrations ($K \cdot [M]_0 > 1, X_b > 0.5$) are necessary to achieve a significant increase in the reaction amplitude. In the case of dye-surfactant systems with low binding constants K the necessary micelle concentrations can be very high, exceeding many times the *cmc* of the surfactant. This has several drawbacks: (1) surfactant solutions are difficult to purify and usually introduce some residual fluorescent impurities. Adding millimolar concentrations of surfactant to nanomolar concentrations of dye can be a serious problem in FCS measurements. (2) At high surfactant concentrations the properties of the micelles, such as size, form or aggregation number may change. (3) The reaction terms with high amplitudes correspond to short reaction times, τ_R (see Eq. (9) and dotted line in Fig. 1), with the mentioned disadvantages.

These problems are reduced by dyes which show an increase in their brightness upon binding, that is that have high values of $q > 1$ ($q = 2$ and $q = 4$ in Fig. 1). In this case the reaction amplitude increases strongly already at low micelle concentrations and reaches its maximum at low fractions of bound dye ($K \cdot [M]_0 < 1, X_b < 0.5$). Comparing two cases of the same 1:4 contrast, for $q = 0.25$ the maximum of the amplitude is reached at $K \cdot [M]_0 = 4$, whereas with $q = 4$ already at $K \cdot [M]_0 = 1/4$, that is a sixteen times lower micelle concentration (note the nonlinear upper scale of $K \cdot [M]_0$ in Fig. 1). Thus for this type of dyes only very small micelle concentrations are necessary for the determination of the reaction term, which in turn appears at longer reaction times, easier to resolve with typical FCS equipment.

Summarizing, Fig. 2 represents the dependence of the reaction time at the reaction amplitude maximum, $\tau_{R,max}$, (Eq. (13)) on the brightness ratio for different typical values of the exit rate constant k_-. For an acceptable determination of the reaction dynamics from series of FCS curves at different micelle concentrations, the FCS curves with high amplitude of the reaction term should be well resolved. The reaction time given by $\tau_{R,max}$, thus indicates the minimum reaction time which has to be well resolved by the

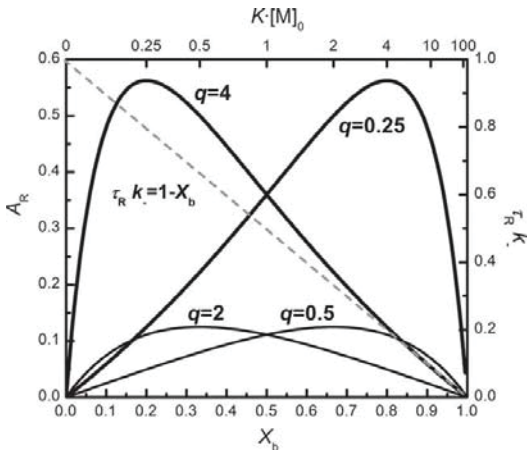

Fig. 1. Reaction amplitude, A_R, at different brightness ratios, q, (left-hand scale, black curves) and the dimensionless product between reaction time and exit rate constant, ($\tau_R\, k_-$) (right-hand scale, grey dashed line), versus the molar fraction of bound dye, X_b (bottom scale), or the concentration ratio $K \cdot [M]_0 = N_b/N_f$ (upper nonlinear scale).

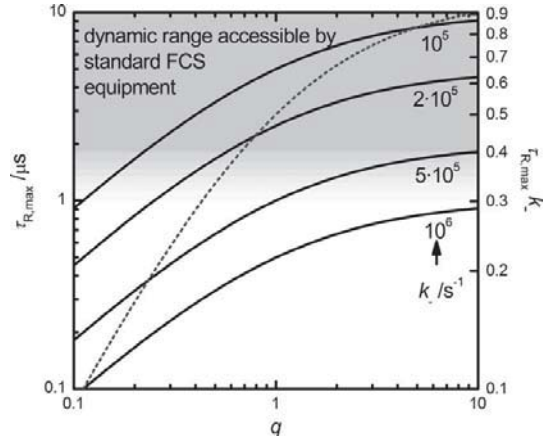

Fig. 2. Left scale and black lines: reaction time at the reaction amplitude maximum, $\tau_{R,max}$ versus the brightness ratio, q, for different exit rate constants k_-. Right scale and grey dotted curve: the dimensionless product of reaction time at the reaction amplitude maximum and exit rate constant ($\tau_{R,max}\, k_-$) versus brightness ratio, q. The grey area indicates approximately the range of reaction times which can be determined with standard FCS equipment.

measurement. Due to dead-time limitations of the counting electronics, standard commercial FCS equipment allows one to determine reaction times down to about one microsecond (although the time resolution itself may be somewhat higher). This accessible reaction time interval is shown as shaded area in Fig. 2. High brightness ratios increase therefore the sensitivity and allow one to study systems with higher exit rate constants. Depending on the exit rate constant of the system, the brightness ratio may be decisive for the accessibility of the reaction dynamics by a given FCS equipment.

4. Results and discussion

4.1. Partition equilibrium

Absorption and fluorescence titration measurements were registered in aqueous solution at a constant concentration of C152 but different concentrations of TX100. Fluorescence emission spectra (Fig. 3) of C152 showed no changes after addition of surfactant at concentrations smaller than the *cmc* of TX100. On the contrary, at higher surfactant concentrations, systematic spectral variations were observed: a significant blue shift and a huge increase in intensity.

The dependence observed indicates a partition equilibrium of C152 between the aqueous solution and the micellar pseudo-phase with an equilibrium binding constant K (Eq. (1)). Under the experimental conditions used (fixed dye concentration and excess of micelles compared to total dye concentration) and in the absence of excited-state association/dissociation processes, the following relation can be deduced between the fluorescence intensity (or the absorbance) at a certain wavelength, $F(\lambda)$, and the concentration of micelles:

$$F(\lambda) = \frac{F_f(\lambda) + F_b(\lambda)\, K[M]_0}{1 + K[M]_0} \tag{14}$$

where $F_f(\lambda)$ and $F_b(\lambda)$ are the limiting fluorescence intensities (or absorbances) at wavelength λ of the dye free in the aqueous solution and bound to the micelles, respectively.

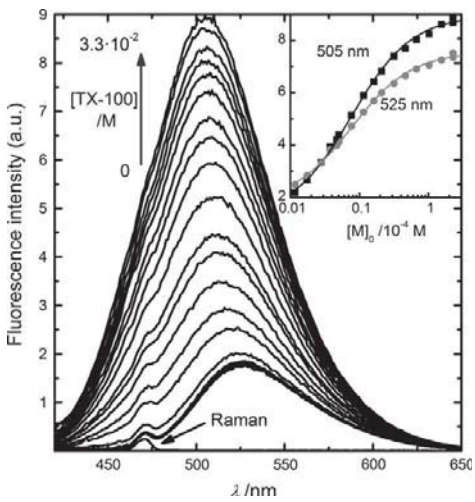

Fig. 3. Fluorescence emission spectra of C152 in the presence of different concentrations of TX100 in aqueous solution ([C152] = 1.98×10^{-7} mol dm^{-3}, λ_{exc} = 405 nm). Inset: Fluorescence intensities of C152 at two wavelengths (505 nm and 525 nm) versus micelle concentration of TX100 (logarithmic scale). Symbols represent experimental data and lines fitted curves of Eq. (14) with the parameters given in the text obtained from a global fit at all measured wavelengths.

Global non-linear analysis using PCGA to the full emission spectra of Fig. 3 yield an excellent fit and a precise value of the equilibrium binding constant (Table 1) as well as the "pure" spectra of the two species involved, i.e., free dye and dye bound to the micelles (Fig. 4).

As compared to the values obtained with R123, the binding constant K of the C152/TX100 system is approximately twice as high (see Table 1). This may be because C152 is a neutral dye whereas R123 has a positive charge, so C152 would have a higher affinity to the apolar micellar pseudo-phase.

Absorption titration data are not shown here, since the spectral change with TX100 concentration is much smaller than that observed in emission. The quantitative analysis of these small changes in absorption is complicated due to several reasons: (1) TX100 shows a residual absorbance that overlaps with that of C152. (2) In order to distinguish the C152 absorbance from that of TX100 relatively high C152 concentration have to be used, much higher than in the emission measurements. Under these conditions the probability that micelles are occupied by more than one C152 molecule (occupancy numbers above 1) is no longer negligible. Assuming that the mean occupancy number is based on Poisson statistics, we use the value of the constant for the 1:1 binding equilibrium determined from our emission data to calculate the probability of double occupancy (see Supplementary Material). This probability remains negligible in the concentrations range used for emission and FCS series, but rises above 10% in the absorption measurements. Therefore, Global fits with the 1:1 complexation model to the absorption data are not satisfactory and we take the measurement at the highest TX100 concentration as an acceptable approximation for the "pure" absorption spectrum of C152 bound to the micelles and use it to estimate the quantum yield of this complex. This approximation does not affect the determination of the brightness ratio.

Fig. 4 shows the "pure" absorption and fluorescence emission spectra of free C152 in aqueous solution and of C152 bound to the micelles of TX100. The corresponding absorption spectra present no significant spectral shift but a higher molar absorption coefficient for bound C152. Emission spectra show a significant intensity increase (which includes that of the absorption at the excitation wavelength) and a small blue shift for bound C152. The ratio between the fluorescence intensities of free and bound C152 that will be observed in FCS measurements with a given excitation wavelength and emission filter, the brightness ratio q, can be determined integrating the corresponding pure fluorescence

Table 1
Binding equilibrium constants, photophysical parameters, and properties determined from FCS of the dye C152 bound to TX100 micelles.

	C152/TX100
$K/10^3$ M^{-1}	129 ± 3
$q = Q_b/Q_f$[a]	3.8 ± 0.2
φ_f[b]	0.064 ± 0.003
φ_b[b]	0.21 ± 0.01
φ_b/φ_f[b]	3.2 ± 0.2
τ_f ms^{-1}	0.122 ± 0.002
τ_b ms^{-1}	1.22 ± 0.03
$D_f/10^{-10}$ m^2 s^{-1}	5.2 ± 0.6
$D_b/10^{-10}$ m^2 s^{-1}	0.52 ± 0.05
$R_{h,f}$/Å^{-1}	4.7 ± 0.2
$R_{h,b}$/Å^{-1}	47 ± 5
$k_-/10^5$ s^{-1}	0.6 ± 0.2
$k_+/10^{10}$ M^{-1} s^{-1}	0.8 ± 0.3
$k_d/10^{10}$ M^{-1} s^{-1}	2

All values are given for 25 °C.

[a] Brightness ratio estimated from emission spectra for λ_{exc} = 405 nm and interference filter: 550/100 nm.

[b] Fluorescence quantum yields of free C152 and C152 bound to micelles.

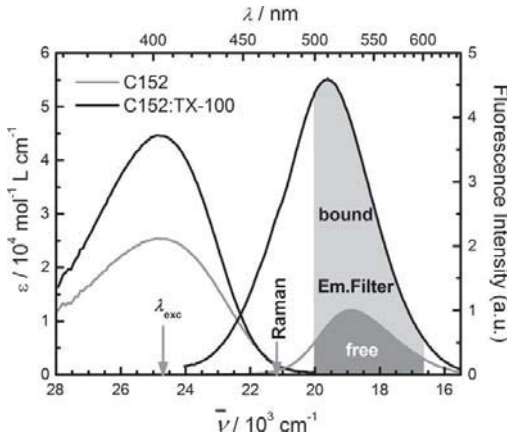

Fig. 4. "Pure" absorption and fluorescence emission spectra of C152 in aqueous solution (gray lines), and bound to TX100 micelles (black lines) obtained as described in the text. Also indicated are the excitation wavelength (λ_{exc} = 405 nm), the Raman band and the range of emission wavelength detected (λ_{em}) in the FCS measurements as determined by the band-pass filter used (CWL = 550 nm, FWHM = 100 nm).

emission spectra within the limits of the emission filters (gray areas in Fig. 4). The relative quantum yields $_b/_f$ are calculated from the same spectra but integrating the full spectral range and correcting for the different molar absorption coefficients of the species at the excitation wavelength. The results are given in Table 1. The boost in the brightness of C152 in the presence of TX100 micelles is determined by the increase of the molar absorption coefficient at the excitation wavelength (405 nm) and especially of the fluorescence quantum yield. This way, the entry/exit processes of C152 into/out of a micelle results in an effective variation ("blinking") of the brightness, which can be observed in FCS measurements.

4.2. FCS measurements

In order to achieve optimal conditions for the determination of the dynamics of the reaction process of a given surfactant – dye system several experimental parameters have to be balanced: (1) a low excitation irradiance avoids saturation, photobleaching and triplet population but may increase the measuring time unacceptably, especially in the case of dyes with low brightness, (2) a bigger confocal volume increases the diffusion time and improves the separation between reaction and diffusion terms ($\tau_R \ll \tau_D$) but also raises the background signal and the probability of photobleaching, especially at high host concentrations, and (3) the range of micelle concentrations in the titration has to be optimized both for the resolution of the reaction term at high amplitudes A_R and for the determination of the diffusional properties of free and bound dye. In the case of a dye with $q > 1$ it may be convenient to separate the determination of the reaction term at low micelle concentrations ($K \cdot [M]_0 < 1$) from the titration at high concentrations ($K \cdot [M]_0 \gg 1$) necessary for the estimation of the diffusion time τ_B of bound dye.

In order to determine the optimal excitation irradiance power series were measured for free and bound C152 under the same experimental conditions as used later for the FCS curves. Saturation and photobleaching at too high irradiance will reduce the apparent diffusion time and introduce therefore significant error in the determination of the diffusional properties [26,27]. Fig. 5 shows a double logarithmic plot of the fluorescence count rate of the dye calculated as the difference between the fluorescence intensity detected from samples with and without dye, versus the mean irradiance ($I_0/2$).

The fluorescence count rate registered from C152 in the absence of TX100 (filled black squares in Fig. 5) increases linearly at low irradiance but levels off at about 50 kW cm^{-2} due to saturation. The addition of an intermediate concentration of TX100 micelles ($[M]_0 = 0.011 \times 10^{-3}$ mol dm^{-3}, $K \cdot [M]_0 \approx 1.4$) increases the registered intensity (filled black circles) according to the expected increase in brightness of the dye. Saturation is observed at approximately the same irradiance. At a much higher micelle concentration ($[M]_0 = 0.10 \times 10^{-3}$ mol dm^{-3}, $K \cdot [M]_0 \approx 13$) the registered intensity (filled black triangles) increases still, but levels off strongly at high irradiance due to saturation and photobleaching, falling even below the intensity found at lower micelle concentrations. Due to the binding equilibrium the presence of micelles increases the mean residence time of the dye in the focal volume which leads to a higher photobleaching probability. The effect of saturation and photobleaching is well appreciated comparing the values of the diffusion time τ_D of C152 determined from FCS curves at different micelle concentrations and at increasing irradiance as indicated as open symbols in the same Fig. 5. At zero or intermediate micelle concentrations τ_D is constant within the experimental error up to about 40 kW cm^{-2}, whereas at high micelle concentrations already at about 30 kW cm^{-2} a strong decrease is observed. At high irradiance the real transit time is not observed but the time until the dye is bleached. In order to minimize the effects of saturation and photobleaching an irradiance of about 26 kW cm^{-2} (207 μW in the sample) was chosen. This irradiance is high enough to assure acceptable measurement times for the determination of the reaction term at intermediate micelle concentrations and is just acceptable for the estimation of τ_D at highest concentrations.

The next step is the evaluation of the influence of the triplet reaction. For this aim FCS correlation curves were measured at different excitation irradiances for C152 in aqueous solution and in the presence of high TX100 concentration ($[TX100] = 14.8 \times 10^{-3}$ mol dm^{-3}, $[M]_0 = 0.10 \times 10^{-3}$ mol dm^{-3}, concentration ratio

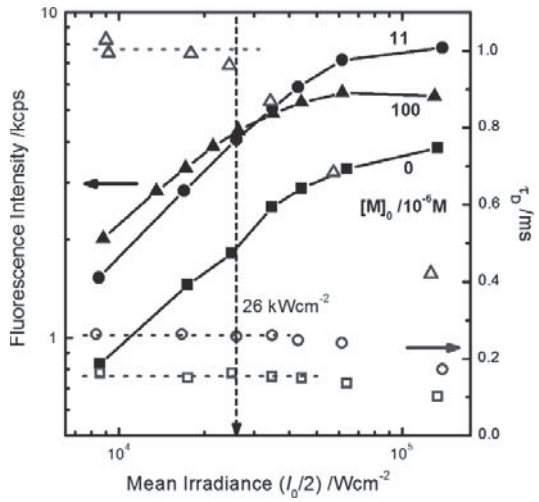

Fig. 5. Detected fluorescence intensity (filled symbols, left scale) and apparent diffusion time (open symbols, right scale) of C125 versus mean irradiance ($I_0/2$) at different micelle concentrations as indicated (squares: $[M]_0 = 0$ M, circles: $[M]_0 = 0.011$ mM, triangles: $[M]_0 = 0.10$ mM). The solvent signal (water or water + TX100) was measured separately and was subtracted from the total photon count for each sample. The vertical dashed arrow indicates the irradiance used for the FCS measurements of the reaction dynamics.

$K \cdot [M]_0 \approx 13$). The triplet-state population depends directly on the excitation power [6,28], whereas the dynamics of the dye-micelle association reflected in the reaction term does not depend on excitation power but changes with the concentration of micelles (see Eqs. (9) and (10)). At all irradiances the curves without TX100 need only one diffusion term for the model to fit satisfactorily. In the presence of TX100 micelles no excitation power dependent term was found and therefore no triplet term has been taken into account in the fits.

As pointed out before, the exchange dynamics are best determined at micelle concentrations which lead to high amplitudes in the reaction term. In this system the maximum reaction term amplitude, A_R, corresponds to a very low micelle concentration of $[M]_{0,max} \approx 0.002 \times 10^{-3}$ mol dm^{-3} ($K \cdot [M]_{0,max} \approx 0.3$) as estimated from Eq. (12) and the values of q and K determined from bulk measurements (Table 1) (see also Fig. 6). For the titration finally five FCS curves were measured at concentration ratios of $K \cdot [M]_{0,max} =$ 0, 0.3, 1.4, 2.3 and 13 as shown in Fig. 6. Beside the curve at $[M]_{0,max}$ other higher concentrations were added in order to improve the statistics and to separate better between diffusion and reaction term in the global fit. The curves at zero and at the highest micelle concentrations contain no information about the reaction, but help to estimate the diffusion coefficients of free and bound dye. For the reasons discussed before, this experiment is not optimized for the determination of the diffusion coefficients or the equilibrium constant. These would require a lower irradiance and a higher number of curves which cover a wide range of at micelle concentrations. This is not the aim of this study and the values of the diffusion coefficients given here are therefore only rough estimations.

Global "Target" Analysis of this series of FCS curves using Eq. (7) lead to satisfactory fits, as shown by the accordance of the fitted curves with the experimental data and the randomly distributed residuals (see Fig. 6). Leaving all parameters of Eq. (7) free in the fits leads to a binding equilibrium constant of $K = (140 \pm 10) \times 10^3$ M^{-1}, in good concordance with the value $K = (129 \pm 3) \times 10^3$ M^{-1} determined from bulk measurements. This later value was then kept fixed in the fits. The brightness ratio of $q = 2.5$ obtained from these fits coincides with that estimated directly from the total fluorescence intensities registered in the FCS measurements, but is significantly smaller than that observed in the bulk (see Table 1). This is probably due to the spectral responses of the FCS-detectors and to polarization effects. The results of the fits are shown in Table 1. The entry rate constant k_+ is not a direct fit parameter, but it is calculated from the binding equilibrium constant K and the exit rate constant k_-.

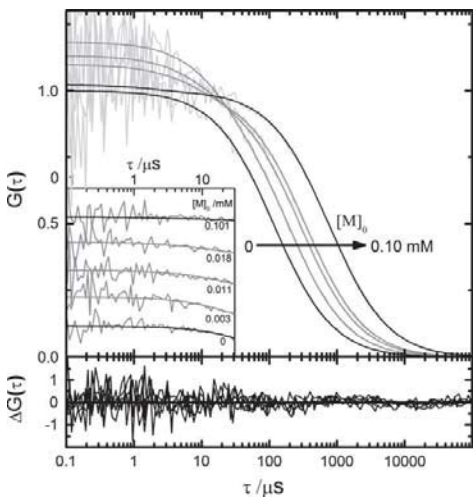

Fig. 6. Upper panel: normalized correlation curves of C152 in aqueous solution in the presence of different concentrations $[M]_0$ of TX100 micelles ($[M]_0$ = 0–0.10 mM corresponding to $K \cdot [M]_0 = 0, 0.3, 1.4, 2.3$ and 13) (gray noisy lines), measured at an irradiance of 26 kW cm^{-2}. The smooth curves are obtained from a global fit of Eq. (7) to the experimental data with fitting parameters given in Table 1. All curves were normalized by multiplication by N, the total number of molecules obtained from the fit. Inset: stacked view of the fast part of the same FCS curves. Lower panel: corresponding weighted residuals in arbitrary units. The weighting amplifies the residuals at long correlation times.

4.3. Diffusional dynamics

The diffusion times obtained from the analysis of the fluorescence correlation curves (Table 1) are converted to diffusion coefficients using Eq. (5) and then to the corresponding hydrodynamic radii R_h applying the Stokes–Einstein relation:

$$R_h = \frac{kT}{6\pi\eta D} \tag{15}$$

where k is the Boltzmann constant and η the viscosity of water (0.8905 cP at 25 °C). The values obtained are also given in Table 1.

As expected, the diffusion coefficient of bound C152 is much lower than that of free dye and coincides well with the diffusion coefficient of empty TX100 micelles determined by Dynamic Light Scattering ($D = 0.54 \times 10^{-10}$ m^2 s^{-1}) [14] (values from some other references are significantly lower but they are not based on such a detailed study as in the reference cited). The presence of a small, noncovalently bound neutral dye has no significant effect on the translational motion of the micelles, as opposed to large fluorescent probes which perturb the micellar structure and lead to a significant decrease of the diffusion constant [29].

A comparison to the values of D_b and R_h obtained for the association of R123 to TX100 micelles shows significant differences [3]. This may be due to the uncertainty in the calibration of the focal area of different FCS equipment, the use of different dyes as references, and the general limitations of standard FCS to accurately determine absolute diffusion coefficients [27]. However, these differences may also be explained by the influence of the micellar concentration itself on the micellar self-diffusion coefficient, D_b, due to changes in shape and aggregation (N_{agg}) of the micelles with increasing surfactant concentration [30].

4.4. Partition dynamics

Table 1 gives the values of the rate constants of dye entry (k_+) and exit (k_-) obtained from the fits of the fluorescence correlation curves. Neither the entry nor the exit processes take place during the lifetime of the excited state, since both the rate at which the coumarine molecules enter into the micelles (k_+[M]) and the exit rate (k_-) are, for all studied concentrations, much lower than the fluorescence deactivation rate of C152. Lifetimes for 7-aminocoumarines range between 0.4 and 5 ns depending on the solvent, that of C152 in water being about 2 ns [12].

The high value obtained for the entry rate constant (k_+) of about 1×10^{10} M^{-1} s^{-1} suggests a diffusion-controlled process for the entry of the neutral dye C152 to the TX100 micelles. The rate constant corresponding to a purely diffusion-controlled association process between dye and the micelle (k_d), can be roughly estimated applying the Smoluchowski equation:

$$k_d = 4\pi D_{DM} R_{DM} N_0 \tag{16}$$

where D_{DM} and R_{DM} are the sums of diffusion coefficients and hydrodynamic radii of the dye (free C152) and the micelles (bound

C152), respectively, and N_0 is the Avogadro constant. Comparing the values of k_+ with that of $k_d \approx 2 \times 10^{10}\ M^{-1}\ s^{-1}$ a good agreement is found, which corroborates a diffusion-controlled entry rate constant (see Table 1). This behaviour of the micelle as a "soft" supramolecular cage is similar to that found before for the entry of the cationic dye R123 in the same micelles [3]. The entry rate constant found in this study are of the same order of magnitude as those reported for other solubilizates and different types of micelles determined with other techniques [1,17,31].

The exit rate constant $k_- = 6 \times 10^4\ s^{-1}$ is much lower than that found for the R123-TX100 system. It is known that the exit rate constant varies strongly with the hydrophobicity of the solubilizate, which is higher in the case of C152. This is reflected in the much higher binding equilibrium constant of the C152 system. Given that in both cases the entry is diffusion limited, the overall affinity of the dyes to the micelles is mainly determined by the exit process.

5. Conclusions

Matter exchange is a fundamental process in colloid and interface science. Fluorescence Correlation Spectroscopy has the potential to reveal these typically very fast exchange-dynamics. The study of hydrophobic interactions in ionic colloidal systems requires neutral fluorescent probes, which typically present a lower brightness, worse photostability and mostly need an excitation at lower wavelength as compared to the charged dyes mostly used in FCS. We have shown in this contribution that the dynamics of the (host–guest) association of a neutral hydrophobic dye to micelles can be studied by FCS in spite of the low quantum yield, low saturation threshold and higher energetic excitation of the dye. The careful selection of the experimental conditions allows one to obtain the dynamic and diffusional properties with reasonable precision. We discuss that the contrast in the brightness of free and bound dye (brightness ratio q) has a strong influence on the sensitivity of the FCS experiment to the association dynamics. A strong contrast $q > 1$ leads to high amplitudes of the reaction term already at low micelle concentrations.

We found again that the micelles act as a soft cage which allows a diffusion-limited entry of the dye into the micelle. Being the association rate constant diffusion-limited, both the binding equilibrium constant and the overall exchange (relaxation) rate of different micellar systems will be determined mainly by the exit rate constant, which shows a strong dependence on the specific interactions between dye and micelle. This leads to a broad dynamic range of the exchange in micellar systems, which can be well covered by FCS.

The use of both neutral and charged dyes opens the way to systematic studies of the dynamics of matter exchange in series of neutral and ionic colloidal systems and to evaluate the role of electrostatic as compared to other weak interactions.

Acknowledgments

J.B. thanks the Ministerio de Ciencia e Innovación for a research scholarship. M.N. and W.A. thank the Ministerio de Ciencia e Innovación and the Xunta de Galicia for financial support (CTQ2007-68057-C02-02, INCITE07PXI209034ES, INCITE08E1R209060ES) and C.A.M. Seidel and S. Felekyan for help with the FCS setup.

Appendix A. Supplementary material

Supplementary data associated with this article can be found, in the online version, at doi:10.1016/j.jcis.2010.01.064.

References

[1] R. Zana, in: R. Zana (Ed.), Dynamics of Surfactant Self-assemblies: Micelles, Microemulsions, Vesicles, and Lyotropic Phases, Taylor & Francis/CRC Press, Boca Raton, 2005.
[2] A. Patist, J.R. Kanicky, P.K. Shukla, D.O. Shah, J. Colloid Interface Sci. 245 (2002) 1.
[3] M. Novo, S. Felekyan, C.A.M. Seidel, W. Al-Soufi, J. Phys. Chem. B 111 (2007) 3614.
[4] W. Al-Soufi, B. Reija, S. Felekyan, C.A. Seidel, M. Novo, ChemPhysChem 9 (2008) 1819.
[5] W. Al-Soufi, B. Reija, M. Novo, S. Felekyan, R. Kühnemuth, C.A.M. Seidel, J. Am. Chem. Soc. 127 (2005) 8775.
[6] R. Rigler, E.S. Elson, Fluorescence Correlation Spectroscopy: Theory and Applications, Springer Verlag, Berlin, 2001.
[7] C. Eggeling, J. Widengren, R. Rigler, C.A.M. Seidel, Anal. Chem. 70 (1998) 2651.
[8] C. Eggeling, J. Widengren, R. Rigler, C.A.M. Seidel, in: W. Rettig, B. Strehmel, S. Schrader, H. Seifert (Eds.), Applied Fluorescence in Chemistry, Biology and Medicine, Springer-Verlag, Germany, 1999, p. 193.
[9] J. Shobini, A.K. Mishra, K. Sandhya, N. Chandra, Spectrochim. Acta, Part A 57A (2001) 1133.
[10] P. Dahiya, M. Kumbhakar, T. Mukherjee, H. Pal, Chem. Phys. Lett. 414 (2005) 148.
[11] R.W. Yip, Y.X. Wen, A.G. Szabo, J. Phys. Chem. 97 (1993) 10458.
[12] G.I. Jones, W.R. Jackson, C.Y. Choi, W.R. Bergmark, J. Phys. Chem. 89 (1985) 294.
[13] A. Chakraborty, D. Seth, P. Setua, N. Sarkar, J. Phys. Chem. B 110 (2006) 16607.
[14] G.D.J. Phillies, J. Stott, S.Z. Ren, J. Phys. Chem. 97 (1993) 11563.
[15] G.D.J. Phillies, J.E. Yambert, Langmuir 12 (1996) 3431.
[16] K.R. Acharya, S.C. Bhattacharya, S.P. Moulik, J. Photochem. Photobiol., A 109 (1997) 29.
[17] K. Kalyanasundaram, Photochemistry in Microheterogeneous Systems, Academic Press, New York, 1987.
[18] D. Granadero, J. Bordello, M.J. Pérez-Alvite, M. Novo, W. Al-Soufi, Int. J. Mol. Sci. 11 (2010) 173.
[19] P.O. Gendron, F. Avaltroni, K.J. Wilkinson, J. Fluoresc. 18 (2008) 1093.
[20] C. Muller, A. Loman, V. Pacheco, F. Koberling, D. Willbold, W. Richtering, Europhys. Lett. 83 (2008).
[21] W. Al-Soufi, M. Novo, M. Mosquera, Appl. Spectrosc. 55 (2001) 630.
[22] J. Widengren, R. Rigler, Cell Mol. Biol. 44 (1998) 857.
[23] J. Widengren, in: R. Rigler, E.S. Elson (Eds.), Fluorescence Correlation Spectroscopy: Theory and Applications, Springer Verlag, Berlin, 2001, p. 276.
[24] E. Haustein, P. Schwille, in: P.R. Selvin, T. Ha (Eds.), Single-Molecule Techniques: a Laboratory Manual, Cold Spring Harbor Laboratory Press, Cold Spring Harbor, NY, 2008, p. 259.
[25] E.L. Elson, D. Magde, Biopolymers 13 (1974) 1.
[26] C. Eggeling, A. Volkmer, C.A.M. Seidel, ChemPhysChem 6 (2005) 791.
[27] J. Enderlein, I. Gregor, D. Patra, J. Fitter, Curr. Pharm. Biotechnol. 5 (2004) 155.
[28] J. Widengren, R. Rigler, Bioimaging 4 (1996) 149.
[29] M.A. Hink, A. Van Hoek, A.J.W.G. Visser, Langmuir 15 (1999) 992.
[30] I.D. Charlton, A.P. Doherty, J. Phys. Chem. B 104 (2000) 8327.
[31] M.H. Gehlen, F.C. De Schryver, Chem. Rev. 93 (1993) 199.

DNA Binding Dynamics

DOI: 10.1002/anie.201201099

Single-Molecule Approach to DNA Minor-Groove Association Dynamics**

*Jorge Bordello, Mateo I. Sánchez, M. Eugenio Vázquez, José L. Mascareñas, Wajih Al-Soufi, and Mercedes Novo**

Chemists have long pursued the design and preparation of small molecules that can recognize specific DNA sequences. Deciphering the human genome and on-going efforts to sequence the genomes of many other organisms have provided a wealth of information about DNA targets of both therapeutic and diagnostic interest, and therefore there is a renewed interest in the development of smart DNA minor-groove binders.[1,2] Despite the detailed structural and thermodynamic information available regarding the interaction of a number of minor-groove binders with DNA, kinetic data are much more scarce. In addition, the very low dissociation rates typical of these agents result in very slow binding dynamics, which are hard to measure experimentally.[3] Typically, stopped-flow methods are used, but this technique can yield complex kinetics and artifacts arise from the relatively high binder concentrations required. Moreover, the dissociation rates are usually obtained with indirect SDS-sequestering techniques that only give apparent rates. Dynamic data of archetypical minor-groove binders such as distamycin or Hoechst 33258 indicate that the association process is very fast and nearly diffusion limited, which is surprising given the severe geometric constraints imposed upon the inclusion of a binder into the narrow minor groove.[4–7]

Cationic bisbenzamidines are able to target AT-rich sequences preferentially over those containing GC pairs. Prominent examples of this family of molecules, such as pentamidine or furamidine, have found clinical applications and are used for the treatment of several major tropical diseases.[8] Nevertheless, the toxic side effects of these bisbenzamidines[9] have encouraged the search for new derivatives with improved efficacy, improved pharmacological properties, and reduced adverse effects.[10] Bisbenzamidines bind short AT-rich DNA sequences by insertion in the narrow minor groove. NMR spectroscopy and X-ray crystallographic studies agree on the general model of the interaction, wherein the positively charged amidinium groups are situated deep in the minor groove, making both direct and indirect hydrogen bonds with the DNA bases and electrostatic contacts with the bottom of the groove.[11]

Recently, we reported several rapid and practical approaches to synthesizing bisbenzamidine DNA binders, some of which can be easily conjugated to functional groups or fluorophores.[12] Using these methods, we made the conjugate **BBA-OG** (Scheme 1), which features an Oregon

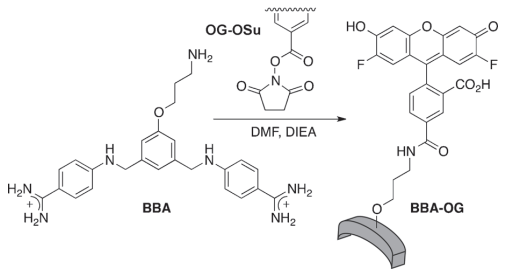

Scheme 1. Synthesis of Oregon Green-labeled bisbenzamidine **BBA-OG**. DMF = dimethylformamide; DIEA = *N*,*N*-diisopropylethylamine.

Green (OG) fluorophore attached to the DNA binder, bisbenzamidine (BBA). We envisioned that the presence of a negatively charged carboxylate in the fluorophore would increase the DNA dissociation rate, and thereby allow us to extract kinetic information using fluorescence correlation spectroscopy (FCS). This technique provides a sensitive single-molecule approach to study the fast kinetics of biomolecular interactions,[13] yielding accurate values for the binding equilibrium constant, the association and dissociation rate constants, and the diffusion coefficients,[14,15] from which the diffusion-controlled rate constants can be estimated.[16] To the best of our knowledge, this technique has not been previously used to analyze the dynamics of minor-groove binders. The wide dynamic range of FCS makes it possible to identify the rate-limiting step in the association event by comparison of the dynamics of the association to DNA with different sequences and chain lengths, and thus to evaluate processes such as sliding or two-dimensional diffusion, which

[*] J. Bordello, Prof. Dr. W. Al-Soufi, Prof. Dr. M. Novo
Departamento de Química Física, Universidade de Santiago de Compostela, Facultade de Ciencias
27001 Lugo (Spain)
E-mail: m.novo@usc.es

M. I. Sánchez, Prof. Dr. M. E. Vázquez, Prof. Dr. J. L. Mascareñas
Departamento de Química Orgánica y Centro Singular de Investigación en Química Biológica y Materiales Moleculares, Unidad Asociada al CSIC, Universidade de Santiago de Compostela
15782 Santiago de Compostela (Spain)

[**] We thank the Ministerio de Ciencia e Innovación (CTQ2010-21369, SAF2007-61015, SAF2010-20822-C02, CTQ2009-14431/BQU, Consolider Ingenio 2010 CSD2007-00006) and the Xunta de Galicia (INCITE09262304PR, INCITE09E2R209064ES, IN845B-2010/094, INCITE09 209 084PR, GRC2010/12, PGIDIT08CSA-047209PR) for financial support. J.B. and M.I.S thank the Ministerio de Ciencia e Innovación for their research scholarships.

Supporting information for this article is available on the WWW under http://dx.doi.org/10.1002/anie.201201099.

have been proposed as likely mechanisms for the binding of proteins to DNA.[16,17]

FCS titrations of **BBA-OG** with three short hairpin (**hp**) oligonucleotides (12 bp + loop) containing as key target sequences AAATTT, AATTT, and a non-target control GGCCC and with a longer dsDNA (50 bp) containing one AAATTT site, were performed. For the **AAATTT-hp**, an additional FCS titration at a higher salt concentration was measured (see Supporting Information for full DNA sequences). Figure 1 shows normalized fluorescence correlation

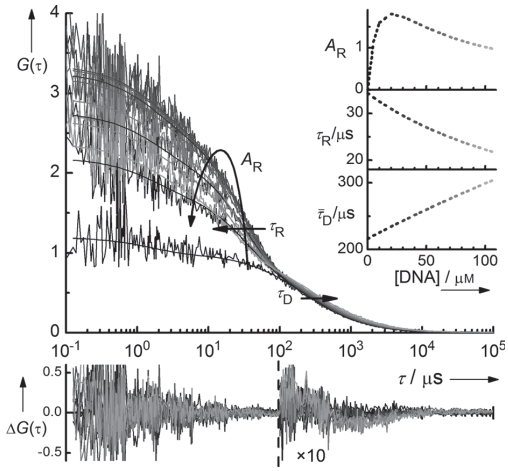

Figure 1. FCS curves of the titration of **BBA-OG** with **AAATTT-ds** and results of a global fit of the dynamic-equilibrium model (Supporting Information, Equation S1–S4). Insets: variation of the mean diffusion time $\bar{\tau}_D$, the relaxation time τ_R, and the relaxation amplitude A_R with the [DNA] calculated from the fit parameters. Lower panel: unweighted fit residuals. The small deviations at high DNA concentrations are from minor fluorescent impurities in the DNA samples. Above 100 μs a factor of 10 was applied.

curves of the binding of **BBA-OG** to the longer dsDNA. Without DNA, only a translational diffusion term of the binder with correlation time τ_D is observed. Addition of DNA increases τ_D, reflecting the slower diffusion of the dye when bound to DNA. Additionally, a new term appears with a shorter correlation time τ_R, which decreases as the concentration of DNA is increased (see insets in Figure 1). τ_R is the relaxation time of the reversible binding process: $\tau_R = (k_+[\mathrm{DNA}] + k_-)^{-1}$ with k_+ and k_- being the association and dissociation rate constants, respectively. The large amplitude A_R of this term is because of the large increase in the brightness of bound **BBA-OG**.[18] The diffusion and relaxation terms show the expected concentration dependence and are independent of the irradiance.[18,19] To reduce parameter correlation, the FCS titration series were analyzed by global target fits[14,15] with a common dynamic-equilibrium model of the diffusion, triplet, and relaxation terms (Figure 1 and Figure S1–S4). The parameters that best fit the whole data set are given in Table 1 and Figure 2.

Table 1: Association (k_+) and dissociation (k_-) rate constants and binding equilibrium constant (K) of **BBA-OG** with dsDNA. The values of k_+ are calculated from the fit parameters k_- and K ($K = k_+/k_-$).

DNA[a]	k_+ [$\times 10^8$ M^{-1} s^{-1}]	k_- [$\times 10^4$ s^{-1}]	K [$\times 10^3$ M^{-1}]
AAATTT-hp[a]	1.36 ± 0.01	3.19 ± 0.02	4.27 ± 0.03
AATTT-hp[a]	0.95 ± 0.01	4.89 ± 0.05	1.95 ± 0.02
GGCCC-hp[a]	0.083 ± 0.003	14.0 ± 0.4	0.059 ± 0.001
AAATTT-ds[a]	1.56 ± 0.02	2.84 ± 0.02	5.47 ± 0.05
AAATTT-hp[b]	0.65 ± 0.03	4.63 ± 0.01	1.41 ± 0.03

[a] [NaCl] = 0.1 M, [b] [NaCl] = 1.0 M. See the Supporting Information for complete oligonucleotide sequences.

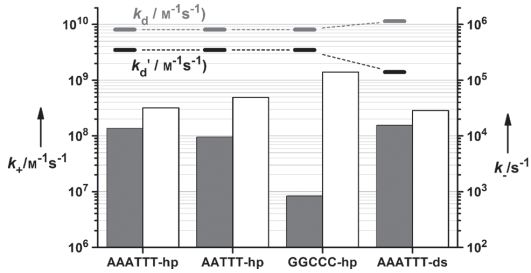

Figure 2. Association (gray, left scale) and dissociation (white, right scale) rate constants of **BBA-OG** with DNA, calculated from FCS measurements. Estimates of the diffusion-controlled association rate contants k_d and k_d', defined in Scheme 2 (see Supporting Information).

Figure 2 shows that the association rate constant decreases by more than one order of magnitude from the AT-rich to the GC-containing sequences, whereas the dissociation rate constant increases three to five times. Both association and dissociation contribute to the specificity for the AT-rich tracts, but the association has a higher effect. This is in agreement with reported results for the binding of the antibiotic distamycin to sequences with different numbers and positions of mismatched sites.[4] Moreover, the absolute values of k_+ for the AT sequences coincide well with those reported for other minor-groove binders[4–7] and show the small decrease with increasing Na^+ ion concentration expected for groove binders,[20] suggesting they might have analogous association mechanisms. Nevertheless, the dissociation rate constants are about four orders of magnitude higher than those of typical minor-groove binders, resulting in much lower binding constants.

The above results indicate much weaker specific interactions between **BBA-OG** and the DNA minor groove, which is probably owing to the electrostatic repulsion between the negatively charged OG moiety and the DNA phosphate backbone. The higher binding constants of unlabeled bisbenzamidines supports this explanation.[12] On this basis, we can consider **BBA-OG** as a valid model for the study of the association process of small molecules binding to the minor groove of DNA.

To determine the rate-limiting step for the association process, we compared the dynamics of binding to the short DNA **AAATTT-hp** with that to the much longer **AAATTT-ds**, which has been designed to avoid additional AT-rich sites.

Curiously, we did not find significant differences in the binding dynamics of these two duplexes (Table 1, Figure 2). The similar dissociation (k_-) is readily explained in terms of similar specific interactions with the AAATTT sequence. However, if diffusion plays an important role, the association dynamics should be affected by the increase of the DNA length.

For a more detailed analysis, we propose a two-step mechanism like that previously used to describe other supramolecular binding processes (Scheme 2).[14,15] The first

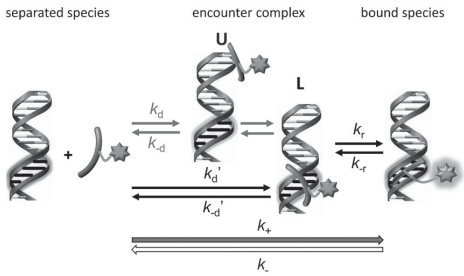

Scheme 2. Two-step mechanism proposed for the binding of **BBA-OG** to DNA involving the formation of an encounter complex, with the binder localized at the DNA reactive site (L) or unlocalized (U).

step is the formation of an encounter complex between DNA and binder, with a diffusion-controlled association rate which can be estimated based on the geometry of the DNA and binder. The second step is the insertion of the binder into the minor-groove with a rate constant k_r, a process which conveys structural rearrangements or the breakdown and reconstitution of the network of water molecules surrounding the interacting species. The experimentally determined k_+ corresponds to the overall reaction described by a single relaxation time and is determined by the rate-limiting step. This mechanism is therefore different to the sequential model proposed for the binding of Hoechst 33258 to DNA[7] which involves two reactions, with their corresponding two observed reaction times.

Assuming a rod-like structure of the DNA with a localized reactive site, we estimate lower bounds (see Supporting Information) of the diffusion-controlled association rate constants k_d and k_d' for the formation of unlocalized (U) and localized (L) encounter complexes, respectively, where the binder is either located arbitrarily at any position of the DNA (U) or already localized near to the reactive site (L) (Scheme 2).[16]

The estimated values of k_d' for the formation of localized complexes L are of course significantly lower than those of k_d corresponding to the formation of U, especially in the case of the long dsDNA (Figure 2). Nevertheless, even for the most specific sequences, both k_d and k_d' are at least one order of magnitude higher than the observed overall rate constant k_+. This shows that the diffusion-controlled formation of the encounter complex is not the rate-limiting step, even if the binder is required to be located near the reactive sequence (L complex). The encounter complexes U and L are in rapid pre-equilibrium with the separated species so that the overall rate of association between **BBA-OG** and DNA is not diffusion limited but determined by the next step of the process, namely the unimolecular inclusion into the minor groove. This step is probably controlled by geometric and orientational requirements, which depend on the critical dimensions of both the binder and the minor groove. The presence of an exocyclic 2-amino group in the minor groove of GC tracts[21] may explain the much lower value of k_+ obtained for **GGCCC-hp**.

We can also conclude that processes that increase the rate of formation of localized encounter complexes, such as sliding or two-dimensional diffusion along the DNA strand,[16,17] do not play a key role in the association rate of **BBA-OG**, and probably also do not for other minor-groove binders.

In summary, our results indicate that the association process of **BBA-OG** to dsDNA is not controlled by diffusion, but by the rate-limiting insertion of the binder into the minor-groove. Moreover, we find that the association process has an important effect on the specificity to AT-rich sites, whereas the differences in the binding affinity are mainly determined by the dissociation rate. This mechanism might constitute a general mechanism for small minor-groove binders, but this should be confirmed with further studies on more typical minor-groove agents. This information should be useful for the design of new DNA binders with optimized properties and for the future understanding of the behavior of these molecules in more complex cellular environments. This work has also shown the potential of FCS for the study DNA binding dynamics of minor-groove binders using labeled derivatives.

Experimental Section

Oligonucleotides were purchased from Thermo Fisher Scientific Inc. Nucleotide sequences and the procedure for reconstitution and annealing are provided in the Supporting Information. Details of the synthesis of the **BBA-OG** can also be found in the Supporting Information. Experimental setup and conditions, as well as the details of the data analysis for the FCS measurements have been published elsewhere[18,22] and are specified for these experiments in the Supporting Information. The uncertainties given in Table 1 represent one standard deviation as obtained by the fits.

Received: February 9, 2012
Revised: March 26, 2012
Published online: June 14, 2012

Keywords: binding dynamics · DNA · fluorescence correlation spectroscopy · minor-groove binders · molecular recognition

[1] a) D. R. Boer, A. Canals, M. Coll, *J. Chem. Soc. Dalton Trans.* **2009**, *3*, 399–414; b) W. C. Tsee, D. L. Boger, *Chem. Biol.* **2004**, *11*, 1607–1617; c) E. Pazos, J. Mosquera, M. E. Vázquez, J. L. Mascareñas, *ChemBioChem* **2011**, *12*, 1958–1973; d) M. E. Vázquez, A. M. Caamaño, J. L. Mascareñas, *Chem. Soc. Rev.* **2003**, *32*, 338–349.

[2] a) M. E. Vázquez, A. M. Caamaño, J. Martínez-Costas, L. Castedo, J. L. Mascareñas, *Angew. Chem.* **2001**, *113*, 4859–

4861; *Angew. Chem. Int. Ed.* **2001**, *40*, 4723 – 4725; b) O. Vázquez, M. E. Vázquez, J. B. Blanco, L. Castedo, J. L. Mascareñas, *Angew. Chem.* **2007**, *119*, 7010 – 7014; *Angew. Chem. Int. Ed.* **2007**, *46*, 6886 – 6890.
[3] a) L. M. Wilhelmsson, P. Lincoln, B. Nordén in *Sequence-Specific DNA Binding Agents* (Ed.: M. Waring), The Royal Society of Chemistry, London, **2006**, pp. 69 – 95; b) T. C. S. Pace, C. Bohne, *Adv. Phys. Org. Chem.* **2007**, *42*, 167 – 223.
[4] R. Baliga, D. M. Crothers, *J. Am. Chem. Soc.* **2000**, *122*, 11751 – 11752.
[5] R. Baliga, D. M. Crothers, *Proc. Natl. Acad. Sci. USA* **2000**, *97*, 7814 – 7818.
[6] S. Y. Breusegem, S. Sadat-Ebrahimi, K. T. Douglas, R. M. Clegg, F. G. Loontiens, *J. Mol. Biol.* **2001**, *308*, 649 – 663.
[7] S. Y. Breusegem, R. M. Clegg, F. G. Loontiens, *J. Mol. Biol.* **2002**, *315*, 1049 – 1061.
[8] a) R. Balaña-Fouce, M. C. Redondo, Y. Pérez-Pertejo, R. Díaz-González, M. R. Reguera, *Drug Discovery Today* **2006**, *11*, 733 – 740; b) I. Midgley, K. Fitzpatrick, L. M. Taylor, T. L. Houchen, S. J. Henderson, S. J. Wright, Z. R. Cybulski, B. A. John, A. McBurney, D. W. Boykin, K. L. Trendler, *Drug Metab. Dispos.* **2007**, *35*, 955 – 967.
[9] a) W. D. Wilson, B. Nguyen, F. A. Tanious, A. Mathis, J. E. Hall, C. E. Stephens, D. W. Boykin, *Curr. Med. Chem. Anti-Cancer Agents* **2005**, *5*, 389 – 408; b) A. H. Fairlamb, *Trends Parasitol.* **2003**, *19*, 488 – 494.
[10] R. R. Tidwell, D. W. Boykin in *DNA and RNA Binders: From Small Molecules to Drugs* (Eds.: M. Demeunynck, C. Bailly, W. D. Wilson), Wiley-VCH, Weinheim, **2003**, pp. 414 – 460.
[11] C. M. Nunn, S. Neidle, *J. Med. Chem.* **1995**, *38*, 2317 – 2325.
[12] a) O. Vázquez, M. I. Sánchez, J. Martínez-Costas, M. E. Vázquez, J. L. Mascareñas, *Org. Lett.* **2010**, *12*, 216 – 219; b) O. Vázquez, M. I. Sánchez, J. L. Mascareñas, M. E. Vázquez, *Chem. Commun.* **2010**, *46*, 5518 – 5520; c) M. I. Sánchez, O. Vázquez, J. Martínez-Costas, M. E. Vázquez, J. L. Mascareñas, *Chem. Sci.* **2012**, *3*, 2383 – 2387; d) M. I. Sánchez, O. Vázquez, M. E. Vázquez, J. L. Mascareñas, *Chem. Commun.* **2011**, *47*, 11107—11109.
[13] a) A. van Oijen, *Curr. Opin. Biotechnol.* **2011**, *22*, 75 – 80; b) D. Magde, E. L. Elson, W. W. Webb, *Biopolymers* **1974**, *13*, 29 – 61.
[14] W. Al-Soufi, B. Reija, M. Novo, S. Felekyan, R. Kühnemuth, C. A. M. Seidel, *J. Am. Chem. Soc.* **2005**, *127*, 8775 – 8784.
[15] W. Al-Soufi, B. Reija, S. Felekyan, C. A. Seidel, M. Novo, *ChemPhysChem* **2008**, *9*, 1819 – 1827.
[16] O. G. Berg, P. H. von Hippel, *Annu. Rev. Biophys. Biophys. Chem.* **1985**, *14*, 131 – 158.
[17] D. Vuzman, A. Azia, Y. Levy, *J. Mol. Biol.* **2010**, *396*, 674 – 684.
[18] J. Bordello, M. Novo, W. Al-Soufi, *J. Colloid Interface Sci.* **2010**, *345*, 369 – 376.
[19] M. Novo, D. Granadero, J. Bordello, W. Al-Soufi, *J. Inclusion Phenom. Macrocyclic Chem.* **2011**, *69*, 1 – 10.
[20] a) W. D. Wilson, F. A. Tanious, H. J. Barton, R. L. Jones, K. Fox, R. L. Wydra, L. Strekowski, *Biochemistry* **1990**, *29*, 8452 – 8461; b) F. A. Tanious, J. M. Veal, H. Buczak, L. S. Ratmeyer, W. D. Wilson, *Biochemistry* **1992**, *31*, 3103 – 3112; c) T. M. Lohman, *CRC Crit. Rev. Biochem.* **1986**, *19*, 191 – 245.
[21] S. Neidle, *Nat. Prod. Rep.* **2001**, *18*, 291 – 309.
[22] D. Granadero, J. Bordello, M. J. Pérez-Alvite, M. Novo, W. Al-Soufi, *Int. J. Mol. Sci.* **2010**, *11*, 173 – 188.

